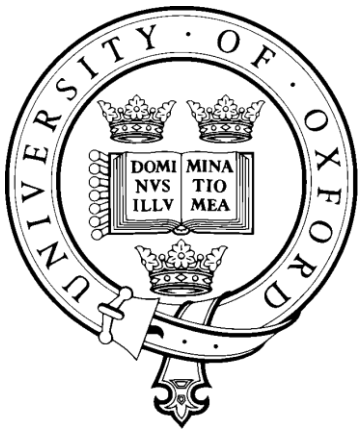

University of Oxford

Neovascularisation of the Heart post-MI: A role for endocardial trabeculation?

Tonia Thomas

St Edmund Hall

Thesis submitted for the degree of Doctor of Philosophy (DPhil) in Physiology, Anatomy & Genetics

Supervisors: Dr Nicola Smart, Dr Amer Rana, Professor Paul Riley

2018

Abstract

Restoring blood flow after myocardial infarction (MI) is essential for the oxygenation of existing and newly regenerated tissue. Proangiogenic therapies have been previously investigated in an attempt to target existing coronary vessels, but with limited success. Endogenous vascular repair processes are poorly understood, therefore we sought to determine whether coronary vessel developmental mechanisms are intrinsically reactivated following injury in the adult mouse heart. Through pulse-chase genetic lineage tracing, we established that de novo vessel formation constitutes a significant component of the neovascular response and revealed that the endocardium is a major contributory source. During development, the endocardium contributes 60% of coronary vessels, this is in large part via compaction of the trabeculated endocardial surface perinatally. We have shown that the adult heart reverts to a hypertrabeculated state between one and five days post-MI and repeats the process of compaction from 7-14 days. This process appears to facilitate endocardium-derived neovascularization, leading to formation of mature sub-endocardial vessels after infarction. To gain insight into the mechanisms that regulate endocardium-derived vessel formation in the ischemic adult heart, we investigated candidate signalling pathways which orchestrate trabeculation and compaction during development. We observed reactivation of the Notch pathway in the endocardium following MI, in keeping with its role as a key regulator of these processes in development. Using Notch1 loss- and gain- of function mouse models targeted by an endothelial-specific Cre, we observed a hypertrabeculation response induced by constitutive Notch activity, and impaired trabeculation with reduced sub-endocardial vessels after disruption of Notch activity. Moreover, our data suggest a role for Notch in driving endothelial-mesenchymal transition (EndMT) to provide smooth muscle support to newly formed vessels. Insight into pathways that regulate endogenous vascular repair, and underlying mechanisms of transient hypertrabeculation and

compaction, may reveal novel targets for therapeutically enhancing neovascularization in heart failure patients.

Acknowledgements

Firstly, I would like to thank my supervisors: Nicola Smart, for supporting me and guiding me through this challenging and rewarding learning experience, Moo Rana, for the invaluable scientific perspective and for being at hand when I needed extra support, this was appreciated so much, and Paul Riley, for being the overarching voice of reason and keeping things on track. This DPhil would not have been possible without the continuing supervision from these experts.

Secondly, thank you to all the members of the Smart, Mommersteeg and Riley labs, it's been great to be part of such a large group of dynamic, knowledgeable and interesting people. Specifically, Sonali, for always being on-hand with lab experiments and animal work from the first day to the last, and answering all of my questions with a welcoming smile! To Mala, for teaching me the MI surgery and supporting me for all those long, tiring days at BMS; I'll never forget those often trying times and our frequent heart-to-hearts! To Andia, for all your help with optimising the animal procedures, and sharing your endless knowledge (and love!) of FACS – the isolation experiments would have been impossible without you! To Ellie, Caroline, Irina, Susann and Will, for listening to me, sometimes for weeks on end, when nothing seemed to be working, and for making me smile despite everything, even if that was by dragging me to after-work drinks when we'd all share our frustrations – life in the lab would have been harder without you! Thank you also to Joey, for always answering my questions, and for your advice after confirmation – the lab are so lucky to have you keeping everyone together!

Thank you to everyone who provided the tools for this research to be achieved: Michal Maj at the Dunn School FACS Facility, Andrew Jefferson at Micron, Angela Curran, Richard Maxwell and the animal technicians on level 2, Ralf Adams for the *Cdh5-Cre* mice and Freddy Ratke for the *Notch1*$^{fl/fl}$ *mice*. Thank you to Tertia Softley, for the organization of the CRM DPhil programme, and to the CRM for giving me the opportunity

to carry out this project. To Carolyn Carr and Duncan Sparrow for your helpful input at the transfer and particularly confirmation stages, and to Carolyn and Helen Phillips for reading and examining this thesis. To Katie and Dee for running the lab meetings, ordering consumables, arranging socials and just keeping the lab going – you're the backbone of our groups!

Thank you to my family, for always believing in me, even if sometimes I did my best to challenge that belief! I wouldn't be here without your constant encouragement and the positive role models you provided growing up. Thank you to my friends for supporting me along this difficult but rewarding journey, for taking me for coffee when I needed a break, and helping me escape Oxford when things got a little too tough! Finally, thank you to Harvey – I wouldn't have got through the final 18 months without you. Thank you for always listening, for your scientific input (even if we didn't always agree) and for your unfaltering emotional support. You stepped in just when I needed to be rescued, and I'll never forget how much you changed my outlook, both mentally and scientifically – helping me reconnect with research was invaluable for motivating the final year of experiments, and I'll forever be thankful to you for listening to my research ordeals and helping me with experimental improvements. ☺

Table of Contents

Thesis Figures

Abbreviations

AVC	Atrioventricular canal
AVN	Atrioventricular node
BMP	Bone morphogenic protein
BSA	Bovine serum albumin
CECs	Coronary endothelial cells
CM	Cardiomyocyte
CoA	Co-activators
cTnI	Cardiac troponin I
CVP	Coronary vascular population
d	Day
DAPI	4',6-diamidino-2-phenylindole
Dll4	Delta like-4 (DLL4)
E	Embryonic
ECG	Echocardiogram
ECs	Endothelial cells
EDTA	Ethylenediaminetetraacetic acid
EFE	Endocardial fibroelastosis
EndMT	Endothelial-mesenchymal transition
FACS	Fluorescence-activated cell sorting
FD	Fractal dimension
FGF	Fibroblast growth factor
FITC	Fluorescein isothiocyanate
FMO	Fluorescence minus one
FSS	Fluid shear stress
GFP	Green fluorescent protein
GoF	Gain-of-function
Hes	Hairy enhancer of split
Hey	Hes-related
HF	Heart failure
HIF	Hypoxia inducible factor
HREM	High resolution episcopic microscopy
IL-1	Interleukin-1

KCl	Potassium chloride
KO	Knockout
LAD	Left anterior descending (coronary artery)
LoF	Loss-of-function
LV	Left ventricle
LVNC	Left ventricular non-compaction
MAML	Mastermind-like
MFng	Manic Fringe
MI	Myocardial infarction
MRI	Magnetic resonance imaging
N1ICD	Notch1 intracellular domain
NACWO	Named animal care and welfare officer
NF-ƙB	Nuclear factor ƙB
NICD	Notch intracellular domain
NPR-C	Natriuretic peptide receptor C (Npr3)
NRG1	Neuregulin-1
OCT	Optimal cutting temperature compound
OFT	Outflow tract
PBS	Phosphate-buffered saline
Pdgfb	Platelet-derived growth factor subunit B
PDGFRβ	Platelet-derived growth factor receptor β
PFA	Paraformaldehyde
PHH3	Phospho-histone H3
PSSL	Purse-string suture-like
RBPJ	Recombination binding protein for ƙJ
RIN	RNA integrity number
RPM	Reps per minute
SM-MHC	Smooth muscle myosin heavy chain
TLRs	Toll-like receptors
TSA	Tyramide signal amplification
VE-Cadherin	Vascular endothelial cadherin
VEGF	Vascular endothelial growth factor
VEGFR2	Vascular endothelial growth factor receptor 2
WGA	Wheatgerm agglutinin

YFP	Yellow fluorescent protein
α-SMA	Alpha-smooth muscle actin

CHAPTER 1

INTRODUCTION

Chapter 1

Introduction

1.1 Neovascularisation of the heart is required for repair post-MI

Cardiovascular diseases are the leading cause of morbidity and mortality worldwide, with over 200,000 people in the UK suffering a heart attack each year (BHF Statistics, 2018).

Myocardial infarction (MI) is defined clinically by loss of normal cardiac myocyte structure, which may include necrosis, myocytolysis, fibrosis and infiltration of inflammatory cells (Meier et. al., 2009). These are the result of a perfusion imbalance between supply and demand, usually caused by occlusion of a major artery, and are detected clinically using biomarkers (e.g. troponin), echocardiogram (ECG) or cardiac imaging (Thygesen et. al., 2007). An important endogenous response to MI is inflammation, and experimental MI has been associated with stimulation of toll-like receptors (TLRs), interleukin-1 (IL-1) signalling, and the resulting activation of the nuclear factor ƙB (NF-ƙB) system and induction of cytokines, chemokines and adhesion molecules. This results in recruitment of infiltrating neutrophils and mononuclear cells, as well as collagen deposition for scar formation (Fang et. al., 2015). Early evidence suggested that inflammation was detrimental for repair post-MI, after a canine model showed reduced infarct size with corticosteroid treatment (Libby et. al., 1973), however a clinical trial using methyl-prednisolone led to increased infarct size and higher incidence of ventricular arrhythmias, and inflammation has more recently been accepted as a reparative response to ischaemia (Roberts et. al., 1976, Frangiogannis, 2014).

Neovascularization post-MI is another essential process employed endogenously to improve blood supply to the ischemic myocardium, and may occur via mechanisms similar to those of vascularization during development (Rivard et. al., 1998). Based on animal studies, proangiogenic therapies held much promise for the treatment of ischemic

heart disease, however more than 25 phase II and phase III clinical trials have assessed the efficacy of angiogenic treatments via protein and gene therapy, with no indications of long-term benefits identified (FIRST Trial, Simons et. al., 2002, The VIVA Trial, Henry et. al., 2003, REVASC Study, Stewart et. al., 2006, Zachary and Morgan, 2011). Most therapies target angiogenic sprouting from existing coronary vessels, via vascular endothelial grow factor (VEGF) or fibroblast growth factor (FGF) signalling, however, alternative mechanisms of vessel formation in development and post-MI, have recently been considered. This poses an opportunity to identify novel mechanisms driving pathological neovascularisation in the adult heart, which could serve to provide therapeutic targets for enhancing regeneration and repair, and improve outcomes for heart failure patients.

1.1.2 Mechanisms of heart development

Regenerative medicine has established a paradigm whereby regenerative mechanisms are underpinned by the recapitulation of developmental mechanisms involved in creating the tissues embryonically. Therefore, when investigating neovascularization post-MI, key insights may be obtained from studying developmental processes involved in the formation of the heart and coronary vasculature.

The heart is derived from the mesodermal layer of cells formed during embryonic gastrulation (Moorman et. al., 2003), and the first structural representation of the heart appears at embryonic day (E) 7.5, when the mesodermal cells move to the anterior region of the embryo to form the cardiac crescent (Aria et. al., 1997). The cardiac crescent is made up of primitive endocardial and myocardial cells which express *Gata4,5,6, Hand1, Hand2* and *Nkx2-5* (Van Vliet et. al., 2012). The migration of these primitive cardiac cells is driven by mesoderm posterior 1 (MESP1) which induces EMT (Kitajima et. al., 2000) to allow cells to ingress under the epiblast (Van Vliet et. al., 2012).

The first source of cardiomyocytes has been identified as the splanchnic mesoderm in the cardiac crescent, which fuses to form the primitive heart tube. The primitive heart tube goes on to form the left ventricle, atrioventricular canal (AVC), sinus venosus and atria (Van Vilet et. al., 2012). The heart tube then undergoes looping and elongation, which is driven by a second source of cardiac progenitors, known as the second heart field, which contributes to the right ventricle and outflow tract (OFT) (Kelly et. al., 2001). Once the cardiac chambers are formed, they undergo a complex maturation process, which allows development from a smooth ventricular structure containing mainly endocardial and myocardial cells, to the complex postnatal structure composed of epicardium, myocardium, endocardium and the intra-myocardial coronary vasculature (Samsa et. al., 2013). The epicardium is derived from proepicardial progenitors, which are a highly active cell population contributing the majority of smooth muscle cells, fibroblasts and a small percentage of endothelial cells to the developing heart (Pomares and de la Pompa, 2011).

The process of ventricular wall maturation is conserved across species (Sedmera et. al., 2000) and genetic disruption of pathways involved in this process result in the clinical manifestation left ventricular non-compaction (LVNC) (Jenni et. al., 2007). In patients with LVNC, the heart morphology resembles that of the embryonic heart, and is characterised by prominent trabeculae and large sinuses between trabeculae (Jenni et. al., 2001). LVNC leads to heart failure, arrhythmias and/or sudden cardiac death (Bhatia et. al., 2011), therefore, a good understanding of the mechanisms driving chamber maturation in development and leading to LVNC cardiomyopathies in the adult heart is of paramount importance.

Ventricular maturation is composed of three distinct processes which result in the formation of a healthy, mature heart; the production of myocardial projections called trabeculae, development of the conduction system, and thickening of the compact myocardium (Samsa et. al., 2013). Myocardial trabeculae are surrounded by a

continuous layer of endocardium, and are produced after cardiac looping to increase cardiac output and oxygen uptake prior to the establishment of coronary vasculature (Lui et. al., 2010). The trabeculae undergo extensive remodelling as the chamber walls mature, which coincides with cardiomyocyte proliferation in the compact myocardium, formation of the coronary vasculature and maturation of the conduction system. The molecular mechanisms driving ventricular trabeculation and compaction are described in further detail in 1.2.2.

1.1.3 Origins of endocardial cells

The exact origin of the endocardial cells remains uncertain, but it has been suggested that a population of progenitor cells which moves into the heart field is predetermined to form either myocardium or endocardium (Cohen-Gould et. al., 1996). More recently, studies have shown a vascular endothelial lineage for endocardial cells, with lineage tracing showing a de novo vasculogenesis process contributing to the endocardium (Ferdous et. al., 2009, Milgrom-Hoffman et. al., 2011). Whilst conclusive evidence of their origin is yet to be provided, endocardial cells have a distinct gene expression profile during development which differentiates them from coronary endothelial cells, including expression of *Nfatc1* (Wu et. al., 2011), with transcripts detectable during endocardial differentiation at E7.5 and protein expression detected at the linear heart tube stage at E8.5 (de la Pompa et. al., 1998). *Gata4* has also been demonstrated for endocardial specificity (Nemer et. al., 2002, Nadeau et. al., 2010), in addition to the coronary endothelial markers *Tie2*, *VE Cadherin* and *CD31* which are also expressed by the embryonic endocardium. Unfortunately the endocardium loses expression of these distinct markers postnatally, and there has been little evidence of a specific endocardial gene expression profile in the adult heart.

1.1.4 Mechanisms of coronary vasculature development

For many years, the origins of the coronary vessels were incompletely defined, with the epicardium widely accepted as the principal source of coronary endothelial cells (Riley and Smart, 2011); however, with the identification of selective markers with which to lineage trace distinct cell sources, recent publications provided support for alternative primary embryonic sources (Redhorse et. al., 2010, Wu et. al., 2012, Tian et. al., 2014, Zhang et. al., 2016, Su et. al., 2018).

The Cre-loxP system allows tissue- and site-specific DNA recombination in transgenic mice (Orban et. al., 1992), proven to be an invaluable genetic tool employed by developmental lineage tracing studies, and utilised in this thesis. Cre recombinase is a protein from the bacteriophage P1 (Sternberg et. al., 1981) which binds a 34 base pair loxP recognition site, and when two loxP sites are present in the same orientation, binding with Cre induces deletion of any intervening DNA, leaving a single loxP (Payne et. al., 2018). This method has been used widely to remove coding regions of interest, and the use of a modified Cre combined with a mutated estrogen receptor binding domain, CreERT2, allows temporal control of gene deletion via induction with tamoxifen (Chandler et. al., 2007). Whilst the Cre-loxP system has become the standard method for genetic loss- and gain-of-function studies, there are limitations that must be considered when utilising such models.

A single Cre-excision event is passed on to all subsequent daughter cells during cell division, rendering it a useful tool for tracing cell lineages (Payne et. al., 2018). However, off-target expression is often observed due to transient Cre expression in an unreported cell type during early development, which is carried through to all cell types derived from this lineage. Attempts have been made to fully characterise transgenic mice utilising the Cre-loxP system, with results incorporated into online databases (Heffner et. al., 2012, Cre Portal, The Jackson Laboratory), but with consideration of generational drift which may result in altered expression changes, it is important to re-characterise any Cre model

used, by crossing with a reporter such as green fluorescent protein (GFP), tdTomato or LacZ, before undertaking targeted loss- or gain-of-function experiments (Song et. al., 2018).

A vast number of endothelial Cre-driven mouse models are available, and a recent review considered the validity of these models (Payne et. al., 2018). The *Tg(Cdh5-Cre/ERT2)*^{1Rha}, commonly referred to as *Cdh5-PAC-CreERT2*, is the most widely used inducible endothelial marker (Wang et. al., 2010), and was used to target adult endothelial cells in this thesis. The *Cdh5-PAC-CreERT2* mouse line is referred to as vascular endothelial cadherin (*VE Cadherin)-Cre* throughout this thesis. Tamoxifen injection at postnatal day (P)1 and P6 induced pan-endothelial cell expression in brain and retina endothelium (Yanagida et. al., 2017), and tamoxifen administration at P14 induced efficient recombination in the endocardium (Zhang et. al., 2016). However, some variability was reported with the efficiency of tamoxifen-induced Cre recombination (Zarkada et. al., 2015), therefore full optimisation and characterisation was undertaken prior to using this model experimentally, which is described in chapter 4.

1.2.1 The origins of coronary endothelial cells

Recent publications initiated a debate surrounding the origins of coronary vascular endothelial cells, with the identification of two sources in addition to the proepicardium, which was found to derive mostly smooth muscle cells and fibroblasts in lineage tracing studies (Cai et. al., 2008, Zhou et. al., 2008). The sinus venosus and the endocardium have been separately identified and are now considered as the main sources of coronary endothelial cells during development (**Figure 1.1**) (Red-horse et. al., 2010, Wu et. al., 2012, Tian et. al., 2014, Zhang et. al., 2016, Su et. al., 2018).

The sinus venosus is the vein that supplies the embryonic heart with blood, and culminates in a large cavity lined with endocardial cells which goes on to form the right atrium and coronary sinus later in development (Red-horse et. al., 2010). The sinus

venosus was identified as a source of coronary endothelial cells using an Apelin-LacZ reporter, contributing via the formation of an immature coronary plexus which undergoes sprouting angiogenesis. The model was later updated and sprouting venous endothelial cells were proposed to gradually decrease expression of venous genes, whilst increasing expression of arterial genes, and upon reaching a threshold towards full arterial differentiation, the coronary plexus commits to forming mature coronary arteries (Su et. al., 2018).

Two concurrent studies identified the endocardium as a major source of coronary endothelial cells. An Nfatc1-Cre line was used to track endocardial cells and demonstrate contribution to the endothelial cell population of 72% major arteries, 81% myocardial vessels, and 37% subepicardial vessels (Wu et. al., 2012). A further study suggested that coronary vessel formation comprises two distinct phases, using separate mechanisms and progenitor populations; the 1st coronary vascular population (CVP) contributes to the fetal ventricular free wall and postnatal outer myocardial wall, and the 2nd CVP contributes to *de novo* formation of vessels in the intramyocardial vessels during myocardial compaction (Tian et. al., 2014).

A later study from the Red-Horse group considered relative embryonic contributions of the endocardium alongside the sinus venosus, and revealed that ApjCreER-traced vessels (sinus venosus-derived) and Nfatc1Cre-traced vessels (endocardium-derived) contribute to complementary and minimally overlapping regions of the heart (Chen et. al., 2014). It was also proposed that 5-10% of coronary endothelial cells were contributed by the proepicardium, which were spread uniformly throughout the heart.

In response to the controversy between sinus venosus and endocardial contributions, the Zhou group (Zhang et. al., 2016) followed up their previous study by generating an Natriuretic peptide receptor C (Npr3)-Cre endocardial-specific mouse line after they reported that their Nfatc1-Cre model labelled sinus venosus endothelial cells at E9.5 and E11.5, preventing the separation of endocardial and sinus venosus derived coronary

endothelial cells. The study showed that Npr3-Cre was expressed specifically by endocardial cells, and it was confirmed that the endocardium minimally contributes to coronary ECs of the ventricular free walls during embryonic stages. However, the study supported their earlier findings of a 2nd CVP contributing to the majority of intramyocardial vessels postnatally. This postnatal contribution coincided with compaction of the trabecular myocardium, and quantification of Nfatc1-Cre labelled vessels established that 60% of the irrigated muscle volume formed between P0 and P28 was of an endocardial origin (Zhang et. al., 2016).

Whilst it remains controversial how, and when, the endocardial and sinus venosus contributions occur, these thorough lineage tracing studies confirm an important role for the endocardium in the development of the coronary vessels, providing strong rationale for its consideration as a source of neovascularistion post-MI.

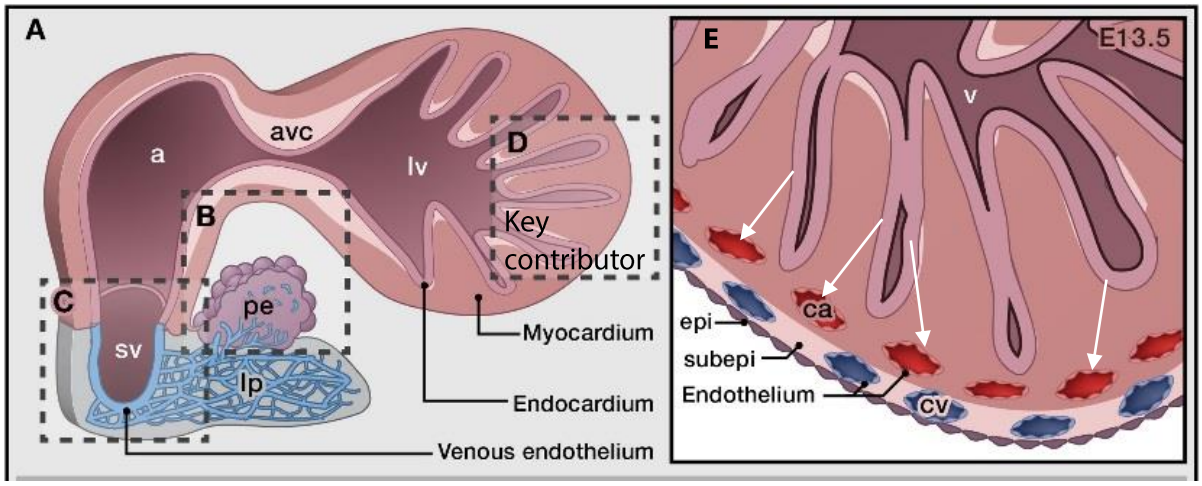

Figure 1.1. The origins of the coronary vessels: Proepicardium, Sinus Venosus and Ventricular Endocardium

This schematic shows the embryonic mouse heart at stage E13.5, with the three sources of coronary vascular endothelial cells outlined (A). The proepicardium (box B), the sinus venosus (box C) and the ventricular endocardium (key contributor, box D) have each been identified as a source of coronary endothelial cells in the developing heart. The close proximity of these tissues to the developing myocardium and coronary vessels (inset) show how these sources interact concurrently to produce the heart vasculature Arrows indicate endocardial contribution to intra-myocardial vessels via trapping mechanism during ventricular compaction (E). *Adapted from G del Monte, R P Harvey, 2012.*

a = atrium, sv = sinus venosus, lv = left ventricle, pe = proepicardium, lp = liver primordium, epi = epicardium, subepi = subepidcardium, cv = coronary vein, ca = coronary artery, v = ventricle

1.2.2 Ventricular patterning in the embryo: Trabeculation and Compaction

The mechanisms of trabeculation and myocardial compaction are intimately associated with the development of the coronary vasculature, with disruptions leading to failed vasculogenesis and LVNC; persistence of heavily trabeculated myocardium (Teekakirikul et. al., 2013). Unexpectedly, our group uncovered evidence of induction of new trabeculae in the adult endocardium post-MI, which may serve to increase surface area for perfusion and, with subsequent compaction, may also be an intrinsic response to enhance neovascularisation of the ischemic myocardium (Dubé, Thomas et. al.,

2017). Understanding the mechanisms of trabeculation and compaction in development will provide a basis to determine whether they are recapitulated after injury.

The development of ventricular trabeculae involves highly coordinated paracrine signalling between the endocardium, myocardium and cardiac jelly which is initiated towards the end of cardiac looping (Moorman et. al., 2003, Paige et. al., 2015). These transduction pathways lead to cell proliferation, differentiation and migration, before the cardiac jelly is later degraded to initiate maturation of the ventricular wall.

These processes are driven by multiple mechanisms such as the cell adhesion molecule Neuregulin-1 (Nrg1) in the endocardium, which acts as a paracrine ligand for ErbB4 in the myocardium, promoting its heterodimerisation with ErbB2, and leading to downstream signal modulation (Yarden and Sliwkowski, 2001). Genetic modulation of NRG1, ErbB2 and ErbB4 has shown that a lack of any components of this mechanism results in early gestational death due to trabeculation defects (Meyer et. al., 1995, Lee et. al., 1995, Gassman et. al., 1995).

Bone morphogenic protein-10 (BMP10) has an important role in regulating trabeculation through signalling via SMAD to modulate gene transcription (Lowery et. al., 2010). BMP10 is expressed in cardiomyocytes in the embryonic and post-natal heart (Neuhaus et. al., 1999), and its global deletion results in severely reduced cardiomyocyte proliferation which leads to embryonic lethality (Chen et. al., 2004). Endocardial Brg1 (chromatic remodelling protein) is involved with signalling through BMP10 (Hang et. al., 2010), to initiate cardiomyocyte proliferation, and later represses the metalloproteinase ADAMTS1 to initiate degradation of the cardiac jelly and terminate trabeculation (Cooley et. al., 2011).

Notch signalling is important throughout cardiac development due to its involvement in valve formation, OFT development and ventricular chamber maturation (Samsa et. al., 2013). Notch1 signalling receptor plays a pivotal role in orchestrating trabeculation and

compaction during development through its expression in the endocardium (Grego-Bessa et. al., 2007, Zhang et. al., 2013), and will be described in more detail later in this chapter.

These mechanisms underlying trabeculation-compaction are summarised in **Figure 1.2**, alongside others which were not considered during this project. Whilst there is currently no evidence of ventricular patterning mechanisms being reactivated in the post-embryonic heart, the observation of injury-induced trabeculae outlined here has prompted their consideration in the pathological setting.

Consideration was primarily focused on Nrg1, Brg1, and Notch1, which were investigated alongside known regenerative processes such as inflammation and angiogenesis.

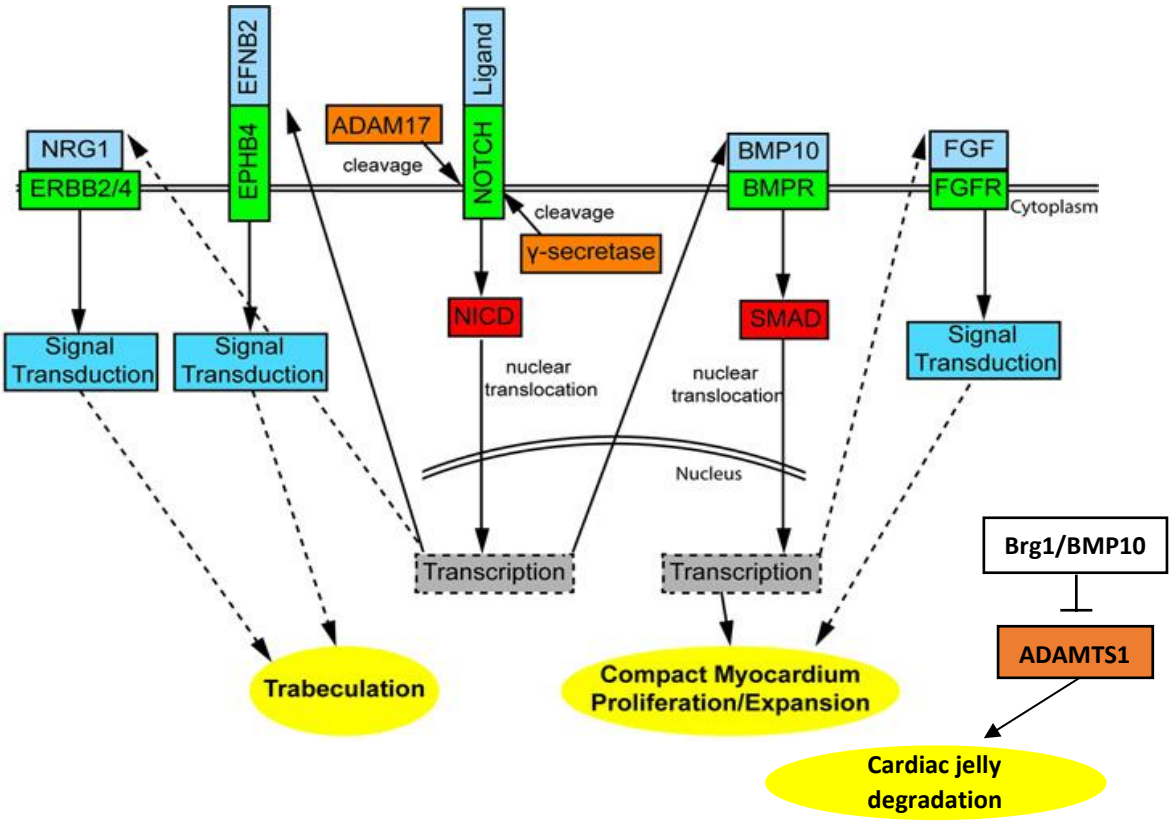

Figure 1.2. Signalling pathways in ventricular chamber maturation

Intrinsic signaling pathways identified as key regulators of cardiac chamber morphogenesis. Canonical NOTCH ligands including Delta and Jagged bind to NOTCH receptors. Upon binding, ADAM17 cleaves the extracellular domain of NOTCH and γ-secretase cleaves the intracellular domain of NOTCH, releasing NICD into the cytoplasm. NICD translocates to the nucleus and modulates gene transcription. NOTCH activation leads to stimulation of EphrinB2 signaling through EPH4 and NRG1 signaling through ErbB2/4, which are essential for trabeculation. NOTCH activation also leads to activation of BMP signaling through BMP10 interaction and FGF signaling through FGFR. BMP and FGF signaling are essential for cardiomyocyte proliferation and expansion of the compact myocardium. Endocardial Brg1 later activates BMP10 to repress ADAMTS1 and initiate degradation of the cardiac jelly to terminate trabeculation. *Adapted from Samsa et. al., 2014.*

1.2.3 The Notch signalling pathway

The Notch pathway is evolutionarily conserved in most multicellular organisms, and orchestrates multiple cell differentiation processes in embryonic and adult life (Artavanis-Tsakonas et. al., 1999). The Notch receptors and their ligands are single transmembrane proteins that allow the Notch pathway to transduce signals between neighbouring cells (summarised in **Figure 1.3**, High & Epstein, 2008). In mammals, there are four Notch receptors (1-4) and five ligands (Delta-like 1,3,4 and jagged 1,2), and these receptors and ligands are specific to different cell types. To activate Notch signalling, the ligand binds with the receptor on a neighbouring cell, which leads to proteolytic cleavage of the Notch intracellular domain (NICD) by the γ-secratase complex, releasing it into the cytoplasm. NICD then translocates to the nucleus where it binds with the DNA binding protein RBPJ, the co-activator mastermind-like (MAML), and other co-activators (CoA), which leads to activation of transcription factors. The most widely described Notch transcriptional targets are the Hairy enhancer of split (Hes) and Hes-related families (Hrt/Hey). These mediate many of the downstream responses of Notch signalling, however the explicit outcome of Notch activation is dependent on the cell type initiating signalling, and the temporal point in development (**Figure 1.3**, High & Epstein, 2008).

Notch signalling has a vital role in the regulation of cardiac development, and haploinsufficiency of its pathway components in human embryogenesis can result in congenital heart defects (Garg et. al., 2005, Luxan et. al., 2013). During early cardiac specification, Notch is downregulated in cardiomyocytes and enriched in the endocardial cell lineage, where it has important functions discussed in detail in section 1.2.4 (Lescroart et. al., 2018). Notch signalling is also important for heart tube patterning, formation of the AVC, and establishment of the conduction system via the atrioventricular node (Macgrogan et. al., 2018). Defective signalling through this pathway leads to structural congenital heart disease and abnormal cardiac conduction (Rentschler et. al., 2011), and ectopic endocardial Notch1 activation via a *Tie2-Cre*

resulted in increased EMT in the AVC and induction of EMT in the ventricles (Kisanuki et. al., 2001). This provides further support of the important role Notch signalling plays during cardiac development, and in particular ventricular patterning; these roles are discussed in more detail below.

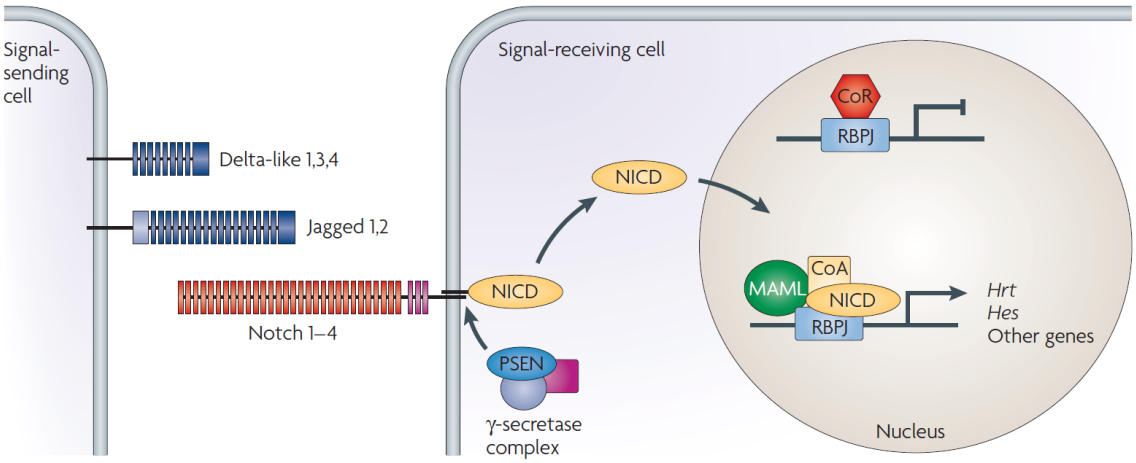

Figure 1.3. The Notch Signalling Pathway in Mammalian Cells

The mammalian Notch signalling pathway is summarised with ligands, Delta-like 1,3,4, and Jagged 1, 2, the Notch receptors 1-4, proteolytic cleavage complex, co-activators MAML, RBPJ and CoA, and transcription factors, Hes and Hrt indicated. *High & Epstein, 2008.*

1.2.4 The role of endocardial Notch signalling in ventricular patterning

Notch signalling is a critical component of cardiovascular development and disease, with roles in regulating cell proliferation, differentiation and maturation for morphogenesis, and in initiating endothelial-mesenchymal transition (EndMT) and sprouting angiogenesis (Garg et. al., 2005, Grego-Bessa et. al., 2007, Luna-Zurita et. al., 2010, Luxán et. al., 2013). Endocardial Notch1 signalling is vital in regulating trabeculation, and genetic studies performed in the mouse have contributed to our understanding of this process. Embryonic knockout (KO) of endocardial Notch1 regulators, such as Jarid2, Fkbp1a and RBPJκ (CBF1), led to impaired trabeculation, decreased CM proliferation and reduced endocardium-myocardium contact (Mysliwiec et. al., 2011, Chen et. al., 2013, Luxán et. al., 2013). Conditional KO of the transcription factor, Jarid2, selectively from endocardium, but not myocardium, epicardium or neural crest, recapitulated the phenotype of the global KO (Mysliwiec et. al., 2011). In mutant embryos, Notch1 pathway genes, including endocardial *Notch1*, *Nrg1*, and *Nrg4*, and myocardial *Dll4*, *ErbB4* and *Hey1* were significantly up-regulated; Notch1 levels remained continually elevated in the endocardium, coinciding with the sustained increase in trabecular projections (Matthew et. al., 2011).

The transcriptional regulator, RBPJκ, interacts with activated endocardial Notch1 (N1ICD) to initiate activation of myocardial Notch target genes *Hey* and *Hes*. RBPJκ-null mice showed attenuated EphrinB2 and NRG1 in the endocardium, and increased myocardial BMP10. However, BMP10 levels were not affected in NRG1 or EphrinB2 mutants, suggesting that Notch1 independently regulates two pathways; cardiomyocyte proliferation via BMP10 and myocardial differentiation to trabecular and compact muscle via EphrinB2 (Grego-Bessa et. al., 2007).

A recent study detailed the coordination of sequential Notch1 signalling for the regulation of ventricular chamber development (D'amato et. al., 2016). $Dll4^{flox}$, $Jag1^{flox}$ and $Jag2^{flox}$ mice, targeted with endothelial- and cardiomyocyte-specific Cre lines, were used to show

the orchestration of endocardial Notch1 signalling by endocardial delta-like 4 (Dll4) and myocardial Jag1 between E8.5-E10.5, followed by a switch to myocardial Notch1 activation by myocardial Jag1 and Jag2 from E11.5. *Dll4*^{flox} targeted to endocardial cells with *Nfatc1Cre* produced severely disrupted trabeculation with a phenotype similar to that seen with Notch1 inactivation. An upregulation of negative regulators of cell proliferation was also observed in the *Dll4*^{flox}*; Nfatc1Cre* mutants by RNA-Sequencing. Early inactivation of Jag1 did not affect trabeculation or expression of N1ICD, however when *Jag1*^{flox} was targeted using a *cTnT-Cre*, mutants showed higher trabeculation and reduced compact myocardium at E16.5. *Jag2*^{flox}*; cTnT-Cre* mice showed a similar phenotype at E16.5 and when both were perturbed, the compact myocardium was 40% thinner than in controls (D'amato et. al., 2016).

This coincided with trabeculation and compaction, respectively, and the switch from Dll4 to Jag1 and Jag2 orchestrated signalling was found to be mediated by Manic Fringe (MFng), which was progressively down-regulated in the endocardium over this period (**Figure 1.3**, D'amato et. al., 2016).

This study is key in improving our understanding of how Notch signalling orchestrates ventricular chamber remodelling, and due to its key role in regulating trabeculation and compaction in this developmental setting, Notch1 signaling is an important consideration for recapitulation post-MI.

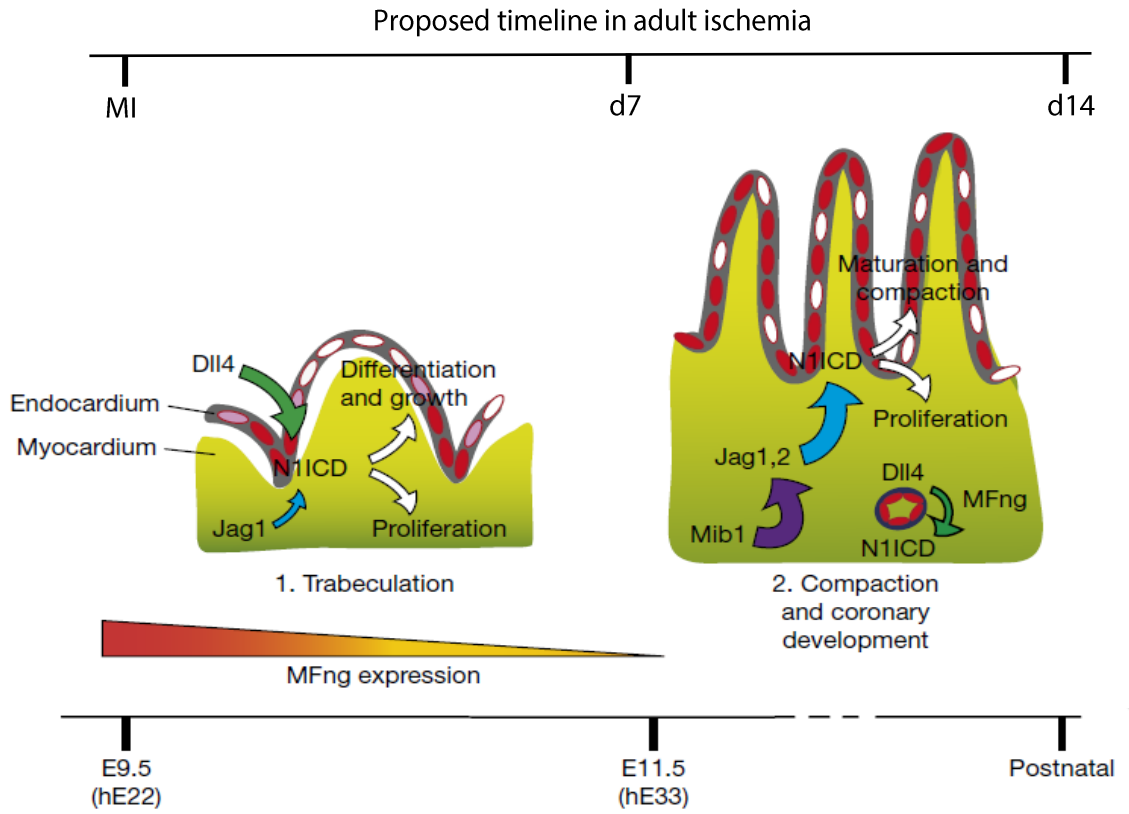

Figure 1.4. Sequential Notch ligand-receptor activation during ventricular chamber development

In the early ventricle, endocardial Notch1 signaling is mediated primarily by Dll4 (1, green arrow), with low myocardial Jag1 expression (1, blue arrow) at this stage. Notch1 activation in the endocardium (red) promotes cardiomyocyte proliferation, trabecular growth and patterning. As chamber patterning develops (2), endocardial Manic Fringe (MFng) expression reduces progressively to allow myocardial Jag1 to activate Notch1 in the myocardium. Jag2 expression is also upregulated in chamber myocardium, where it acts together with Jag1 to promote proliferation, patterning and trabecular compaction (2, blue arrow). This process occurs between E9.5 and early postnatal stages in the developing heart, and it is proposed that a similar mechanism may occur in the adult heart between 24 hours and 14 days post-MI.

Adapted from *D'amato et. al., 2016.*

1.2.5 Notch signalling in valve formation and EndMT

Elsewhere in the developing heart, Notch plays a role in activating endocardial EndMT in the AVC and OFT regions to contribute mesenchymal cells to the mitral, tricuspid and outflow tract valves (de Lange et. al., 2004). Notch1 is expressed in the cardiac crescent during early heart development, and then throughout the endocardium with raised expression in the AVC and OFT, followed by heightened levels in the cardiac cushion mesenchyme at E9.5 (Williams et. al., 1995). Transgenic models have been used to uncover the role of Notch1 in orchestrating EndMT in this setting. A gain-of-function (GoF) model with constitutive endothelial/endocardial Notch activation (Tie2-Cre;N1ICD) showed initiation of a mesenchymal gene programme in the ventricular endocardium (Luna-Zurita et. al., 2010), and loss-of-function (LoF), through global RBPJ KO, caused a loss of cushion mesenchyme in the AVC, reduced expression of Snai1, an EndMT transcriptional regulator, and collapsed endocardium (Timmerman et. al., 2004). More recently, endocardial cells have been identified as a source of mesenchymal progenitors of pericytes and coronary vascular smooth muscle cells via EndMT during development of the coronary vasculature (Chen et. al., 2016). These data confirm an important regulatory role for endocardial Notch1 in controlling embryonic EndMT (**Figure 1.5**), and support consideration for the endocardium as a source of mesenchymal, as well as endothelial, cells post-MI.

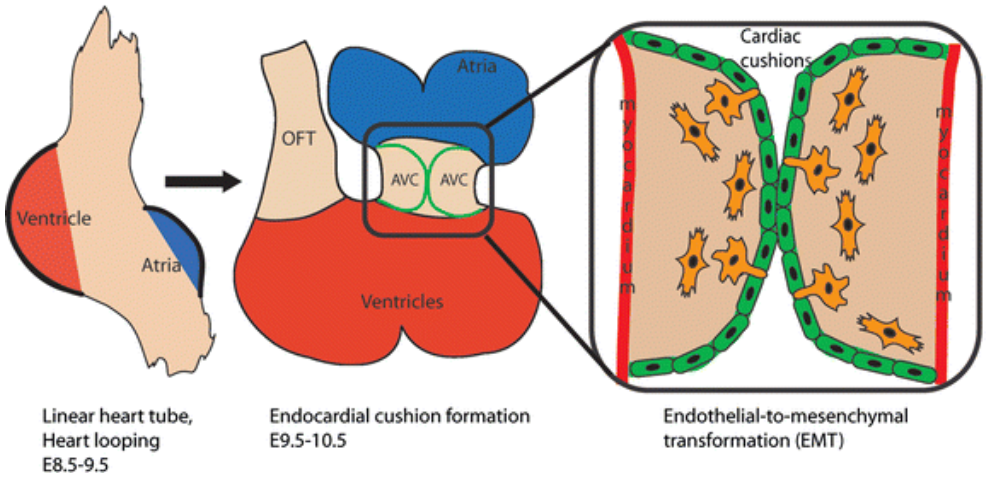

Figure 1.5. EndMT in the developing AVC

After looping of the linear heart tube, the endocardium lining the AVC (green) contributes mesenchymal cells to the cardiac cushion (yellow), in preparation for formation of the mitral, tricuspid and outflow tract valves. Notch1 expression in the endocardium drives EndMT in this setting. *Garside et. al., 2013.*

1.3 Neovascularisation and endocardial remodelling in the injured adult heart

1.3.1 A murine model of myocardial infarction for insight into clinical pathologies

Heart failure (HF) is defined in patients as insufficient cardiac output to meet the metabolic demands of the body, and the leading cause of HF is coronary artery disease resulting in MI (Braunwald, 2013). Within minutes of myocardial ischemia, billions of cardiomyocytes and many blood vessels are lost through necrosis, which leaves a lasting scar in the myocardium preventing the heart from functioning as usual (Krijnen et. al., 2002). Currently there are no treatments to reverse HF, and all therapeutic approaches aim to alleviate symptoms. Investigations into the endogenous repair mechanisms and attempts to activate regeneration are of paramount importance for improving patient outcomes of this condition.

In order to investigate the endogenous response to MI, a suitable mammalian model is required to replicate the period of ischemia caused by MI in patients. Murine models of

ischemia are favoured due to the lower costs involved with housing, and the availability of genetically modified animals for investigating specific genes and signalling pathways. Three main surgical models are used in rodents: permanent coronary ligation, temporary coronary ligation (ischemia reperfusion) and cryoinjury (Madeddu et. al., 2006). All models provide a useful simulation of the clinical pathology, however each also has its caveats. Ischemia reperfusion is often favoured due to its similarity to the clinical treatment of MI which involves inserting a stent to reopen the occluded vessel and restore blood flow to the myocardium, however this murine surgical procedure requires an experienced surgeon to prevent unwanted surgical trauma which could contribute to the inflammatory response that is characteristic with myocardial reperfusion (Nossuli et. al., 2000). Cryoinjury is an accurate and reproducible method of inducing myocardial ischemia, however the necrosis of such a large region of the left ventricle is less replicative of the clinical pathology, and damage to the epicardium may hinder important regenerative processes that support cardiac repair (Smart and Riley, 2012). The model adopted by most groups, including ours, is permanent ligation of the left anterior descending coronary artery (LAD), which was first described in 1960 (Selye et. al., 1960). Whilst permanent coronary ligation is less representative of the clinical pathology as permanent ligation in patients would quickly lead to death, it is a useful method for investigating the chronic effects of HF without maintaining animals on a severe protocol for many months. The “no-reflow phenomenon” has been described which refers to a section of the microvasculature that does not restore blood flow despite re-opening of the occluded large artery (Kloner, 2006). The area of “no-reflow” is suggested to expand over time, with extensive “no-reflow” zones shown to correlate with more left ventricular remodelling (Reffelmann et. al., 2003). This phenomenon is contributing a growing challenge for the selection of suitable therapeutic interventions in MI patients, and successfully modelling it in mice could provide insight into how to combat the issue clinically (Ramjane et. al., 2008). The short period of ischemia induced by the temporary ligation model is unlikely to accurately represent the clinical “no-reflow” phenomonen,

and when investigating vascular remodelling post-MI, consideration of this pathological adaptation is important. The combined benefits of studying a chronic HF model, and one in which the “no-reflow” phenomenon is replicated, makes permanent LAD ligation the method of choice for this study. Reproducibility can be a challenge with both the temporary and permanent ligation models, but if care is taken to exclude outlying samples with very small or very large infarcts, results remain reliable. The LAD ligation method is commonly performed in Oxford which also proved beneficial for training and monitoring of the procedure, and expertise for analysing this type of injury have been well established within the group.

Whilst it is important to remember that a murine model will never fully replicate the clinical pathology, when comparisons to human studies and observations are made alongside animal models, there is potential for uncovering interesting and relevant therapeutic mechanisms.

1.3.2 Neovascularisation of the heart post-MI

Vascular growth in the embryo and neovascularisation in adult pathologies occur through four main processes: vasculogenesis, angiogenesis, arteriogenesis and collateral growth. Vasculogenesis is driven by the coalescence of circulating endothelial progenitors to form de novo vessels, and mostly occurs during development to produce de novo vessels from blood islands in the yolk sac (Silvestre et. al., 2008). Sprouting angiogenesis involves the expansion of pre-existing vessels to form an extended capillary network, through degradation of the basement membrane and endothelial cell proliferation (Flamme et. al., 1998). Angiogenesis can be followed up by arteriogenesis which allows pre-existing arterioles to form collateral arteries, through recruitment of mural cells and generation of extracellular matrix (Kern, 2007). Collateral growth is employed to form bridges between pre-existing vessels, which can occur in the adult if another blood vessel cannot sufficiently supply blood to an organ or vascular bed (Taybejee et. al., 2004).

Angiogenesis has frequently been the target of therapeutic approaches to neovascularisation in limb ischemia and coronary artery disease, with the majority of recent trials targeting VEGF signalling in the ischemic heart (FIRST Trial, Simons et. al., 2002, The VIVA Trial, Henry et. al., 2003, REVASC Study, Stewart et. al., 2006). After the treatment of over 2500 patients with cardiovascular disease, no substantial benefit was observed with delivery of VEGF protein or other proangiogenic therapies, which was disappointing after the early promise from preclinical studies (Zachary and Morgan, 2011). Suggestions have been made for targeting the processes which regulate neovascularisation, such as hypoxia, via hypoxia inducible factor (HIF) signalling, or fluid shear stress (FSS) (Silvestre et. al., 2008). However, since the delivery of VEGFA via protein and gene therapy was shown to be safe and efficacious, but without beneficial therapeutic outcomes, it is unlikely that interrogating the same pathway through its regulatory mechanisms will result in further success. Consideration should instead be extended to alternative mechanisms that may drive endogenous neovascularisation in the ischemic heart, and strategies investigating recapitulation of developmental mechanisms, employed by the regenerative medicine field, may uncover novel mechanisms for therapeutic approaches to pathological neovascularisation.

With recent advances in developmental biology identifying the sinus venosus and the endocardium as primary sources of vascular endothelial cells for coronary vessels, their derivative tissues in the adult have been considered in the injury setting. Our group published findings which proposed angiogenic sprouting from the coronary sinus vein, the adult derivative of the sinus venosus, and the emergence of alpha-smooth muscle actin $(\alpha\text{-SMA})^{+}$ cells suggestive of recapitulated angiogenesis and EndMT similar to that shown by the sinus venosus in development (Dubé et. al., 2017). This in vivo observation was confirmed in vitro; atrioventricular sulcus explant cultures produced vascular sprouts expressing the endothelial marker CD31, a finding which was not observed when using explant cultures from ventricular portions of the heart. Whilst lineage tracing studies are

required to confirm these findings, they are supportive of the rationale for considering recapitulation of developmental mechanisms in the adult injury setting.

Since the endocardium has been described as the major contributor of coronary vessels within the myocardium perinatally, recent publications have considered reactivation of the endocardium as a neovascular process after infarction. Two studies have provided evidence to support occurrence of endocardial angiogenesis post-MI which leads to sprouting subendocardial vessels and branching into the myocardium (Miquerol et. al., 2015, Kobayashi et. al., 2017), while a third suggests that the endocardium minimally contributes to vascular endothelial cells after infarction using an Npr3-Cre lineage trace (Tang et. al., 2018). These studies were published during the course of this project, and will therefore be discussed later, in the context of the results shown here, however a diagram summarising the known sources of endothelial cells in development and regeneration is shown in **Figure 1.6**. Many cell sources have been considered for post-MI neovascularistion, which are indicated by arrows from the regeneration side; solid arrows represent sources which have been clearly evidenced in literature, dotted lines indicate contested sources, and the endocardium poses a question which is addressed throughout this thesis.

1.3.3 Investigating the adult endocardium

The recently developed Npr3-Cre model (Zhang et. al., 2016) provides the first possibility of specifically targeting the adult endocardium, however the model requires full characterisation to determine its suitability for accurately investigating neovascularisation, and was not available until 2018. Meanwhile, the field was limited to descriptive studies; the lineage-specific markers employed effectively in embryonic studies, such as Nfatc1 (Wu et. al., 2011) and Gata4 (Nemer et. al., 2002, Nadeau et. al., 2010), are either silenced postnatally or expressed in all cardiac endothelial cells, regardless of their embryonic origin (Dubé et. al., 2017). Endocardial cells are derived from a population of vascular endothelial progenitors in the cardiogenic mesoderm, and express specific markers such as Nfatc1, that are distinct from cardiomyocyte and

endothelial markers in the developing heart (de la Pompa et. al., 1998, Milgrom-Hoffman et. al., 2011). However, later in development and in the adult heart, Nfatc1 is not expressed, including after MI (our unpublished data and personal communication from Lucile Micquerol). The lack of specific genetic tools to label the endocardium prompted consideration of other methods for distinguishing endocardial and endothelial cells in the adult.

He et al., 2017, used a pulse chase strategy to investigate expression of three endothelial Cre models before and after MI. *Cdh5-CreER*, *AplnCreER* and *Fabp4-CreER* were each crossed with a tdTomato reporter and injected with tamoxifen embryonically and postnatally to induce Cre recombination and labelling of endothelial cells. After 10 weeks, ischemia-reperfusion surgery was performed and samples were harvested 14 days post-MI for analysis of neovascularisation. The study concluded that almost 100% vessels pre- and post-MI were labelled by all three endothelial models, suggesting that pre-existing endothelial cells are the source of all vascular endothelial cells post-MI. However, these models label the endocardium as well as coronary endothelial cells in the adult heart, and this technique does not differentiate between endocardial and endothelial cells. Interestingly, we identified another endothelial marker, Platelet-derived growth factor subunit B (Pdgfb), to label coronary endothelial, but not endocardial, cells in the adult heart. Pdgfb is expressed in vascular endothelial cells and interacts with the Platelet-derived growth factor receptor β (PDGFRβ). An inducible Pdgfb-CreER2 model was developed to study endothelial cells in the adult heart, which allows postnatal Cre recombination using tamoxifen, enabling a similar lineage tracing strategy to those used by He et. al., 2017 (Claxton et. al., 2008). This model labelled 98% of all endothelial cells in the adult heart (capillary, venous and arterial), but did not label endocardial cells (Dube et. al., 2017), and since the only discernible difference between this endothelial Cre and those tested by He et. al., is the lack of endocardial labelling, we can infer that vessels unlabelled by Pdgfb-Cre may be endocardial-derived. Whilst we cannot exclude a possible contribution from a circulating or resident endothelial progenitor, those

characterised by other groups to date express Pdgfb, and thus would likely have been labelled in our mice.

Whilst this model proved useful for describing subendocardial vessels post-MI, in order to target processes in the endocardium with a gain- or loss-of-function, an endocardial-expressed marker must be utilised. Whilst pan-endothelial labelling is a strong caveat for using any endothelial model to target the endocardium, it is currently the only reliable method of targeting the tissue in the adult. Therefore, the VE Cadherin-Cre (*Cdh5-Cre*) model was identified as a suitable method for targeting Notch in the endocardium for this study.

1.4.1 Recapitulating trabeculation and compaction in the adult heart?

An understanding of the pathways coordinating ventricular chamber development may prove informative when investigating a role for endocardial trabeculation post-MI, and Notch1 would appear to be a prime candidate for a pathway involved with neovascularisation of the ischemic heart. Once coronary vasculature formation is complete by P28, the embryonic finger-like trabeculae which increase surface area for myocardial perfusion are no longer necessary. The adult mammalian endocardium appears to be a predominantly smooth surface, without perceptible projections, with exception of the papillary muscles. However, upon ischemic injury, the endocardial surface becomes hypertrabeculated and, by day 2 post-MI, large finger like projections can be seen adjacent to the infarct region (**Figure 1.7A-B**). Endocardial projections persist at day 7 (**Figure 1.7C-E**), and then appear to compact concurrently with the formation of subendocardial vessels by day 14 post-MI (**Figure 1.7F**). This phenomenon seems like a plausible response to ischemic myocardial tissue since the endocardium, as a large source of endothelial cells interfacing with the blood-filled ventricular lumen, may provide a useful surface to enhance reperfusion.

A mechanism of induced hyper-trabeculation has also been reported in other contexts of increased cardiac preload, such as during pregnancy, in patients with sickle cell anaemia (Gati et. al., 2013) and in highly trained athletes (Gati et. al., 2013). During pregnancy,

25% of women examined developed increased left ventricular trabeculations; when re-examined post-partum, 73% demonstrated complete resolution, with a further 19% showing a marked reduction in trabeculation (**Figure 1.7G-J**, Gati et. al., 2014). When considered alongside this model, the transient increase in trabeculation post-MI may reflect a similar mechanism, with increased preload (left ventricular end diastolic volume) induced by injury. The induced hypertrabeculation and subsequent compaction appears also to be a recapitulation of the developmental process, which contributes to coronary vessel formation via the endocardium (the trapping of endocardial cells within the myocardial wall after compaction) (Tian et. al., 2014), and was observed in the adult purse string suture-like (PSSL) model, also involving entrapment of endocardial cells (Tang et. al., 2018). Thus, we propose that hypertrabeculation-compaction represents an additional example of an embryonic mechanism, associated with cardiac growth, reactivated to perform a similar function in the injury setting.

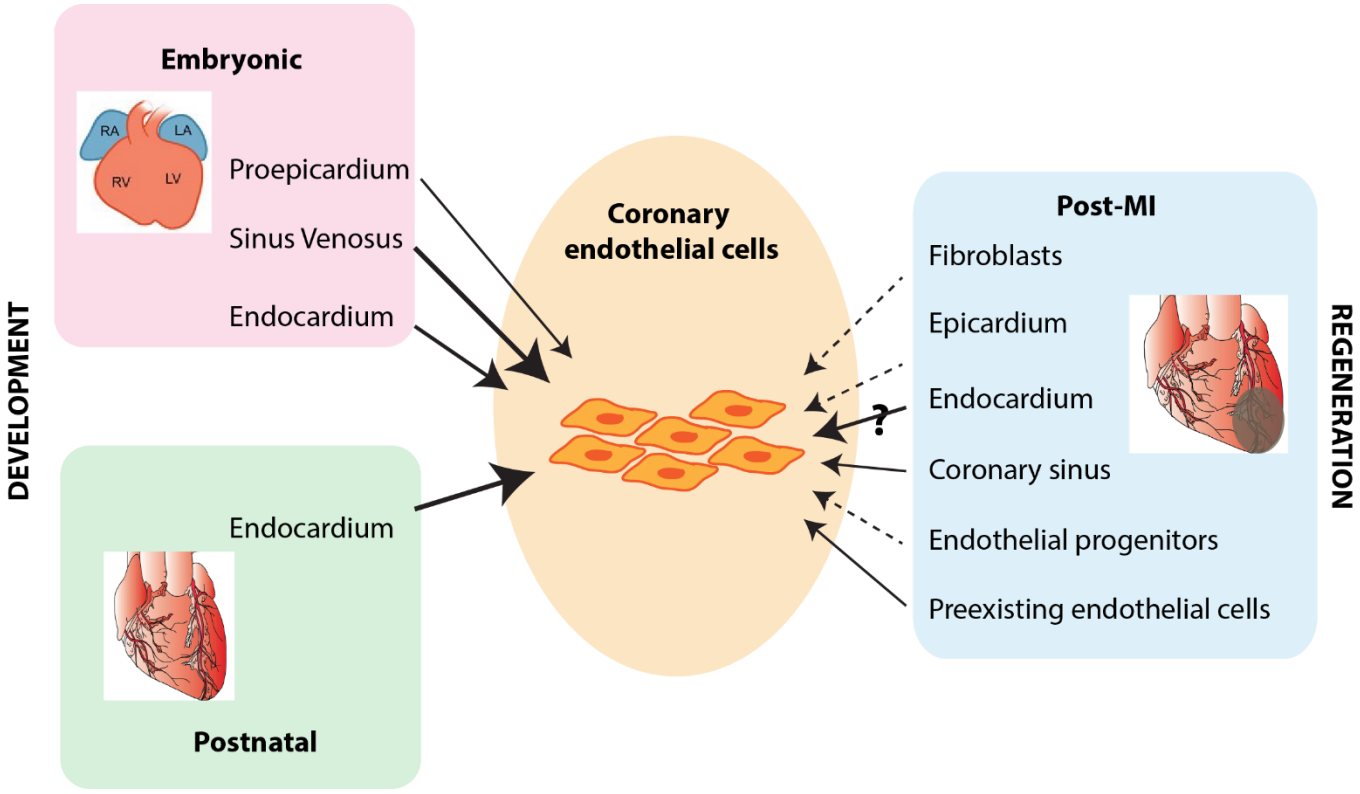

Figure 1.6. Sources of coronary endothelial cells in development and regeneration

Schematic summarising sources of endothelial cells during development and regeneration. In development there is a distinction between embryonic and postnatal processes that are important for the formation of coronary vessels. During embryonic development, known sources are the sinus venosus, endocardium and proepicardium (arrow size indicates relative contributions). The main postnatal source of coronary endothelial cells is the endocardium via compaction and "entrapment".

In the post-MI setting, many sources have been considered which are indicated; the coronary sinus and pre-existing endothelial cells are confirmed sources, the epicardium, fibroblasts and endothelial progenitors are contested sources, and the endocardium will be investigated as a source in this thesis.

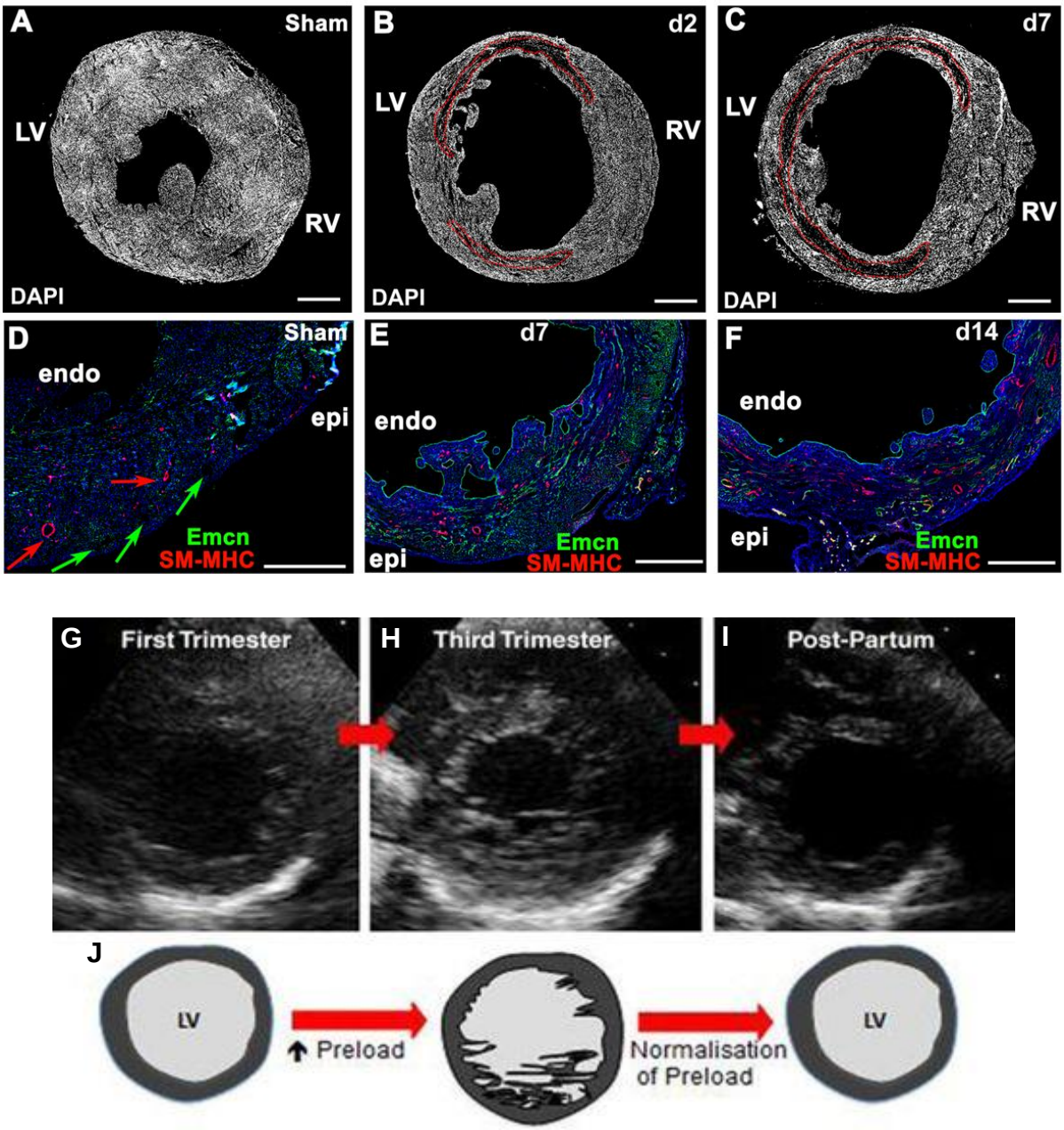

Figure 1.7. Hypertrabeculation is induced after MI in the adult mouse heart and observed in a clinical study of pregnancy

The adult heart maintains a relatively smooth endocardial surface after P28, except the papillary muscles (A, asterisks), but between 2-7 days post-MI, endocardial projections appear overlaying the infarct (B-C, infarct red outline). Hypertrabeculation was not observed in sham hearts (D). Extensive remodelling shown at day 7 (E) appeared to compact by day 14 (F), coinciding with the formation of subendocardial vessels. A similar observation was made in a clinical study of pregnancy, where 25% of women showed hypertrabeculation during the third trimester which was resolved in most patients by postpartum check-ups (G-I). Increased preload was suggested as a trigger for this response (J). *(A-F),Dubé and Thomas et. al., 2017, (G-J), Gati et. al., 2014*

1.5.1 Original Hypothesis

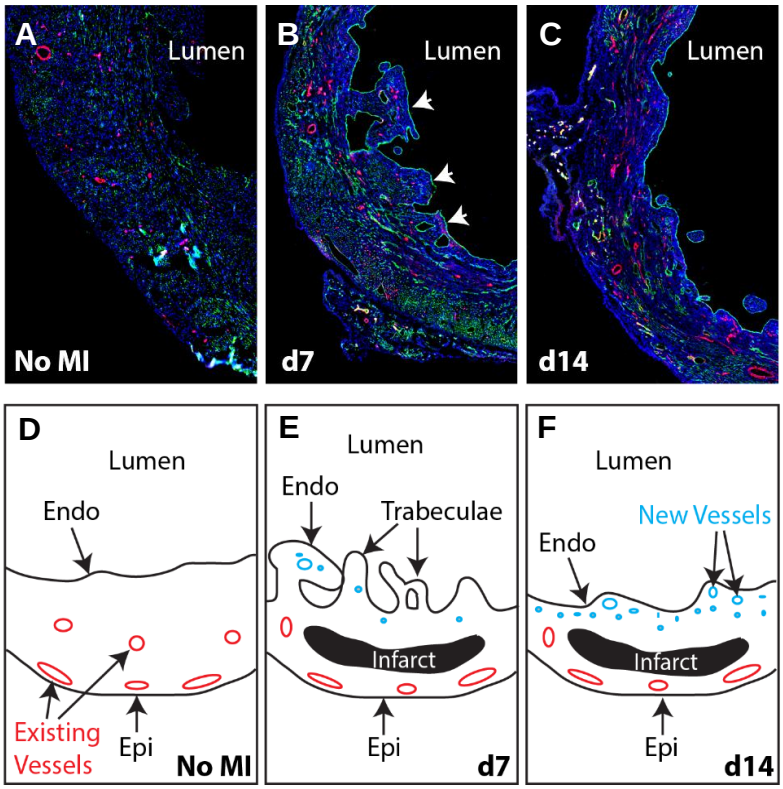

Figure 1.8. DPhil Hypothesis

Observations have been made of a hypertrabeculation response to MI in the mouse heart, with endocardial finger-like projections appearing by day 7, which compact concurrently with the formation of subendocardial vessels from 7-14 days post-MI (A-F). The mechanism hypothesised to be partly responsible for this is a recapitulation of endocardial Notch1 signalling, which is mediated by Dll4 and Jag1 ligands.

Original Hypothesis: In response to myocardial infarction, regions of the endocardium closest to the injury show increased trabeculation to facilitate blood flow to ischemic areas of myocardium. Trabeculation occurs, in part, via the Notch1 pathway, recapitulating embryonic development; at later time points post-MI trabeculae undergo compaction and EndMT to form of *de novo* sub-endocardial vessels.

1.5.2 Project Aims

Objective 1:* To *characterise endocardial remodelling post-MI and screen for reactivated developmental pathways

- Use Pdgfb-Cre to negatively trace endocardial- and endothelial-derived vessels
- Analyse wild-type MI hearts to characterise the extent of remodeling post-injury
- Use immunohistochemistry to identify molecular regulators induced in remodeling regions, and possible recapitulation of developmental mechanisms post-MI
- Optimise isolation method for extraction of endothelial and endocardial cells from the adult mouse heart
- Use Pdgfb;TdTomato labelling to sort isolated cells using flow cytometry, and extract RNA for analysis

Objective 2: Development of surgical, analytical and genetic tools to investigate trabeculation and the role of endocardial Notch1 post-MI

- Develop LAD ligation procedure within Smart group, introducing general and strain-specific refinements to improve survival
- Develop and optimise digital methods for analysing infarct size and trabeculation in post-MI hearts
- Optimise induction of *VE Cadherin-Cre* in adult mice
- Develop endothelial Notch1 loss- and gain-of function models to investigate the role of Notch1 in endocardial remodelling post-MI

Objective 3: Investigate the role of Notch1 in endocardial remodelling and neovascularisation post-MI

- Use Notch reporter mouse line, *CBF:H2B-Venus* to analyse Notch1 activity post-MI and compare with uninjured and embryonic hearts
- Use loss-of-function *Notch1*$^{lox/lox}$ and gain-of-function *Rosa*^{N1ICD} mouse lines to investigate the role of Notch1 in endocardial remodeling
- Use inducible *VE Cadherin-Cre* lineage tracing to investigate a role for EndMT post-MI
- Assess involvement of EndMT in endocardium-derived neovascularisation and interrogate role of Notch 1 using *Notch1*$^{lox/lox}$ and gain-of-function *Rosa*^{N1ICD} mouse lines

CHAPTER 2
MATERIALS AND METHODS

Materials and Methods

Standard lab chemicals and materials were purchased from Sigma or VWR.

2.1 Animal Work

2.1.1 Mouse Strains

Mice were housed and maintained in a controlled environment and all procedures involving the use and care of animals were performed in accordance with the Animals (Scientific Procedures) Act 1986, (Home Office, United Kingdom) and approved by University of Oxford Animal Welfare and Ethical Review Boards.

*Cdh5(PAC)*CreERT2 (referred to as *VE Cadherin-Cre*) mice were developed in the Adams group (gift from Ralf Adams, Max Planck Institute for Molecular Biomedicine, Muenster) with an inducible Cre under the control of the vascular endothelial promoter *Cdh5(PAC),* enabling inducible Cre recombinase activity in vascular endothelial cells *(Sorensen, 2009)*. *VE Cadherin-Cre* mice were crossed with *Gt(ROSA)26Sor*$^{tm14(CAG-tdTomato)Hze}$/J reporter mice (purchased from The Jackson Laboratory, stock no: 007908) to generate *VE Cadherin-Cre*; *Gt(ROSA)26Sor*$^{tm14(CAG-tdTomato)Hze}$/J mice and Cre recombination was induced by five daily IP injections of 100mg/kg tamoxifen in peanut oil at least 10 days prior to harvesting (for uninjured samples) or LAD ligation surgery (for MI samples).

*Pdgfb*CreERT2 mice (gift from Marcus Fruttiger, UCL, London), with insertion of a tamoxifen inducible form of Cre recombinase into the open reading frame of the *Pdgfb* gene, have previously been reported *(Claxton, 2008)* and were crossed with either *Rosa26R (R26R)-EYFP* (yellow fluorescent protein) reporter mice *(Srinivas, 2001)* (gift from Shankar Srinivas, University of Oxford, to generate *Pdgfb*CreERT2; R26R-EYFP mice, or with *Gt(ROSA)26Sor*$^{tm14(CAG-tdTomato)Hze}$/J reporter mice to generate PdgfbCreERT2; *Gt(ROSA)26Sor*$^{tm14(CAG-tdTomato)Hze}$/J mice. Expression of EYFP or v

vTdTomato in endothelial cells was induced by three consecutive IP injections of 50mg/kg tamoxifen in peanut oil at least 10 days prior to harvesting for flow cytometry or LAD ligation surgery.

Tg(*Cp-HIST1H2BB/Venus*)47Hadj mice (purchased from The Jackson Laborotary, stock no: 020942) express the nuclear fluorescent protein Venus under the control of the CBF1 binding site and SV40 promoter to label canonical CBF1-mediated Notch activity at single cell resolution.

Notch1$^{loxP/loxP}$ mice (gift from Freddy Radtke, École Polytechnique Fédérale de Lausanne, *(Radtke, 1999)*) have LoxP sites flanking an exon encoding the signalling peptide of the Notch1 gene, and were therefore used to generate an inducible vascular endothelial knockout of Notch1 by crossing with *VE Cadherin-Cre* to produce *VE Cadherin-Cre*; *Notch1*$^{loxP/loxP}$ mice. Inactivation of vascular endothelial Notch1 was induced by five consecutive IP injections of 100mg/kg tamoxifen in peanut oil at least 10 days prior to harvesting for uninjured samples or LAD ligation surgery for MI samples. Antibodies were used to detect expression of the N1ICD and Hes1, a transcription factor activated by Notch1, to confirm successful Notch1 inactivation.

Gt(ROSA)26Sor$^{tm1(Notch1)Dam}$*/J* mice (purchased from The Jackson Laboratory, stock no: 008159) contain a truncated cytoplasmic fragment encoded by an intracellular portion of the Notch1 sequence, causing constitutive signalling activity. *Gt(ROSA)26Sor*$^{tm1(Notch1)Dam}$*/J* mice were crossed with *VE Cadherin-Cre* mice to produce an inducible vascular endothelial specific Notch1 gain-of-function. Constitutive activation of vascular endothelial Notch1 was induced by five consecutive IP injections of 100mg/kg tamoxifen in peanut oil at least 10 days prior to harvesting for uninjured samples or LAD ligation surgery for MI samples. RNA Scope was used to analyse Hes1 expression to confirm successful constitutive activation of Notch1 in endothelial cells.

All strains were maintained on a C57Bl6/J background for more than 20 generations, with the exception of Tg(*Cp-HIST1H2BB/Venus*)47Hadj mice which were maintained on FVB/NJ background (The Jackson Laboratory, stock no: 001800).

2.1.2 Genotyping

Ear biopsies were taken at age 10-14 days of all strains for genotyping. Tissue was digested in 100µl digestion buffer (50mM Tris-HCl (pH 8.5), 1mM Ethylenediaminetetraacetic acid (EDTA), 0.5% Tween 20, 50µl/ml of 10mg/ml Proteinase K) for 2 hours at 56ºC, reaction was stopped by 10 mins incubation at 95 ºC. illustra PuReTaq Ready-To-Go PCR Beads were used which contain 200 µM dNTP in 10 mM Tris-HCl (pH 9.0 at room temperature), 50 mM potassium chloride (KCl) and 1.5 mM $MgCl_2$ when reconstituted to 25µl. 1µl DNA, 1µl each of forward and reverse primers and 22µl NF water were added to the beads, and tubes were placed in an Applied Biosystems Veriti 96-well Thermal cycler and run on a programme based around the following: Reactions were denatured at 95˚C for 10 minutes before cycling through a programme of denaturing for 15 seconds at 92˚C, and annealing for 1 minute at 60˚C. After 40 cycles the reaction was cooled rapidly to 4˚C. Exact temperatures and annealing time were provided by The Jackson Laboratory or the groups gifting the mice. After the reactions were completed, the PCR product was run on a 2% agarose gel at 125v for 1 hour with 5µl orange G/GelRed loading dye per sample.

Primers

*Cdh5(PAC)*CreERT2 (VE Cadherin-Cre)

Fwd: 5’-TCCTGATGGTGCCTATCCTC-3’
Rev: 5’-CCTGTTTTGCACGTTCACCG-3’
Transgene = 548 bp

Gt(ROSA)26Sor$^{tm14(CAG-tdTomato)Hze}$/J

WT Fwd: 5’-AAG GGA GCT GCA GTG GAG TA-3’
WT Rev: 5’-CCG AAA ATC TGT GGG AAG TC-3’
Wild type = 297 bp

Mut Fwd: 5’-CTG TTC CTG TAC GGC ATG G-3’
Mut Rev: 5’-GGC ATT AAA GCA GCG TAT CC-3’
Mutant = 196 bp

*Pdgfb*CreERT2
5

Fwd: 5’-CCAGCCGCCGTCGCAACT-3’
Rev: 5’-GCCGCCGGGATCACTCTCG-3’

Tg(*Cp-HIST1H2BB/Venus*)47Hadj

Fwd: 5’-ATC TGC ACC ACC GGC AAG-3’
Rev: 5’-TCA TGT GGT CGG GGT AGC-3’
Transgene = 97bp
0

Notch1$^{loxP/loxP}$

Fwd: 5’-CTGAGGCCTAGAGCCTTGAA-3’
Rev: 5’-TGTGGGACCCAGAAGTTAGG-3’
Floxed = 500bp
WT = 445bp

Gt(ROSA)26Sor$^{tm1(Notch1)Dam}$*/J*

Rosa26-R primers
5´-AAAGTCGCTCTGAGTTGTTAT-3
5´-GCGAAGAGTTTGTCCTCAACC-3´
5´-GGAGCGGGAGAAATGGATATG-3´
WT = 500bp
Mut = 250bp

GFP Primers
Fwd: 5’-ATGGTGAGCAAGGGCGAGGA-3’
Rev: 5’-CCTCCTTGAAGTCGATGCCC-3’
Transgene = 426bp

2.1.3 Permanent ligation of the left anterior descending coronary artery (LAD)

All animal procedures were performed under strict home office guidelines. Wild type and transgenic mice (<35g, aged 10-18 weeks) underwent ligation of the left anterior descending artery to induce MI, using aseptic technique.

For each surgical procedure, the mouse was weighed and anaesthetised using isoflurane (4%/96% O_2), and injected with buprenorphine (0.06mg/kg) for analgesia. Lacri-lube eye gel was applied and mouse suspended on an intubation platform by upper molars. Once secured in place with a continuous flow of isoflurane to the mouth, intubation was completed by directing a cannula through the vocal cords and into the trachea using a fibre optic cable to illuminate the throat. Once intubated, the ventilator was set to 200bpm and 200 units of volume (for 25g mouse); a rectal probe was inserted and secured to monitor temperature, and pain reflexes were checked to ensure adequate surgical anaesthesia.

Isoflurane was reduced to 2%/96% O_2 at this stage, and the mouse limbs were secured to the surgical mat. The left chest area was shaved, and disinfected with Hibiscrub Antibacterial Skin Cleanser before making an incision parallel to the ribs approx. halfway between the top and bottom of the ribcage. Blunt forceps were used to separate skin from the muscle, and then the major pectoral muscle from the minor equivalent. Muscles and skin were held in place throughout surgery with retractors. The 4^{th} intercostal muscle was pierced and an opening made to insert the rib retractors, the ribs were then separated by gradually opening the retractors. The heart was positioned so that the surface was visible, and an 8.0 ethilon suture was inserted through the mid-left ventricular wall, tied with a surgical knot, followed by two single knots. When ligation was successful, blanching of the tissue beneath the suture was evident. The organs were re-positioned and the retractors removed, then a 7.0 prolene suture was used to re-secure the ribs. The pectoral muscles were replaced and the skin secured using a 7.0 prolene

suture, the isoflurane was then switched off and the mouse recovered in a warm incubator.

Mice were closely monitored in the initial 24 hours following surgery, and for the next few days. Vetergesic jelly was provided for self-medicated pain relief, and a second dose of buprenorphine was administered if additional pain relief was required.

For sham samples, mice underwent the same procedure, excluding ligation of the LAD by omitting the tying of the suture after insertion into the myocardial wall.

2.2 Tissue Preparation and Analysis

2.2.1 Fixation and Preparation of tissue for cryosectioning

Mice were sacrificed by cervical dislocation and hearts were harvested at 24hrs, 2, 4, 7 and 14 days after LAD ligation surgery. Sham samples were harvested at 7 days post-injury. The heart was fixed in diastole by injection of 1M KCl into the right atrium and perfused with 4% paraformaldehyde (PFA); samples remained in PFA for 2 hours at room temperature. Tissues were then rinsed with phosphate-buffered saline (PBS) and equilibrated overnight in 30% sucrose/PBS at 4°C. Sucrose was gradually removed with addition of 50:50 30% sucrose:Tissue-Tek optimal cutting temperature compound (OCT), then 100% OCT. Tissue was embedded in a mould and placed in -80°C freezer until cryosectioning. Sections were cut at a thickness of 11µm using a Bright OTF5000 Cryostat, collected on SuperFrost Plus slides and stored at -80°C prior to staining.

2.2.2 Immunofluorescence

Slides were removed from -80°C freezer and left at room temperature for 10 mins to dry, then rinsed in PBS to remove OCT. Sections were permeabilised with 0.5% Triton X-100 in PBS for 10 mins, then rinsed again in PBS. Immedge pen was used to separate sections, preventing the mixing of antibody solutions, and the slides were arranged in a humid, foil-covered box. Sections were blocked for 1 hour at room temperature using 1%

bovine serum albumin (BSA), 10% donkey serum, and 0.1% Triton X-100 in PBS. Sections were washed and incubated with primary antibodies (**Table 2.1**) diluted, as indicated, in blocking buffer at 4°C overnight. Slides were rinsed (x3) and washed (x3) using 0.1% Triton X-100, and then sections were incubated with AlexaFluor secondary antibodies (488/546/647, Invitrogen, 1:200), diluted in blocking buffer, at room temp for 1 hour. 3 further rinses and washes were completed before incubating with 300nmol/µl 4',6-diamidino-2-phenylindole (DAPI) in PBS for 5 mins, and mounting with 50:50 glycerol:PBS underneath 24x60mm coverslips. Slides were imaged using Leica DM6000 fluorescent microscope or Olympus FV1000 Confocal Microscope. Extent of myocardial infarction was assessed in each heart by immunofluorescence against DAPI, and CD68 for 24 hours, 2 days and 4 days post-MI, and wheatgerm agglutinin (Alexa 488-conjugated, Invitrogen) for 7 days and 14 days post-MI. Pre-defined exclusion criteria was set as hearts with 10-30% of the LV infarcted for inclusion in the analysis, with the exception of examples in section 4.2 where infarct size is stated.

Sections examined were between 10 µm and 5 mm from the suture placement, and 20-30 sections per heart were visualised microscopically. At least 5 sections per heart from similar regions were imaged and analysed for quantification throughout, and n numbers throughout refer to total number of hearts analysed.

Table 2.1. Antibodies and dilutions for immunofluorescence

Antibody	Species	Supplier	Cat. No.	Dilution
anti-cleaved Notch1	Rabbit	Cell Signalling Technology	4147	1:50
anti-Hes1	Rabbit	Abcam	ab108937	1:50
anti-Dll4	Rabbit	Abcam	ab7280	1:50
anti-CD31	Armenian Hamster	Abcam	ab119341	1:100
anti-Jag1	Goat	Santa Cruz Biotechnology	sc-6011	1:50
anti-Notch4	Rabbit	Santa Cruz Biotechnology	sc-5594	1:100
anti-CD68	Rat	AbD Serotec	MCA1957	1:50
anti-CD45	Rabbit	Abcam	ab10558	1:100
anti-Brg1 (H-88)	Rabbit	Santa Cruz	sc-10768	1:50
anti-Hey1	Rabbit	Abcam	ab22614	1:100
anti-GFP	Chicken	Abcam	ab13970	1:1000
anti-Endomucin	Rat	Santa Cruz Biotechnolgy	sc-53941	1:50
anti-SM-MHC	Rabbit	Abcam	ab125884	1:1000
anti-Ki67	Rat	eBioscience	14-5698	1:100
anti-SMA Cy3 Conjugated	Mouse	Sigma	C6198	1:200
anti-Apelin	Rabbit	Abcam	ab59469	1:500
anti-VEGFR2	Goat	R&D Systems	AF66	10µg/ml
anti-MLC2	Rabbit	Abcam	ab79935	1:140
anti-Snail	Rabbit	Abcam	ab82846	1:50
anti-pHH3	Rabbit	Santa Cruz	Sc-8656-R	1:100
anti-NRG1	Rabbit	Abcam	ab180808	1:100
anti-Sarc α-actinin	Mouse	Abcam	ab9465	1:500
anti-Periostin	Rabbit	Abcam	ab92460	1:100
Anti-cTnI	Rabbit	Abcam	ab47003	1:200

All antibodies have been validated for use in immunofluorescence by 1Degree BIO, or by the manufacturer, and were optimised for use with heart sections.

2.2.3 RNA Scope

RNAScope fluorescence in situ hybridisation was carried out using the manufacturers' guidelines (ACD Biotechne). In brief, cryosections were air-dried for 20 mins at room temperature and washed for 5 mins in 1x PBS. Slides were incubated with hydrogen peroxide for 10 mins, to quench endogenous peroxidase activity, and washed for 2 x 15secs with deionised water. Slides were boiled at 97°C for 10 mins, washed for 15secs with deionised water and for 3 mins with 100% ethanol. A hydrophobic Immedgepen was used to enclose each section and then they were incubated with RNAscope protease plus for 30 mins at 40°C. Slides were washed for 15secs with deionised water, the probes were added in combination (**Table 2.2**, sequences not provided by ACD) and incubated for 2 hours at 40°C. Sections were washed for 2 x 2 mins with 1X wash buffer then incubated with Multiplex Amp1, Amp2 and Amp3 each for 30 mins at 40°C with 2 x 2 mins wash buffer washes between. After Multiplex Amp3 and the final washes, sections were incubated at 40°C with each HRP (C1, C2 and C3) for 15 mins, followed by tyramide signal amplification (TSA) Fluorescein/Opal520 for 30 mins and HRP Blocker for 15 mins for each channel, with 2 x 2 mins washes between every step. DAPI was used for nuclear labelling (30 secs incubation) before Prolong Gold Antifade was added underneath 24x50mm coverslips to preserve the sections. Slides were kept at 4°C and imaged within two weeks using Leica DM6000 fluorescent microscope or Olympus Confocal FV1000.

Table 2.2 Probes for RNAScope

Channel 1	Channel 2	Channel 3
DLL4 (319971-C1)	**TdTomato** (317041-C2)	**Pecam** (316721-C3)
TdTomato (317041-C1)	**Hes1** (417701-C2)	
	Hey1 (404651-C2)	

2.3 Cell Isolation and Analysis

2.3.1 Endothelial/Endocardial Isolation and Flow Cytometry

Mice were euthanized using 50µl Pentoject. Once reflex response was lost, the chest was opened, the aorta severed, and 1ml heparin (2U/mL) was slowly injected into the left ventricle to remove blood clots from the heart. The heart was then removed and rinsed in ice cold PBS. A microscope was used to remove the atria and cut the ventricles in half (long axis), then the two halves of the ventricle were transferred to a fresh petri dish with cold PBS and cut into <3mm pieces. Tissue was collected and transferred to a 15mL Falcon tube containing 5mL digestion solution at 37°C (2mg/mL type IV collagenase, 1.2U/mL dispase II, 2mM $CaCl_2$ in PBS). Tissue was incubated at 37°C in an orbital shaking incubator, with speed set to 70 reps per minute (RPM) for 45 mins. Every 15 mins the solution was carefully removed and collected with a disposable pipette, then filtered through a 70µm cell strainer into a 50mL Falcon tube. 5mL neutralising buffer (15% horse serum in PBS, 5mM EDTA) was added and the fraction kept on ice. The digest solution was replaced with fresh enzyme solution (kept at 37°C) and a disposable plastic pipette was used to carefully agitate the tissue. After 45 mins, a disposable plastic pipette was used to carefully collect the remaining cell suspension which was filtered through a 70µm cell strainer attached to a 50mL Falcon tube. Another 5mL neutralising buffer was added and all fractions for each sample were pooled. The filtered, digested suspension was centrifuged at 4°C for 10 mins at 300xg in an Eppendorf 5804R Centrifuge. The digestion solution was decanted, leaving the cell pellet, which was resuspended in 5mL 1 X Red Cell Lysis Buffer (room temperature) with 0.1mg/mL DNase 1 for 5 minutes. After 5 minutes, 5mL neutralising buffer was added, and thoroughly pipetted to wash. The solution was centrifuged at 300xg at 4°C for 5 mins, the solution decanted, pellet resuspended in 1mL 2%FBS/PBS and counted. Cells were again centrifuged at 300xg at 4°C for 5 mins, resuspended in 200µl of relevant antibodies (**Table 2.3**) in a 96 well plate, and incubated for 30 mins in darkness at room

temperature. Compensation controls were prepared as listed in **Figure 2.1**, and also incubated for 30 mins. After 30 mins, 200µl 2% FBS/PBS was added, mixed using a pipette and spun at 300xg at 4°C for 5 mins. Cells were resuspended in 500µl 2% FBS/PBS, pipetted well and filtered into polystyrene, round-bottom tubes for flow cytometry. Cells were sorted using a BD FACSARIA III at the Dunn School of Pathology Flow Cytometry Facility.

Cells were lysed with Trizol reagent (Invitrogen) and stored at -80°C until ready for sequencing. RNA extraction and sequencing was performed by the Functional Genomics Dept, University of Cambridge.

Table 2.3. Antibodies and dilutions for flow cytometry

Antibody	Fluorescence Spectra	Supplier	Cat. No.	Dilution
CD31	FITC	Biolegend	102406	1:100
CD31	BV605	Biolegend	102427	1:100
CD45	APC	Biolegend	103112	1:100
Lineage Cocktail	APC	BD Bioscience	558074	1:200
CD144	BV421	Biolegend	138013	1:100
NPR-C	Alexa 700 Secondary	Abcam	Ab177954	1:100

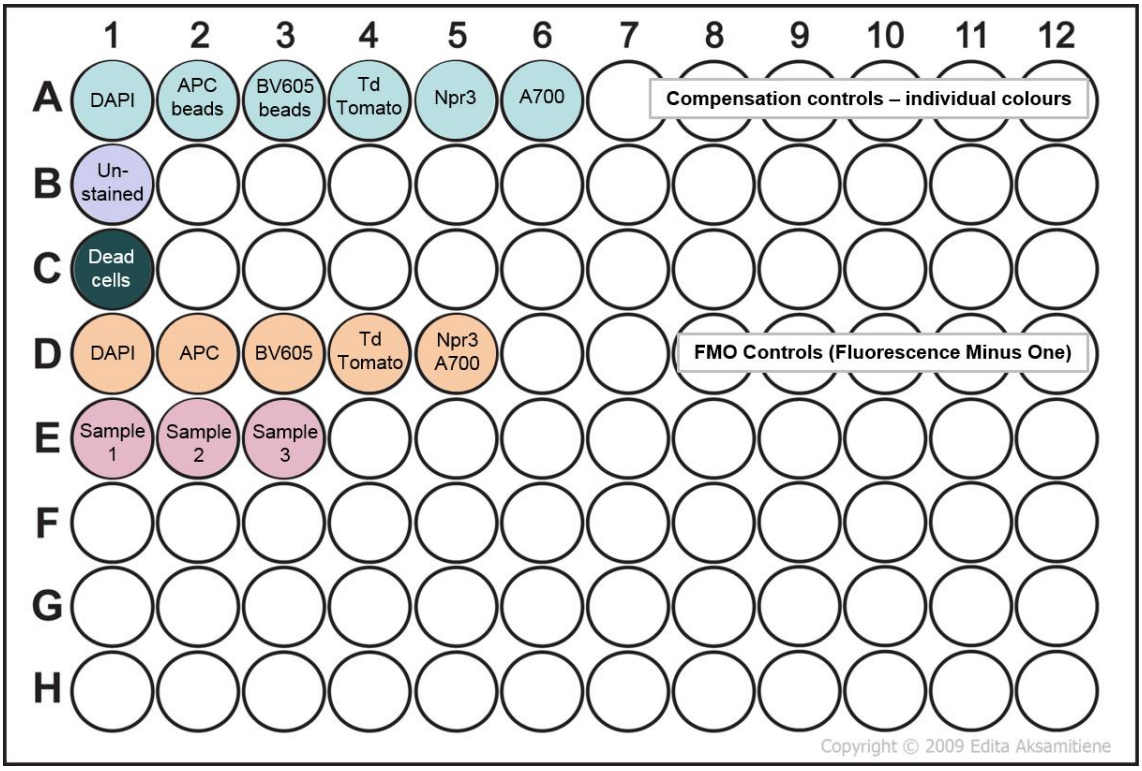

Figure 2.1. 96-well plate set-up for Flow Cytometry

Compensation controls were set up with individual fluorescent antibodies using either compensation beads (A2, A3) or cells (A1, A4, A5, A6) to analyse fluorescence of each individual colour. Unstained and dead cells (with DAPI) were also included to compensate for auto fluorescence and control for DAPI stained nuclei. Fluorescence minus one (FMO) controls were used, where for each sample all fluorescent antibodies were added minus one. These controls were used for each flow cytometry experiment, to set gates for positive cells. This method ensured that all cells captured were either endothelial or endocardial.

2.3.2 RNA Isolation and Analysis (performed by Functional Genomics Dept, University of Cambridge)

Cells isolated by flow cytometry were resuspended in TRIzol® Reagent, frozen at -80°C, and shipped to Cambridge on dry ice. Samples were defrosted and TRIzol® Reagent volume topped up to 500µl. Samples were vortexed for 30 secs to ensure complete lysis, then allowed to warm up to room temperature. Samples were transferred to a 2ml heavy phase lock tube (5prime), and 0.2 mL of chloroform per 1 mL of TRIzol® Reagent was used for homogenization (tube shaken vigorously for 15secs, incubated for 2-3 mins at room temp and centrifuged for 15 mins at 4°C). The colourless, aqueous phase of the sample was removed by angling the tube at 45° and pipetting the solution out, and placed into a new tube for RNA isolation. 0.5 mL of 100% room temperature isopropanol was added to the aqueous phase, per 1 mL of TRIzol® Reagent used for homogenization. Samples were incubated at room temperature for 10 minutes, then centrifuged at 12,000 × *g* for 10 minutes at 4°C. The supernatant was removed, leaving only the RNA pellet. The pellet was washed twice with 1 mL of ice cold 75% ethanol per 1 mL of TRIzol® Reagent used in the initial homogenization (ethanol added to the RNA pellet, the pellet was gently loosened, then the tube was centrifuged at 8000 × *g* for 10 minutes at 4°C, and ethanol removed). After the second wash, the pellet was left to dry for 5-10 mins.

Since the RNA pellets obtained from the isolated endothelial and endocardial samples were very small, they were re-suspended in 11µl of nuclease free water and 1µl from this was removed for QC purposes and diluted in 1µl water (1 in 2 dilution). 1µl was measured using a qubit HS RNA quantification kit, but the RNA was too dilute to obtain a concentration. The remaining 1µl of RNA was used in an Agilent Pico RNA chip to measure the concentration and the RNA Integrity number (RIN). The results from this are shown in Chapter 3. Libraries were prepared from two endothelial cell samples using the KAPA stranded RNA-seq with RiboErase, although they were small due to the low starting material. These were sent for RNA Sequencing.

2.4 Quantification and Statistics

2.4.1 Digital detection and quantification of endocardial trabeculation

Low resolution DAPI images of the whole left ventricle were captured using Leica DM6000 fluorescent microscope. Images were uploaded to imageJ (NIH, US) and converted to 8-bit, then Auto Threshold applied to produce a white image on a black background. This was converted to binary, and holes filled to produce a solid object. The "Find Edges" tool was used to identify edges of the object and all lines except the endocardium were removed. This resulted in an endocardial trace which was suitable for fractal analysis. The FracLac plugin (H. Jelinek, NIH) for ImageJ was used to perform this analysis; box sizes were set to a minimum of 2% of the total image size, and a maximum of 45% of the total image size, with 20 sizes of box between 2 and 45% allocated per image. The number of boxes fitted along the endocardial trace was used in combination with the pixels detected per box to calculate the fractal dimension (FD).

2.4.2 Digital analysis of fluorescent area for quantification of infarct size

Images of the whole left ventricle were captured using Leica DM6000 fluorescent microscope and uploaded to ImageJ. Channels were split to show individual fluorescence, converted to 8-bit images and Auto Threshold applied to produce a white image on a black background. The "Analyse Particles" tool in imageJ was used to calculate the total pixels shown in a given area (the left ventricle), and WGA pixels were analysed as a percentage of DAPI pixels to produce a percentage infarct size. This method was also used in cases where overlap between two antibodies was analysed, e.g. Hes1:Endomucin for percentage Hes1 expression in endothelial cells.

2.4.3 Statistics

Statistical analysis was performed using Excel. For comparison between two groups, a student T-test (two-tailed) was used, and for the correlation analysis, the correlation coefficient was calculated. A P-value of less than 0.05 was used to define statistical

significance, which confirms that reasonable evidence has been provided to allow rejection of the null hypothesis.

CHAPTER 3
RESULTS CHAPTER 1

Chapter 3

Results 1: Characterisation of endocardial remodelling post-MI and screen for recapitulation of developmental pathways

3.0 Introduction

Whilst angiogenesis has been extensively studied in the context of MI (Deveza et. al., 2012), there has been less consideration for de novo vessel formation, and controversy exists surrounding the source of new vessels in response to injury. Previous work carried out by the Smart group revealed remodelling of the endocardium after infarction, which is suggested to contribute to neovascularisation.

Development of the coronary vessels is well characterised, with the endocardium contributing up to 60% of coronary endothelial cells through the processes of trabeculation and compaction (Tian et. al., 2014, Paige et. al., 2015), and when investigating neovascularization post-MI, key insights may be obtained from studying developmental processes. Consideration was therefore given to the mechanisms driving trabeculation and compaction in development, in order to investigate their possible redeployment in response to injury. One such pathway which is important for both trabeculation and compaction in development is Notch1 signalling (D'amato et. al., 2015), and after observations that elements of this pathway are reactivated after MI, full characterisation was undertaken to determine its relevance in this setting.

For many years, the origins of the coronary vessels were incompletely defined, with the epicardium widely accepted as the primary source of coronary endothelial cells (P Riley, 2011); however recent publications provided evidence for the endocardium as an

embryonic and perinatal source (Wu et. al., 2012, Tian et. al., 2014, Zhang et. al., 2016). Suggestions have also been made for the endocardium being a source of endothelial cells via angiogenesis in pathological settings (Miquerol et. al., 2015, Kobayashi et. al., 2017), and previous work from the lab supports a role for the endocardium in neovascularisation post-MI (Dube, Thomas, et. al., 2017).

Studying the endocardium in the adult heart is challenging, due to a lack of genetic tools that label the endocardium specifically, so lineage tracing of endocardial cells is not possible for this application. Instead, the lab previously identified that the *Pdgfb*CreERT2 (Marcus Fruttiger, UCL) model can be used to label all endothelial cells in the heart, except the endocardium, when crossed with a suitable reporter. This was therefore a useful tool in identifying *de novo* vessels post-MI that were either derived from pre-existing endothelial cells (labelled) or from another source such as the endocardium (unlabelled). Cre recombination was induced two weeks prior to LAD ligation by IP injection of tamoxifen to label $Pdgfb^{+}$ cells with YFP or TdTomato. Since tamoxifen has a half-life of 12 hours, this protocol allowed full depletion from the circulation prior to MI, to ensure that only pre-existing endothelial cells were labelled.

The aims for this chapter were to further characterise the formation of subendocardial vessels post-MI in order to validate the hypothesis of an endocardial contribution to neovascularisation in the ischaemic adult heart. Consideration was extended to recapitulation of developmental pathways involved in endocardial trabeculation and compaction, and established mechanisms involved in ventricular patterning of the embryonic heart were examined with the aim of identifying a candidate mechanism for full characterisation in the ischaemic heart. The screening process and methodology for investigating each mechanism, and subsequent rationale for investigating Notch1 signalling is described throughout the results section below.

3.1 Results

3.1.1 The endocardium contributes to neovascularisation post-MI

This work continued from previous work from the group and MI samples for initial studies were generated by Karina Dubé, prior to my learning and optimisation of the LAD ligation surgical model. Contributions of other group members to the data in Figures 3.1 and 3.3 is acknowledged in the legends.

Myocardial infarction was performed on *Pdgfb;YFP* mice, however, due to weak YFP fluorescence, the *Pdgfb*CreERT2 line was later crossed with *Gt(ROSA)26Sor*$^{tm14(CAG-tdTomato)Hze}$/J reporter mice (breeding strategy shown in **Figure 3.1A**), which are shown without injury in **Figure 3.1B**. Arrows indicate the endocardium, which was labelled with CD31 (endothelial cell adhesion molecule marker, green) but not TdTomato, and endothelial cells in coronary vessels were observed by co-expression of CD31 and TdTomato (yellow).

After MI, expansion of the capillary network in the infarct border zone was observed, and capillaries co-stained with endomucin (endothelial cell marker) and YFP suggest a pre-existing endothelial source (**Figure3.1C-E**, closed arrows). Notably, however, open arrows in the same panel indicate cells labelled by endomucin, but negative for YFP, suggesting an alternative source to pre-existing endothelial cells, which may be the endocardium or another cell type, such as a circulating or resident endothelial progenitor. Larger capillaries were also observed extending into the infarct region (**Figure 3.1F-H**), and these endomucin labelled vessels appeared to contain both YFP^+ (closed arrows) and YFP^- endothelial cells, suggesting combined endothelial and non-endothelial sources.

Vessels were also identified between the infarcted myocardium and the endocardium, referred to throughout as the *sub-endocardium,* and these were entirely unlabelled with YFP (Dubé et. al., 2017). A detailed characterisation over the timecourse of sub-

endocardial remodelling (that appeared to give rise to these vessels) was undertaken and is shown in **Figure 3.2A-H**, with the sub-endocardial region indicated (**Figure 3.2C**, yellow). At 2 days post-MI, very few smooth muscle-myosin heavy chain (SM-MHC)$^+$ cells or vessels were observed (**Figure 3.2A-B**, arrows), however this increased over time (**Figure 3.2C-H**, closed arrows), suggestive of an adaptive response to ischemia. In addition to this sub-endocardial expansion of SM-MHC$^+$ cells, the formation of sub-endocardial holes that appear morphologically similar to vessel lumina were observed (**Figure 3.2D, F, H**, open arrows), which were unsupported by SM-MHC$^+$ cells. It is unclear whether these lumina go on to acquire smooth muscle support later, retain a more venous-like morphology, or are structures referred to as “endocardial tubes” in recent literature (Tang et. al., 2018), however their expansion in response to injury suggests a beneficial role in repair. **Figure 3.2I** demonstrates very few and sub-endocardial “lumina” or SM-MHC$^+$ smooth muscle-lined vessels without infarction.

Sub-endocardial vessels were quantified in sham, day 7 and day 14 post-MI hearts (**Figure 3.3A-C**) by counting the SM-MHC$^+$ (**Figure 3.3B**) and SM-MHC$^-$ (**Figure 3.3C**) lumina between the endocardium and infarct within a 3mm segment (**Figure 3.3A**, dotted line). Vessels were grouped by size as follows: <20µm, 20-80µm and >100µm; 1-way ANOVA with Bonferroni correction revealed a significant increase for all vessel sizes at day 7 and day 14 post-MI (**Figure 3.3D**; ** = $P \leq 0.01$, *** = $P \leq 0.001$ versus sham).

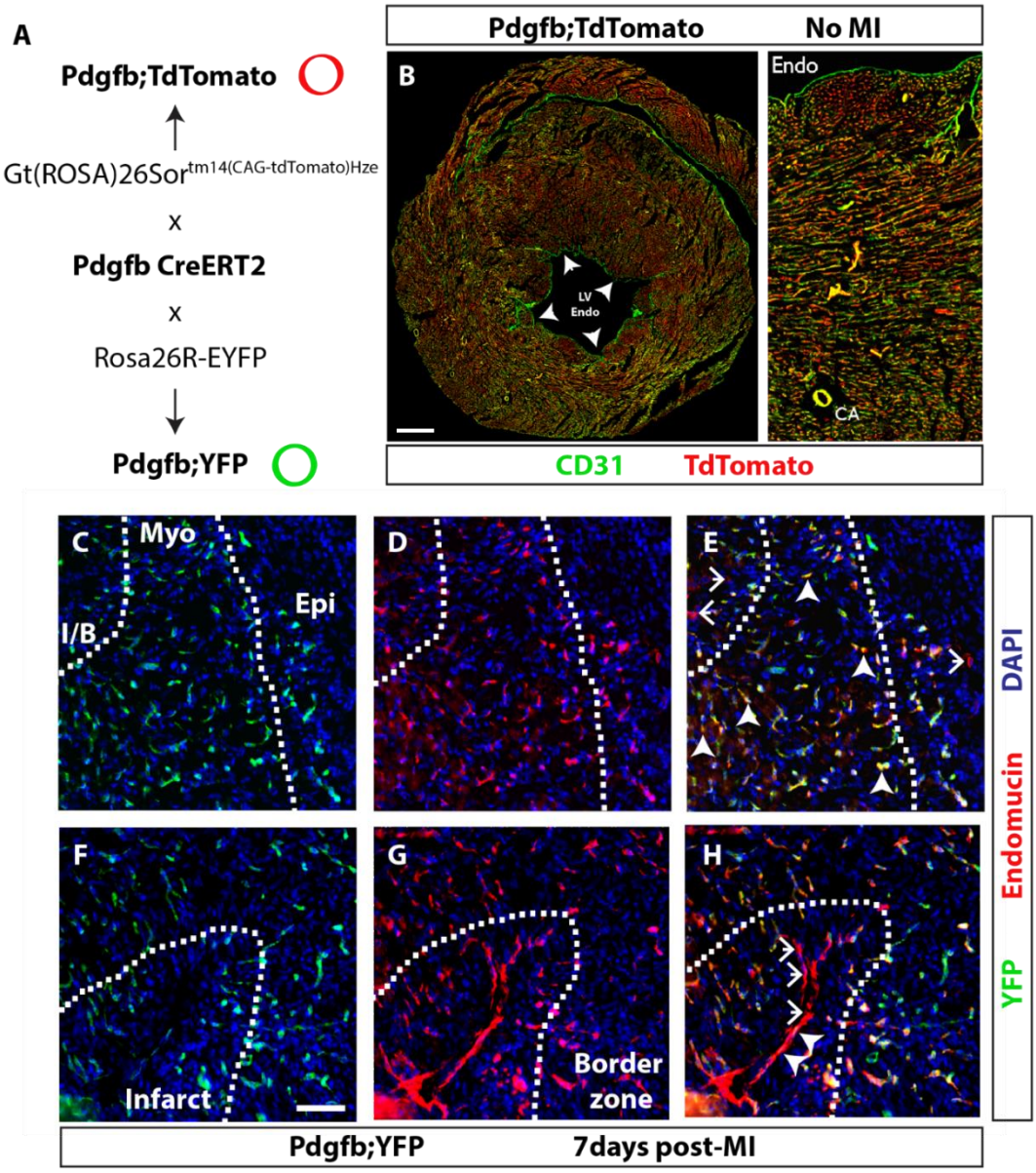

Figure 3.1. *Pdgfb Cre* lineage trace negatively labels the endocardium and de novo vessels in infarct border zone

Pdgfb Cre was used to negatively trace endocardium-derived vessels following myocardial infarction (MI). (A) shows the breeding strategy for labelling *pdgfb Cre* positive cells with YFP (green) or TdTomato (red) and (B) demonstrates that the endocardium is unlabelled by TdTomato in non-injured hearts (endocardium labelled by CD31 in green). In the post-MI setting, expansion of the capillary network was observed with YFP positive vessels co-stained with endomucin (red) (C-E, closed arrows), suggesting a pre-existing endothelial source, however YFP negative capillaries were also observed in the infarct border zone (C-E, open arrows), suggesting a non-endothelial source or endocardium. Larger YFP^- capillaries were also observed extending into the infarct region (F-H, open arrows) labelled by endomucin (red), alongside co-stained endothelial cells (F-H, closed arrows), suggesting that both pre-existing endothelial cells and non-endothelial or endocardial cells contribute to neovascularisation post-MI.

Endo: endocardium, CA: coronary artery, myo: myocardium, epi: epicardium, I/B: infarct border. Scale bars: B = 1mm, C-H = 50µm. N = 4 injured hearts, 3 uninjured hearts. MI surgeries performed by Karina Dubé, imaging of YFP vessels completed by Nicola Smart. (Dubé, Thomas et. al., 2017).

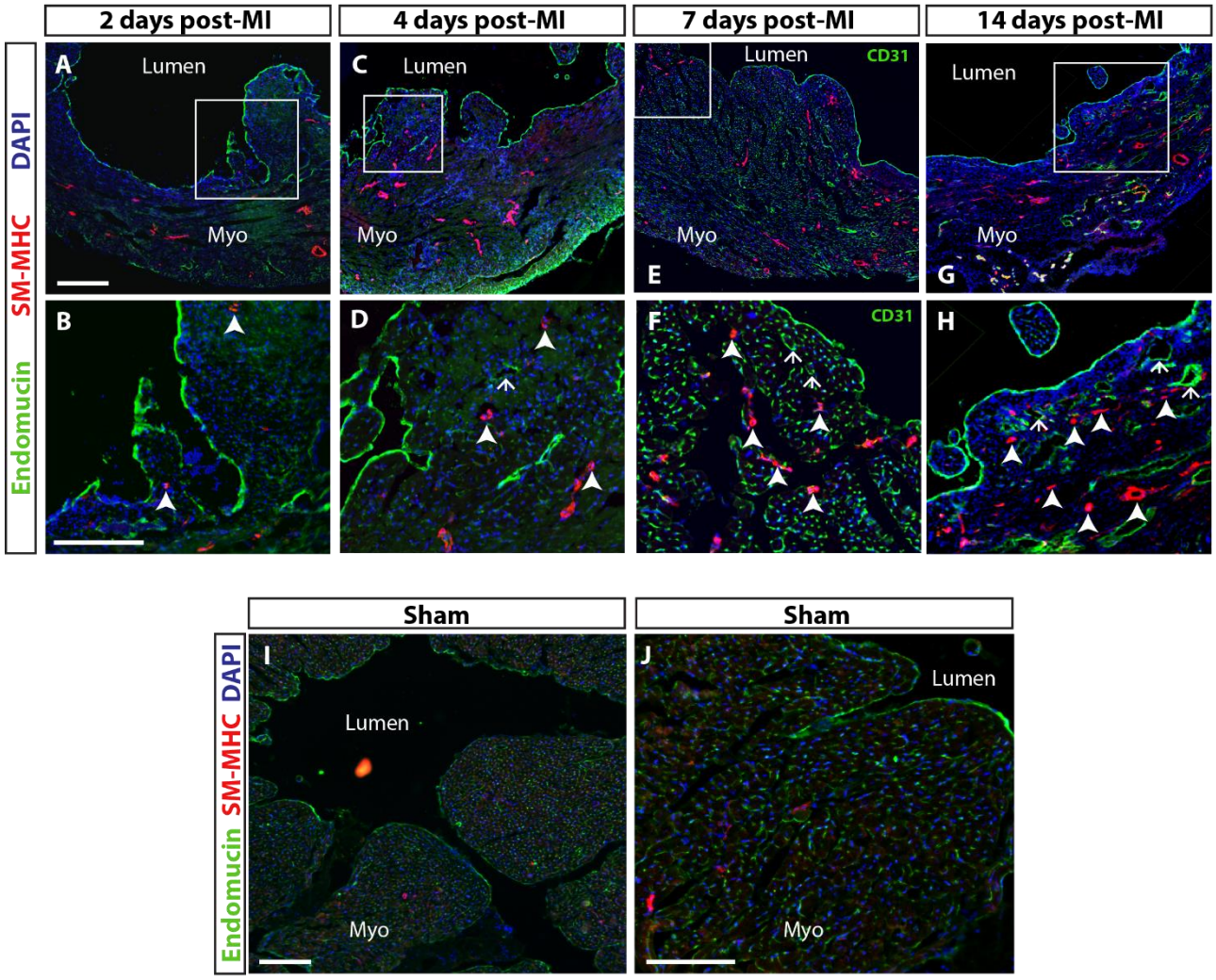

Figure 3.2. Temporal vascular remodelling in the sub-endocardium overlaying infarcted myocardium

A time course of vascular remodelling in the sub-endocardium (between endocardium and infarct, region indicated by yellow dotted line and arrows, C) post-MI is shown by immunofluorescence imaging between days 2 and 14 post-MI. High power inserts (B, D, F & H) are shown by white boxes in A, C, E & G, respectively. Sub-endocardial vessels are labelled with SM-MHC (closed arrows) in the region between the endocardium (labelled by endomucin, green) and the infarct, and an increase in number from B to H is demonstrated. There is also an increase in endomucin labelled lumina without SM-MHC positive cell support in this region, and these are highlighted by open arrows in D, F and H. Panels I and J show the sub-endocardial region of a sham heart comparatively stained with SM-MHC.

Wild type hearts analysed. Scale bars: A, C, E, G, I = 500μm, B, D, F, H, J = 100μm, representative of n = 4 injured, 2 sham.

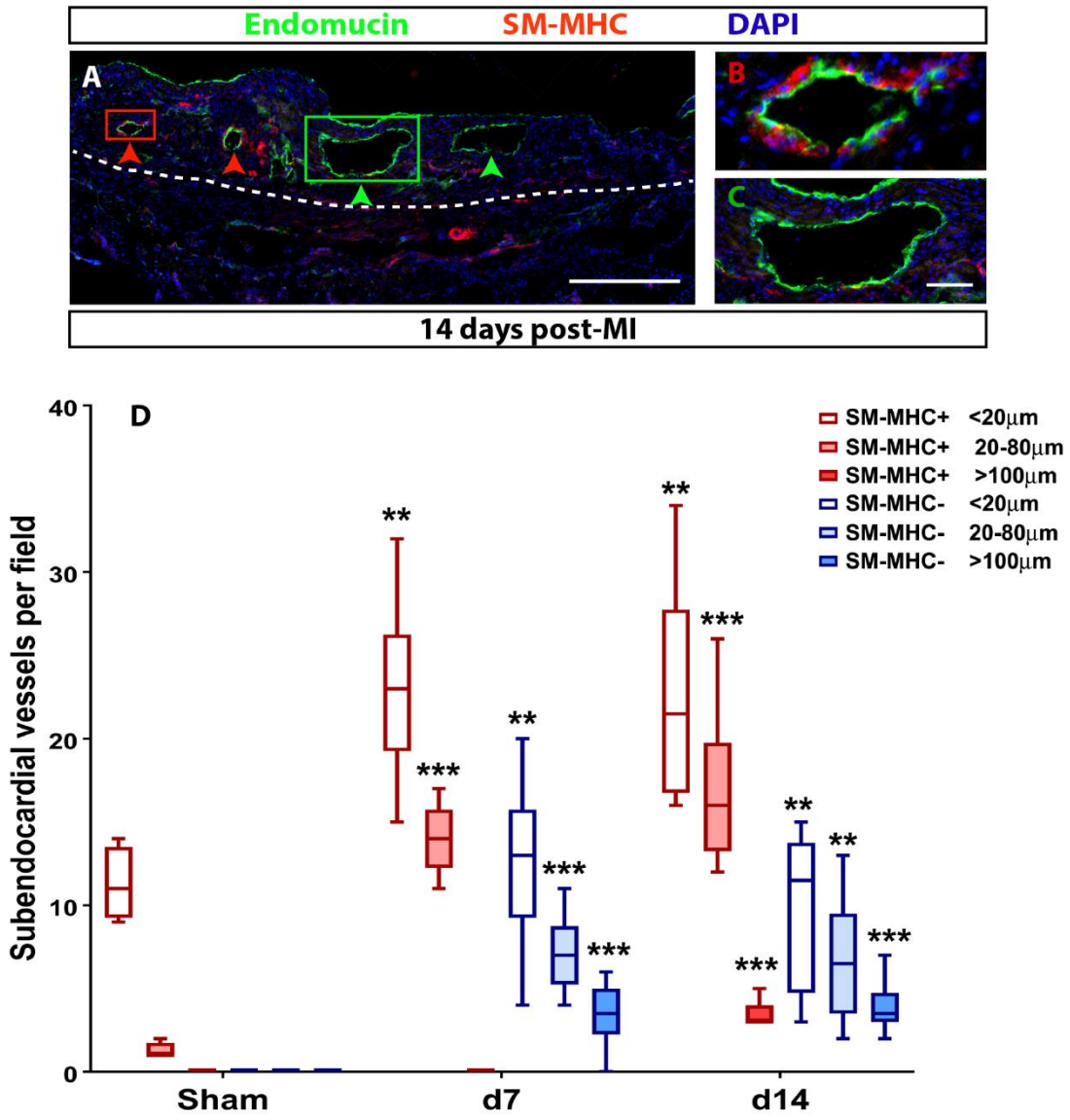

Figure 3.3. Subendocardial vessels quantified post-MI

Sub-endocardial vessels were quantified at days 7 and 14 post-MI, and compared with sham. Vessels per 3mm segment were counted between the endocardium (labelled with endomucin, green) and the white dotted line, and split into categories as follows: SM-MHC+ (labelled red) (B) or SM-MHC- (C), and <20µm, 20-80µm or >100µm. N = 4 sham, n = 8 d7, n = 8 d14. A 1-way ANOVA with Bonferroni correction was performed to determine significance. D shows this data as a box and whisker chart with significance indicated (** = P≤0.01, *** = P≤0.001 versus sham). *Scale bars: H = 500µm, J = 50µm.*

Wild type hearts used for analysis. Vessel count performed by Nicola Smart. (Dubé, Thomas et.

3.1.2 Trabeculation and Compaction in the infarcted adult heart

In an attempt to understand the signalling pathways driving the observed expansion of sub-endocardial vessels, consideration was given to developmental processes that may be redeployed in a pathological setting. In the embryonic heart, ventricular trabeculation increases the surface area of the myocardium in contact with the ventricle lumen, whilst the coronary vessels are developing (Sedmera et. al., 2000). Trabeculae later compact down in a process that intimately couples formation of a compact myocardium with the emergence of the coronary vasculature. Indeed, evidence from mouse studies suggest that the endocardium contributes up to 60% of coronary endothelial cells by P28 via the process of trabecular remodelling (Tian et. al., 2014).

Previous observations of the lab showed that the characteristically smooth endocardial surface of the adult heart (**Figure 1.6**) appears to develop protrusions into the lumen after injury, which partly resemble trabeculations of the embryonic heart. At later stages, the endocardium returns to a smoother state, coinciding with the formation of sub-endocardial vessels. An observational timecourse was made to investigate a possible recapitulation of trabeculation and compaction in the injured adult heart (**Figure 3.4**). At 24 hours post-MI, folds appeared to form in the endocardium which protrude into the myocardium below (**Figure 3.4A, B**, arrows). At day 2, endocardial folds had opened up further to form large projections into the lumen and “holes” in the myocardium below (**Figure 3.4D, E**, arrows). Arrows indicate the base of trabeculae in **Figure 3.4A-E**, and in **Figure 3.4F** subendocardial “lumina” began to develop. By days 5 and 7 post-MI, the trabeculae appeared to fuse, creating large, fully enclosed lumina below the endocardial surface; closed arrows in **Figure 3.4G-J** indicate regions of endocardium/myocardium that appear to be “fusing”. At 14 days post-MI the endocardial surface appeared smoother and the remaining sub-endocardial lumina were smaller, with the presence of more vessel-like structures (**Figure 3.4K-L**, open arrows). Interestingly, by analysing serial sections 250μm apart, sub-endocardial lumina were visualised open (**Figure 3.5A**,

arrows), partly enclosed (**Figure 3.5B**, arrows) and fully enclosed (**Figure 3.5C**, arrows), respectively, supportive of a transitional process of vessel or endocardial tube formation.

3.1.3 Sub-endocardial vessels acquire support from α-SMA+ cells

In combination with subendocardial remodelling, α-SMA^{+} cells were detected in and immediately below the endocardium (**Figure 3.5D-F**, arrows). These cells may be smooth muscle cells recruited for vascular support, or endocardium-derived mesenchymal cells which are an intermediary in the process of EndMT. Whilst some endocardial cells (**Figure 3.5F**, open arrows) also expressed α-SMA, suggesting that they may be the source of mesenchymal cells, there is currently no lineage tracing evidence to support this, and further investigation is required to determine their origin.

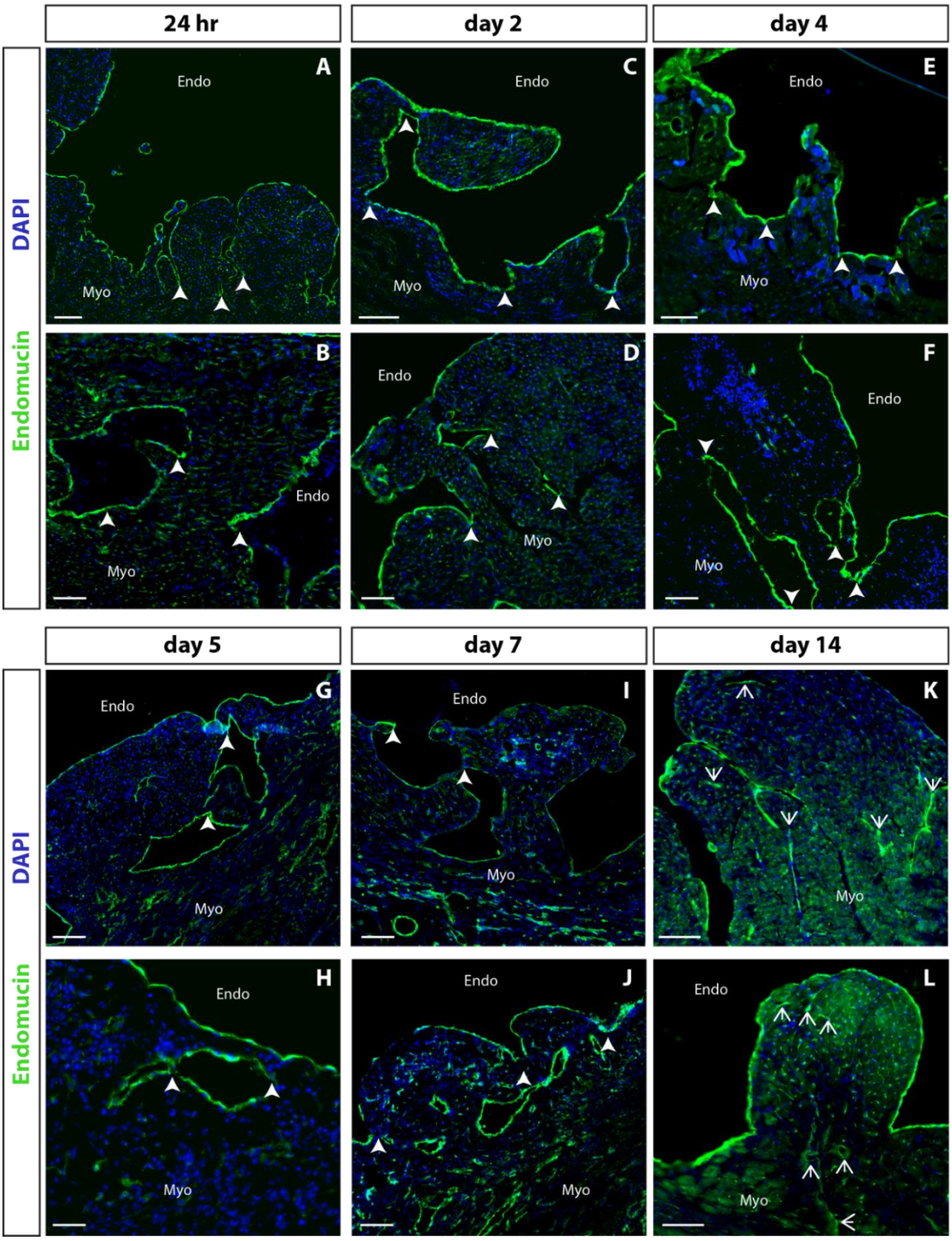

Figure 3.4. Endocardial remodelling 24 hours - 14 days post-MI: Trabeculation and compaction

Endocardial remodelling was observed between 24 hours and 14 days after infarction, resembling that of trabeculation and compaction in the developing heart. Endomucin (green) labelled endothelium. Closed arrows in panels A-F highlight the base of "trabeculae" which have formed close to the endocardial surface. At later stages, days 5-7, these trabeculae appear to compact (G-J) to form enclosed sub-endocardial "lumina". Closed arrows here (G-J) indicate points of fusion where the endocardium is no longer connected to the main left ventricle lumen, and is instead enclosed by the myocardium. Panels K and L show fully integrated vessel-like structures in the sub-endocardial region (open arrows) which are formed by day 14 post-MI.

Wild type hearts imaged. Scale bars: A, C, G, I, J, K L = 100µm, E, B, D, F, H = 50µm. Representative of n = 2 for d2, d5, n = 4 for d2, d4, d7, n = 3 for d14.

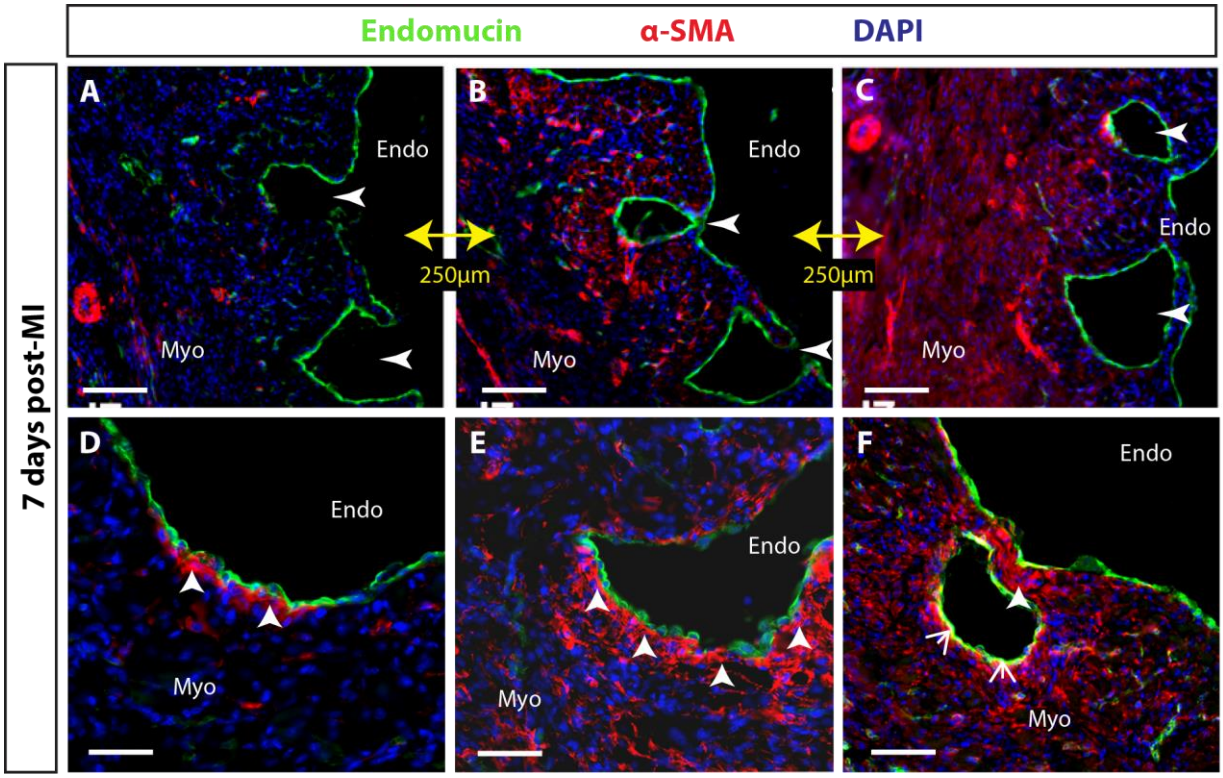

Figure 3.5. Sub-endocardial lumina are enclosed and are supported by α-SMA positive cells

Panels (A-C) are images taken of cryosections 250μm apart in wild type heart, showing sub-endocardial "trabeculae" progressively enclosed by myocardium (arrows, A-C). α-SMA staining (red) demonstrates that these sub-endocardial "lumina" also acquire support from mesenchymal or smooth muscle cells at day 7 post-MI (D-F). Endothelium labelled by endomucin (green). Arrows indicate α-SMA$^+$ cells below the endocardial surface (D), in the surrounding sub-endocardial lumina (E-F) and in the endocardium (F, open arrows).

Scale bars: A, B, C, F = 100μm, D, E = 200μm, n = 4.

3.2 Developmental signalling pathways are recapitulated following infarction in the adult heart

Reciprocal signalling between the endocardium and myocardium elicits proliferation and migration of endothelial cells in the embryonic heart (Paige et. al., 2015). Whilst these signalling processes are essential for early myocardial patterning, after E15.5 in the embryonic mouse they are no longer required, and persistence can lead to LVNC (Teekakirikul et. al., 2013). There is currently no evidence of recapitulation of endocardial signalling pathways in a pathological setting. Therefore, based on our observations of trabecular projections after MI, involvement of known developmental signalling pathways was investigated.

3.2.1 Expression of Brg1 in post-MI endocardium during trabeculation

Endocardial expression of Brg1, a chromatin remodelling protein, is required to repress ADAMTS1 during trabeculation, to allow the cardiac jelly to support trabecular growth. Brg1 is later switched off to allow ADAMTS1 to support the degradation of cardiac jelly and termination of trabeculation (Stankunas et. al., 2008).

Expression of Brg1 was not identified in the uninjured adult heart (**Figure 3.6A, B**), but observations at early time points post-MI showed expression in remodelling regions. At day 2, endocardial and myocardial Brg1 was expressed (**Figure 3.6C-D**, arrows). At 5 days post-MI, endocardial Brg1 was evident (**Figure 3.6E-F**, arrows), with clusters of $Brg1^{+}$ cells also observed in the myocardium below. These data support a putative role for Brg1-regulated processes in MI-induced trabeculation post-MI.

3.2.2 Nrg1 in endocardial remodelling post-MI

Neuregulin 1 (Nrg1) is an endocardial paracrine signalling molecule that binds the receptor ErbB2, leading to its dimerization with ErbB4 during trabeculation (Paige et. al., 2015), to induce signalling cascades that modulate cell growth and migration (Yarden et. al., 2001).

Expression of Nrg1 was observed in the endocardium of remodelling regions at 2 – 7 days post-MI (**Figure 3.7A-F**, arrows), providing further support for recapitulation of developmental signalling post-MI. Nrg1 was not seen in the adult heart without infarction (**Figure 3.7G,H**).

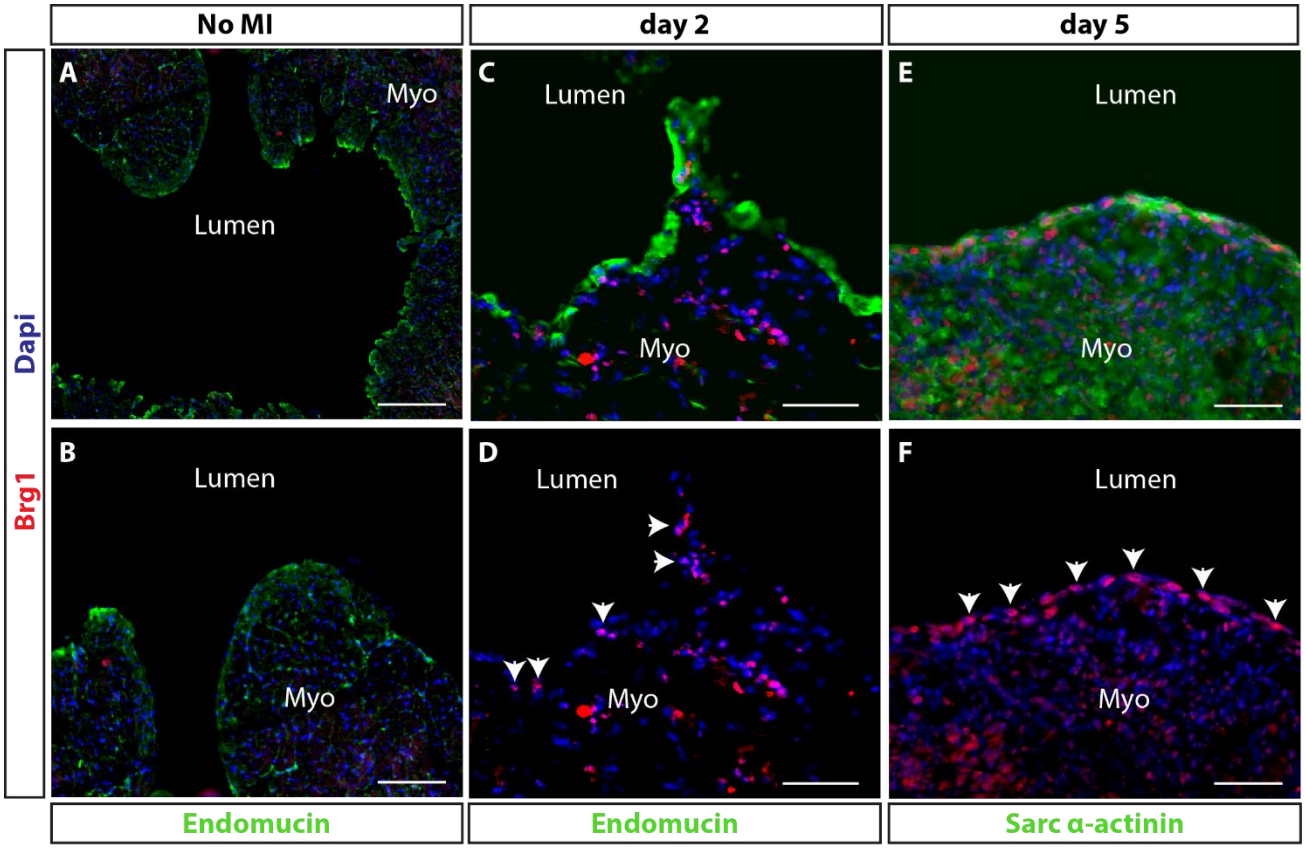

Figure 3.6. Molecular signalling pathways screened for endocardial remodelling post-MI: Brg1

Consideration was given to Brg1 due to its role in repressing ADAMTS1 in endocardial trabeculation during coronary vessel development. Panels (A,B) show that there is no expression of Brg1 in the endocardium or underlying myocardium in the uninjured adult heart (Brg1 labelled red, endomucin labelled green). Panels (C-F) indicate Brg1 expression in the endocardium and sub-endocardial region at days 2 and 5 post-MI (arrows), with sarc α-actinin labelling cardiomyocytes in E.

Wild type hearts analysed. Scale bars: A = 250μm, B = 200μm, C-F = 100μm. n = 2 for No MI, n = 4

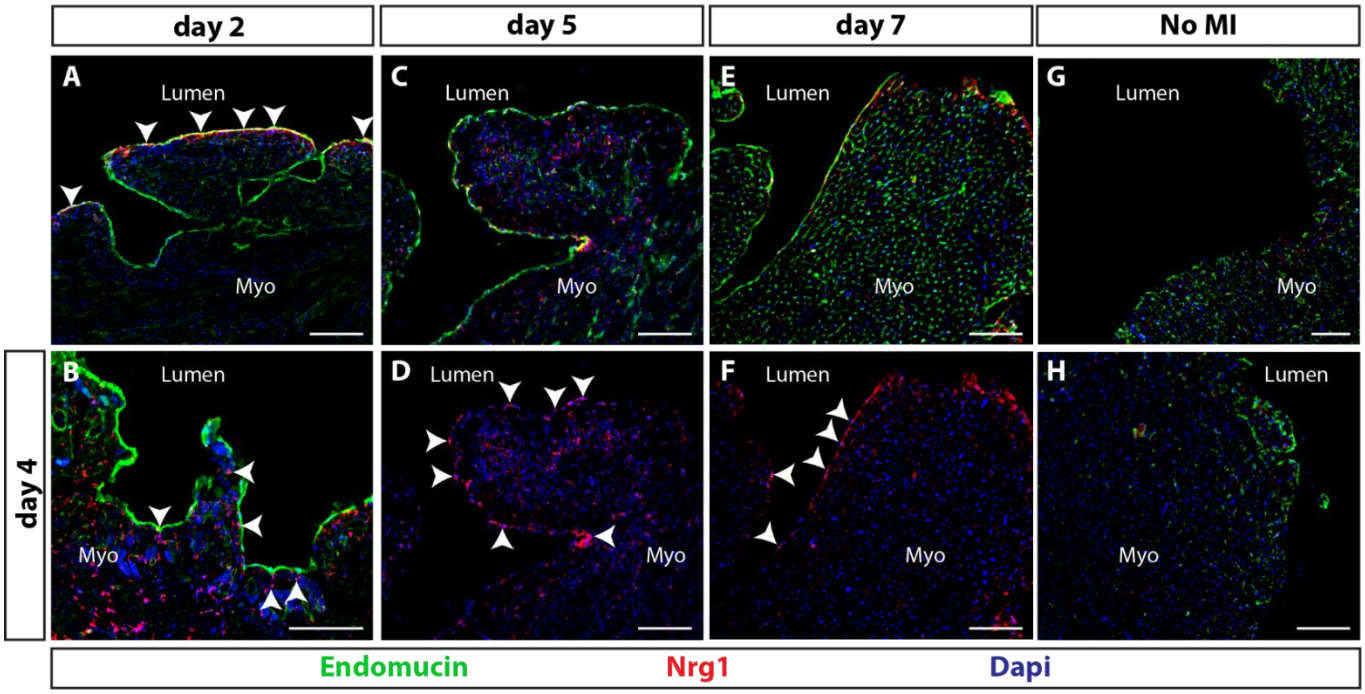

Figure 3.7. Molecular signalling pathways screened for endocardial remodelling post-MI: Nrg1

Neuregulin 1 (Nrg1) is a paracrine signalling molecule implicated in cell migration and adhesion during trabeculation in development. Nrg1 was identified in the endocardium at 2 days, 5 days and 7 days post-MI (labelled red, A, C-F arrows) co-stained with endomucin (green), and immediately beneath the endocardium at 4 days post-MI (B, arrows). The uninjured adult heart is shown (G,H) indicating that there is no Nrg1 expression without MI.

Wild type hearts analysed. Scale bars: A = 200μm, B-H = 100μm. n = 4 for d2, n = 2 for d5, n = 4 for d7, n = 2 for No MI.

3.2.3 Angiogenesis and proliferation in the infarcted adult heart

Proliferation is a key process required for trabeculation during development, which is coordinated by endocardial and myocardial signalling mechanisms, and results in proliferation of the endocardium from the base of trabeculae as well as underlying cardiomyocytes. Ki67, a marker of proliferation, and phospho-histone H3 (PHH3) which indicates mitosis, were used to assess proliferation in the post-MI setting, and to compare this with proliferation in the embryonic heart. Proliferation of cardiomyocytes in the adult heart has been established at a rate of ~1.3-4% per year, however this is proposed to increase post-MI (Malliaras et. al., 2013). In regions of endocardial remodelling, proliferation was observed in clusters beneath the endocardium at 24 hours post-MI (**Figure 3.8A**, arrows) and in the endocardium at days 4 and 7 post-MI (**Figure 3.8B-D**, arrows). PHH3 expression is also shown at the base of trabeculae, which is replicative of the developmental pattern (D'amato et. al., 2015).

Figure 3.8E, F showed the presence of many proliferating cells (arrows) in the trabecular myocardium at E15.5. Endomucin (green) labelled the endocardium in **Figure 3.8F** which highlights the extent of trabeculation at this stage of development.

Whilst these data indicate that proliferation plays a role in the trabeculation observed, the number of proliferating cells does not appear to account for the extent of remodelling taking place. Consideration was therefore given to other processes which could contribute, such as inflammation, cell migration and transitions between cell types.

The endocardium has recently been implicated as a source of neovascularisation post-MI, however angiogenesis has been suggested as the primary mechanism for this contribution (Miquerol et. al., 2015, Kobayashi et. al., 2017). Both *Kobayashi et. al.* and *Miquerol et. al.* highlighted VEGF signalling as a mechanism for endocardial-derived angiogenesis post-MI, via VEGF receptor 2 (VEGFR2) in pre-existing endothelial cells.

Despite careful observation, we were not able to detect expression of VEGFR2 in the endocardium post-MI ((Dubé et. al., 2017) and **Figure 3.8G-I**). Arrows in **Figure 3.8G** indicate a representative region of remodelling endocardium at 7 days post-MI, labelled by endomucin (green), which is VEGFR2 negative. Capillaries were observed in the same panel expressing VEGFR2, suggestive of an angiogenic role in pre-existing capillary expansion. Similarly, larger pre-existing vessels are shown within the myocardium that express VEGFR2 (**Figure 3.8H,I**, open arrows), suggesting that post-MI, angiogenesis is driven by pre-existing endothelial cells, rather than the endocardium. Apelin was also used as a marker of angiogenesis at day 4, but minimal expression was seen in remodelling regions of the endocardium (**Figure 3.8J,K**), although apelin expression was previously observed in the coronary sinus, which undergoes angiogenic sprouting post-MI (Dubé et. al., 2017). These data together suggest that angiogenesis does have a role in neovascularization post-MI, but that the primary mechanism of endocardial remodelling is likely to be independent of this.

3.2.4 An inflammatory role in endocardial remodelling post-MI?

Infiltrating cells were observed in regions of endocardial remodelling post-MI, and macrophages were considered due to their role in remodelling the coronary plexus during early embryonic vasculature development (Leid et. al., 2016). Infiltration of inflammatory cells was also considered as a mechanism for the formation of subendocardial cavities, due to their well-established reparative role in response to cardiac injury (Lambert et. al., 2008). Clusters of $CD68^+$ cells (macrophages) were observed in the myocardium of remodelling regions, particularly in locations where lumina were developing (**Figure 3.9A-E**). Clusters were also observed on or near the endocardial surface of remodelling regions at 24 hours and 2 days post-MI (**Figure 3.9C**). Cell clusters in remodelling endocardial regions were also $CD45^+$ (**Figure 3.9F-I**), which labels leukocytes, and this joint expression profile supports a possible role for inflammatory cells in cardiac remodelling post-MI.

3.2.5 A role for EndMT in endocardial remodelling post-MI?

Endothelial cells show high levels of plasticity in various settings and the process by which they obtain characteristics of mesenchymal cells (α-SMA, vimentin) and lose their endothelial cell phenotype (CD31, VE-Cadherin) is called EndMT (Eisenberg and Markwald, 1995). During development, the endocardium undergoes EndMT in the atrioventricular canal and outflow tract regions to contribute mesenchymal cells to the mitral, tricuspid and outflow tract valves (de Lange et. al., 2004) and smooth muscle cells to the coronary vasculature (Chen et. al., 2016). Studies have been undertaken to investigate endocardial EndMT in pathological settings, however there is some controversy surrounding this and whilst *Xu et. al., 2015,* found endocardial fibroelastosis (EFE) tissue to be derived from the endocardium via EndMT, *Zhang et. al., 2015,* used an Npr3-Cre model to show that the postnatal endocardium and coronary endothelial cells seldom contribute to fibrosis.

Moore-Morris et.al., 2014, concluded that in the injured adult heart, the endocardium does not undergo EndMT, and that the two major sources of fibroblasts post-MI are pre-existing coronary endothelial cells (CECs) and pre-existing coronary fibroblasts which were traced back to an epicardial origin during development, however further investigation is required to conclusively prove this (Li et. al., 2018).

Given the importance of EndMT during development, and inconclusive roles in adult pathologies, analysis was made for markers of EndMT in our post-MI samples. Snai1, a transcription factor that drives EndMT, was observed in the endocardium in remodelling regions at 24 hours, 2 days, 4 days and 7 days post-MI (**Figure 3.10A-F**, arrows). The endocardium is labelled with endomucin (green) in these sections, and of note, is the newly formed lumen at day 4 (**Figure 3.10D**) which clearly expresses Snai1 in the remodelled endocardium lining the vessel-like structure. Alongside this, the *pdgfb-Cre* model was used as a negative tracing tool, and whilst the endocardium was unlabelled by TdTomato, pre-existing endothelial cells were clearly labelled (red), with some

showing co-expression of α-SMA (yellow) (**Figure 3.10G-J**, open arrows). This suggests that EndMT occurs from pre-existing endothelial cells, which supports the current literature. However, interestingly, a large cluster of α-SMA^{+} cells, reminiscent of those shown in **Figure 3.5**, appeared to be unlabelled by TdTomato (**Figure 3.10I,H**, arrows). This suggests a source which is non-endothelial, and considering the proximity of these cells to the endocardium, it seems plausible that they could be endocardial-derived, alongside, or rather than contributed via pre-existing fibroblasts, the other major source suggested by recent literature.

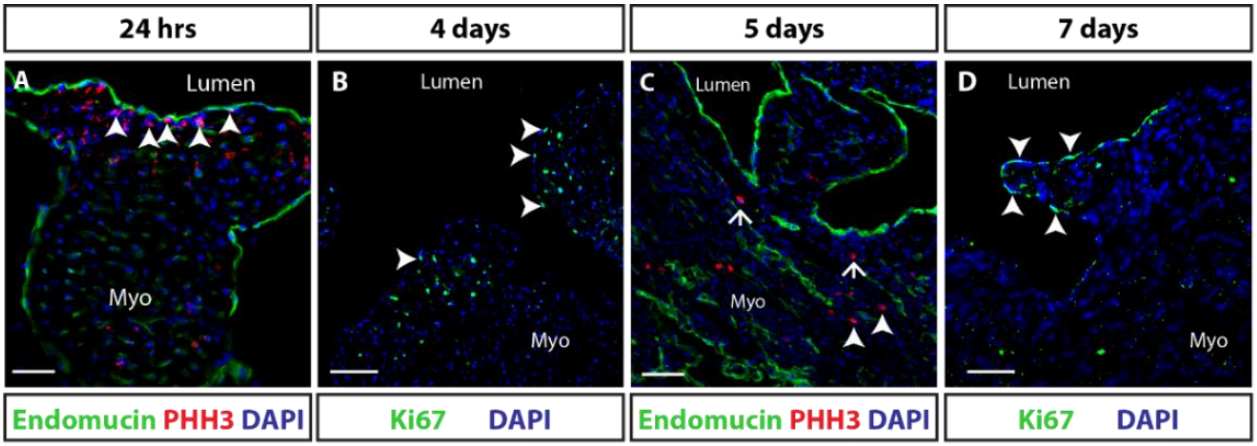
24 hrs
4 days
5 days
7 days
A
Lumen
Myo
B
Lumen
Myo
C
Lumen
Myo
D
Lumen
Myo
Endomucin PHH3 DAPI
Ki67 DAPI
Endomucin PHH3 DAPI
Ki67 DAPI

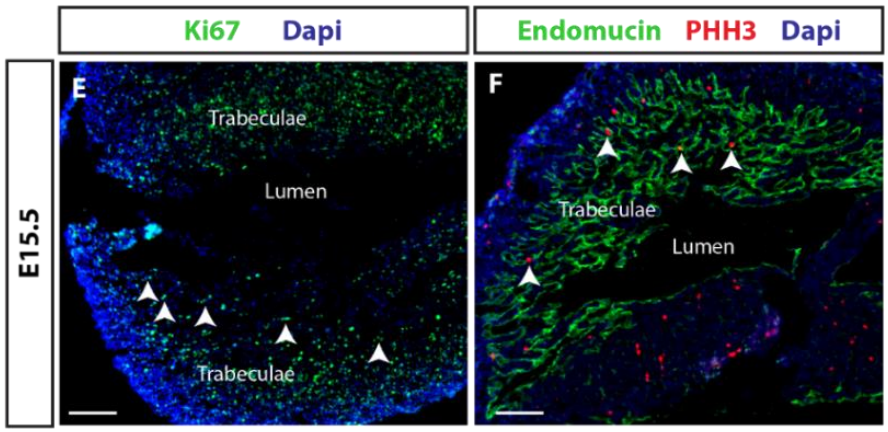
Ki67 Dapi
Endomucin PHH3 Dapi
E15.5
E
Trabeculae
Lumen
Trabeculae
F
Trabeculae
Lumen

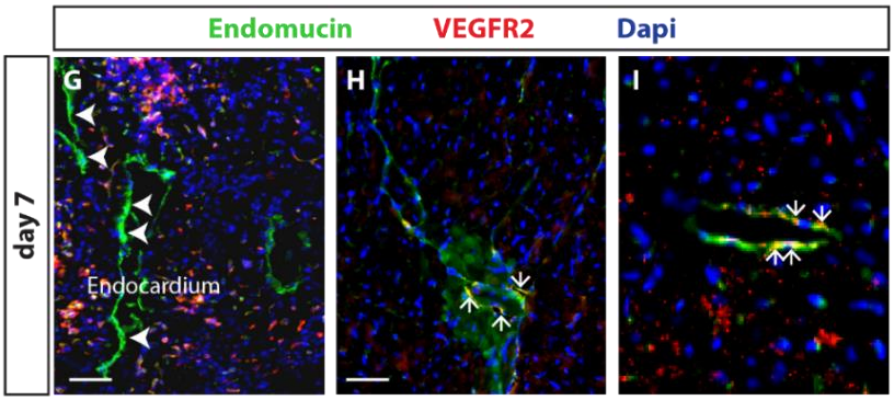
Endomucin VEGFR2 Dapi
day 7
G
Endocardium
H
I

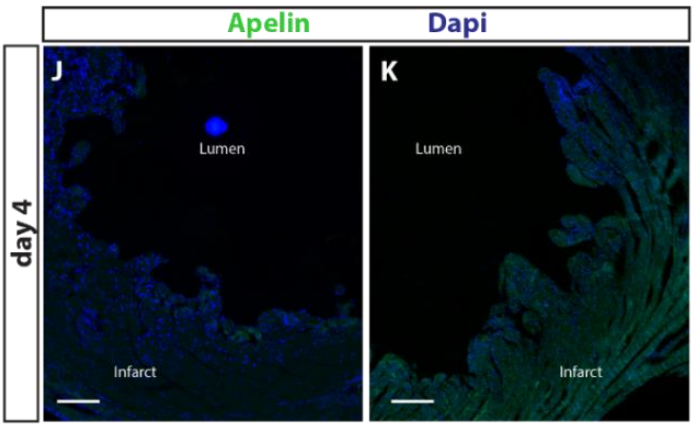
Apelin Dapi
day 4
J
Lumen
Infarct
K
Lumen
Infarct

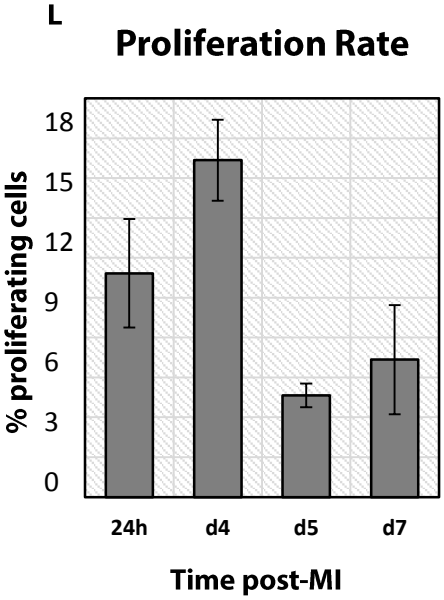
L
Proliferation Rate
% proliferating cells
18
15
12
9
6
3
0
24h
d4
d5
d7
Time post-MI

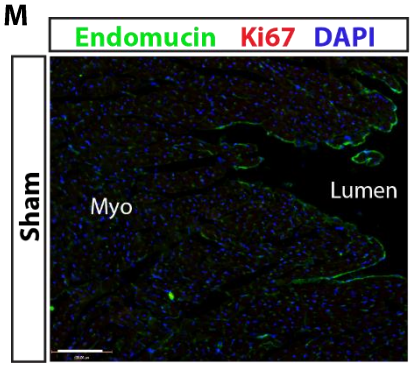
M
Endomucin Ki67 DAPI
Sham
Myo
Lumen

Figure 3.8. Minimal proliferation and angiogenesis in regions of endocardial remodelling post-MI

Proliferation was observed in regions of endocardial remodelling, although only in a small number of cells. (A) indicates PHH3 positive cells (red) underlying the endocardial surface (labelled by endomucin, green) at 24 hour, showing a small degree of mitosis. A few endocardial cells were labelled by Ki67 (green) at 4 days and 7 days post-MI (B, D arrows), indicating that the endocardium can undergo proliferation in this setting. At 5 days post-MI, PHH3 positive cells are localised to the remodelling sub-endocardial region, although they do not appear to be endothelial cells (C) (unlabelled by endomucin, green). These data are quantified in (L), which shows total % of proliferating cells in the sub-endocardium, as a percentage of DAPI. Ki67 expression in a sham heart is shown in (M) as a comparison. (E) and (F) show developmental proliferation as a comparison, which highlights the extent of proliferation required for the formation of coronary vessels. Ki67 (green) and PHH3 (red) are localised to the base of trabeculae in these examples, which has not been observed in the injury setting. (G – I) show minimal VEGFR2 (red) in the endocardium at 7 days post-MI, where endomucin labels the endocardium (G, closed arrows) suggesting little, if any, angiogenesis from the endocardium. Vessels found further within the myocardium co-express VEGFR2 and endomucin, suggesting that any angiogenesis post-MI arises from pre-existing vessels. Apelin was not observed in the endocardium or endothelial cells at day 4 post-MI (J-K).

Wild type hearts analysed. Scale A, B, D, G, H, M = 100µm, C = 50µm E,F = 250µm. n = 2 for 24hrs, d5, n = 4 for d4, d 7, n = 2 for E15.5

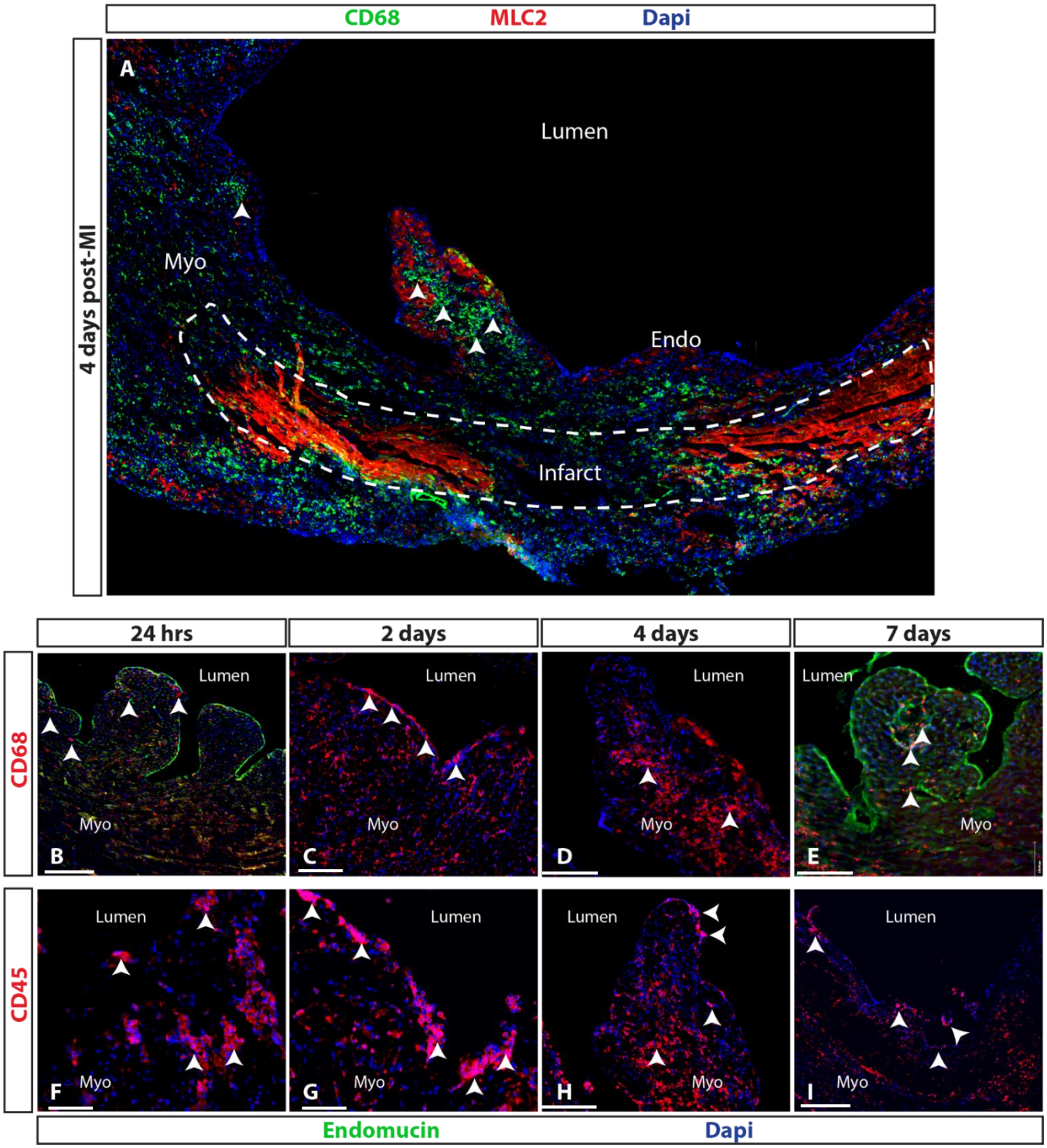

Figure 3.9. Possible role for macrophages in endocardial remodelling post-MI

A role for immune cells was investigated in the post-injury setting by immunofluorescent staining for CD68 (macrophages) and CD45 (leukocytes). Panel (A) shows clustering of macrophages in regions of endocardial remodelling (arrows) overlaying the infarcted myocardium (dotted line), where MLC2 labels cardiomyocytes. Additionally, macrophages were observed in the endocardium (labelled by endocmucin, green) at 24hrs and 2 days post-MI (B, C arrows), and clustering in regions where sub-endocardial "lumina" are forming at days 4 and 7 post-MI (arrows). Clearly labelled clusters of CD45 positive cells were observed in regions of endocardial remodelling at all time points (F-I, arrows), suggesting a role for inflammatory signalling in neovascularisation post-MI.

Wild type hearts analysed. *Scale bars: A = 500μm, B = 200μm, C-D = 100μm, F-G = 50μm, H = 100μm, I = 200μm. N = 2 for 24hrs, n = 4, for d2-d7.*

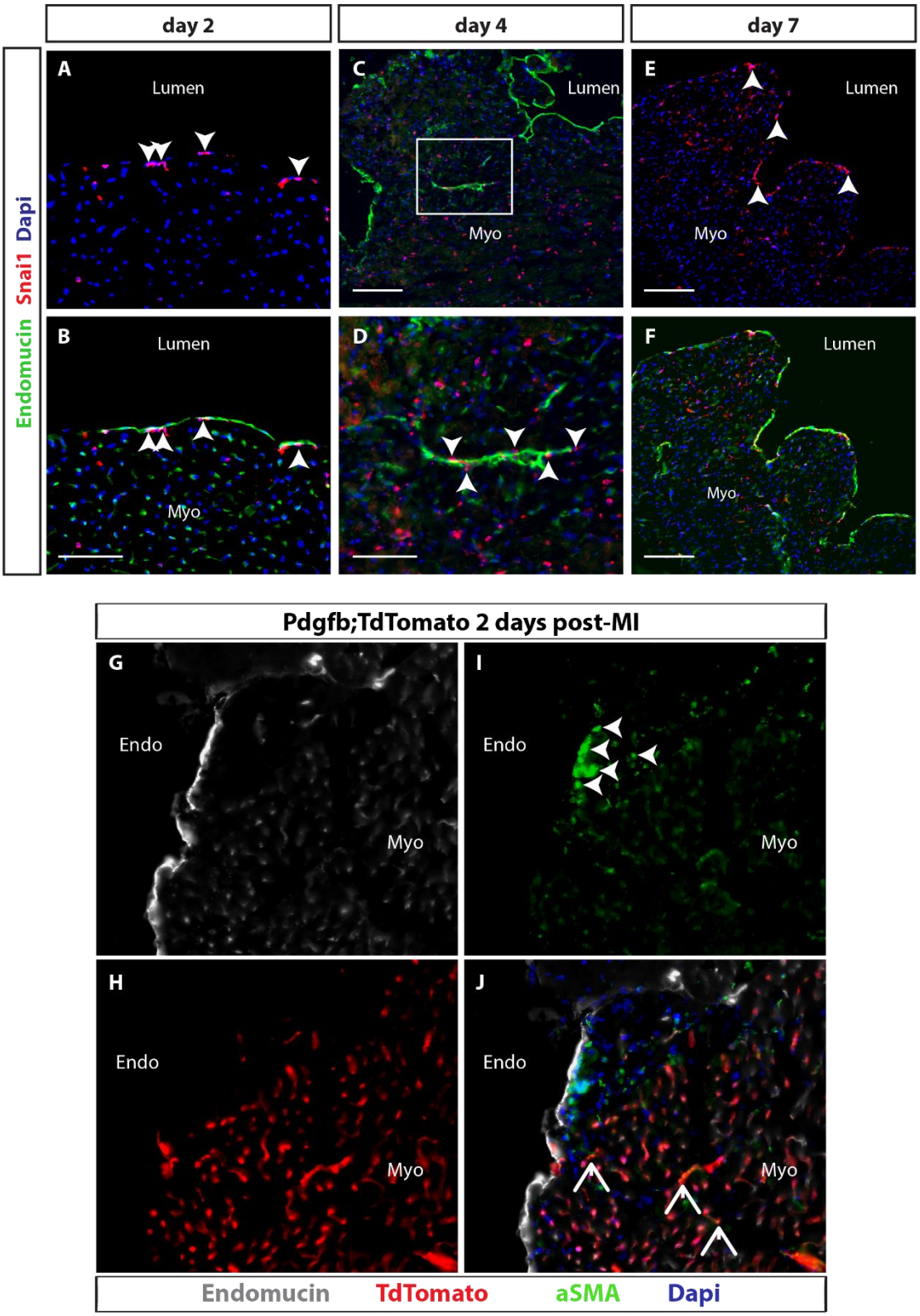

Figure 3.10. Contribution of endocardial-to-mesenchymal transition to de novo vessels post-MI?

The possibility of an endocardial contribution to de novo vessels post-MI via endothelial-to-mesenchymal transition (EndMT) was investigated using immunofluorescence analysis of wild type hearts in A-F. Snai1, an EndMT-driving transcription factor was observed in the endocardium at 24 hours and 7 days post-MI (A, B, E, F, arrows) and in new sub-endocardial "lumen" at 4 days post-MI (C,D). To support this theory, α-SMA positive cells were observed below the endocardium (G) appearing to move away towards the myocardium at 2 days post-MI (I, arrows). Whilst some of the α-SMA^{+} cells in the *Pdgfb Cre* heart (G-J) were labelled with TdTomato (J, open arrows), suggesting an endothelial origin, those near the endocardium were unlabelled (I, arrows), suggesting a possible endocardial origin, although (myo)fibroblasts cannot be excluded. *Scale bars: B = 100μm , C, E, F = 200μm, D, H = 50μm. n = 4 per timepoint.*

3.3 Multiple markers suggest a role for Notch1 signalling in endocardial remodelling post-MI

The Notch pathway is well-characterised in cardiac development, and is a key regulator of cell proliferation, migration and EndMT during the processes of trabeculation, compaction and valve formation (Grego-Bassa et. al., 2007, Garside et. al., 2013). As stated, trabeculation is driven by endocardial Dll4-mediated Notch1 activation which induces proliferation and differentiation from the base of trabeculae, and after a reduction in MFng expression there is a switch to myocardial Jag1,2-mediated Notch1 activation, leading to maturation and compaction of trabeculae (**Figure 3.11A**, D'amato et. al., 2015).

Notch1 is also implicated in controlling EndMT for cardiac valve development; Notch1$^{-/-}$ mice show severely reduced Snai1 expression, abnormal endocardial adhesion and a lack of cushion mesenchyme indicating disrupted endocardial EndMT (Timmerman et. al., 2004). These data together highlight the importance of endocardial Notch1 signalling for trabeculation, compaction and EndMT, and provide a strong rationale for its consideration in the post-MI setting.

3.3.1 Components of the Notch pathway are expressed in regions of endocardial remodelling post-MI

Notch1 plays a vital role in mammalian cardiac development, which was confirmed between mouse E9.5 and E12.5 (**Figure 3.11B-G**). Notch1 intracellular domain (N1ICD), indicating active Notch1, was present in the trabecular endocardium (**Figure 3.11B-D**, arrows) at stages E9.5 and E11.5, as well as in the highly proliferative myocardium (**Figure 3.11C,D**, Ki67, red). Jag1, a ligand for Notch1 which was shown in development to drive myocardial-mediated Notch1 signalling, was observed between E10.5 and E12.5 (**Figure 3.11E-G**, arrows). This expression profile replicates the findings of D'amato et.

al., 2015 (**Figure 3.11A**), and validates the N1ICD and Jag1 antibodies for use in investigating their role in the post-MI setting.

The post-MI analysis began with analysing Notch components known to be expressed and active in endothelial cells during development (Niessen et. al., 2008). Receptors analysed were Notch1 and Notch4, ligands investigated were Dll1, Dll4, Jag1, and Jag2, and the transcription factors, Hes1, Hey1, Hey2 and HeyL were considered due to their downstream activation through Notch. With the antibodies tested, reliable expression of Notch1, Dll4, Jag1, Hes1 and Hey1 was observed, which is described below.

Notch1 ligands Dll4 and Jag1 have both been shown to activate endocardial Notch1 during developmental trabeculation and compaction (D'amato et. al., 2015). Dll4 expression was observed in the endocardium at days 2, 5 and 7 post-MI (**Figure 3.12A-F**) and was restricted to remodelling regions (**Figure 3.12B,D,F**, arrows). Endomucin (green) labelled the endocardium and co-expression was clearly shown by yellow regions (**Figure 3.12A,C,E**, yellow arrows). Jag1, was observed in cardiomyocytes beneath the endocardium in remodelling regions at days 5, 7 and 14 post-MI (**Figure 3.12G-J**, arrows). These findings appeared to depict the developmental signalling pattern which switches from being driven by endocardial Dll4 at early stages to initiate trabeculation, to myocardial Jag1 at later stages to induce maturation and compaction (**Figure 3.10A**, D'amato et. al., 2015). Minimal expression of Dll4 and Jag1 was observed in sham hearts (**Figure 3.11K-L**).

The presence of the activated receptor, N1ICD was also investigated and endocardial expression was observed at 24 hours, 2, 4 and 5 days post-MI (**Figure 3.13A-H**, arrows).The endocardium was labelled by endomucin (green) and clear coexpression was observed in remodelling regions with cells appearing yellow/white (**Figure 3.13A,C,E,G**, arrows) due to the combination of all three colours, indicating nuclear N1ICD expression in endocardial cells. This expression pattern was localised to regions of endocardial projections (**Figure 3.13D**), "fusion" of sub-endocardial lumina (**Figure**

3.13F) and the base of trabeculae (**Figure 3.13H**), suggesting that Notch1 may play an active role in endocardial remodelling post-MI. In contrast, expression of N1ICD in the uninjured adult heart was minimal (**Figure 3.13I**).

Hey1 and Hes1 are transcription factors activated by Notch1 in the endocardium during development (D'amato et. al., 2015) and antibodies for these proteins were used as the final tool to confirm Notch activity in remodelling endocardial post-MI. Hey1 was observed in remodelling regions of the endocardium at 24 hours, 2 and 4 days post-MI (**Figure 3.14A-F**, arrows) and appeared to be localised to the endocardium with co-expression of endomucin (green). High expression of Hes1 was observed in remodelling regions between 24 hours – 7 days post-MI (**Figure 3.14G-N**, arrows). Co-expression of endomucin and Hes1 (yellow/white cells) was observed in endocardial projections, sub-endocardial lumina and base of trabeculae at days 2-7 post-MI (**Figure 3.14I, K, M**), which matches the profile seen with N1ICD, supporting a role for Notch1 signalling in endocardial remodelling. Additionally, expression of Hes1 was observed in a pre-existing vessel at 24 hours (**Figure 3.14H**, red box), suggesting a possible role for Notch signalling in the pre-existing endothelial cell contribution to neovascularisation post-MI. Hey1 and Hes1 were not detected without MI (**Figure 3.14O, P**).

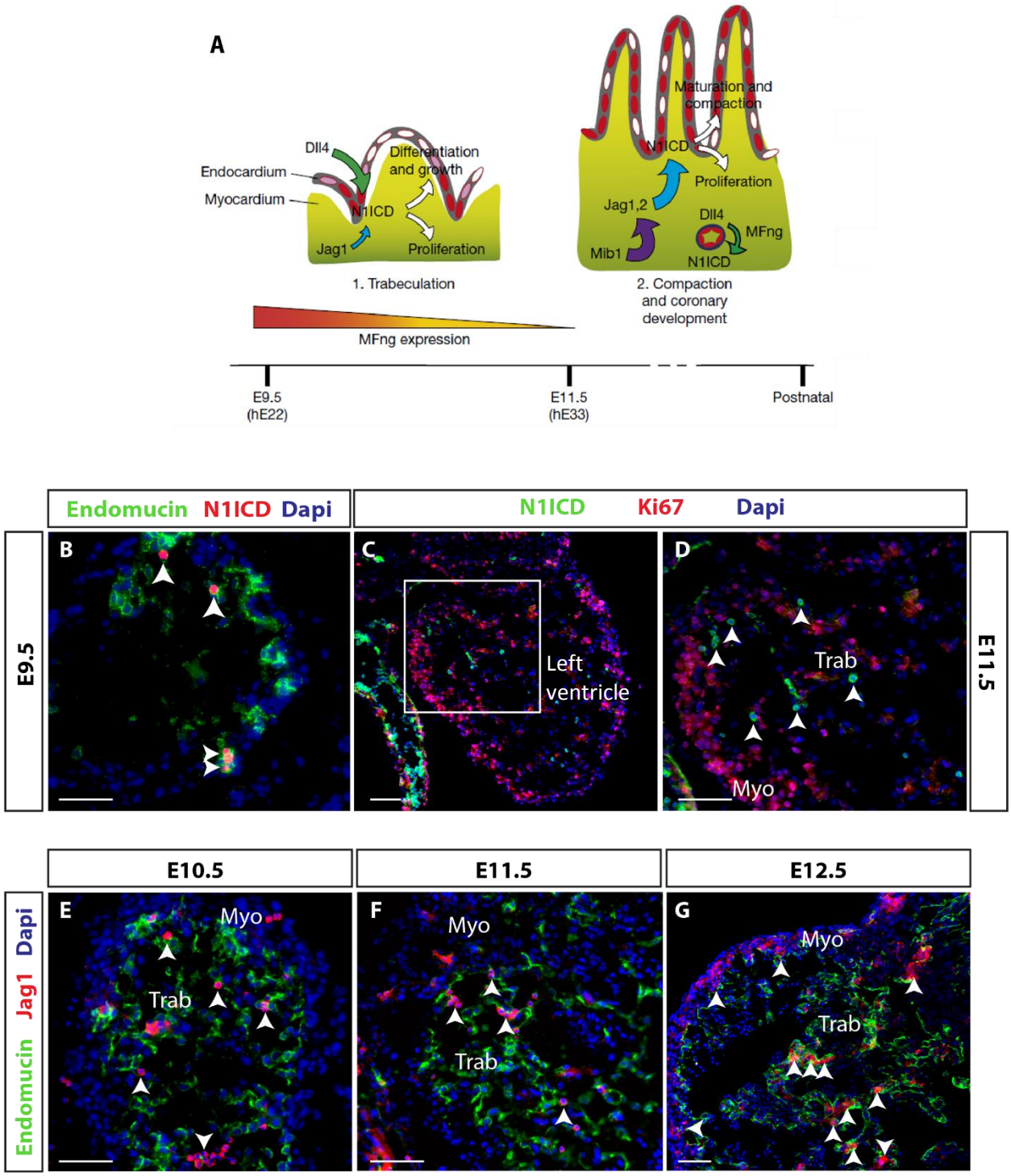

Figure 3.11. Notch signalling orchestrates trabeculation and compaction in the developmental heart

Notch1 signalling has been implicated in developmental trabeculation and compaction (A), *D'amato et. al. 2015,* and immunofluorescent imaging was used to confirm this in embryonic sections of the developing heart (B-G). N1ICD was observed in trabecular endocardium at E9.5 (B-D, arrows) alongside Ki67 expression (C, D) which demonstrates high levels of proliferation at this stage of development. Jag1, the ligand mediating Notch1 signalling from the myocardium at later stages of development (A), was observed at E10.5, E11.5 and E12.5 (E-G, arrows). This also served as validation for these antibodies prior to using them in the adult setting. *Scale bars: B, D, E, F = 20μm, C, G = 50μm. n = 2 per timepoint. Myo = myocardium, Trab = trabeculae.*

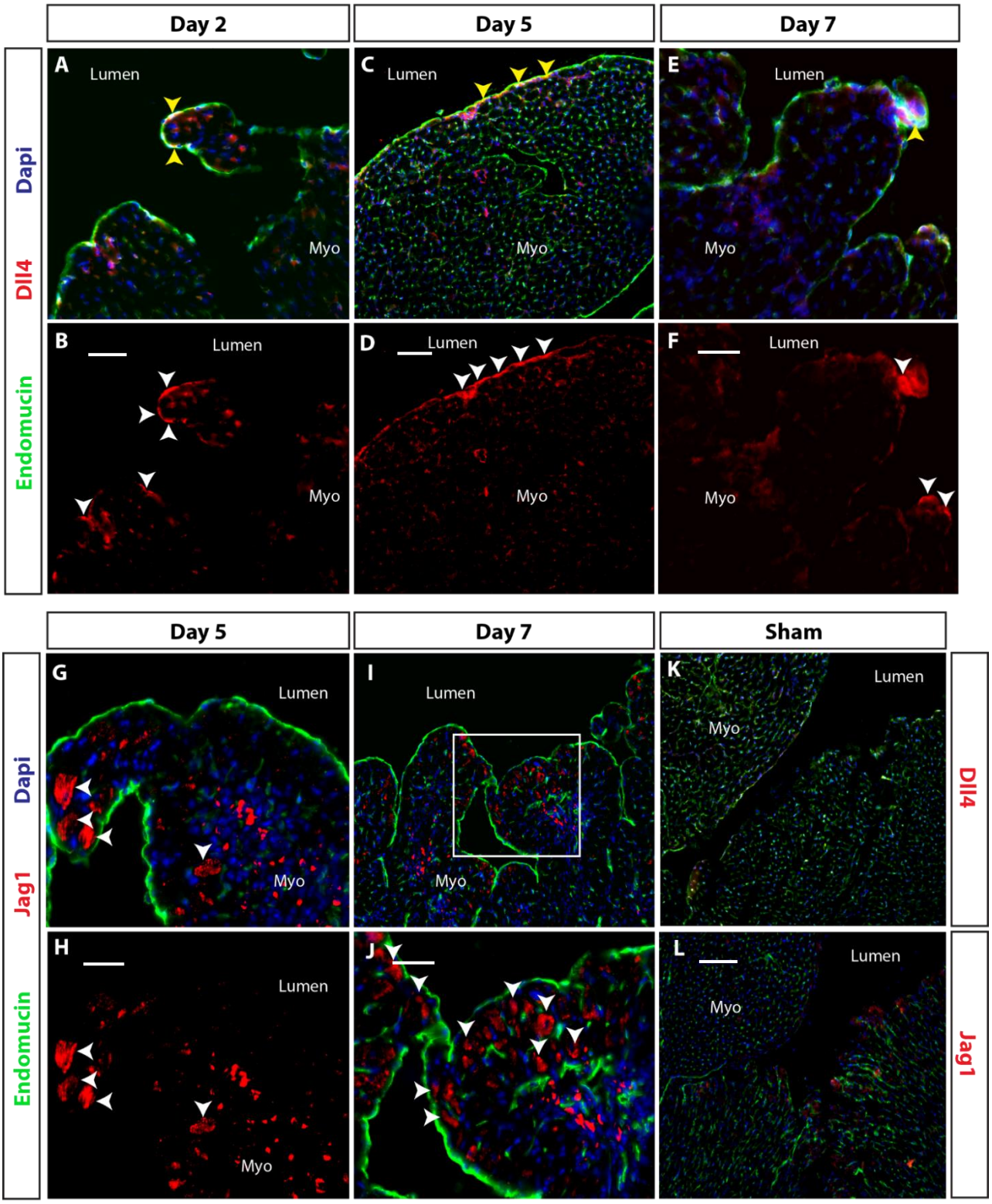

Figure 3.12. Expression of Notch pathway ligands in regions of endocardial remodelling post-MI

Dll4 (red), a ligand which activates Notch1 signalling in developmental trabeculation through endocardial signalling, was observed in remodelling regions of the endocardium at days 2, 5 and 7 post-MI (A-F, arrows), co-stained with green endomucin (yellow arrows). Jag1 (red) expression was observed in cardiomyocytes underlying the endocardium (endomucin, green) at later stages, days 5 and 7 post-MI (G-L, arrows) which fits with the developmental timeline of Notch1 mediated trabeculation and compaction. Panels (K,L) show that Dll4 and Jag1 expression in the sham heart is negligible. *Analysis of wild type hearts. Scale bars: A, E, G = 50μm, C, I, K, L = 100μm. n = 4 for d2, d7, n = 2 for d5, sham.*

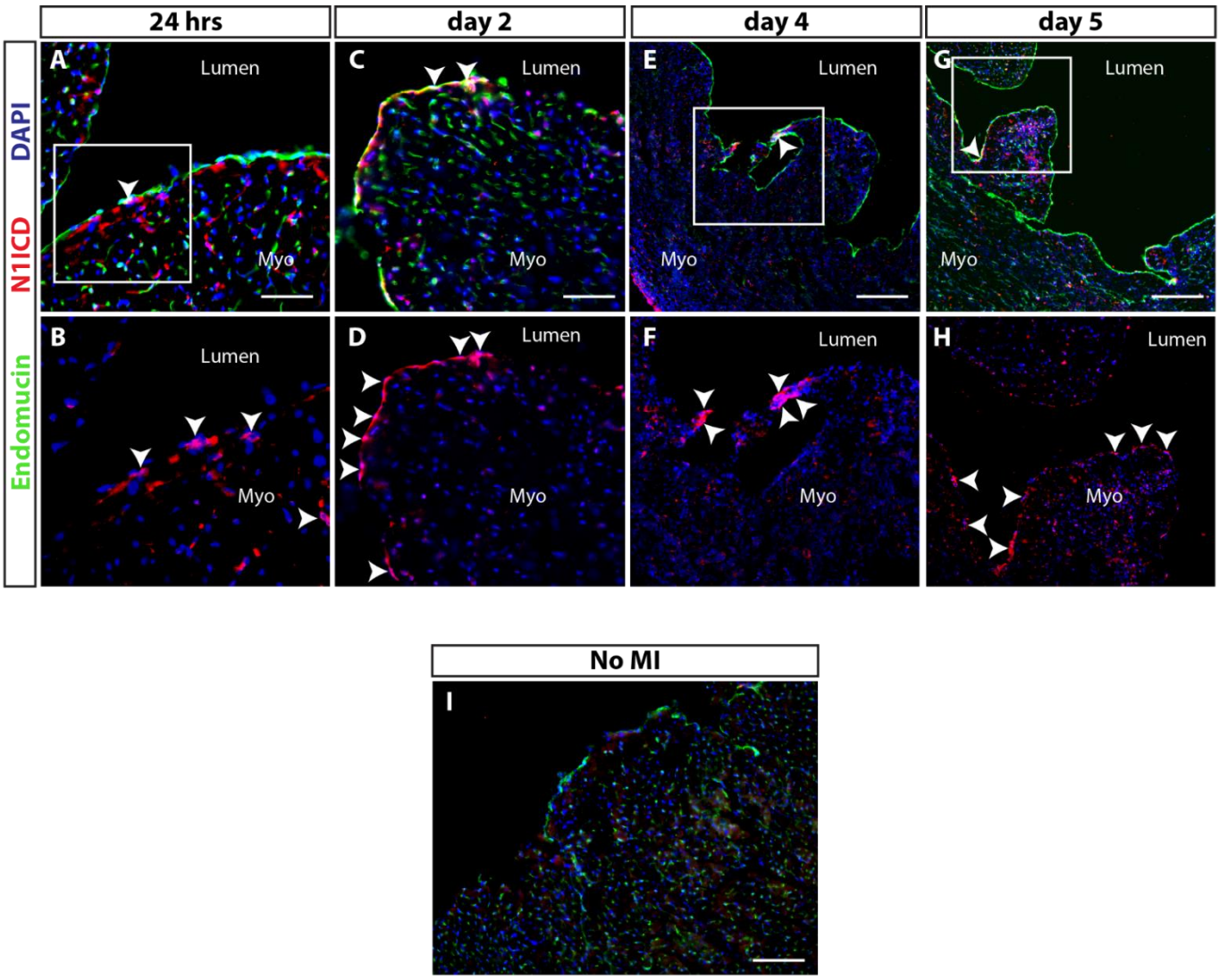

Figure 3.13. Expression of Notch1 intracellular domain in regions of endocardial remodelling post-MI

Notch1 activity was explored using N1ICD expression (red) as a readout and endocardial co-staining (endomucin, green) was observed in remodelling regions over a time course of 24 hours – 5 days post-MI (A-H, arrows). Insets in B, F, H show boxed regions in A, E, G respectively. Clusters were seen in the endocardium (B, D, arrows), areas of forming "lumina" (F, arrows), and at the base of trabeculae (H, arrows), suggesting a possible role for Notch1 signalling in endocardial remodelling post-MI. Panel (I) shows that there is no endocardial or sub-endocardial expression of N1ICD in the uninjured adult heart. *Scale bars: A, C - 50um, E, G, I - 200uM. n = 2 for 24hrs, d5, n = 4 for d2, d4.*

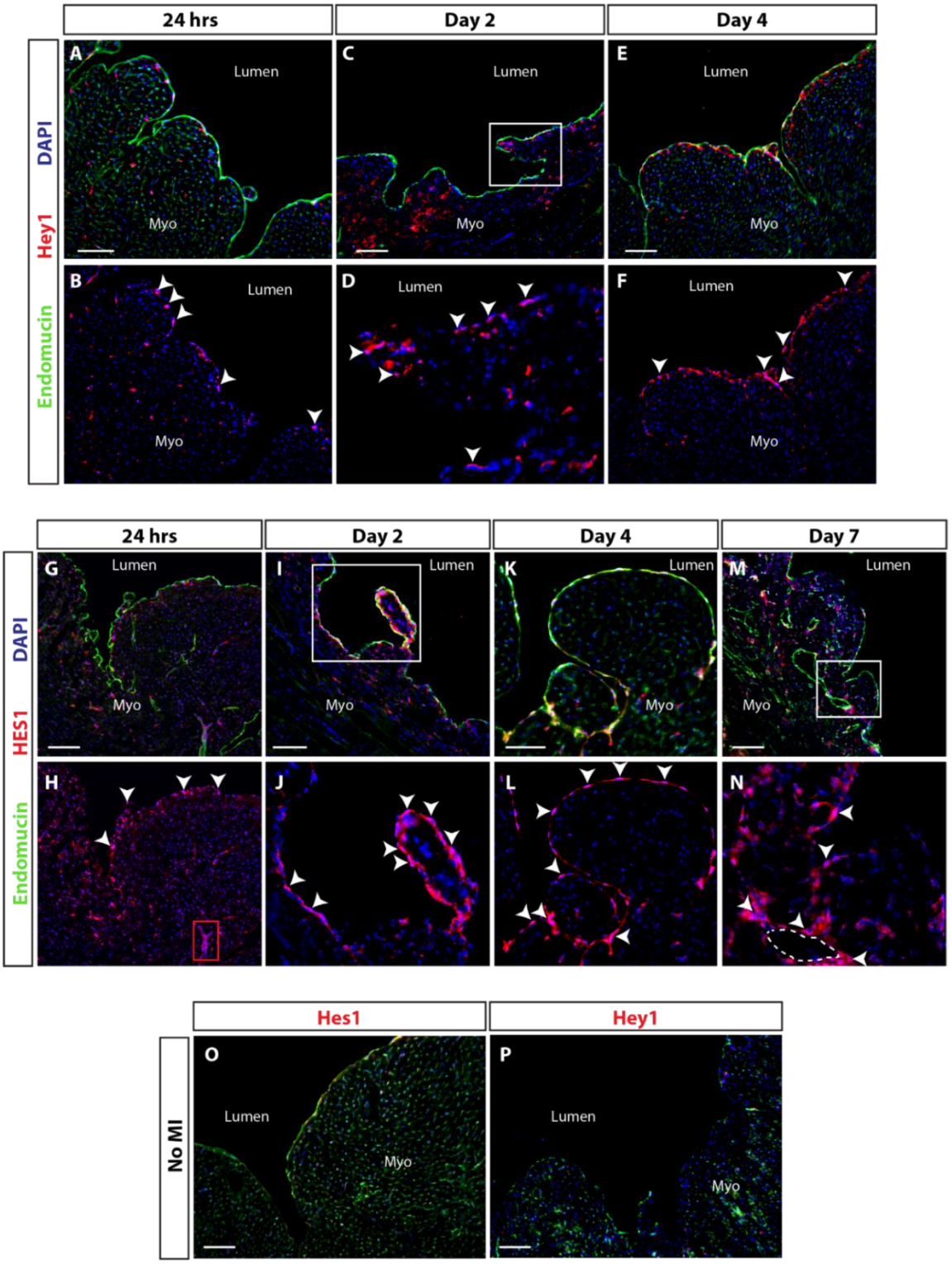

Figure 3.14. Expression of transcription factors downstream of Notch1 in regions of endocardial remodelling post-MI

Transcription factors Hes1 and Hey1, activated by Notch1, were investigated in regions of endocardial remodelling post-MI. Hey1 (red) was observed in the endocardium, co-stained by endomucin (green) at 24 hours, 2 days and 4 days post-MI (A-F, arrows). High expression of Hes1 was observed between 24 hours and 7 days post-MI, and appeared to be localised to the endocardium of remodelling regions (G-N). J and N show insets of boxes in I and M respectively. Expression was also seen in a vessel close to the endocardial surface at 24 hours (H, red box) and in an enclosed sub-endocardial "lumen" at 7 days (N, dotted line) post-MI. Panels (O,P) show minimal expression of Hes1 and Hey1 in the uninjured adult heart.

Wild type hearts analysed. *Scale bars: 100um. n = 2 for 24hrs, No MI, 4 for d2, d4.*

3.3.2 Notch signalling post-MI is orchestrated via endocardial Dll4-Notch1-HES1 interaction

In order to determine how the Notch1 ligands, receptor and transcription factors interact, it was necessary to detect either ligand-receptor expression in adjacent cells or co-expression of N1ICD and effector transcription factors in the same endocardial cell. Unfortunately, the availability of suitable antibodies prevented their combination. Instead, serial sections 12µm apart were used to examine the Notch1 pathway elements in the same remodelling regions. Expression of N1ICD and Hes1 was observed in the endocardium at 5 days post-MI (**Figure 3.15A-D**). In a remodelling region, arrows indicate apparent co-expression of N1ICD and Hes1 in endocardial cells (**Figure 3.15B,D**), although this cannot be conclusively determined with this technique.

At 7 days post-MI, Dll4 was observed in a remodelling region of the endocardium in cells that appeared to be adjacent to Hes1-expressing endocardial cells (**Figure 3.15E-H**, arrows). In addition to the immunofluorescence data, RNA Scope was used to label Hes1 and DLL4 at 2 days post-MI and RNA expression of the ligand (green) and transcription factor (red) was observed in adjacent cells on the same section (**Figure 3.15I**). This expression profile supports the theory that Notch1 signalling described in development is recapitulated in response to injury (**Figure 3.10A**, D'amato et. al., 2015), to drive endocardial remodelling and support neovascularisation.

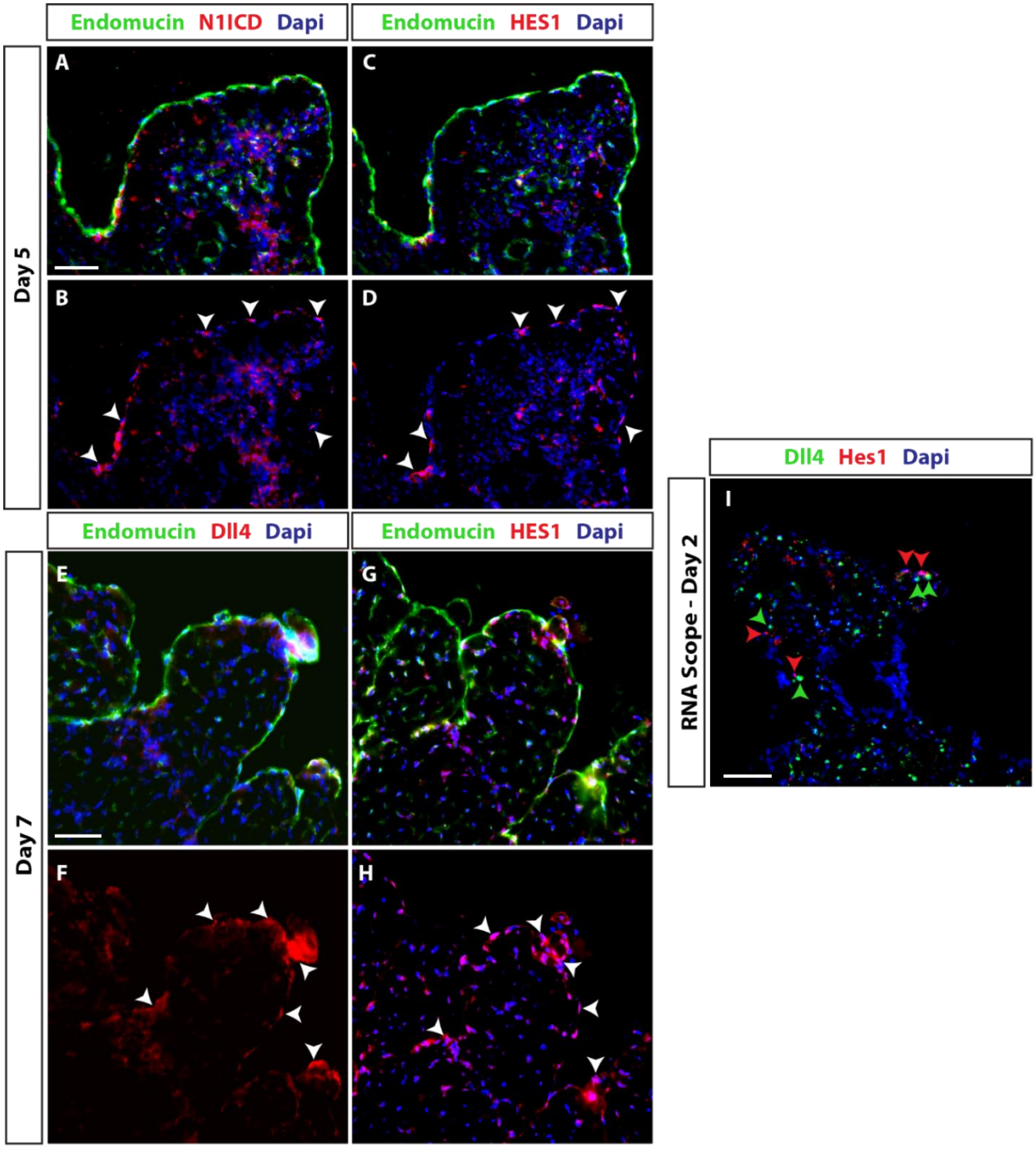

Figure 3.15. Combined components of Notch1 pathway in regions of endocardial remodelling post-MI

Antibodies raised in the same species were unable to be used in combination, so serial sections 12 µm apart showing the same region were used to identify signalling in adjacent cells. At day 5, N1ICD (red) (A, B) was observed in the endocardium, with coexpression of endomucin (green). In a serial section, expression of Hes1 (red) was observed in the same region (C, D), arrows in (B) and (D) indicate the cells showing expression of both the activated receptor and the transcription factor, demonstrating Notch1 signalling in endocardial cells at this stage. At day 7, the ligand, Dll4 (red) (E,F) was observed in the same endocardial region as Hes1 (red) (G,H), although in this case the expression appears to be in adjacent cells, which fits with mode of action of Notch1 intercellular signalling. RNA Scope allowed labelling of Hes1 and Dll4 in combination, which supports the protein expression pattern observed. (I) shows Hes1 RNA (red arrows) and Dll4 RNA (green arrows) in adjacent cells of the endocardium. *Scale bars: 50µm. N = 2 for d5, 4 for d7, 3 for RNA Scope.*

3.4.1 Isolation of endocardial cells from the adult mouse heart

Due to the challenges associated with targeting the endocardium specifically in the adult mouse heart, the *Pdgfb-Cre* model, which specifically labelled endothelial cells and not endocardial cells in the adult heart, was identified as a useful tool for separating endothelial and endocardial cells ex vivo. Isolating endocardial and endothelial cells from the same sample would enable a transcriptomic comparison, which could lead to the identification of specific markers of endocardial cells, and a better understanding of the differences between endocardial and endothelial cell behaviours through gene ontology studies.

A protocol was developed for isolating endothelial cells from the adult mouse heart, using uninjured adult hearts from the *Pdgfb;tdTomato* line, through the adaption of an isolation method described by Pratumvinit et. al., 2013. The full method is described in Chapter 2, but in summary, the ventricles were cut into <3mm pieces and incubated in a digestion solution for 45 mins at 37°C. Every 15 mins during digestion, dissociated cells were removed and the enzymes neutralised to prevent over-digestion. Fresh enzymes were then added to the remaining tissues, and returned to incubation. Once a single cell suspension was achieved, cells were counted and incubated with relevant antibodies, and then filtered for sorting by Fluorescence Activated Cell Sorting (FACS) (**Figure 3.16**).

A representative sorted sample is shown in **Figure 3.17A-D**. After optimisation, *Pdgfb-Cre* samples consistently produced approx. 1 million live cells, with mean 13% endothelial, and 1% endocardial cells isolated across 13 samples (**Figure 3.17E**). Live cells were gated using DAPI fluorescence; cells were not permeabilised meaning that any cells expressing DAPI were dead, as they were unable to extrude the dye (**Figure 3.17A**). CD31 was used to select endothelial and endocardial cells, and a haematopoietic lineage cocktail excluded non-endothelial cells that express CD31, such as macrophages (**Figure 3.17B**). TdTomato expression allowed isolation of $CD31^{+}tdTomato^{+}$ endothelial cells and $CD31^{+}tdTomato^{-}$ endocardial cells (**Figure**

3.17D). 12 samples were sent to our collaborators at the University of Cambridge who performed the RNA extraction in preparation for sequencing.

Unfortunately, the chosen method for RNA extraction did not recover enough RNA from the endocardial samples to generate sequencing libraries. These examples are shown in **Figure 3.18**, where the ladder represents the base pairs (**Figure 3.18A**) recorded for each sample and the graphs represents ribosomal RNA peaks (**Figure 3.18B-E**). The tdTomato negative samples (**Figure 3.18B-C**) showed no band on the RNA ladder, and no clear ribosomal peaks resulting in a calculated RNA integrity number (RIN) of 1, which indicated a low concentration of very degraded RNA. However, the endothelial samples (**Figure 3.18D-E**) produced RNA bands on the ladder, and clear ribosomal peaks which allowed an accurate calculation of the RIN for these samples. These values were 6.50 and 6.90, which suggests some possible RNA degradation, but sufficient RNA was isolated from these samples to create libraries for sequencing.

Since the aim of this experiment was to compare endocardial and endothelial cells, this was not followed up. However, the successful RNA isolation from endothelial samples validates the isolation and cell sorting method optimised, and this experiment may be repeated in future work with a suitable RNA isolation technique optimised for low cell numbers.

A summary table detailing the expression of all proteins considered in this chapter, the pathways or processes they reflect and the timing after infarction that observations were made is shown in **Figure 3.19**. The Notch signalling pathway and EndMT were identified as key processes from this exploratory analysis and were followed up in chapter 5.

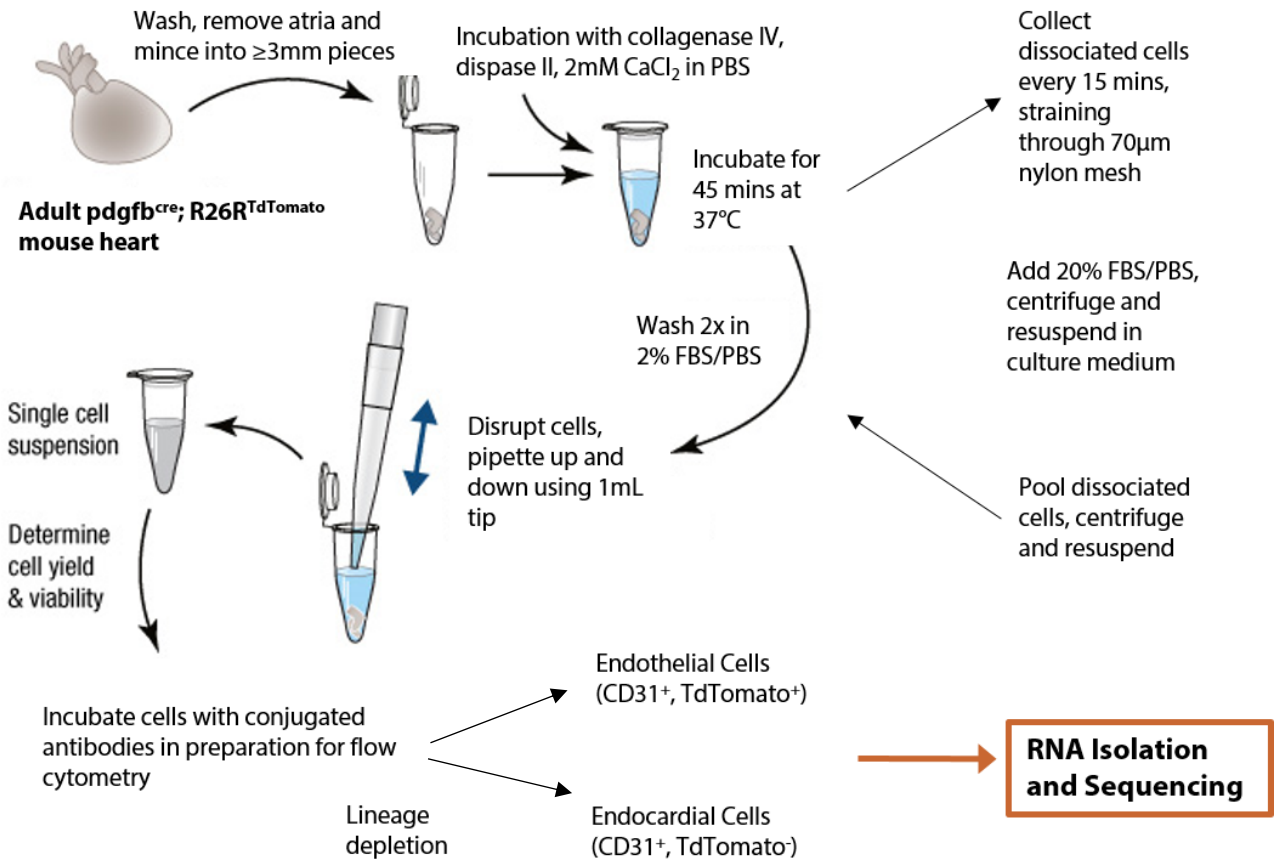

Figure 3.16. Optimised endothelial cell isolation protocol

Protocol adapted and optimised from Pratumvinit et. al., 2013 for isolation of endothelial and endocardial cells from adult mouse hearts in preparation for flow cytometry.

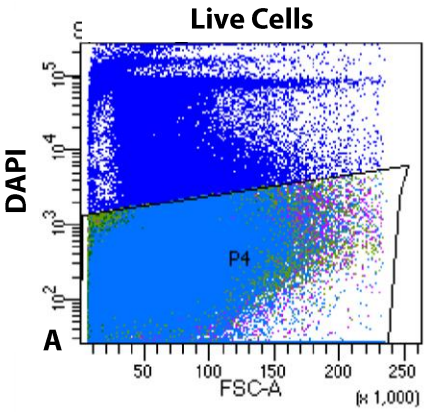

C

Population	Events	% Live Cells
P4 (Live cells)	938479	100
P5 (Lineage-)	871073	93
Endocardial	10401	1
Endothelial	87850	9

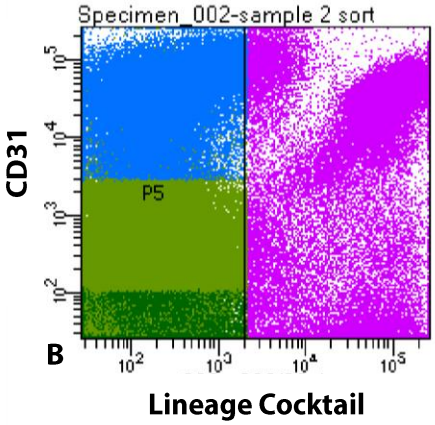

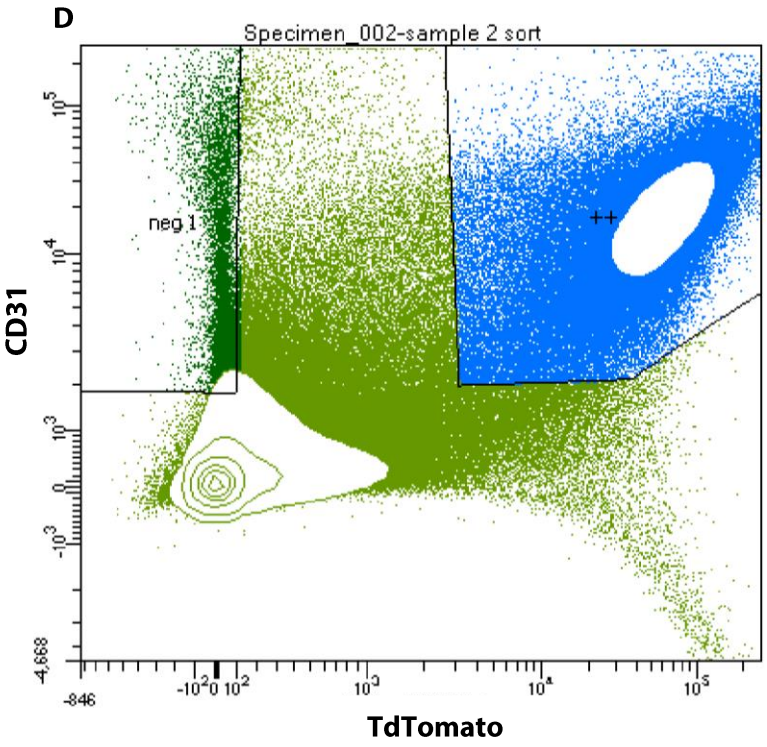

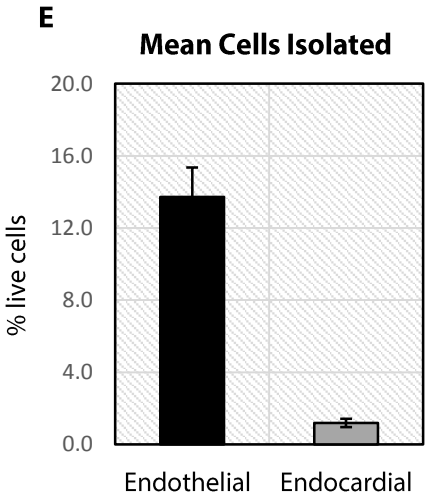

Figure 3.17 FACS data confirms isolation of endothelial and endocardial cells from *Pdgfb-Cre;tdTomato* hearts

A representative sample of multicolour flow cytometry data for a single cell isolation digested from a *Pdgfb-Cre;TdTomato* adult mouse heart, optimised to enrich endothelial/endocardial cells. Live cells were gated using DAPI fluorescence (A), then CD31 was used to identify endothelial cells, and a haematopoietic lineage cocktail was used to exclude non-endothelial cells expressing CD31 (B). TdTomato was used to distinguish between Pdgfb^{+} (endothelial) cells and Pdgfb^{-} (endocardial) cells (D), with 1% cells isolated TdTomato^{-} (endocardial), (dark green), with 10% cells isolated endothelial (blue). (E) shows the mean cells isolated as a percentage of total live cells for TdTomato^{+} (endothelial) (13% +/- 1.6%) and TdTomato^{-} (endocardial)(1% +/- 0.2%) populations. *n = 13.* Further validation by qPCR is required to confirm endothelial/endocardial cell profiles.

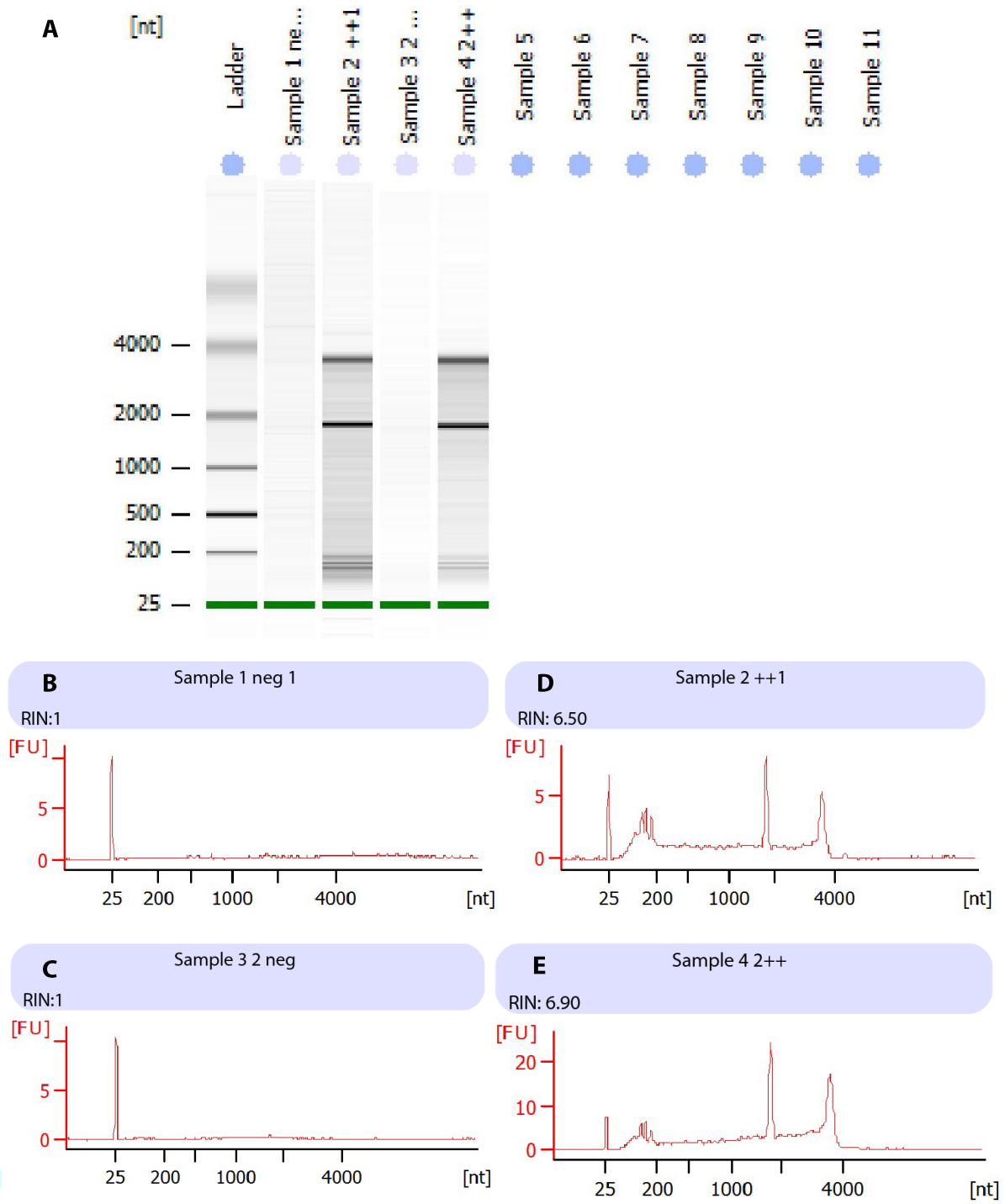

Figure 3.18 Bioanalyser data for RNA extracted from endothelial and endocardial cells

Representative samples showing RNA integrity from bioanalyser (A). RNA isolated from endocardial cells was of very low quantities and showed considerable degradation (B-C), and RNA isolation from endothelial samples achieved higher quantities of less degraded RNA (D-E). Endothelial, but not endocardial, samples were taken forward to make libraries for sequencing. *Representative of n = 12.*

Protein	Pathway/process	Location	Timepoint
Brg1	Trabeculation (BMP signalling)	Endocardium and sub-endocardium	d2 – d5
Nrg1	Trabeculation (ErbB2/4 signalling)	Endocardium	d2 – d7
PHH3	Proliferation	Subendocardium and infarct	24 hrs – d2
Ki67	Proliferation	Endocardium and subendocardium	d2 – d7
CD68	Inflammation and CV development	Endocardium and subendocardial lumina	24 hrs – d7
CD45	Inflammation and EndMT	Trabecular clusters	24 hrs – d7
SM-MHC	De novo neovascularisation	Sub-endocardium	d7 – d14
α-SMA	EndMT	Sub-endocardium	d7
Snail	EndMT	Endocardium, subendocardial vessels	d2 – d7
Dll4	Trabeculation (Notch signalling)	Endocardium	d2 – d7
Jag1	Trabeculation (Notch signalling)	Myocardium	d5 – d7
N1ICD	Trabeculation (Notch signalling)	Endocardium (trabeculae)	24 hrs – d5
Hes1	Trabeculation (Notch signalling)	Endocardium	24 hrs – d7
Hey1	Trabeculation (Notch signalling)	Endocardium	24 hrs – d4

Figure 3.19 Summary table of protein expression post-MI

Table summarising expression of proteins detected by immunofluorescent staining in post-MI wild type hearts. Notch signalling and EndMT were identified as the most important findings from this exploratory study and taken forward for further exploration.

3.5.1 Discussion

Lineage tracing endocardial cells in the adult is very challenging due to the lack of a suitable gene expressed specifically in the endocardium, and not in other coronary endothelial cells. Attempts were made to label the endocardium with developmental markers such as Nfatc1 and GATA4, but these are not expressed in the adult tissue. Recent evidence has suggested that Npr3 is specifically expressed in the adult endocardium and Bin Zhou's group have made use of an Npr3-CreERT2 to lineage trace endocardial cells (Zhang et. al., 2016). However, my attempts to label the endocardium with Npr3 antibodies were unsuccessful and whilst we have recently purchased Npr3-Cre mice for future studies, the availability of this model did not coincide with my DPhil project. Therefore, the most suitable model available at the time has been used for consideration of an endocardial contribution to neovascularisation.

The tamoxifen-inducible *PdgfbCreERT2* (Claxton et. al., 2008) model was used to label endothelial cells, and in the adult heart, the endocardium remains unlabelled. Pdgfb is also known to be expressed by other cells of the hemogenic endothelium lineage (Ulvmar et. al., 2016), and macrophages (Tomlinson et. al., 2018), however for this application recombination was induced in adulthood to prevent labelling of cells with a similar origin, and any labelled macrophages did not appear to affect the interpretation of results.

Whilst we can hypothesise that unlabelled vessels observed in the infarct region are derived from the endocardium, definitive evidence can only be provided by a positive endocardial-specific lineage trace. A previous study used inducible endothelial lineage tracing to show that 100% of vessels pre and post-MI are labelled by three different endothelial reporters *Cdh5CreER*, *AplnCreER* and *Fabp4CreER* (He et. al., 2017), concluding that there is no non-endothelial source for neovascularisation post-MI. However, the endocardium is labelled by all three of these traces, and the *pdgfbCre* model is the only system that does not label 100% of endothelial cells post-MI (Dubé et. al., 2017), which, by comparing conclusions of the respective studies, is supportive of an

endocardial contribution. In addition to this, a marker profile for sub-endocardial vessels was derived, alongside those of capillaries, veins, arteries and endocardium, with full overlap shown only between the sub-endocardial vessels and the endocardium. Both cell types were positive for endomucin and endoglin, and negative for Cx40-EGFP, VEGFR2 and *PdgfbCreERT2*, with veins being the most similar of the other vessels, showing weak expression of VEGFR2 (Dubé et. al., 2017). This profile, in combination with the "negative lineage trace" and contrasting pan-endothelial lineage traces is the most conclusive evidence of an endocardial contribution that can be provided with the current tools available. The possibility is further supported by the injury-induced remodelling reported which provides a mechanism by which endocardium can become internalised within the myocardium to form de novo coronary vessels, as discussed below.

A recent study used the Npr3-Cre model to lineage trace endocardial cells post-MI and they concluded that an increase in "endocardial tubes" was observed with infarction, which appear similar to the sub-endocardial vessels observed here. However, in their samples, maturation of endocardial tubes was not seen, and no smooth muscle support acquired (Tang et. al., 2018). The conclusion of this study was that endocardial cells minimally contribute to vascular endothelial cells in the adult heart, and traced endocardial cells were only observed to change fate to vascular endothelial cells in a PSSL model which forces entrapment of the endocardium. The disparity between the conclusions of Tang et. al. and our findings cannot easily be reconciled. However, at least two possible explanations exist. Firstly, Tang et. al. analysed a relatively small number of samples at a single time point, 21 days post-MI and, and half of these (n=5) were described to have a severe injury which, as discussed in Chapter 4, appears to inhibit trabeculation; moreover, in the frontal sections shown, only a small border zone region existed even in the moderate injury group where endocardium-derived vessels might have been detected. Secondly, we have concerns surrounding the heterozygous

deletion of Npr3, resulting from Cre knock-in to the endogenous locus. Npr3 has an established role in endothelial cell proliferation and vascular homeostasis, and possible involvement with EndMT post-MI (Pedram et. al., 1997, Khambata et. al., 2011, El Andalousi et. al., 2013). For this reason we have recently obtained Npr3-Cre mice from Bin Zhou to enable us to test, in our hands, the utility of the line, given the possibility of a role for Npr3 in neovascularisation post-MI, and to specifically target the endocardium if the model proves to be suitable.

Alongside characterising the Npr3-Cre model, further attempts will be made to optimise the RNA isolation from endocardial and endothelial cells isolated from *Pdgfb-Cre* hearts. The methodology for cell isolation and FACS was successfully optimised here, however the method used for RNA isolation was inadequate, involving Trizol reagent, due to our collaborators having experience primarily with high numbers of cultured cells. RNA extraction has been optimised within our group for isolation from low cell numbers, and this method can be utilised for use with small populations of sorted cells in future work.

The evidence provided for recapitulation of trabeculation and compaction post-MI is entirely descriptive, although extensive remodelling coinciding with appearance of sub-endocardial vessels, a response that is temporally induced post-MI, provides a convincing case for a similar process to ventricular morphogenesis in development. It would be beneficial to visualise the remodelling observed in sections using a 3-dimensional approach, to determine how the sub-endocardial vessels merge and whether they become incorporated with the coronary vasculature.

The phenomenon of hypertrabeculation induced in the adult heart is not entirely novel, as clinical studies have identified a mechanism involving increased cardiac preload such as during pregnancy, in patients with anaemia and highly trained athletes (Gati et. al., 2013). During pregnancy, 25% of women examined developed increased left ventricular trabeculations; when re-examined post-partum, 73% demonstrated complete resolution, with a further 19% showing a marked reduction in trabeculation (Gati et. al., 2014). When

considered alongside this model, the transient increase in trabeculation post-MI, may reflect a similar mechanism, with increased preload (left ventricular end diastolic volume) induced by injury. However, ensuing neovascularisation was not assessed in these studies, so further investigation is needed to determine whether these mechanisms are associated or independent. More specifically, these findings and ours, support the value of assessing whether endocardial remodelling occurs in human MI patients and if it appears to support neovascularisation.

The observation of support from α-SMA^{+} cells demonstrates the development of a more mature vessel phenotype post-MI, which was not observed by Tang et. al., 2018, and is not seen in the sub-endocardial region without infarction. Further investigation is required to determine the source of these cells and how migration is triggered. One possibility, that they may derive from the endocardium, via EndMT, will be further explored in Chapter 5.

Consideration was given to various signalling pathways and molecular mechanisms in an attempt to uncover the forces driving endocardial remodelling post-MI. Whilst inflammation was found to be present in regions of remodelling, this was not elaborated, but kept as a contingency option if the chosen lines of investigation proved redundant.

Similarly, whilst Brg1 has an important role during cardiac development in supporting the growth of cardiac jelly, this direction was also not prioritised due to the lack of literature on trabeculation post-MI, posing the question of whether an “adult cardiac jelly” exists. This line of investigation would require full exploration and characterisation of subendocardial matrix, before analysing alterations post-MI that may drive neovascularisation. Whilst this would be an interesting objective to follow up, Notch1 was deemed the most interesting target and prioritised.

Angiogenesis was considered due to its suggested role in neovascularisation post-MI, which has resulted in attempts to therapeutically target growth factors and promote

angiogenesis in the clinic. Unfortunately, these trials have proven unsuccessful (Simons et. al., 2002, Henry et. al., 2003), however consideration has recently been given for an endocardial contribution to angiogenesis in the injury setting (Miquerol et. al., 2015, Kobayashi et. al., 2017). Whilst we have seen expression of VEGFR2 in pre-existing vessels, this was not observed in the endocardium (Dubé et. al., 2017), suggesting that the endocardial contribution proposed here is not through angiogenesis. This, therefore may be a different process and mechanism entirely to that described by *Miquerol et. al., 2015* and *Kobayashi et. al., 2017*. The mechanisms proposed by these studies may also recapitulate development, but the embryonic contribution (E12.5-E14.5), via sprouting, rather than the perinatal contribution by trabecular compaction that we observed to be recapitulated in the adult.

Proliferation is another key process that drives coronary vessel development and although proliferating cells were observed in sub-endocardial remodelling regions, levels were much lower than in other regions of the heart (Dubé et. al., 2017). Therefore, whilst a role for proliferation cannot be excluded, particularly as only a few time points post-MI were analysed, the mechanism of trabeculation appears to be driven by morphological reorganization of the endocardial surface, rather than a primarily proliferative mechanism.

The expression of Nrg1 was investigated due to its role in trabeculation, and expression was identified in the endocardium of remodelling regions. Interestingly, Nrg1 activation is dependent on endocardial Notch1 signalling (Grego-Bassa et. al., 2007, VanDusen et. al., 2014), so whilst this mechanism was not followed up, reactivated Notch1 in endocardium post-MI is likely to impact Nrg1 signalling downstream. If these intrinsic developmental mechanisms are recapitulated in the MI setting, dysregulated Notch1 signalling may lead to impaired cell growth and migration downstream of Nrg1.

Evidence has been provided here to suggest that EndMT may be involved in neovascularisation post-MI, and while this process is well-established during the

development of valves and smooth muscle cells (Chen et. al., 2016) in the embryonic heart, there is currently no evidence to indicate reactivation in the adult. The localisation of α-SMA^{+} cells to the endocardium and sub-endocardial vessels is supportive of an endocardial source, however this cannot be concluded from the data provided. Lineage tracing is required to conclusively identify the source of these cells, although given the observation of Snai1 in the endocardium, a role for endocardial EndMT is of interest for further investigation.

Evidence has been provided here for recapitulation of Notch1 signalling in the post-MI setting. We hypothesise that the mechanism described as driving trabeculation and compaction in development (D'amato et. al., 2015) plays a similarly important role in neovascularisation post-MI. Endocardial Notch1 signalling in the embryonic heart is mediated by endocardial Dll4 at early stages, before switching to myocardial Jag1-mediated signalling later in development. Evidence for a similar process post-MI has been suggested here, with Dll4-mediated signalling to induce trabeculation 24 hours – 5 days post-MI, followed by Jag1-mediated signalling to activate compaction 7-14 days post-MI. In order to investigate the role of Notch1 signalling further in this context, endothelial-specific augmentation and attenuation of Notch1 signalling is required, which is described in further detail in chapter 5.

3.5.2 Conclusions

- The endocardium contributes to neovascularisation post-MI
- Sub-endocardial vessels are observed, some with SM-MHC^{+} supporting cells between days 7 and 14 post-MI
- Extensive endocardial remodelling takes place post-MI which may be reminiscent of trabeculation and compaction in the developing heart
- *Pdgfb-Cre;tdTomato* and FACS provide a suitable tool for isolating Pdgfb^{+} and Pdgfb^{-} endothelial cells ex vivo
- Some pathways involved in trabeculation and compaction post-MI are recapitulated in response to myocardial injury
- Notch1 signalling, in particular, appears to play a role in endocardial remodelling post-MI
- Endocardial EndMT may contribute mesenchymal cells to *de novo* sub-endocardial vessels post-MI

CHAPTER 4

RESULTS CHAPTER 2

Chapter 4

Results 2: Development of genetic models, analysis tools and surgical optimisations for investigating a role of endocardial Notch1 in neovascularisation post-MI

4.0 Introduction

In order to investigate the role of Notch1 signalling in neovascularisation post-MI, relevant genetic models were identified, and LAD ligation surgery optimised for use in these strains. Suitable analysis tools were then optimised to rigorously determine any effect of modulating Notch1 signalling in endothelial cells, on neovascularisation post-MI. The aims of this chapter were, therefore, to optimise the LAD ligation procedure, identify and validate quantitative methods to analyse infarct size and trabeculation, and generate endothelial-specific Notch1 LoF and GoF models to investigate the effect of modulating Notch1 signalling on pathological neovascularisation in the heart. It was hypothesised that endocardial trabeculation is a reparative response to MI in multiple mouse species, that the extent of trabeculation correlates with infarct size, and that endothelial-specific Notch1 LoF and GoF models are suitable for investigating a role for Notch signalling in the infarcted heart.

Permanent ligation of the LAD coronary artery is a procedure that is commonly used to induce symptoms that replicate clinical myocardial infarction and heart failure (Muthuramu et. al., 2014, Xu et. al., 2014). However, variability of coronary artery anatomy in mice can lead to variable infarct size when performing the LAD ligation procedure (Fernandez et. al., 2008, Chen et. al., 2017). Since these variables have been identified through operating on mice of the same strain, it is particularly important to

optimise the surgical procedure when working with new strains, especially when investigating a novel morphological observation. Endocardial remodelling observed in Chapter 3 was demonstrated in C57/BL6 wild type or *Pdgfb Cre* mice, and it was therefore important to validate the "trabeculation" phenotype in the *VE Cadherin-Cre* model, and to optimise the LAD ligation procedure in this strain to ensure consistent technique for Notch1 LoF and GoF studies.

The LAD ligation procedure is classified as "severe" by the UK home office, which results in regular checks for aseptic technique and opportunities to improve the procedure with support from veterinary services. The government is committed to the replacement, reduction and refinement (3 R's) of the use of animals in research, and refinements were made, where possible, during the development of an additional surgical set-up within the group. Surgical refinements introduced and strain-specific experimental optimisations are described in this chapter, alongside associated improvements in output.

An important factor to consider when optimising the LAD ligation surgery is how to reliably and accurately measure cardiac injury. Detection of fibrosis is the main method used to identify the extent of injury, and picrosirius red staining is well-established for labelling collagen in fibrotic tissue (Wittaker et. al., 1994, Colber et. al., 2009). Whilst this method is a useful and reliable tool for determining fibrosis in the infarcted heart, the optimal protocol involves embedding sections in paraffin and detection via bright field microscopy (Vogel et. al., 2015). Since the analysis shown throughout this thesis is reliant on immunofluorescent antibody staining of PFA fixed cryosections, picrosirius staining is not a compatible method for detection of infarction as co-staining of the same samples with detection of multiple markers using antibodies by these methods would not be possible. Therefore, consideration was given to other methods for detecting fibrosis in the infarcted heart. Wheatgerm agglutinin (WGA) has been used extensively as a cell surface and T-tubule stain (Savio-Galemberti et. al., 2008) and recently has been published for its benefits as a reagent to quantify cardiac fibrosis after MI (Emde, B et.

al., 2014). When compared with picrosirius staining, WGA was found to be useful for labelling cardiac fibrosis in cryosections, and also suitable for co-immunostaining with antibodies. Additionally, the study found that WGA staining could be used to reliably quantify the infarct size using analysis tools in ImageJ; WGA was therefore tested in *VE Cadherin-Cre* MI samples and consequently used as a method of analysing infarct size.

Endocardial remodelling, and specifically trabeculation, is a novel observation in the mouse post-MI heart, and determining the most suitable method for detecting and quantifying this is challenging. Whilst the endocardium of the adult heart is relatively smooth, free from perceptible projections except papillary muscles, when in its contracted state the heart has many endocardial folds which could skew an automated digital analysis, so it was important to identify a digital method to accurately recognise and quantify endocardial morphology. Clinical studies investigating endocardial remodelling and trabeculation through magnetic resonance imaging (MRI) have used fractal analysis to determine the complexity of the endocardium (Captur et. al., 2015, Lin et. al., 2016). Fractal analysis has become popular as a method of analysing patterns, due to its ability to reveal information that may not otherwise be apparent (Jelinek et. al., 2005). The method used to determine FD in the clinical endocardial studies is box counting, which is an approximation of the mathematically rigorous FD, applicable when analysing self-similar objects (Jelinek et. al., 2005). This method involves allocating boxes of various sizes to an image to determine the complexity of its pattern, by counting how many boxes of each size fit along the line of the pattern. When using this method it is important to ensure that the minimum and maximum box size, and the number of box sizes for each sample remains consistent. It is also important that the same scale is used for each image analysed. The clinical studies were able to effectively use this method to analyse the complexity of the adult endocardium, and conclusions were made such as trabeculation being influenced by race and/or ethnicity, cardiac loading conditions and comordities such as hypertension (Captur et. al., 2015). These data not only support our

rationale for investigating pathological endocardial remodelling, but also provide a useful tool for analysing trabeculation in post-MI samples.

As described in previous chapters, at the point of developing mouse models to investigate the effect of Notch1 signalling in the endocardium post-MI, there were no adult endocardial specific genes which could be used to drive targeting selectively via Cre. However, since developing the models for this project, the Npr3-Cre mouse was published to be endocardial-specific (Zhang et. al., 2016), and will be used for future experiments by the group to validate any phenotype observed here. From those tools available to target endothelial cells, the *Cdh5(PAC)*CreERT2 (referred to as *VE Cadherin-Cre* throughout) (Sorensen, 2009) is the most commonly used, and was provided by Ralf Adams. VE Cadherin is a cell-cell adhesion protein which is part of the cadherin family of proteins and present at intercellular junctions of endothelial cells (Corada et. al., 2001). The mouse model was developed to investigate Notch signalling in vascular development (Sorensen, 2009) and has been used in various developmental studies since (Deng et. al., 2013, Kasaai et. al., 2017), and a tamoxifen regime has been established accordingly for induction in embryonic mice. However, limited adult studies have been undertaken, and therefore optimisation was required to induce Cre recombination in the adult heart.

Suitable Notch1 loss- and gain-of-function models were identified to allow the study of Notch1 signalling for neovascularisation. The *Notch1*$^{loxP/loxP}$ mouse was developed by Radtke et. al., 1999, to investigate the role of Notch1 in T-Cell fate, and the exon encoding the signal peptide of the Notch1 locus was flanked with loxP sites for deletion when combined with a suitable Cre. The *Rosa*^{Notch1} mouse was developed by Murtaugh et. al., 2003, to investigate Notch signalling in the pancreas, after studies had shown effects of losing Notch function, but a constitutive activation model was required to indicate when and how the Notch pathway acts in this setting.

The findings of this chapter provide the surgical, genetic and analytical tools to enable the investigation of a role for endothelial Notch1 signalling in neovascularisation of the post-MI heart, with the specific aim of trying to infer endocardial roles in this process.

4.1 Results

4.1.1 LAD ligation surgical proficiency was established

It was important to ensure full competence in the LAD ligation surgical technique, since there is variability with the method even by accomplished surgeons, due to anatomical and strain differences. The surgery had been established in the Riley group, and assistance during training was provided by Mala Rohling using the Riley equipment, before establishing a surgical set-up within our group. This provided an opportunity to improve and refine the surgical protocol and, in collaboration with the named veterinary surgeon, adjustments were made, which are described later in this chapter.

The final surgical protocol used for Notch1 LoF and GoF experiments is shown in **Figure 4.1**. The procedure was performed under strict home office guidelines and the full protocol is described in chapter 2. **Figure 4.1A** shows the location of the LAD coronary artery, the suture tied around the artery, and the resulting region of infarction, which can be visualised immediately by blanching of the tissue and later by the development of a scar. Samples were harvested between 2 and 14 days after the ligation procedure and hearts were fixed in 4% PFA, then sectioned in transverse orientation using a cryostat (**Figure 4.1A**). The surgical procedure was photographed with permission from the named animal care and welfare officer (NACWO) and is shown in images (**Figure 4.1B-J**). Mice were anaesthetised (**Figure 4.1B**), then administered with buprenorphine for pain relief, and suspended from a purpose-built platform at 45° (**Figure 4.1C**). This equipment contained two tubes, one to deliver, and one to scavenge isoflurane, which ensured a consistent dose of anaesthetic was administered via the nose cone. A fibre optic cable was inserted inside the cannula to illuminate the airway enabling visualisation

of the vocal chords and trachea. The cannula was inserted and attached to a ventilator which maintained breathing rate and isoflurane supply throughout the operation, the chest was shaved, and antimicrobial cleanser (HiBiSCRUB) was applied. Sterile cling film and sterile drapes were used to cover the animal and a small hole was cut to allow access to the chest (**Figure 4.1D**). An incision was made at the midpoint between the upper and lower ribs, and muscle retractors were used to hold the muscles apart (**Figure 4.1E**). An incision was made in the 4th intercostal space to gain access to the chest cavity, pericardial fat was removed and the heart was revealed (**Figure 4.1F**). Since the LAD is mostly concealed in mice, the position and depth of the suture is determined based on knowledge of the anatomy and by surgical experience. Muscle retractors were used in place of rib retractors to secure the ribs, to reduce damage to tissue beneath. A size 8.0 ethilon suture needle was passed through the myocardial wall of the upper left ventricle, with care taken not to pass into the ventricle lumen. The suture was then secured, and blanching was observed if the ligation was successful (**Figure 4.1G**). The pericardial fat was replaced, and three individual stitches using a size 7.0 prolene suture secured the ribs (**Figure 4.1H**). A continuous stitch using a size 7.0 prolene suture was used to secure the skin (**Figure 4.1I**). The isoflurane dose was gradually reduced and the mouse recovered in an incubator set to 32°C. Animals were monitored every 12 hours for the first 48 hours after surgery, and daily thereafter. Additional analgesic was administered if required. Samples were harvested at the required time point and a scar was observed in hearts that had a clear infarction (**Figure 4.1J**).

Due to known variability with LAD ligation surgery, the procedure was compared across strains, and endocardial remodelling examined. **Figure 4.2** shows examples from five strains at various time points post-MI to demonstrate that trabecular projections occur in multiple strains after infarction. The infarct region of each heart is indicated with a dotted line and was visualised by reduced DAPI staining (**Figure 4.2A-E**). White arrows highlight endocardial projections, with the papillary muscles indicated by red asterisks

and the septum, which separates the right and left ventricles, labelled accordingly (**Figure 4.2A-E**). An example of the *pdgfb-Cre* strain at 2 days post-MI shows that trabecular projections are induced at an early stage in response to injury (**Figure 4.2A**), which was expected as samples from this strain were used for most of the observations in Chapter 3. The *VE Cadherin-Cre*, which was used to target Notch in the endothelium also responded by 2 days post-MI with clear endocardial projections overlaying the infarct region (**Figure 4.2B**). The *CBF:H2B-venus* strain, which will be introduced in Chapter 5, is shown here at 4 days post-MI, with a large infarct and endocardial projections overlaying the entire ischemic region (**Figure 4.2C**). This heart in particular, is unusual, as projections were not observed on the septal side of most infarcted hearts, however, this large injury induced endocardial remodelling on both sides of the left ventricle. The Notch1 LoF and GoF strains are shown at 7 days post-MI and both showed endocardial projections overlaying the infarct region (**Figure 4.2D,E**). The morphology and number of projections observed in these strains will be discussed further in Chapter 5, however the preliminary data here support the use of *VE Cadherin-Cre* to target Notch1 signalling in endocardium, as well as coronary endothelium, post-MI. These data provide validation of the surgical procedure and technical competency achieved in preparation for the LoF and GoF studies.

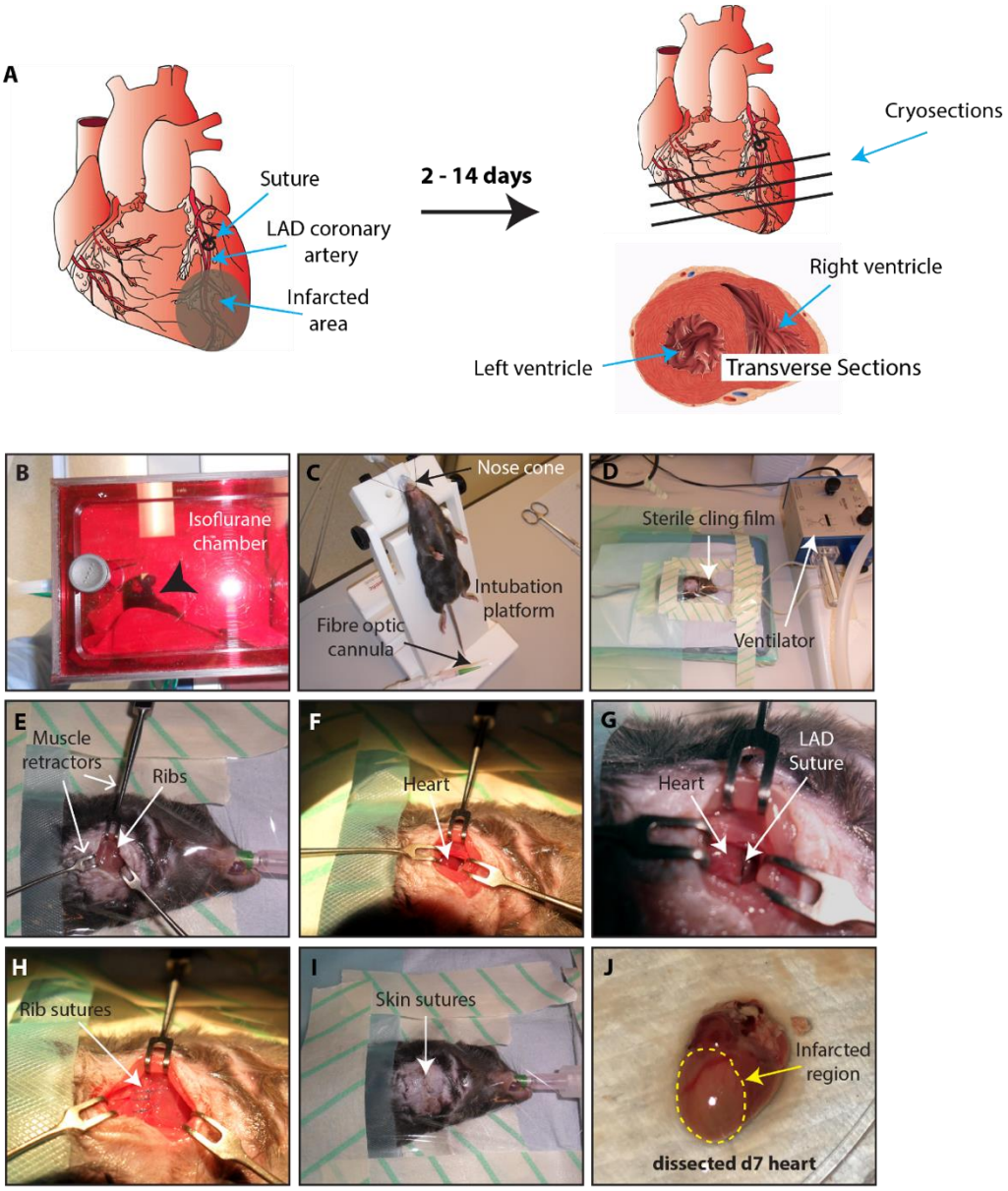

Figure 4.1. Schematic and images of refined LAD ligation surgery protocol

LAD Ligation surgery was performed under strict home office guidelines. Schematic (A) shows location of left anterior descending (LAD) coronary artery, suture, and resulting region of infarction (left ventricle). Samples were harvested between 2 and 14 days after the ligation procedure and hearts were fixed in 4% PFA, then sectioned in transverse orientation using a cryostat. The surgical procedure was photographed and is shown in images (B-J). In brief, mice were anaesthetised (B), then administered with buprenorphine for pain relief, and suspended from a platform for intubation using a fibre optic cable inside a cannula (C). Cannula was attached to ventilator which maintained breathing rate and supply of isoflurane, chest was shaved, hibiscrub applied and mouse was adhered in place on heat mat (D), sterile cling film and sterile drapes were used to cover the animal and a small area remained open for access to the chest. An incision was made approximately halfway between upper and lower ribs, and muscle retractors were used to hold muscles apart (E). An incision was made in the 4th intercostal space to gain access to the chest cavity, pericardial fat was removed and the heart revealed (F). A size 8.0 prolene suture was used to secure the LAD, and blanching was observed if ligation successful (G). Three individual stitches using a size 7.0 prolene suture were used to secure the ribs (H) and a continuous stitch using size 7.0 prolene stitches secured the skin (I). The isoflurane dose was reduced gradually and the mouse recovered in an incubator set to 32°C. An example d7 post-MI heart is shown (J) with the scarred region indicated.

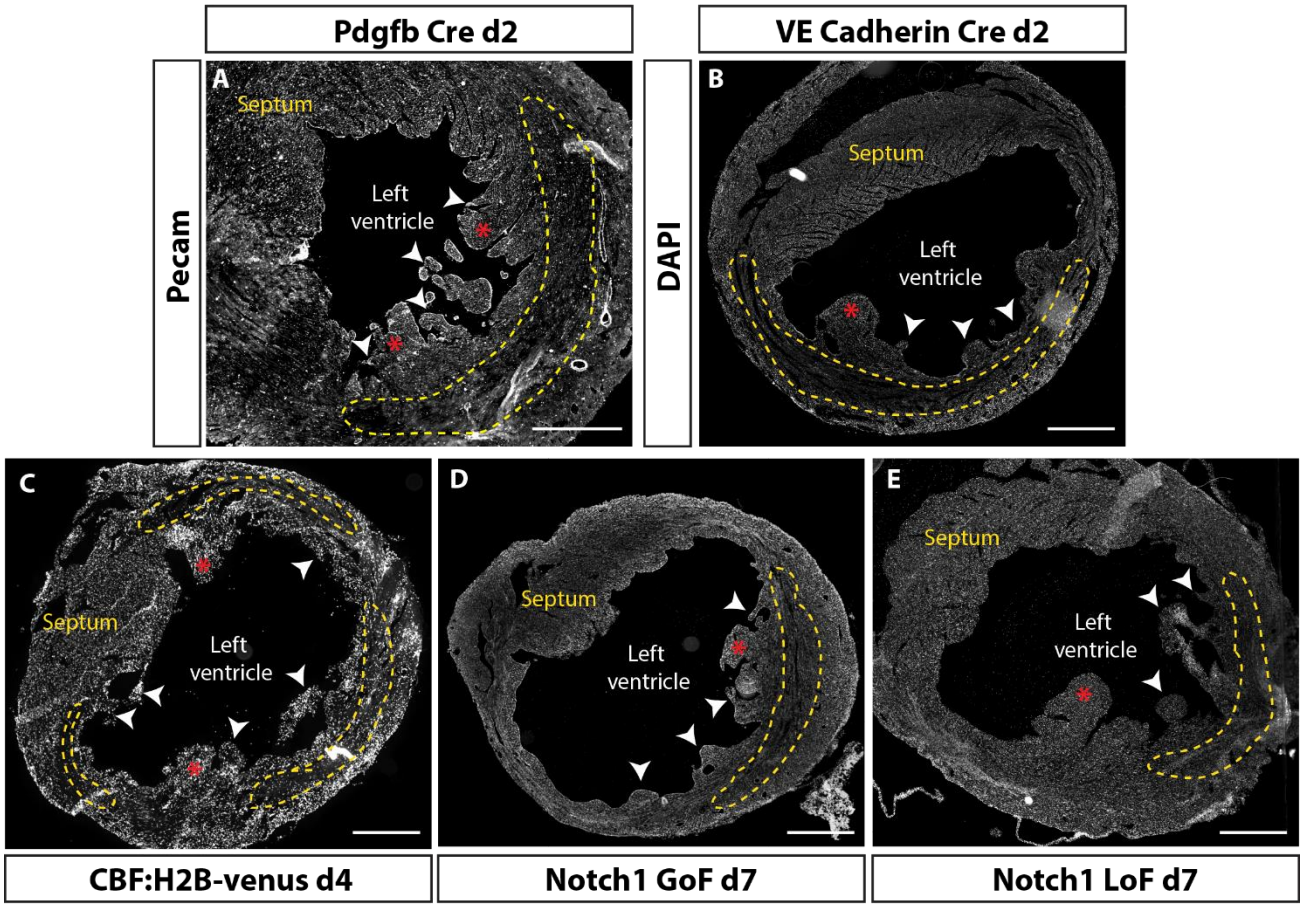

Figure 4.2. LAD ligation induces endocardial projections in multiple strains

LAD ligation was performed on five different mouse strains and endocardial projections were observed in all. The dotted yellow line indicates the infarct (A-E), white arrows indicate endocardial projections (trabeculation), red asterisks show papillary muscles which are present in all adult hearts. (A) shows *pdgfb*^{CreERT2};*TdTomato* at 2 days post-MI, (B) is *VE-Cadherin*^{CreERT2};*TdTomato* at 2 days post-MI, (C) is *CBF:H2B-venus* model at 4 days post-MI, (D) is *GtRosa26*$^{(Notch1)}$;*VE-Cadherin*^{CreERT2} at 7 days post-MI and (E) is *Notch1*$^{fl/fl}$;*VE-Cadherin*^{CreERT2} at 7 days post-MI. Endocardial projections (arrows) are localised to the endocardial region overlaying the infarct which in most cases is not on the septal side (labelled), except in (C), where the infarct extends to the septal side of the ventricle. *Scale bars = 1mm. n = 4 per strain.*

4.1.2 Refinements and Optimisations of LAD ligation protocol

As mentioned, there were several optimisations and refinements made in collaboration with veterinary services during the establishment of the surgery within the group, and these are summarised in **Figure 4.3A**. The first recommendation from the veterinary surgeon was to improve aseptic technique, and the refinements introduced to support this were: sterilisation of tools between animals, rather than washing between animals and sterilising between cages, use of fresh sterilised gloves for each animal, and use of secure sterile drapes to cover the animal throughout surgery, with a small hole for surgical access. Next, there was a recommendation to stabilise anaesthesia, and this was initiated with the use of a new intubation platform which allowed two tubes to connect to the nose cone, permitting isoflurane to be carried in and scavenged away during intubation. The final suggestion was to improve the intubation methodology and this was also achieved with the new intubation kit, which allowed the position of the head to be adjusted easily, and provided an LED and fibre optic cable to illuminate the airways for improved visibility. The new intubation protocol also allowed this part of the procedure to be performed without a microscope, which reduced the time needed to adjust the microscope between various steps of the surgical procedure.

In addition to the general refinements, it was also necessary to make strain-specific optimisations due to the high dose of tamoxifen required to induce recombination of the *VE Cadherin-Cre*. Initially the LAD ligation surgery was performed 3 days after the last tamoxifen injection, however, this cohort did not respond well to the combination of recent tamoxifen, buprenorphine and isoflurane, and respiratory difficulties were observed, resulting in increased mortality rate. A review of the literature confirmed known interactions between tamoxifen and opiates that contribute to respiratory depression (Huh et. al., 2012, Whithey et. al., 2017), therefore optimisations were trialled and introduced to the protocol to improve survival rate for subsequent cohorts (**Figure 4.3B**). The final refinements incorporated a minimum of 10 days break after tamoxifen

treatment, prior to the LAD ligation, a reduction in the rate of isoflurane provided during the procedure, whilst close monitoring was undertaken to ensure adequate anaesthetisation, and administration of the buprenorphine in two parts: 50% before the procedure and 50% after. Animals were then closely monitored and provided with additional analgesia post-operatively for 48 hours.

The effect of these optimisations was monitored and is shown in **Figure 4.4**. Cohort 1 was performed prior to the strain specific optimisations, and each cohort thereafter was performed with incremental optimisations, with the final protocol (from **Figures 2 & 3)** reflected in cohort 4. Survival rate improved from 35% to 72% (**Figure 4.4**, green), validating the benefit of the optimisations made. MI success was measured as a % of those survived (**Figure 4.4**, purple), and was relatively consistent (between 62% and 75%) but with the 3rd and 4th cohorts showing most success (72% and 75%, respectively). These results validate both the surgical technique and the improved equipment, and most samples analysed for the Notch1 study were obtained in cohorts 3 and 4 to ensure findings were consistent.

A

Recommendation	Refinement
Improve aseptic technique	Sterilise tools between animals Sterile gloves replaced between animals Secured sterile drape to cover animal Small hole in transparent sterile drape for surgical access
Stabilise anaesthesia	Intubation kit containing nose cone for anaesthesia delivery and scavenging
Improve intubation methodology	Intubation kit containing platform with adjustable head positioning LED and fibre optic cable illuminates airway for enhanced visualisation

B

Strain specific difficulties	Refinement
VE Cadherin Cre High dose of tamoxifen combined with opiates causes respiratory problems	Additional 10 days to recover from tamoxifen injections Reduced isoflurane dose (1.5% during procedure) Buprenorphine administered 50% prior to procedure, 50% afterwards Additional pain relief provided post-operatively for 48 hours

Figure 4.3. Optimisations and refinements for LAD ligation surgery

(A) shows refinements to LAD ligation surgery in collaboration with veterinary services; refinements were introduced to improve aseptic technique, stabilise anaesthesia and improve intubation. (B) indicates refinements adopted in response to strain-specific challenges related to high tamoxifen dose required for Cre recombination.

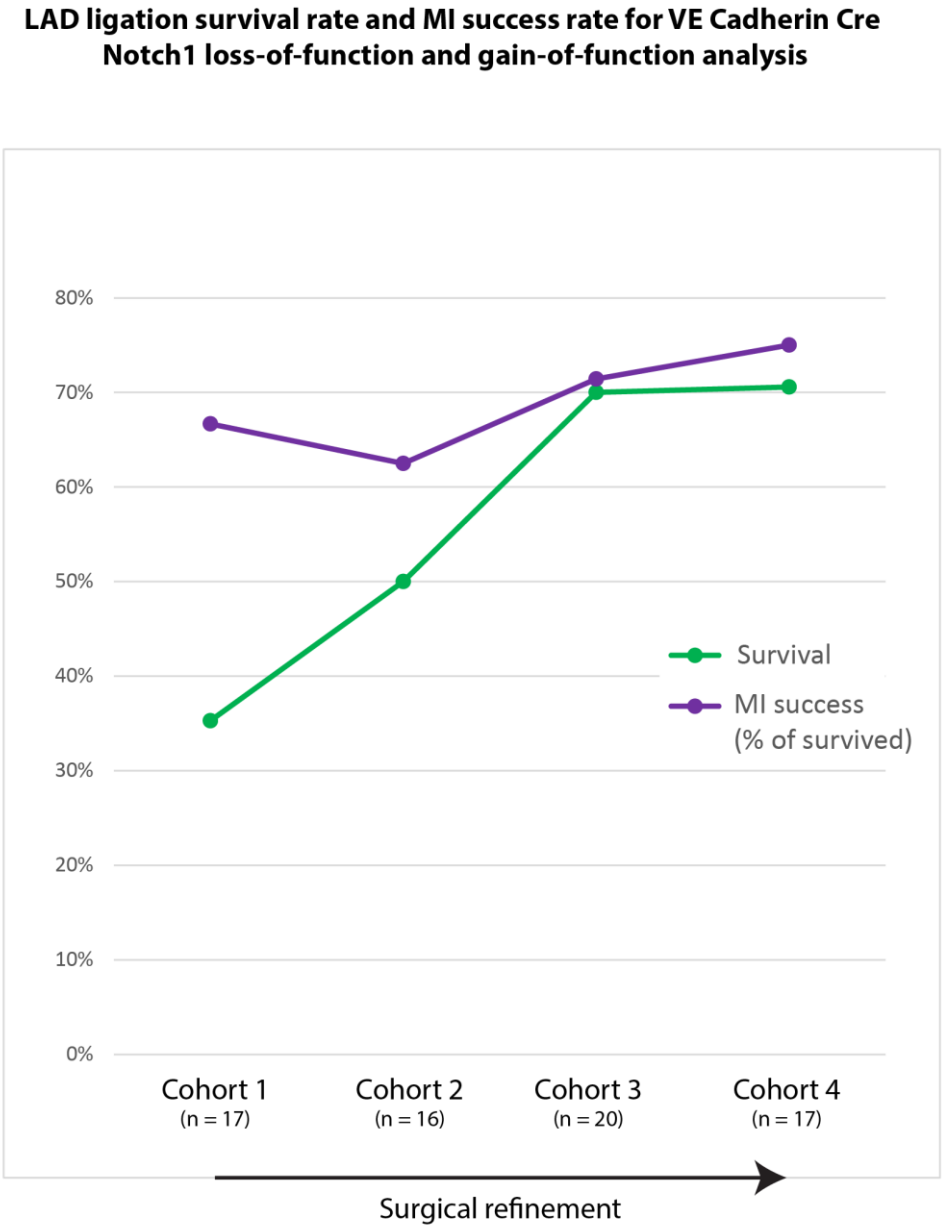

Fig 4.4. Effect of surgical refinements and procedure optimisation on survival rate and success of LAD ligation for gain-of-function and loss-of-function studies

Graph demonstrates percentage survival rate (green) and percentage that had a successful infarct (of those survived) (purple) in response to surgical refinements adopted over a 6 month period, as described in figure 4.3. Each cohort of mice had an n number of 16-20; the survival rate improved from 36% to 71% and the MI success improved from 67% to 75% over the course of 4 cohorts. This demonstrates the benefit of the refinements made, and improved consistency of surgical technique. *n = 70.*

4.2.1 Quantitative methods to determine infarct size and remodelling post-MI

Wheatgerm agglutinin (WGA) has been recently established as a marker of fibrotic tissue, which can be used to quantify the scar region in cryosections post-MI. WGA-Flourescein isothiocyanate (FITC) was applied to cryosections of day 7 MI hearts for one hour in combination with the secondary antibodies for immunofluorescence, and the fibrotic tissue was clearly labelled (**Figure 4.5A**, green). This example shows extensive neovascularisation in the infarct region, with vascular expansion labelled by TdTomato.

In order to quantify the area stained by WGA, ImageJ was used to auto threshold the images of individual channels, and the "analyse particles" tool was used to calculate the area. DAPI-autothreshold was used to calculate the total area of the left ventricle (**Figure 4.5B,D,F,H**, pink dotted line), and WGA-autothreshold to calculate the infarcted region of the left ventricle (**Figure 4.5C,E,G,I**). The percentage of WGA vs DAPI was calculated and this was used as a measure of infarct size. Examples are shown in **Figure 4.5B-I**, with uninjured (**Figure 4.5B,C**) and medium sized infarcts (**Figure 4.5D-G**) and large infarct (**Figure 4.5H-I**). This analysis was undertaken for day 7 and day 14 post-MI hearts and the results were plotted as a box and whisker chart in **Figure 4.5J**. The median infarct size at day 7 post-MI was 13.5% of the left ventricle, and at day 14 was 17.5% of the left ventricle. A range of 10-30% infarct size, which represents the majority of samples, was chosen for inclusion in the Notch1 LoF and GoF analysis in order to exclude outlying responses induced by extreme infarcts and to accurately model typical human MI.

Fractal analysis has been used as a method to determine the complexity of a pattern, and box counting is one form of fractal analysis that can be used to analyse shapes that are self-similar (Jelinek et. al., 2006). The FracLac plugin for ImageJ was used to perform this analysis on mouse heart sections post-MI. An example of this analysis is shown in a non-injured adult heart in **Figure 4.6**. Box sizes were set to a minimum of 2% of the total image size, and a maximum of 45% of the total image size. Percentages were used

instead of pixels to ensure that results were not affected by varying heart sizes or ventricle diameter. 20 sizes of box between 2 and 45% were allocated to each image, and the number of boxes fitting along the pattern was used in combination with the pixels detected per box to calculate the fractal dimension FD. Each image began as an immunostained whole heart (**Figure 4.6A**), which was used to create an autothreshold image, applying the same threshold limits every time. The image was then made binary and lined egdes detected using imageJ. All lines except the endocardium were removed from the image manually, and the remaining outline (**Figure 4.6C**) was run through the FracLac plugin with the relevant parameters set, as above. FracLac produced an image for each box count (x20 sizes, three examples shown in **Figure 4.6D-F**), and a summary of the box number and pixels which were used to calculate FD. The FD value is always between 1 and 2, and the more complex the pattern, the higher the FD. This analysis method was checked and parameters optimised to ensure an accurate representation of the remodelling observed.

Examples of post-MI endocardial traces, after 'autothreshold' and 'find edges' were applied to DAPI stained samples, are shown in **Figure 4.7A-C**. A correlation calculation was undertaken between infarct size (% WGA/DAPI from **Figure 4.5**) and trabeculation FD, analysis as described in **Figure 4.6**), and the results are plotted in **Figure 4.7D**. Endocardial traces shown in **Figure 4.7A, B and C** are indicated on the graph (**Figure 4.7D**), and trabeculation appears to correlate with infarct size up to an infarct size of 30%, after which there appears to be no trabeculation, consistent with visualisation of such sections, as in **Figure 4.7C**. This was confirmed by the calculation of a correlation coefficient which is shown in **Figure 4.7E**. When all samples were included in the calculation, the correlation coefficient was 0.11, indicating low correlation, however when only samples with an infarct size of 1-30% were included, the correlation coefficient was 0.92, indicating high correlation. This data supports the exclusion of samples with infarct size above 30%, as defined in **Figure 4.5,** for the Notch1 LoF and GoF analysis.

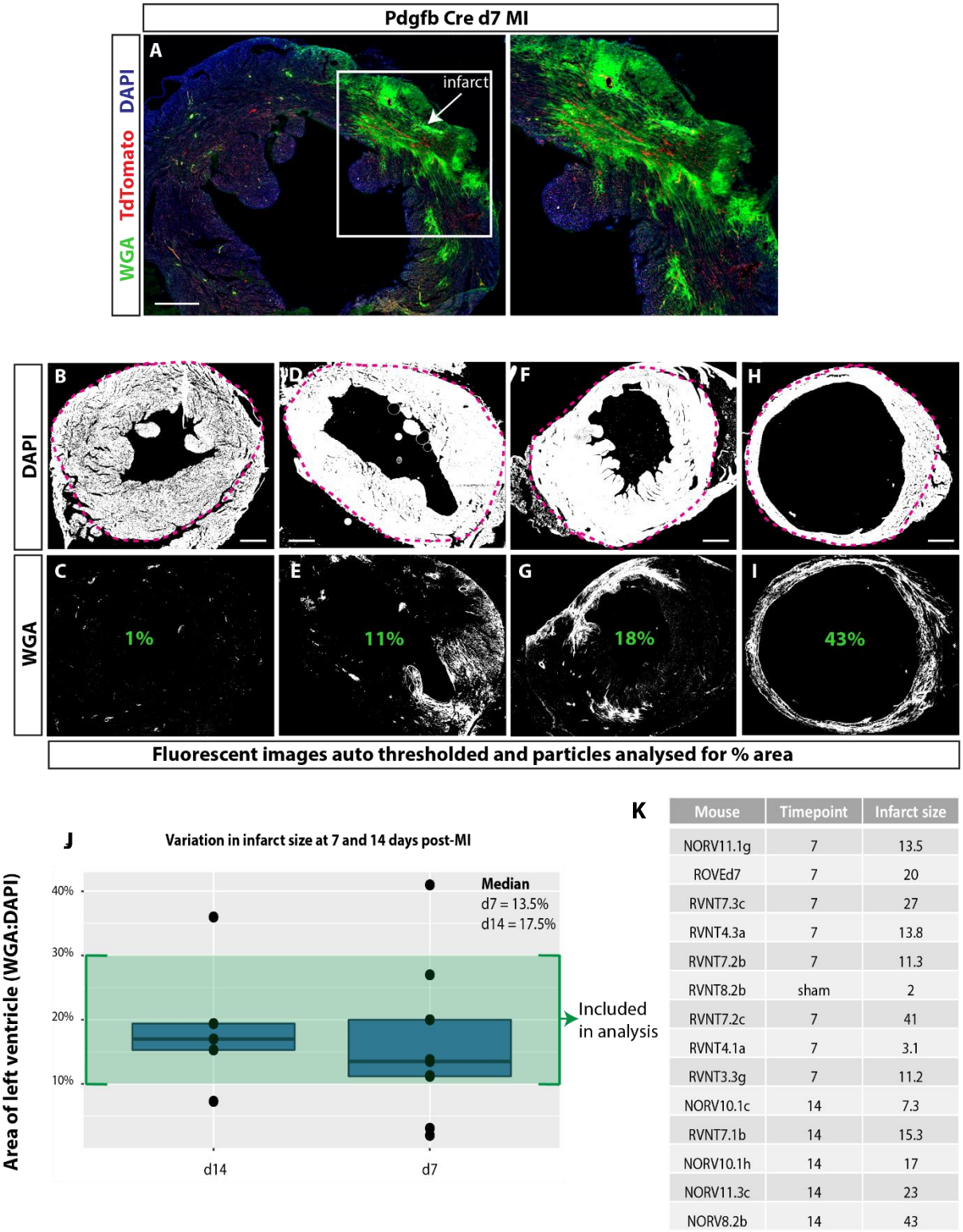

K

Mouse	Timepoint	Infarct size
NORV11.1g	7	13.5
ROVEd7	7	20
RVNT7.3c	7	27
RVNT4.3a	7	13.8
RVNT7.2b	7	11.3
RVNT8.2b	sham	2
RVNT7.2c	7	41
RVNT4.1a	7	3.1
RVNT3.3g	7	11.2
NORV10.1c	14	7.3
RVNT7.1b	14	15.3
NORV10.1h	14	17
NORV11.3c	14	23
NORV8.2b	14	43

Figure 4.5. Quantification of infarct size for loss-of-function and gain-of-function studies, using wheat germ agglutinin to label fibrotic tissue

WGA was used to label fibrotic tissue in the scar region, and provided a useful tool for quantifying the size of infarct (A, box, green labelling). ImageJ was used to auto threshold images of DAPI staining in sham (B-C) and infarcted hearts (D-I) and particles were analysed in left ventricle (B, D, F, H, pink dotted lines) to provide a measure for the ventricle area. The "auto threshold" was then used on the WGA staining of the left ventricle (C, E, G, I) and percentage area calculated by dividing the area of left ventricle WGA by the area of left ventricle DAPI. The variation of infarct size was plotted as a box and whisker diagram (J, data in K), with median infarct for day 7 and day 14 indicated. The green area of the graph shows the infarct size selected for analysis in chapter 5 as 10-30%. *n = 7 for d7, n = 5 for d14. Scale bars: A = 500μm, B-H = 1mm.*

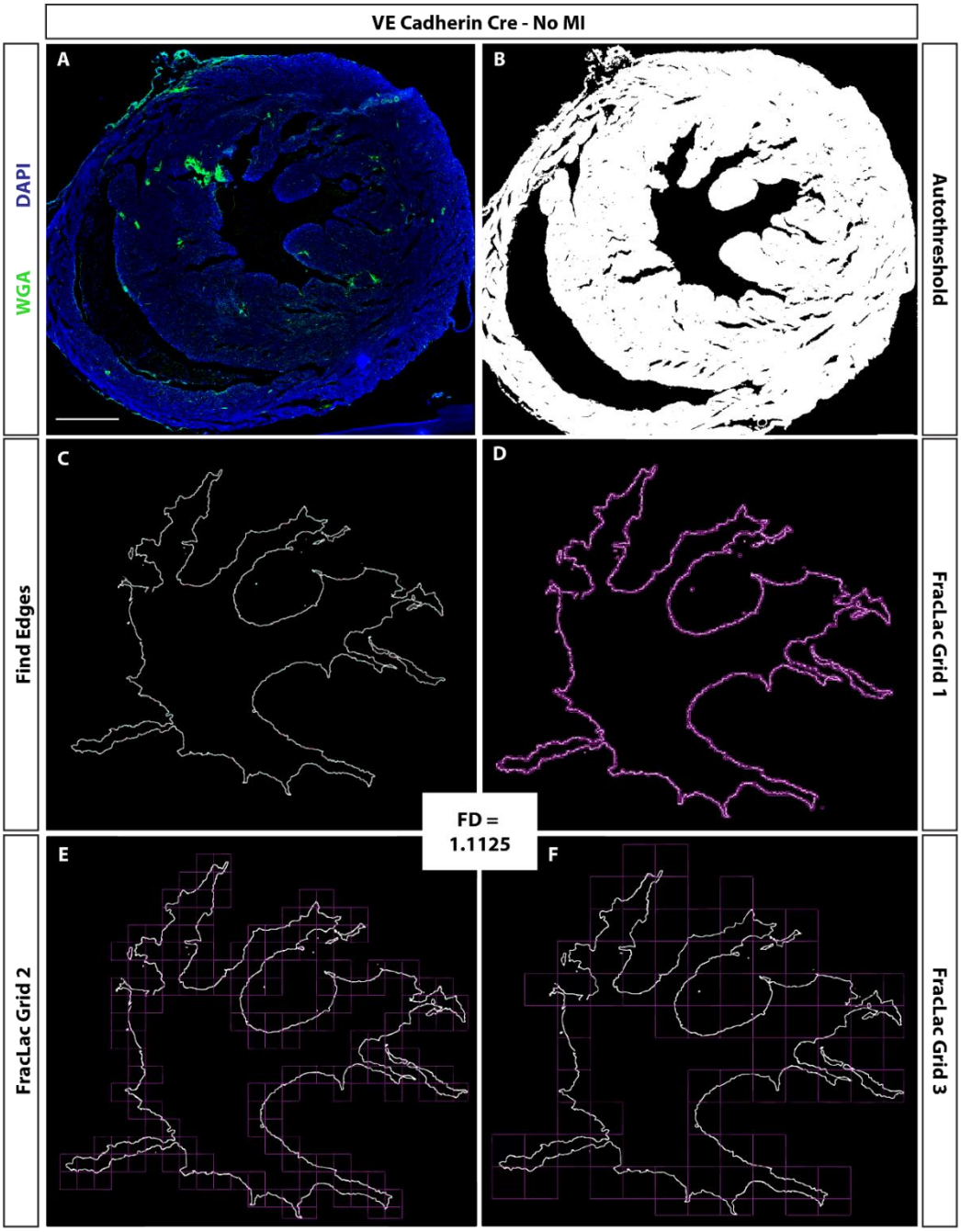

Figure 4.6. Fractal analysis as a method of automated quantification of trabeculation in transverse heart sections

Fractal analysis was used as a method to determine trabeculation post-MI. (A) shows DAPI and WGA immunofluorescent staining of an uninjured, adult heart. (B) shows the same image after the "auto threshold" tool was applied using imageJ. The "find edges" tool in imageJ was used to identify edges of auto threshold image, and all lines except the endocardium were removed (C). The FracLac plugin for imageJ was used to analyse the complexity of the endocardium in this image (D-F). Fractal dimension was calculated by allocating boxes of 20 sizes to the endocardial trace. The smallest boxes were 2% of the total image size (D) and the largest boxes were 45% of the total image size (not shown), with 18 sizes between 2 and 45% also allocated. The number of boxes that could be allocated to the endocardial trace for each box size was recorded, as well as the pixels contained per box, and these data were used to calculate the fractal dimension. A lower value for fractal dimension indicates fewer boxes/pixels, and less complexity; a higher value for fractal dimension indicates more boxes/pixels and more complexity. The scale was kept consistent throughout analysis to ensure accurate comparison. *Scale bar = 1mm. Representative of n = 3.*

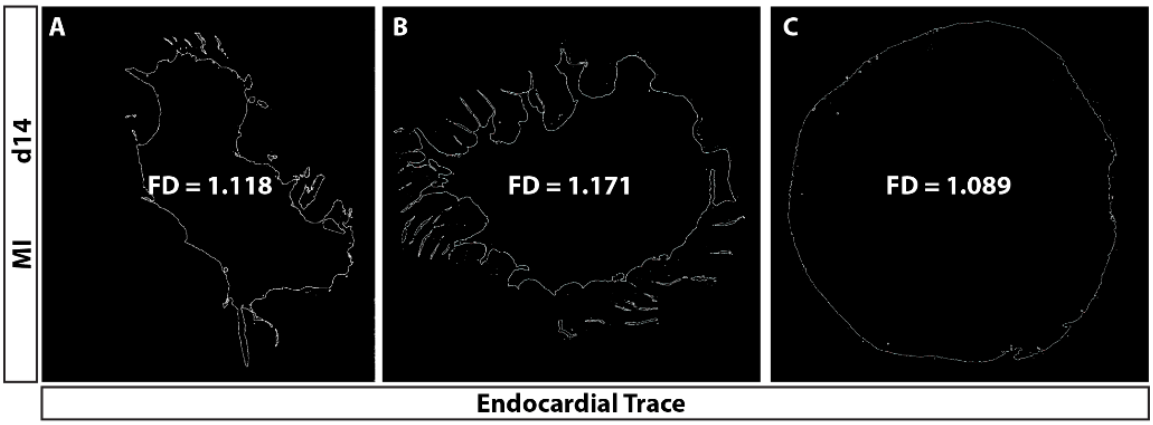

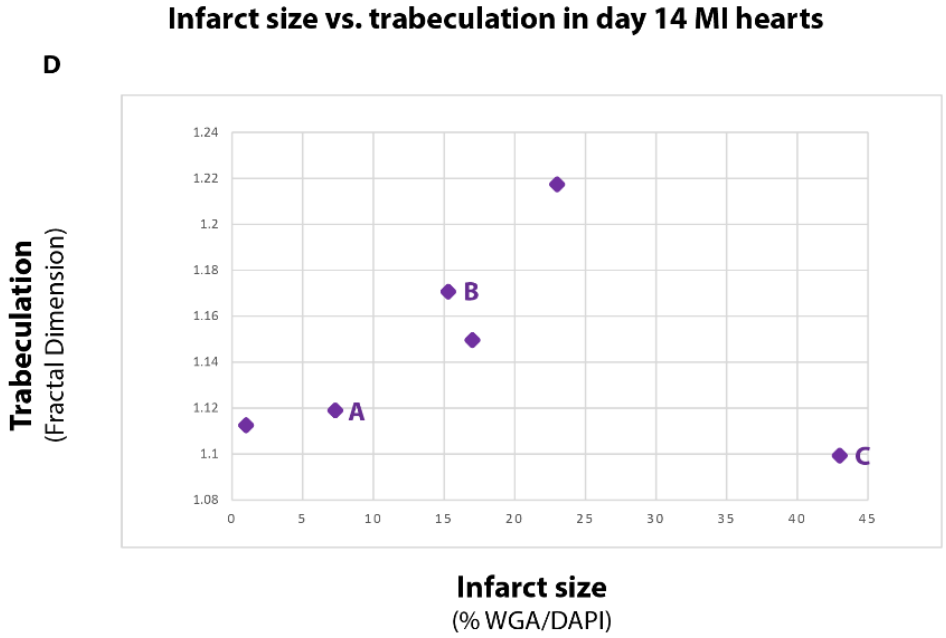

E

Correlation analysis of infarct size vs. trabeculation in day 14 MI hearts

Correlation Coefficient (r) - 1 - 40% injury

	Infarct Size	*Fractal Dimension*
Infarct Size	1	
Fractal Dimension	0.11	1

Correlation coefficient (r) - 1 - 30% injury

	Infarct Size	*Fractal Dimension*
Infarct Size	1	
Fractal Dimension	0.92	1

Figure 4.7. Comparison of infarct size and trabeculation in d14 MI hearts

To determine whether there was a correlation between infarct size and trabeculation in day 14 post-MI hearts, infarct size (from figure 4.5) was plotted against trabeculation (fractal analysis) (D). Fractal dimension is shown in images A, B and C, with corresponding points indicated in the graph (D). Correlation analysis was performed using excel and results shown in (E). When all samples were included, with a range of 1 – 40% infarct size, the correlation coefficient is 0.11 indicating low correlation, however when samples with infarct size 1 – 30% were included the correlation coefficient was 0.92, indicating high correlation. These data support the exclusion of hearts with an infarct size above 30% area of the left ventricle, as described in figure 3.5. $n = 6$.

4.2.2 Identifying infarction before fibrosis develops

As established above, WGA is a useful tool for determining infarction at days 7 and 14 post-MI, however earlier time points have not shown collagen recruitment for scar formation. It was therefore necessary to find another method for determining success of the LAD ligation procedure at earlier time points. At 4 days post-MI, various antibodies were tested to identify a suitable marker, and both WGA (**Figure 4.8A**) and Periostin (**Figure 4.8B**) confirmed the lack of fibrosis at this timepoint, suggesting that a collagen marker would also not be relevant. Instead, consideration was extended to markers of inflammation and proliferation, and whilst Ki67 showed higher expression in MI hearts when compared with non-injured samples, CD68 appeared to be the most accurate indicator of infarction, with expression shown in both the endocardium, epicardium and throughout the myocardium of day 4 MI hearts (**Figure 4.8C**). CD68, which highlights infiltration of macrophages, was also tested at 2 days post-MI, the earliest timepoint for the Notch1 LoF and GoF analysis, and there was a clear increase throughout the heart, with increased clusters of macrophages in the infarct zone and endocardium overlaying the infarct, which correlated with infarct size when compared with an uninfarcted sample (**Figure 4.8D,E**). CD68 was therefore used as a marker of infarction for day 2 and day 4 timepoints post-MI, however this was difficult to quantify and size of injury was less well defined at these stages.

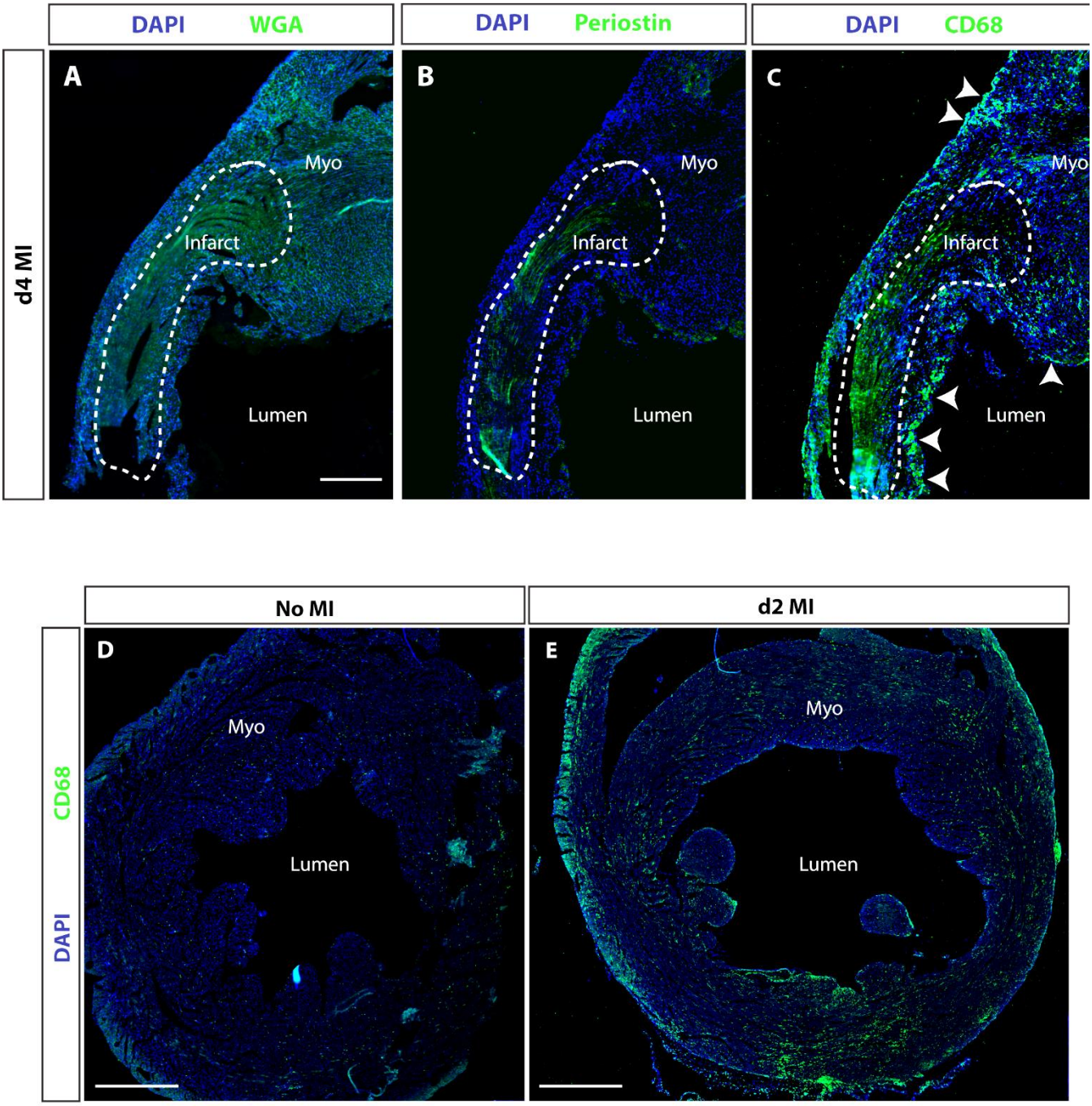

Figure 4.8. CD68 labelling to determine infarct success prior to development of fibrosis

Whilst WGA is a good marker of fibrosis at 7 and 14 days post-MI, the early infarct is more difficult to detect. A day 4 MI heart was stained with WGA-FITC (A) and periostin (B), two established markers of myocardial injury at later stages post-MI, however there was no labelling observed before day 7 post-MI. CD68 was instead used as a marker of injury for earlier stages, as infiltration of macrophages occurs by this time point (C). Arrows indicate CD68 expression in the endocardium overlying the infarcted region, and in the epicardium, which is characteristic of the infarcted heart at this stage. CD68 expression without injury is shown in (D) and increased CD68 is detected as early as 2 days post-MI (E). Expression of CD68 was used to determine successful infarction at 2 and 4 days post-MI, however it is more difficult to determine the size of infarct with this method, so hearts with no infarct or a very large infarct suspected to exceed 30% of the ventricle were excluded, with all other injured samples included in analysis for this timepoint. *Scale bars: A = 200μm, D, E = 1mm. N = 4.*

4.3.1 Development of genetic models for investigation of endothelial Notch1 post-MI

Due to the lack of an endocardial-specific Cre model at the time of developing this model, the only way to target the endocardium in the adult heart was by targeting all endothelial cells. *VE Cadherin-Cre* was used due to its expression in cell-cell adhesion junctions of all coronary endothelial cells, including the endocardium, and was crossed with a TdTomato reporter line to label the cells which were targeted. The resulting mice produced were inducible for *VE Cadherin-Cre;TdTomato* (**Figure 4.9A**), and all mice used were Cre positive and either heterozygous or homozygous for TdTomato, since the fluorescent protein is strong enough to be visualised easily in both heterozygous and homozygous samples.

This *VE Cadherin-Cre;TdTomato* line was then used to specifically target endothelial cells with either a loss or gain of Notch1 activity. For the LoF, the $Notch1^{LoxP/LoxP}$ mouse has LoxP sites flanking an exon encoding the signal peptide of the Notch1 gene, which resulted in an inducible endothelial cell deletion when combined with the VE-Cadherin-Cre;TdTomato mouse (**Figure 4.9B,D**). For this line, only homozygous Notch1 LoF mice were used in the analysis, as heterozygosity may or may not manifest in a consistent clear phenotype.. The GoF, $Rosa^{Notch1}$ mouse contains a truncated cytoplasmic fragment encoded by an intracellular portion of the Notch1 sequence, flanked by LoxP sites, which induced constitutive Notch1 activity in endothelial cells when combined with the *VE Cadherin-Cre* (**Figure 4.9C,E**). For this line, heterozygous mice were used, as recommended and used in the original publication (Murtaugh et. al., 2003), as a single allele is sufficient for constitutive Notch1 activation. This also allowed the mice to be TdTomato heterozygous as both constructs were targeted to the Rosa26 locus; TdTomato proved to be a much brighter fluorescent protein than the inserted EGFP tagged to Notch1, which was weak even with antibody staining.

4.3.2 Optimisation of *VE Cadherin-Cre* recombination

Since most published studies using the *VE Cadherin-Cre* are developmental, induction using tamoxifen has mainly been optimised for embryonic mice. It was therefore necessary to undertake a dose response study to determine the optimal tamoxifen dose for recombination of the loxP in the adult setting. The lowest dose tested was a total of 150mg/kg over 3 consecutive days which was the same as the dose used for the *Pdgfb-Cre* in our other studies, and the highest dose tested was a total of 500mg/kg over 5 consecutive days (Mahmoud et. al., 2015). Recombination efficiency was analysed by detection of TdTomato in endothelial cells of uninfarcted adult hearts. With the lowest dose, low TdTomato expression was observed (**Figure 4.10A-C**, red) in endothelial cells, which were co-labelled with endomucin (green). With a total dose of 250mg/kg over 5 consecutive days, improved endothelial recombination was observed, but TdTomato expression remained low in the endocardium (**Figure 4.10D-F**). With the maximum dose, efficient recombination was observed in both endothelial and endocardial cells of uninfarcted and post-MI hearts (**Figure 4.10G-L**). Overlap of TdTomato with endomucin was calculated as a percentage and an 8-fold increase was seen with 500mg/kg when compared with 150mg/kg and a 4-fold increase compared with 250mg/kg (**Figure**

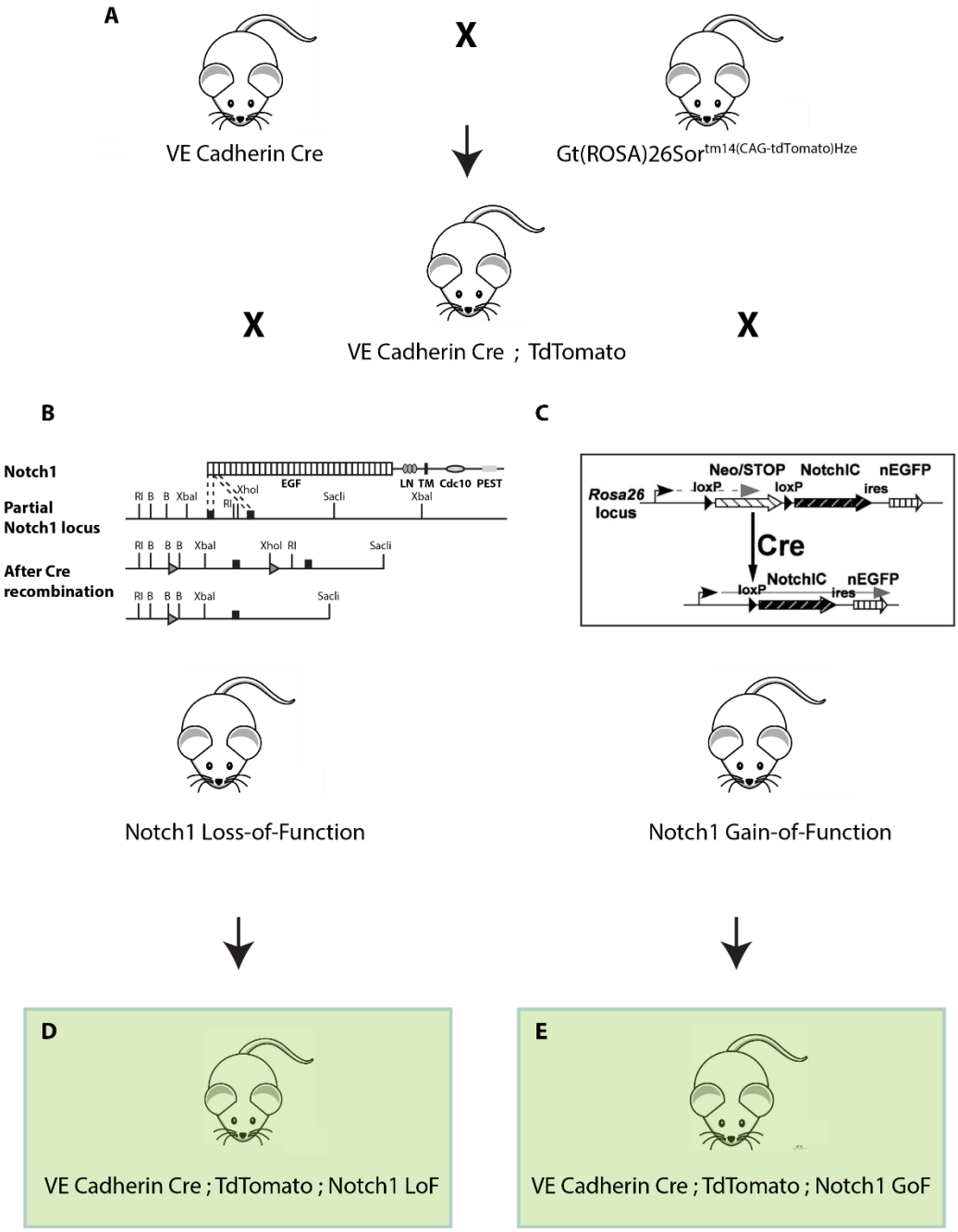

Figure 4.9. Development of endothelial specific Notch1 gain- and loss-of function mouse models

Schematic shows breeding strategy for development of endothelial specific Notch1 loss- and gain-of-function (LoF and GoF) models. *VE Cadherin-Cre* (Sorensen, 2009) were crossed with *Gt(ROSA)26Sor*$^{tm14(CAG-tdTomato)Hze}$/J mice to generate an inducible model with tomato labelled endothelial cells (A). This *VE Cadherin-Cre;TdTomato* line was then used to target endothelial cells specifically with either the Notch1 LoF (*Notch1*$^{loxP/loxP}$, Radtke et. al., 1999) or the Notch1 GoF *(Gt(ROSA)26Sor*$^{tm1(Notch1)Dam}$*/J*, Murtaugh et. al., 2003). The Notch1 LoF mouse has LoxP sites flanking an exon encoding the signal pepide of the Notch1 gene, which resulted in an inducible deletion when combined with the Cre (B). The Notch1 GoF mouse contain a truncated cytoplasmic fragment encoded by an intracellular portion of the Notch1 sequence, flanked by LoxP sites to induce constitutive activity when recombined by the Cre (C). The resulting models developed were an endothelial-specific Notch1 LoF with targeted cells labelled by TdTomato (D) and an endothelial-specific Notch1 GoF with targeted cells labelled by TdTomato (E).

4.10M). A slight decrease in percentage overlap was observed in post-MI hearts, however this difference was not significant, and is likely to be caused by the variability of MI and the characteristic increase in endomucin expression frequently observed by the group. Strong overlap of TdTomato with endomucin in the endocardium at 7 days post-MI is indicated by arrows at higher magnification (**Figure 4.10N**), supporting a dose of 500mg/kg for induction of the *VE Cadherin-Cre*.

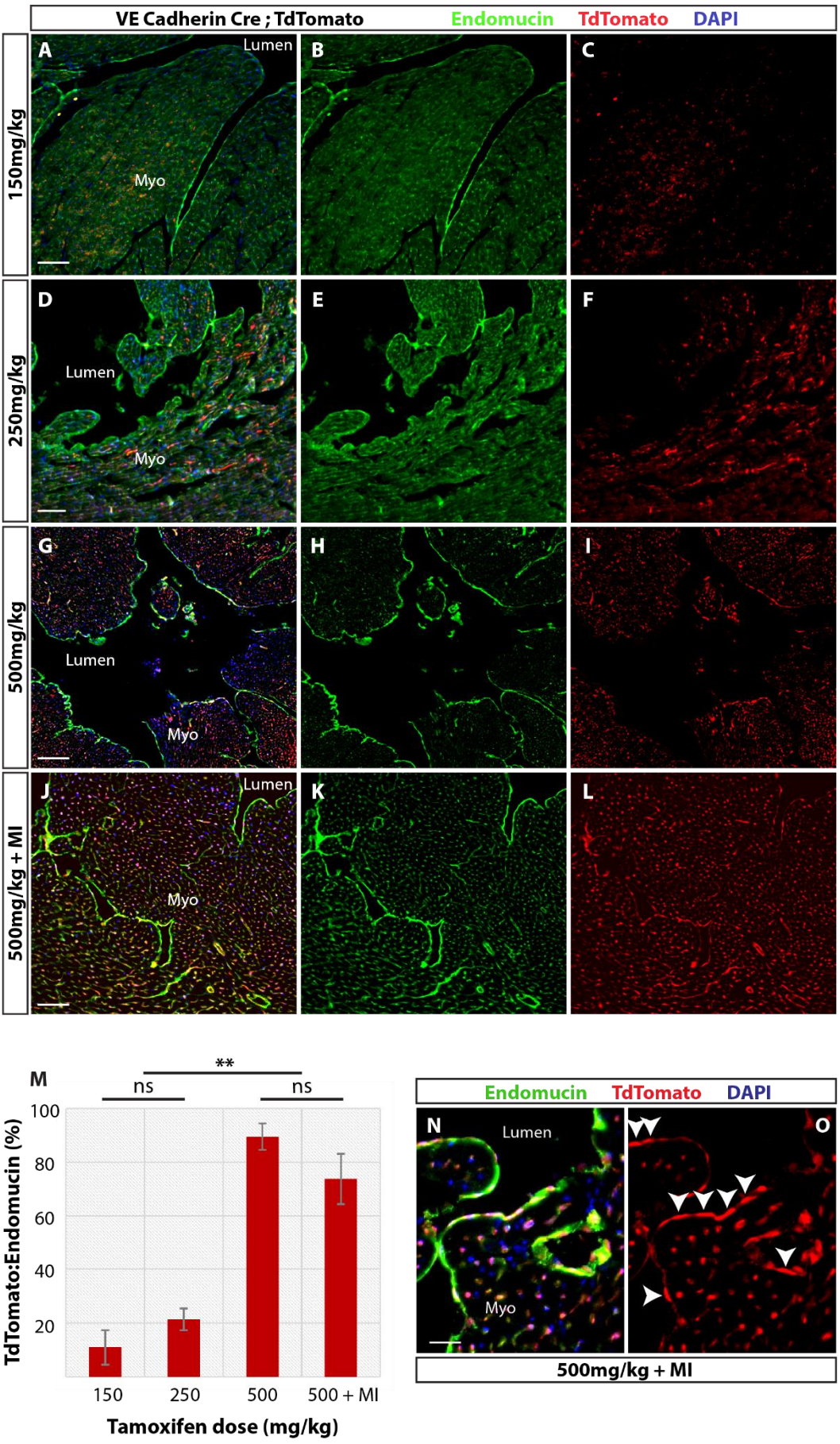

Fig 4.10. Optimisation of tamoxifen dose for induction of VE Cadherin Cre

Figure 4.10. Optimisation of tamoxifen dose for induction of *VE Cadherin Cre*

The dose of tamoxifen required for *VE Cadherin Cre*-mediated recombination was optimised with and without MI. (A-C) show recombination with 150mg/kg; endomucin labelled endothelial cells (B) and low tdTomato expression was observed (C). Administration of 250mg/kg (D-F) showed improved recombination in endothelial cells, but low tdTomato expression in the endocardium (E,F). Administration of 500mg/kg via 5 consecutive IP injections was more efficient and overlap was observed in both endothelial and endocardial cells (G-I). TdTomato expression was also analysed with MI and overlap was observed (J-L). These data were quantified (M) by analysing particles in ImageJ and calculating the % overlap between endomucin and tdTomato. A significant improvement in overlap was observed with the 500mg/kg dose compared to 250mg/kg. Approx. 90% overlap was observed with 500mg/kg, although this was reduced after MI, the difference was not statistically significant (P=0.17). TdTomato expression in endocardium is shown in (N) demonstrating clear overlap with endomucin (arrows). *Two-tailed T-test performed, n = 3 per condition. Scale bars: A, D, J = 100μm, D = 200μm, N = 50μm.*

4.3.3 Loss of Notch1 signalling in endothelial cells

To validate the Notch1 LoF, changes in protein expression were tested by immunofluorescence. N1ICD was used initially, which indicates the presence of the activated Notch1 receptor, and was also used in Chapter 3 to investigate Notch signalling in development and post-MI. Developmental studies utilising this antibody have used a TSA kit to amplify expression (D'amato et. al., 2016), and similar challenges were experienced in the adult setting. The amplified antibody showed expression in some endocardial cells of some control MI samples, but results were unreliable and the antibody was therefore not used for validating Notch activity in the LoF (**Figure 4.11A-C**, arrows).

Hes1 provided a more reliable read out of Notch1 activity, as a transcription factor and functional effector, downstream of Notch1 activation. Therefore, Hes1 was used as a measure of Notch1 activity for the comparison between control and LoF hearts post-MI, and expression at 2 days post-MI is shown in **Figure 4.11D-G**. Control hearts at day 2 show clear expression of Hes1 in the endocardium (**Figure 4.11D,E**, arrows), and a

visible reduction was observed in the LoF endocardial remodelling region at 2 days post-MI (**Figure 4.11F,G**, arrows). An N of 3 per group were analysed at 2 days post-MI, and the percentage of Hes1:Endomucin was calculated for both groups. A significant reduction in Hes1 expression was observed, with the mean dropping from 22% to 6% endothelial cells expressing Hes1 per region counted (**Figure 4.11H**).

Expression levels were also confirmed by RNA scope in these samples, which allowed for the analysis of Hes1 alongside Dll4, a Notch1 ligand (Figure 4.12A-F). Whilst expression levels of Dll4 remained relatively unchanged between control and LoF at 2 days post-MI (**Figure 4.12A,B,E,F**, green), expression of Hes1 was clearly reduced in the LoF samples (**Figure 4.12C-F**, red). This data suggests that the reduction in Notch1 activity is caused by interrupted signalling between the ligand, Dll4 and the transcription factor, Hes1, which is supportive of the protein expression data and confirms what we would expect with the genetic disruption of the Notch1 receptor.

4.3.4 Notch1 GFP was identified in endothelial cells

The Notch1 GoF was validated by isolating targeted endothelial cells using FACS. The GoF construct, targeted to the Rosa26 locus, contains a GFP reporter and successful recombination was confirmed using multicolour flow cytometry by co-staining a single cell suspension with CD31 and VE Cadherin for detection in GFP^+ cells.

Mice were injected with tamoxifen to induce the endothelial Notch1 GoF and hearts were harvested after two weeks. The protocol described in Chapter 3 was used to isolate an endothelial-enriched single cell suspension, and after staining with DAPI, CD31 and VE Cadherin, the cell suspension was analysed by flow cytometry. **Figure 4.13** shows the live cell population (**Figure 4.13A**) and cell counts (**Figure 4.13B**): 30% (50k) live cells were GFP^+ (**Figure 4.13C**), confirming successful induction of the GoF. Of this population, 36k were negative for the haematopoietic lineage cocktail (**Figure 4.13D**), and 26k were VE $Cadherin^+CD31^+$ (**Figure 4.13E**), which confirmed that the GoF was

successfully targeted to endothelial cells in this model. Attempts were made to extract RNA from this cell population to confirm increased expression of Notch1 transcription factors, however this method requires further optimisation for small starting material containing small numbers of fragile FACS sorted cells.

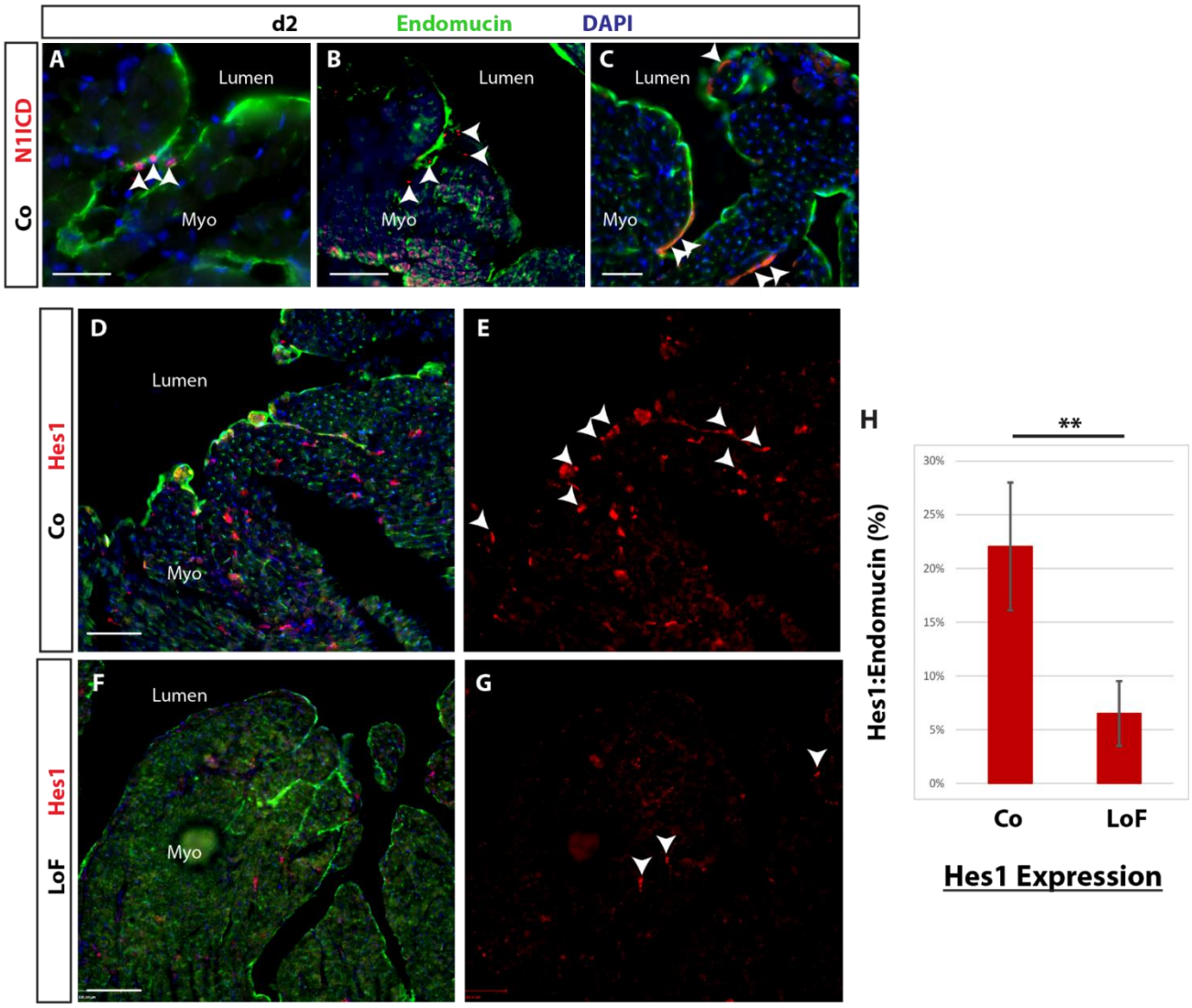

Figure 4.11. Successful knock down of Notch1 activity in endothelial cells

N1ICD expression was analysed in control hearts at 2 days post-MI (A-C) but due to an unreliable antibody for detection, this was not used to analyse Notch1 activity in the LoF. Hes1, a transcription factor activated by Notch1 was instead used to determine Notch1 activity in the endocardium of control (D,E, arrows) and LoF (F,G, arrows) hearts at 2 days post-MI. A significant reduction was observed (H) when particles were analysed and % Hes1 expression calculated against endomucin expression. *Two-tailed T-test performed, n = 3 per condition, P = 0.014. Scale bars: A,C = 50μm, B, D = 100μm, F = 200μm.*

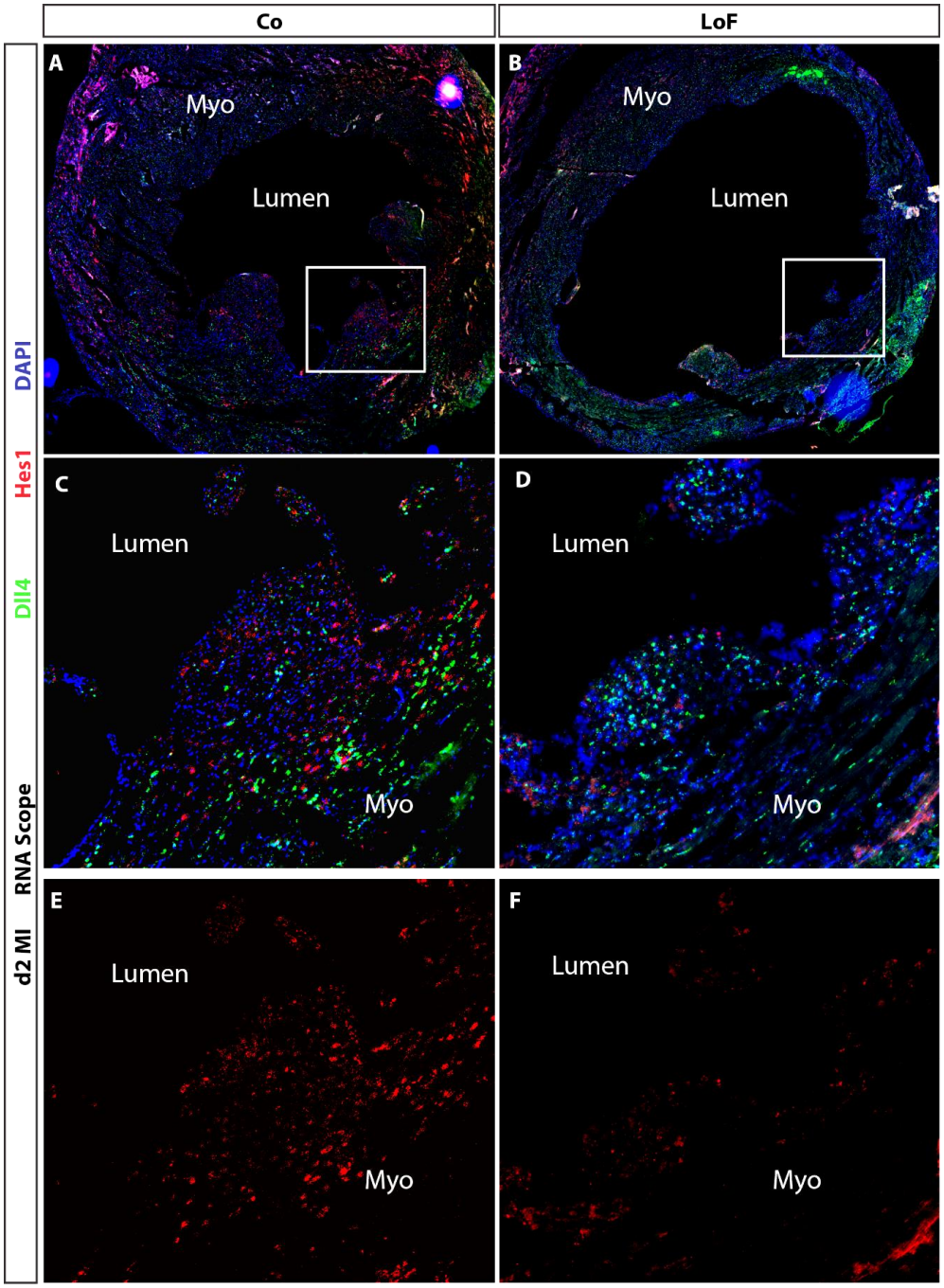
Co
LoF
d2 MI RNA Scope DAPI Hes1 Dll4
A
Myo
Lumen
B
Myo
Lumen
C
Lumen
Myo
D
Lumen
Myo
E
Lumen
Myo
F
Lumen
Myo

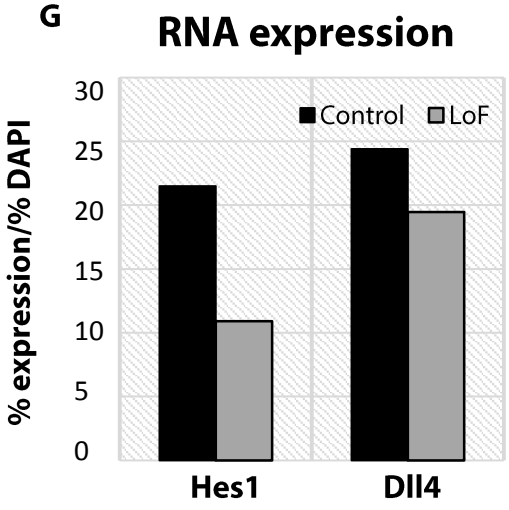
G
RNA expression
% expression/% DAPI
30
25
20
15
10
5
0
Control
LoF
Hes1
Dll4

Figure 4.12. RNA Scope confirms knock down of Notch1 in endothelial cells at 2 days post-MI

RNA Scope was used to investigate RNA expression levels of Dll4 and Hes1, in order to confirm the knock down shown by protein expression in Figure 4.11. (A) shows a control whole heart section 2 days post-MI with expression of Hes1 (red) and Dll4 (green). (C-D) show higher magnification images of insets from (A-B) which are localised to regions of endocardial remodelling. Dll4 expression (green) levels are relatively consistent in these images, however Hes1 expression (red) appears to be reduced in the LoF (D). Hes1 expression alone is shown in panels (E-F), highlighting the reduced expression in regions of endocardial remodelling. Overall quantification is shown in (G) which was calculated as a percentage of DAPI. *Representative of n = 3. Scale bars: A-B = 1mm, C-D = 100µm.*

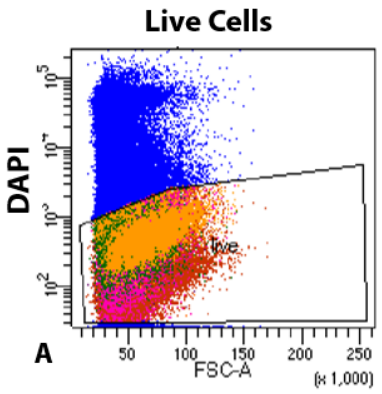

B

Population	Events	% live cells
Live Cells	166532	100
GFP+	49959	30
Lineage-	36637	22
CD31⁺ VE Cadherin⁺	26611	16

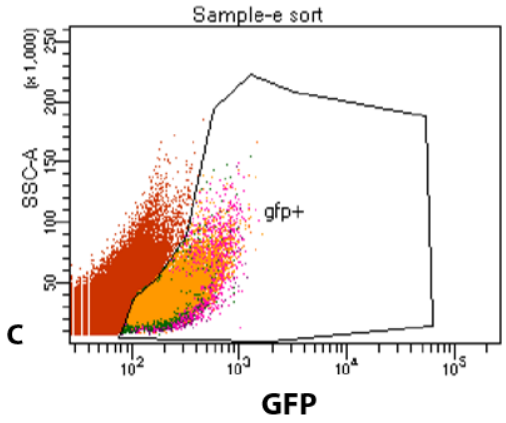

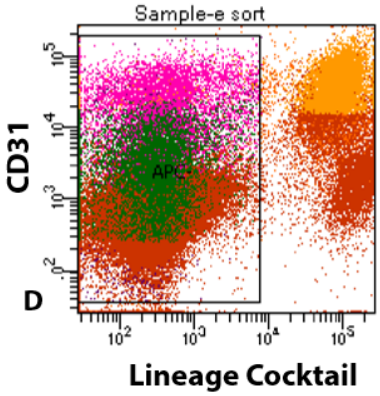

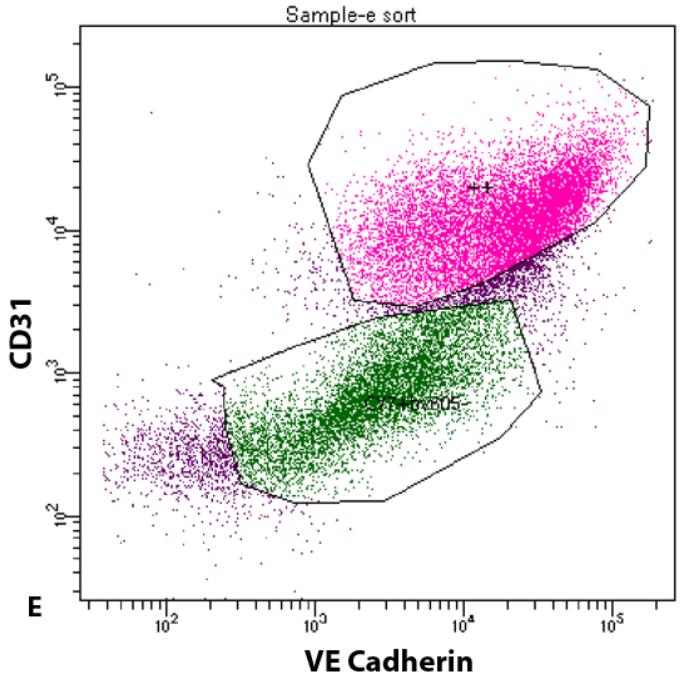

Figure 4.13. Isolation of GFP⁺ VE Cadherin⁺ CD31⁺ cells by FACS confirms Endothelial Notch1 GoF

GFP fluorescence was used to detect cells targeted by the Notch1 GoF, as the inserted construct of the *Rosa*^{N1ICD} contains a GFP reporter. Live cells were gated (A) and the cell count recorded (B). 166k live cells were isolated, with 30% GFP⁺ (C). Of this population, 36k were negative for the haematopoietic lineage cocktail (D) and 26k were VE Cadherin⁺CD31⁺ (E), confirming that endothelial cells had been successfully targeted with the Notch1 GoF. *N = 4 Co, 4 GoF.*

4.4.1 Discussion

Challenges and caveats associated with the LAD ligation procedure have been described in the introduction of this chapter. Optimisations were made to reduce the effects of variability associated with this procedure, on the outcome of the Notch1 loss- and gain-of-function studies. Evidence has been provided for endocardial remodelling and trabecular projections occurring in multiple strains, which supports the hypothesis that this is an adaptive response to ischemic cardiac injury. Endocardial projections have been consistently observed overlaying the infarcted area of myocardium, suggesting that this may be a morphological response to improve blood flow to the ischemic tissue, reverting to be more like the embryonic trabecular myocardium which serves to provide blood to the muscle prior to the formation of the coronary vasculature (Sedmera et. al., 2000). The presence of endocardial remodelling in the *VE Cadherin-Cre* mouse validates its suitability as a model for investigating post-MI remodelling via targeted Notch1 signalling, and the consistency shown across strains confirms technical capacity for undertaking this study.

To ensure that variability remained minimal within the limitations of the surgical procedure, surgical refinements and strain-specific experimental optimisations were introduced. The impact of these changes has been outlined in this chapter, and a clear improvement in both survival rate and success of producing infarction was seen. However, additional considerations could further improve outcomes of the LAD ligation procedure on tamoxifen inducible genetic mice. The *VE Cadherin-Cre* is a particularly inefficient model in terms of inducing Cre recombination, and requires more than three times the tamoxifen dose used for the *Pdgfb-Cre*. Whilst optimisations were made to accommodate this high dose of tamoxifen, for future studies involving a complicated surgical procedure, the tamoxifen dose required should be considered when identifying suitable genetic models. Additionally, due to the importance of experience and consistency when undertaking this complex surgery, benefits may be gained from

employing a technician to carry out the procedure which would remove the time taken to gain surgical competency in addition to that needed for optimising the procedure for each new strain. Within the budget and resources available, feasible improvements and refinements were made and experimental proficiency has been demonstrated by the improved outcomes for the Notch1 LoF and GoF cohorts. Therefore, within the time constraints of this project, a suitable protocol was successfully developed to enable the analysis of endocardial remodelling post-MI.

The next step in developing the tools to investigate remodelling of the endocardium post-MI was to determine suitable analysis methods to define both infarct size and degree of trabeculation. WGA-FITC staining was identified as a reliable marker of cardiac fibrosis post-MI and this was used as a method for quantifying infarct size. The incorporation of a digital method for calculating the area labelled by WGA removed human bias, and the exclusion of samples with infarcts covering less than 10% or more than 30% of the left ventricle ensured that any findings identified from the Notch1 LoF and GoF were representative of the cohort majority. However, the exclusion of hearts with very small or very large infarcts may result in missing a phenotype only induced by severe injury, or discrete effects of a minimally injured heart.

Fractal analysis has proven to be a useful tool for measuring endocardial remodelling in clinical MRI studies, however the method has not been previously employed for the analysis of mouse hearts. Therefore, the technique required significant optimisation in order to establish a protocol that was reliable, and representative of the endocardial remodelling observed by eye. The key challenge here was identifying the optimal way to create an image that the FracLac software could accurately read, since the low quality of MRI scans is well-suited to this analysis, whereas immunofluorescence imaging provided unnecessary, excessive detail for this software to analyse. The outcome of these trials was to capture a low magnification image of a whole heart section stained with DAPI, with binning increased to create an image with lower resolution. This was the

image subjected to autothreshold and “find edges” using ImageJ, however this method did not account for folds in the endocardium or damage to the section, which may have influenced the fractal dimension calculated. Other steps were taken to ensure consistency across measurements, such as using KCl to harvest the heart in diastole, reducing the extent of endocardial folding, and analysing sections at the same distance from the LAD suture placement.

The comparison of infarct size with trabeculation provided validation of the optimised fractal analysis technique for measuring endocardial remodelling. It was suspected that extent of trabeculation was correlated to infarct size, however this had not been proven by the group due to a lack of unbiased tools for evaluating trabeculation. The correlation coefficients calculated in this chapter confirmed our hypothesis and provided support for using fractal analysis to interpret endocardial remodelling in the mouse.

The other main aim for this chapter was to develop and test the Notch1 genetic models that would permit investigation of a role for endocardial Notch1 in neovascularisation post-MI. The complex breeding strategy has been shown here, and some challenges were encountered with developing two triple-cross models. The Notch1 GoF mouse contains an EGFP construct which is activated by Cre, however difficulties were encountered with detecting GFP and even when using an anti-GFP antibody, the expression was very weak. Therefore, to accurately trace endothelial cells in both Notch1 models, future experiments should be carried out with the TdTomato reporter.

The Notch1 GoF model produces constitutively active Notch1 signalling in endothelial cells when Cre recombination is induced, and this signalling can be detected both with and without MI. To gain a quantitative measure of Notch1 activation in these cells, qPCR experiments were attempted. This technique involved the isolation of endothelial cells, using the method optimised in Chapter 3, labelling the single cell suspension with a VE Cadherin antibody, and sorting the cells for VE Cadherin, CD31 and GFP (collecting cells that were positive for all three). RNA was extracted from these cells, however the yield

was very low and qPCR was not possible. Further optimisations are needed for extracting RNA from small cell numbers and, if successful, this would provide an opportunity to analyse the expression of Notch1 signalling genes as well as markers of pathways that may be induced by Notch1 signalling in this model.

In summary, this chapter has defined and validated the tools utilised for investigating a role for Notch1 in endocardial remodelling post-MI.

4.4.2 Conclusions

- LAD ligation surgery was optimised for use with *VE Cadherin-Cre* with resulting improvements in survival rate and success of MI
- WGA is a useful tool for detecting and quantifying infarction in mice
- Fractal analysis is a valid method for measuring trabeculation in the infarcted mouse heart
- Extent of trabeculation is correlated with size of infarction when up to 30% of the left ventricle is damaged
- *VE Cadherin* is a valid tool for targeting endothelial cells in the adult heart
- The Notch1 LoF model induced a knock down in endothelial cells of the adult heart post-MI
- The Notch1 GoF model was successfully targeted to endothelial cells in the uninjured adult heart

CHAPTER 5
RESULTS CHAPTER 3

Chapter 5

Results 3: Endothelial Notch1 signalling is required for neovascularisation post-MI, with an apparent endocardial contribution.

5.0 Introduction

Notch1 signalling was identified as a key pathway in remodelling regions of the endocardium post-MI, and genetic mouse models were developed to investigate its role. The aim of this chapter was to determine whether attenuation or augmentation of endothelial Notch1 signalling affects endocardial remodelling and neovascularisation in the ischaemic heart.

The Notch signalling pathway is important for regulating cell fate and cell proliferation in many developmental processes and has many roles in maintenance of adult tissues (Bray, 2006). The Notch receptors are transmembrane proteins that receive signals from ligands on neighbouring cells, leading to cleavage of the receptor and promotion of transcription factors. Most Notch studies in the developing and adult heart have focused on signalling in cardiomyocytes, however recent studies have highlighted the fundamental role of Notch signalling in the endocardium, which coordinates various developmental processes in the heart (De La Pompa et. al., 2012).

D'amato et. al., 2015 showed that Notch1 in endocardial cells orchestrates trabeculation through Dll4 mediated Notch1 activation, which leads to proliferation and differentiation, followed by Jag1/Jag2 mediated Notch1 activation to induce myocardial patterning, maturation and compaction. In the developing atrioventricular canal, endocardial Dll4-Notch1 signalling acts in coordination with myocardial BMP2 and WNT4 to induce

expression of SNAIL transcription factors, leading to EndMT (Luna-Zurita et. al., 2010). Patterning of the atrioventricular canal is important for the formation of the atrioventricular valves and cardiac conduction via the atrioventricular node (AVN) (MacGrogan et. al., 2018). The role of endocardial Notch in these developmental processes is vital for the formation of a healthy mammalian heart, however there has been little consideration for their recapitulation in a pathological setting to support cardiac remodelling and neovascularisation post-MI.

Endocardial Notch signalling induces EMT during atrioventricular canal maturation in the developing embryo, but in the post-MI setting, most studies have focused on epicardial EMT (Zhou & William, 2011). However, consideration has been given to pre-existing coronary vessels as a source of endothelial cells for MI-induced EndMT. Canonical Wnt signalling was found to drive EndMT in the post-MI heart, and the process was replicated in cultured endothelial cells (Aisagbonhi et. al., 2011). This study described migratory mesenchymal cells as an intermediary expressing CD31 and SMA, which could go on to form new blood vessels or contribute myofibroblasts to the scar tissue. However, this is a controversial subject, and more recent evidence has disputed the contribution of endothelial cells to fibroblasts and vascularisation in the post-MI heart, (Li et. al., 2018). Whilst the endocardium has an important role in EndMT during development, it has not yet been considered in the adult, and this chapter aims to address the potential for pathologically induced endocardial EndMT.

The endocardium has recently been suggested as a source of angiogenesis post-MI, with VEGF signalling leading to endocardial branching into the infarct zone (Miquerol et. al., 2015, Kobayashi et. al., 2017). Whilst these data support the hypothesis of endocardial-derived vessels being formed in response to injury, since angiogenic therapies have been unsuccessful in the clinic, angiogenesis from pre-existing capillaries may not be the primary mechanism. A recent study in the zebrafish, which is used as a model of heart regeneration, identified the endocardium as being highly dynamic during

regeneration with morphological, behavioural and transcriptomic changes observed (Münch et. al., 2017). The group also highlighted a role for the endocardium in activating cardiomyocyte proliferation through Notch signalling, which was previously described as a cardiomyocyte driven process (Zhao et. al., 2014). Pharmacological inhibition of Notch signalling led to reduced endocardial remodelling and increased prevalence of endocardial protrusions which failed to mature/compact in the zebrafish, however, it was unclear which ligands and receptors this mechanism acted through (Münch et. al., 2017). These data highlight the rationale for considering the endocardium, and specifically Notch signalling in the endocardium, post-MI, with the aim of uncovering a targetable pathway for improving neovascularisation clinically.

This chapter employs the use of a Notch reporter model, as well as the endothelial specific transgenic models, and analysis techniques described in Chapter 4 to rigorously investigate a possible role for Notch1 signalling in endocardial remodelling and neovascularisation post-MI. It was hypothesised that the endothelial knockdown of Notch1 would lead to disrupted trabeculation or compaction, leading to a reduction in subendocardial neovascularisation post-MI, and that the GoF model may produce a hypertrabeculation (LVNC) phenotype.

5.1 Results

5.1.1 *CBF:H2B-Venus* reporter of Notch activity confirmed Notch signalling in the remodelling endocardium

To expand on the data provided in Chapter 3, which identified elements of the Notch pathway in remodelling regions of the heart, a Notch reporter was employed to label cells with active Notch signalling. The *CBF:H2B-Venus* mouse was developed to provide a single cell readout of Notch activity, and incorporates an H2B-Venus construct linked to CBF1 (also known as RBPJ) via the SV40 promoter (Nowotschin et. al., 2013). When a Notch ligand binds the receptor, the NICD is cleaved, releasing it into the cytoplasm where it binds co-factors, including CBF1, before translocating to the nucleus. This results in nuclear Venus expression when the Notch receptor is activated, providing a single cell resolution reporter of Notch activity. In order to identify the cell types that display Notch activity in remodelling regions post-MI, markers of cardiomyocytes, macrophages and endothelial cells were stained for in *CBF:H2B-Venus* heart sections and typical observations are described below

The transgene fused to CBF1 is shown in (**Figure 5.1A**), and Venus expression occurs when N1ICD binds CBF1 and translocates to the nucleus. This produces a fluorescent green nuclear signal in cells with active Notch signalling. Baseline Notch activity was shown by Venus expression in the sham heart (**Figure 5.1B-C**), which was widely present across the myocardium. At 24 hours post-MI, Venus was clearly expressed in the nuclei of remodelling vessels close to the endocardial surface (**Figure 5.1D-G**, arrows). At 4 days post-MI, an example region of enclosed endocardium is shown, which had remodelled to form a new lumen (**Figure 5.1H**, box). Endocardial expression of Venus is indicated in this region (**Figure 5.1I**, arrows), and was particularly clear in the endocardial cells lining the newly formed lumina (**Figure 5.1J-K**, arrows, dotted lines indicate lumina). At 7 days post-MI, Venus expression persisted throughout the heart (**Figure 5.1L**), however, clusters of Venus-positive cells were observed in remodelling

regions of the endocardium (**Figure 5.1M**, arrows). A representative example of remodelling is highlighted in the single channels by yellow boxes (**Figure 5.1N-O**).

Cardiac troponin I (cTnI) was used to visualise cardiomyocytes (**Figure 5.2A-F**, grey) and in a remodelling region around a newly formed lumen (**Figure 5.2A, C**, yellow), Venus-positive nuclei appeared to be clustered in three clear areas (**Figure 5.2B-C**, pink dotted lines). Area 1 was directly beneath the endocardial surface, where lower cTnI expression was observed, area 2 was around the newly formed vessel lumen, and area 3 was a region of damaged myocardium, indicated by the low cTnI expression (**Figure 5.2C**). These data suggest that at 4 days post-MI, there is little or no Notch activity in cardiomyocytes. At day 7, cTnI was used in combination with Ki67 in an attempt to identify proliferating cells. Some cells appeared to co-express Venus and Ki67, indicating that some cells undergoing active Notch signalling were also proliferating (**Figure 5.2D**, yellow/white nuclei). Venus and Ki67 expression are each shown in combination with cTnI (**Figure 5.2E-F**), however it is difficult to conclude from these images whether the Venus or Ki67 positive nuclei belong to the cardiomyocytes or another cell type closely localised to the cardiomyocytes, such as fibroblasts or pericytes. CD68 was used as a marker of macrophages, to investigate whether infiltrating inflammatory cells were signalling through Notch. At 7 days post-MI, infiltrating macrophages were clearly labelled with CD68 (**Figure 5.2G-I**, red), however, Venus-positive nuclei were not associated with these cells. Therefore, at 7 days post-MI, whilst infiltrating macrophages and Notch signalling cells appear to be localised to remodelling regions of the endocardium, the macrophages are not signalling via Notch in these areas. The only cell marker that was consistently observed to overlap with Venus was endomucin, which was used to label the endocardium and endothelial cells. Representative images from 24 hours, 4 days and 7 days post-MI clearly showed Venus-positive nuclei in endothelial cells of small capillaries (**Figure 5.2J**) and larger vessels (**Figure 5.2K-L**). This,

combined with the images shown in **Figure 5.1**, confirm Notch activity in the endocardium and endothelium of remodelling sub-endocardial regions post-MI.

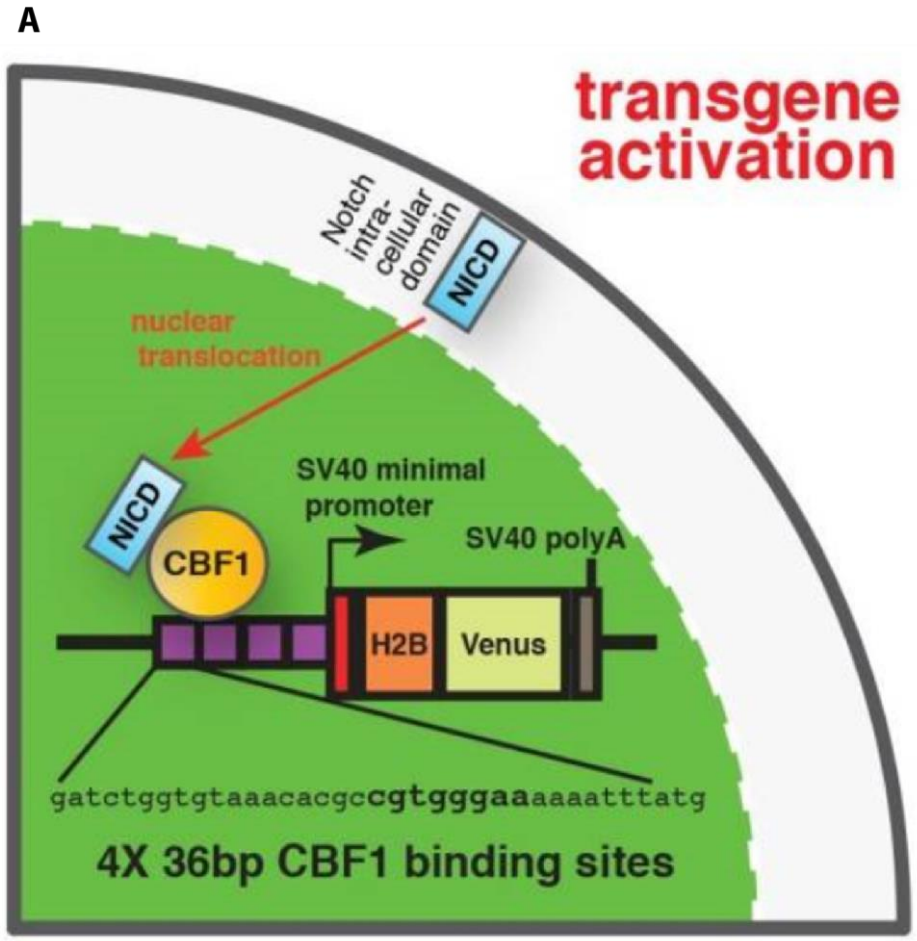

Figure 5.1. *CBF:H2B-Venus* provide a readout of Notch activity post-MI

The *CBF:H2B-Venus* mouse has incorporated an H2B-Venus construct fused to CBF1 (also known as RBPJ) which binds to Notch intracellular domain (NICD) after activation of the Notch receptor, before translocating to the nucleus (A). This results in Venus being expressed when the Notch receptor is activated, providing a single cell readout of Notch activity. This model is not specific to the Notch1 receptor, and labels activation through all Notch receptors (1-4).

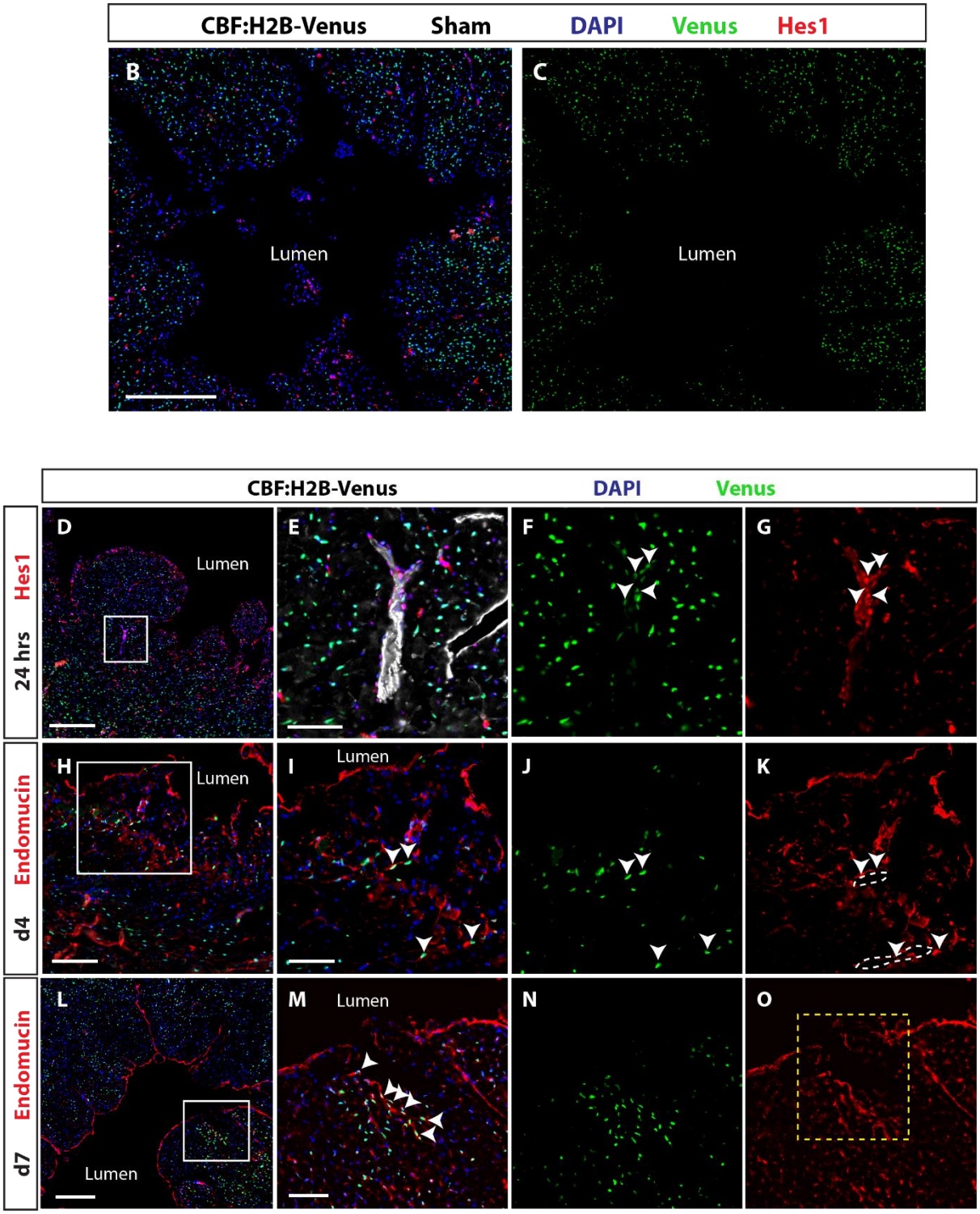

Figure 5.1. *CBF:H2B-Venus* provide a readout of Notch activity post-MI

Venus (green) expression in the left ventricle of a sham heart is shown in (B, C), with Hes1 (red), and represents low-level Notch activity in the myocardium without MI. After MI, Venus expression increased, with localisation to remodelling vessels and endocardium observed. (D-G) shows endothelial cells (G, red) expressing Venus (F, green) in a remodelling vessel close to the endocardial surface (D,E). At 4 days post-MI clusters of Venus positive cells (H-K, arrows) were observed in the endocardium around a remodelling region, where subendocardial lumina were found (K, dotted lines). At 7 days post-MI Venus expression was observed throughout the myocardium (L), and clusters of cells in the endocardium were observed in a remodelling region (M-O, arrows, box). *Scale bars: B = 500μm, D, H = 200μm, E = 50μm, L = 250μm, I, M = 100μm. n = 3 per timepoint.*

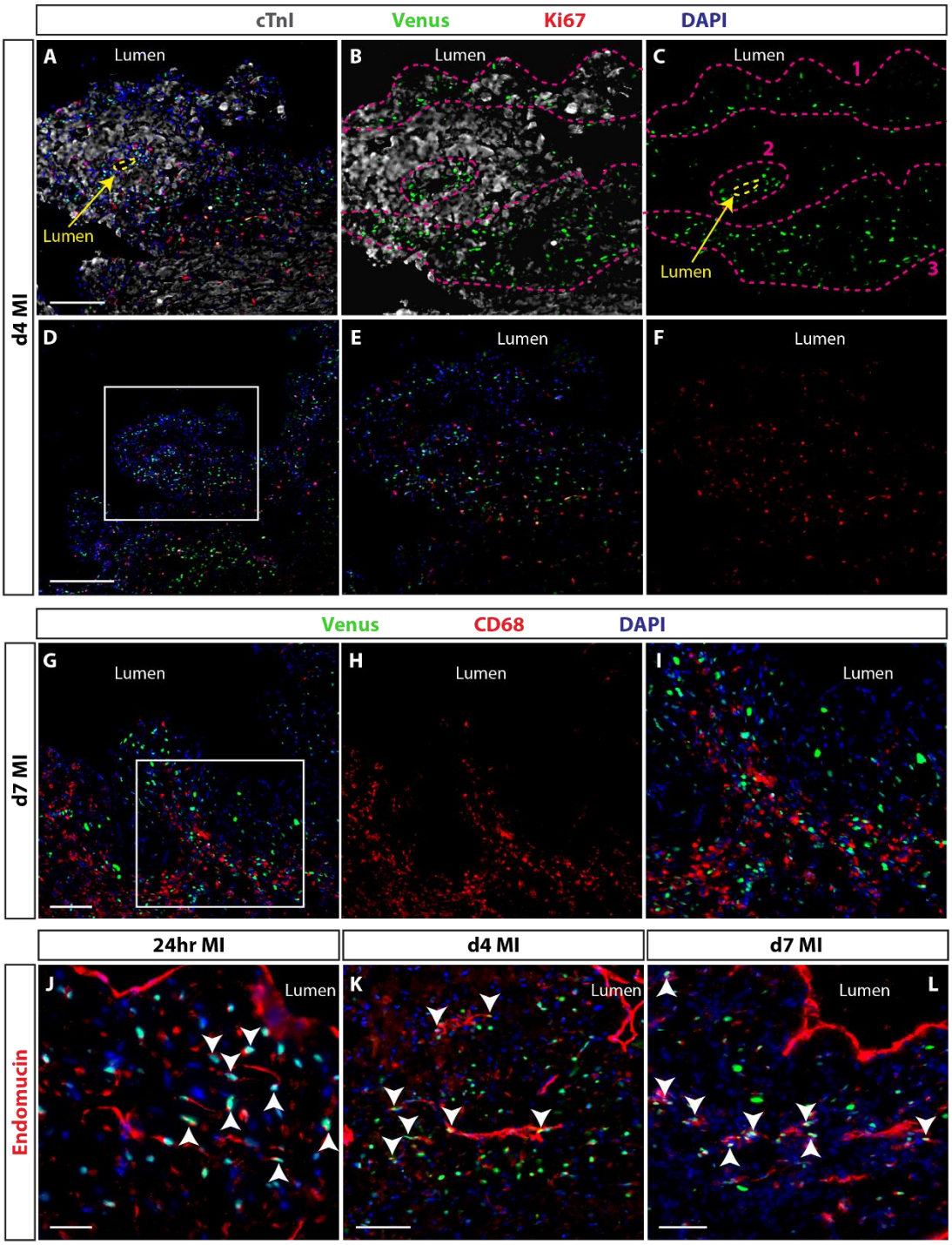

Figure 5.2. *CBF:H2B-Venus* demonstrates Notch activity and proliferation in endothelial cells

To determine which cell type was involved in Notch signalling, co-staining is shown with markers of cardiomyocytes, macrophages and endothelial cells in post-MI samples. cTnI was used to label cardiomyocytes (A-C, grey), and at 4 days post-MI, Venus positive nuclei appear to be localised to areas of damaged myocardium (B, C, pink dotted lines) and around a remodelling vessel (A, C, yellow dotted line). At this stage, some Venus positive nuclei (green) appear to overlap with Ki67 (red), showing Notch signalling in proliferating cells at this stage (D-F). However, it is unclear what cell type the Venus positive nuclei (E, green), or Ki67 expressing nuclei (F) belong to from these images. CD68 was used to label macrophages and there appears to be no Notch signalling in macrophages at this stage (G-I). Endomucin was used to label endothelial cells at 24 hours, 4 days and 7 days post-MI (J-L), and overlap between Venus positive nuclei and endomucin labelled endothelial cells was observed at all stages (J-L, arrows). *Scale bars: A, G = 100μm, D = 500 μm, J = 20μm, K, L = 50μm. n = 3 per timepoint.*

5.2.1 Loss of endothelial Notch1 has no effect on endocardial trabeculation without MI

Endocardial remodelling was analysed in the endothelial-specific Notch1 LoF model. Low magnification, low resolution DAPI images (**Figure 5.3A, D**) were subjected to "Autothreshold" (**Figure 5.3B, E**) and "Find Edges" tools in ImageJ, and endocardial traces (**Figure 5.3C, F**) were run through the FracLac software, using the parameters outlined in Chapter 4. No significant difference in endocardial morphology was observed by fractal dimension in the Notch1 LoF model without MI (**Figure 5.3G**). This confirmed that any trabeculation phenotype observed after MI was in response to the LAD ligation, and not induced by the Notch1 LoF at baseline.

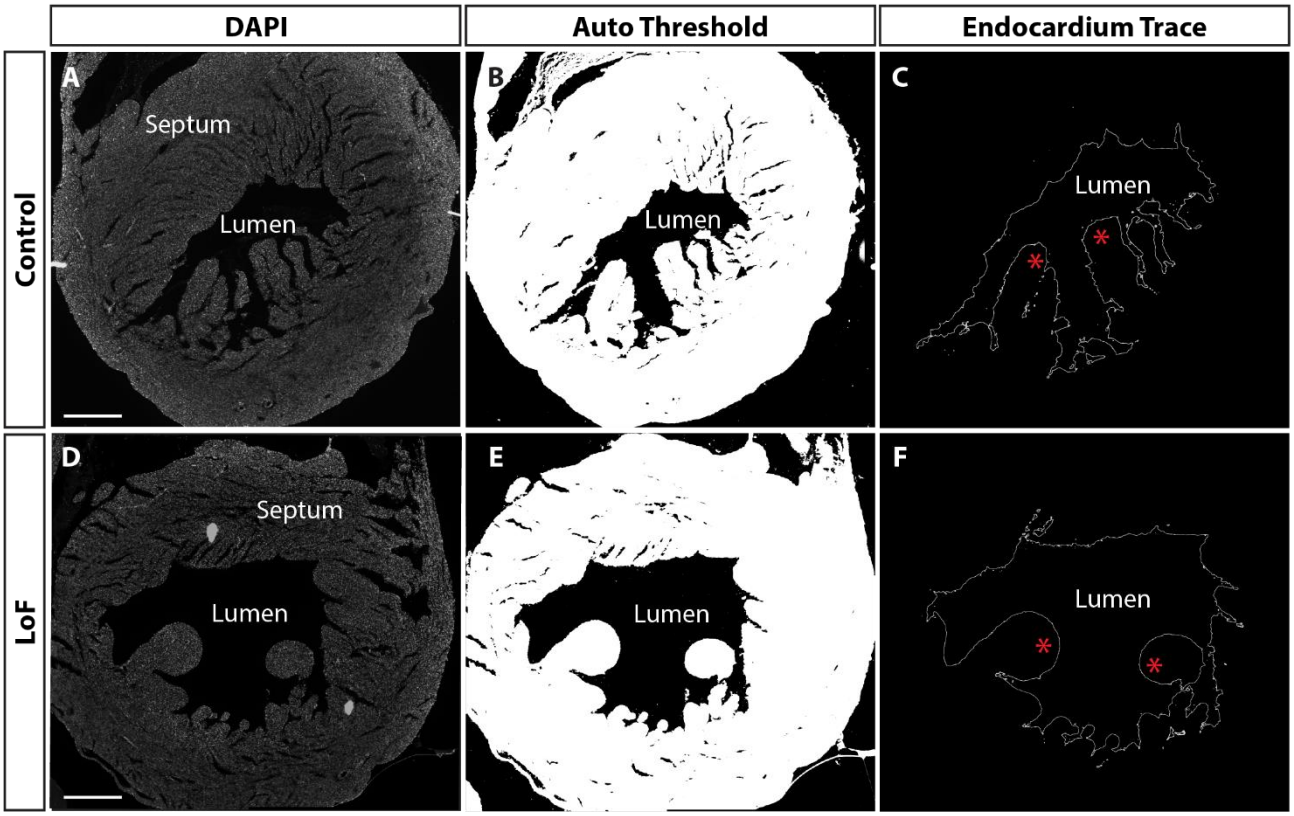

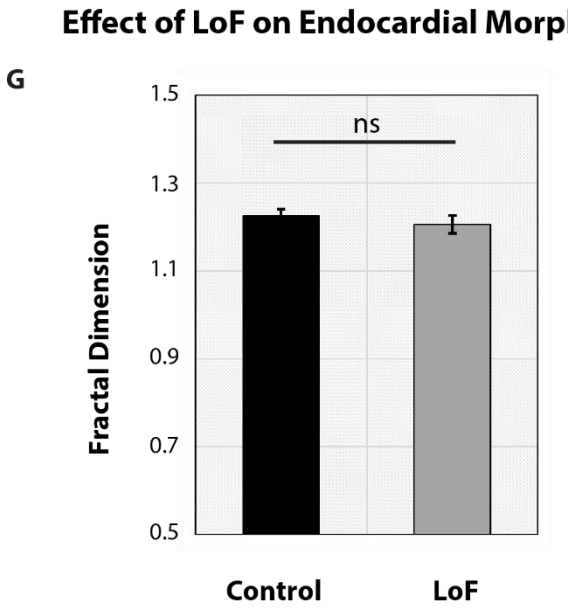

Figure 5.3. Fractal dimension demonstrates that loss of endothelial Notch1 has no effect on endocardial morphology in sham hearts

Fractal dimension was calculated for control and Notch1 LoF sham hearts. DAPI images of control (A) and Notch1 LoF (D) sections were converted to Auto threshold (B, E) and Edges identified using ImageJ. All outer edges and holes in myocardium were removed manually to produce endocardial traces of each image (C, F, asterisks = papillary muscles). Traces were run through FracLac plugin software to calculate FD. No significant difference was observed in FD between control and Notch1 LoF (G), therefore, loss of Notch1 does not affect endocardial morphology in sham hearts. *Scale bars = 1mM. N = 3 per condition.*

5.2.2 Loss of endothelial Notch1 leads to reduced trabeculation in post-MI hearts

Trabeculation was analysed in samples at 2 days post-MI using FracLac software. First, samples were checked for consistency of infarct size using CD68 expression (**Figure 5.4A-E**). After exclusion of samples with no clear infarct visible, the percentage of CD68 was calculated against total DAPI in the left ventricle using the “analyse particles” tool in ImageJ, and no significant difference was observed in CD68 expression between control and Notch1 LoF. The fluorescent DAPI images were then used to create endocardial traces (**Figure 5.4F-G**) and analysed using FracLac software. Whilst some samples appeared to show reduced remodelling, this was not replicated across all samples and no significant difference in FD was observed between the control and Notch1 LoF hearts at 2 days post-MI (**Figure 5.4H**).

At 7 days post-MI, infarct size was calculated using WGA expression (**Figure 5.5A-D**). The total WGA was calculated as a percentage of DAPI using the “analyse particles” tool in ImageJ, and after exclusion of those with infarcts outside the defined experimental range (10-30%), no significant difference in infarct size between control and Notch1 LoF was shown (**Figure 5.5E**). DAPI fluorescence was used to create endocardial traces (**Figure 5.5F-G**) and these were analysed using FracLac. A reduction in trabeculation was observed in the Notch1 LoF hearts, which can be clearly visualised by the representative traces (**Figure 5.5F-G**) and was calculated as statistically significant.

At 14 days post-MI, infarct size and trabeculation were analysed using the same methods. WGA expression was used to calculate infarct size and, whilst a trend towards increased fibrosis was seen in the Notch1 LoF samples (**Figure 5.6A-D**), the difference was not significantly different (**Figure 5.6E**). DAPI fluorescence was used to create endocardial traces (**Figure 5.6F-G**) and the morphology was clearly affected in the Notch1 LoF. This was quantified and shown to be statistically significant (**Figure 5.6H**).

These data together provide evidence of an essential role for Notch1 signalling in endocardial remodelling post-MI, which supports the hypothesis that developmental mechanisms driving trabeculation and compaction for ventricular patterning are recapitulated in the adult pathological setting. Some hearts imaged may not have been arrested in diastole due to challenges with efficiency using KCl; this should be considered when examining trabeculation and is one of the reasons that a high sample size is required to unequivocally prove these results.

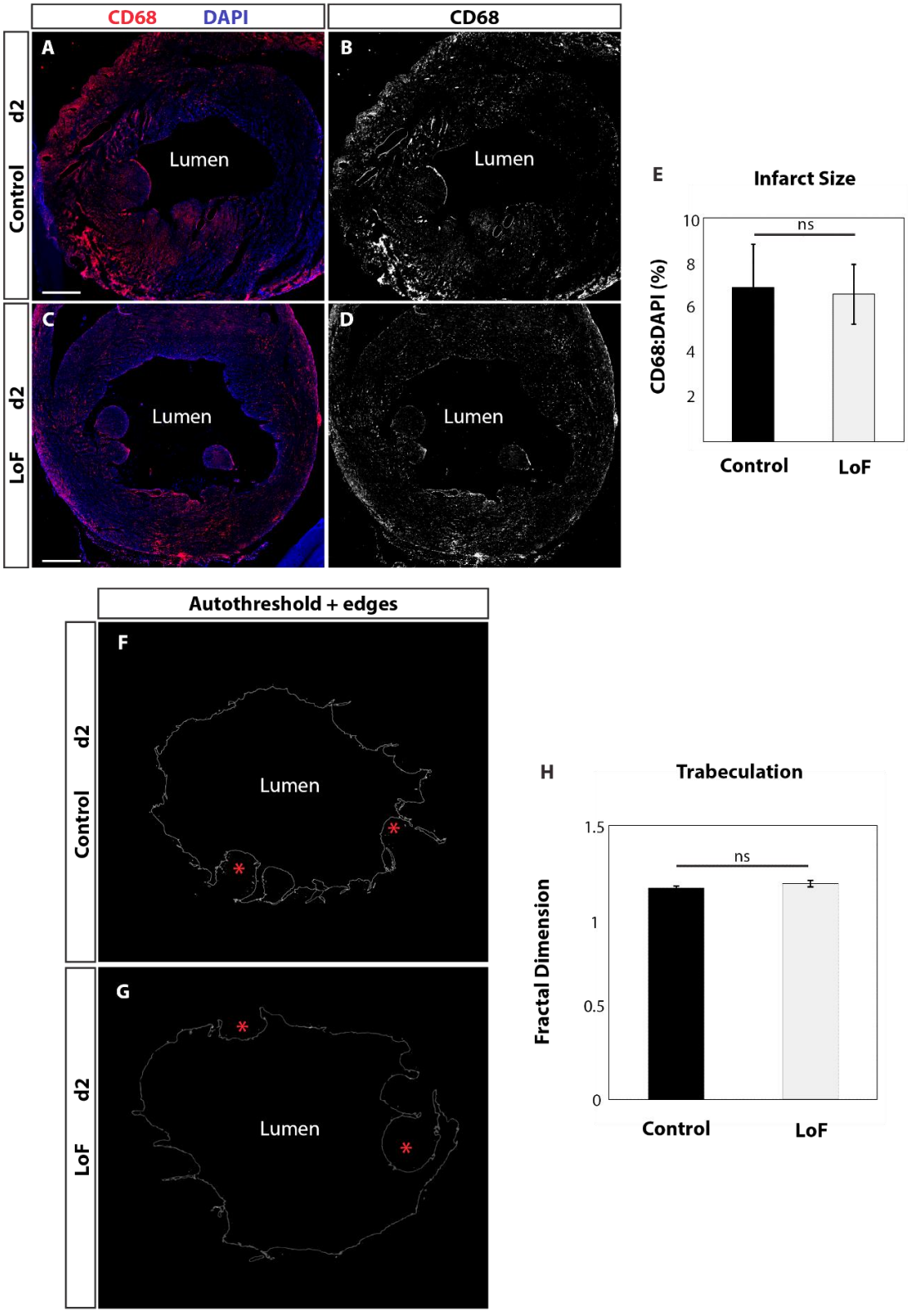

Figure 5.4. Infarct size and endocardial remodelling in Notch LoF 2 days post-MI

Endocardial remodelling was analysed at 2 days post-MI in control and Notch1 LoF hearts. Size of infarction was measured by CD68 expression, as a percentage of total left ventricle DAPI staining using the "analyse particles" tool in ImageJ (A-E), and there was no significant difference in infarct size across samples. Endocardial traces were created and trabeculation was measured using FracLac software plugin (F-G). FD was compared between control and Notch1 LoF samples, and there was no significant difference shown in trabeculation at this stage (H). *N = 3 hearts per group, scale bars = 1mM.*

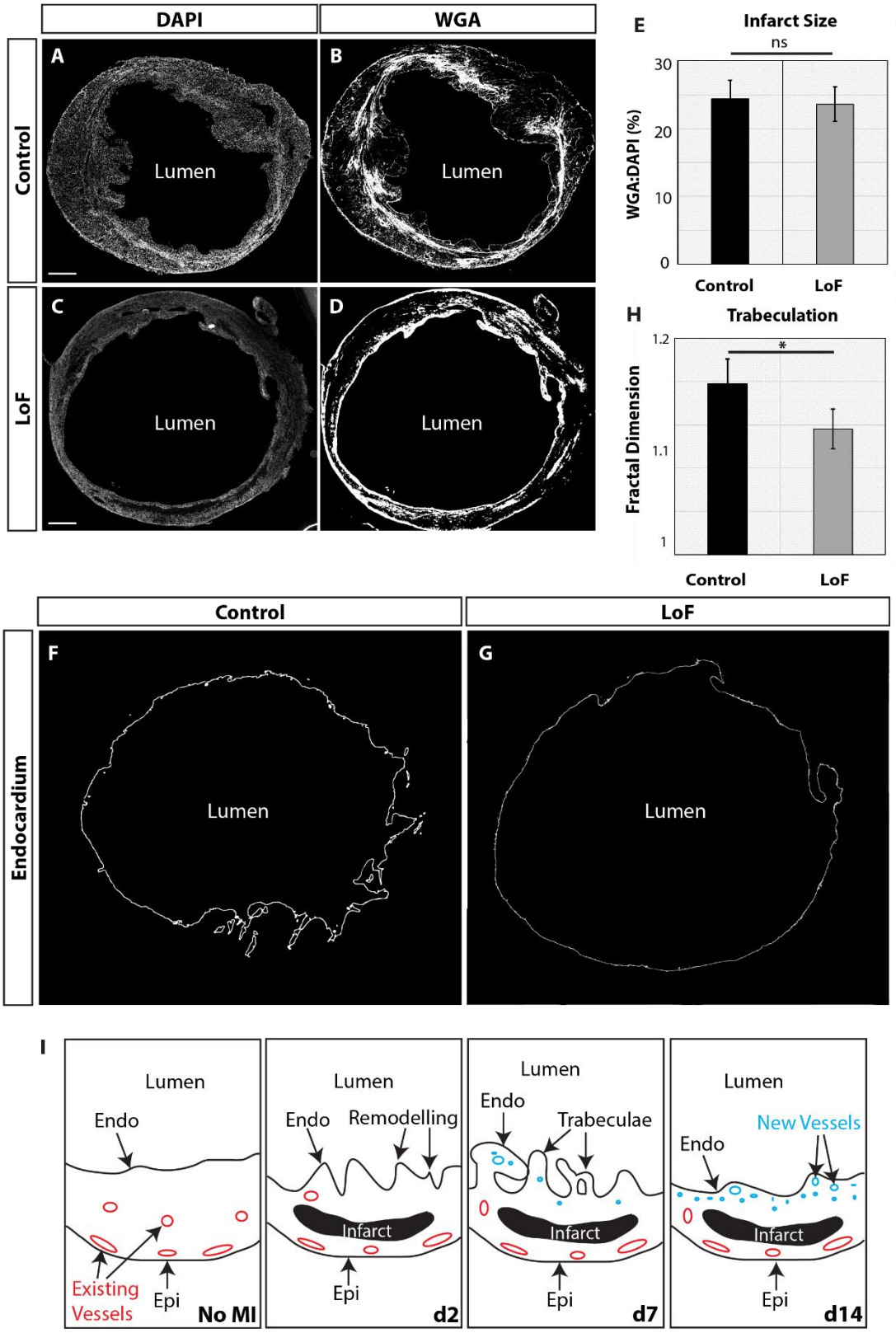

Figure 5.5. Endocardial remodelling is reduced in Notch1 LoF 7 days post-MI

The effect of Notch1 LoF on endocardial remodelling 7 days post-MI was analysed. Infarct size was calculated using WGA and DAPI staining (A-C) and no difference was observed in infarct size between control and LoF groups (E). Endocardial traces were created from DAPI stained images for control and LoF groups (examples in F-G) and fractal dimension calculated. A significant reduction was shown in fractal dimension of LoF hearts (H). A schematic illustrating the timeline of trabeculation in wild type hearts is shown in (I). *n = 4 hearts per group, P = 0.03, scale bars = 1mM.*

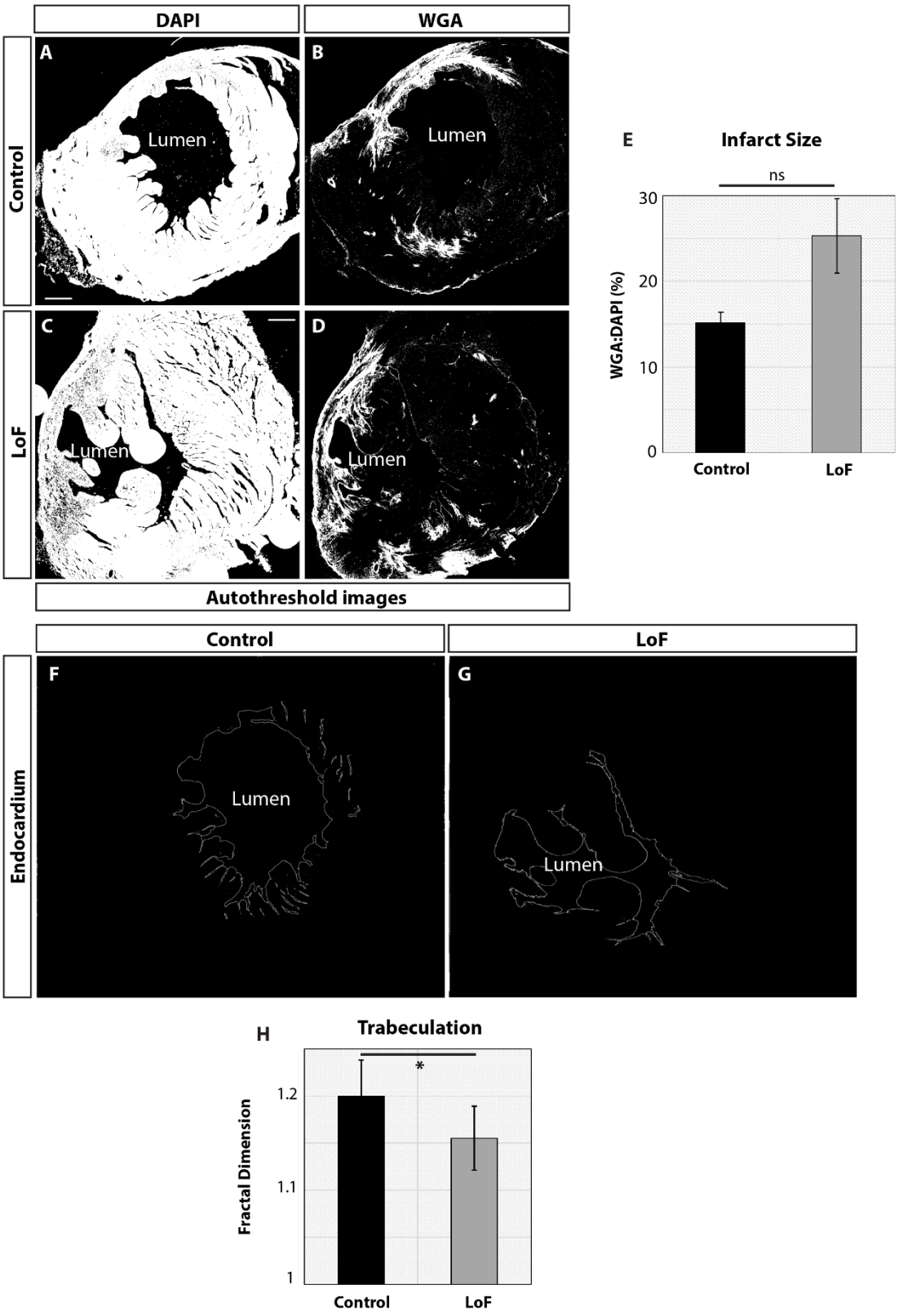

Figure 5.6. Endocardial remodelling is reduced in Notch1 LoF 14 days post-MI

Endocardial remodelling was examined at 14 days post-MI in control and LoF hearts. Infarct size was measured using WGA and DAPI staining (A-D), and whilst there is a trend for larger infarcts in the Notch1 LoF group, this was not significant (E). The same samples were used to create endocardial traces (F-G) and the morphology is clearly unusual for the LoF hearts. Fractal analysis was applied to these traces and a significant reduction was shown in trabeculation at this stage (H). *n = 3 per group, P = 0.14 for infarct size, P = 0.03 for trabeculation, scale bars = 1mM.*

5.2.3 Loss of endothelial Notch1 leads to reduced subendocardial vessels post-MI

The number of subendocardial vessels overlaying the infarct region were counted at 7 and 14 days post-MI. The "subendocardium" was defined as between the endocardium and the infarct border zone (**Figure 5.7A-B**, arrows). Vascular expansion also occurred within the infarcted myocardium, but this is thought to be mostly endothelial-, and not endocardial- derived (Dubé et. al., 2017). Subendocardial vessels were counted and grouped into small/medium (<50µm) or large (>50µm) categories. Representative control images (**Figure 5.7C-F**) indicate large (pink arrows) and small/medium (blue arrows) subendocardial vessels. Neovascularisation was clearly observed in control hearts at 7 days post-MI with SM-MHC$^+$ vessels in the subendocardial region overlaying the infarct (**Figure 5.7D, F**). In contrast, representative images for the Notch1 LoF show fewer SM-MHC$^+$ subendocardial vessels (**Figure 5.7G-J**), with an obvious reduction in small/medium vessels (**Figure 5.7J**, blue arrows). These data were analysed and a significant reduction in small/medium vessels was observed in the Notch1 LoF at 7 days post-MI (**Figure 5.7K**). There was no significant difference observed in the number of large subendocardial vessels at this stage.

Vessels were counted at 14 days post-MI using the same methodology as the 7 day analysis. A clear reduction in SM-MHC$^+$ subendocardial vessels was observed (**Figure 5.8A-D**), with small/medium (blue arrows) and large (pink arrows) vessels indicated in representative control and Notch1 LoF images at 14 days post-MI (**Figure 5.8C-D**). Interestingly, SM-MHC expression appeared to be reduced in the infarct region of these hearts, as well as in the subendocardium (**Figure 5.8A-D**). Additionally, representative images of the control and Notch1 LoF are shown (**Figure 5.8E-H**), and similarly to the day 7 samples, the Notch1 LoF still appeared to have some large subendocardial vessels at day 14 (**Figure 5.8F-H**, pink arrows). Statistical analysis showed a significant reduction in small/medium subendocardial vessels, and a trend towards reduced large subendocardial vessels in the Notch1 LoF at 14 days post-MI (**Figure 5.8I**).

These data provide the first evidence of a role for Notch1 in subendocardial neovascularisation post-MI. Whilst the consistent observation of large subendocardial vessels in both control and Notch1 LoF hearts suggests that other mechanisms may also be involved, the clear reduction in SM-MHC^{+} subendocardial vessels confirms an important role for endothelial Notch1 in maturation of new vessels post-MI.

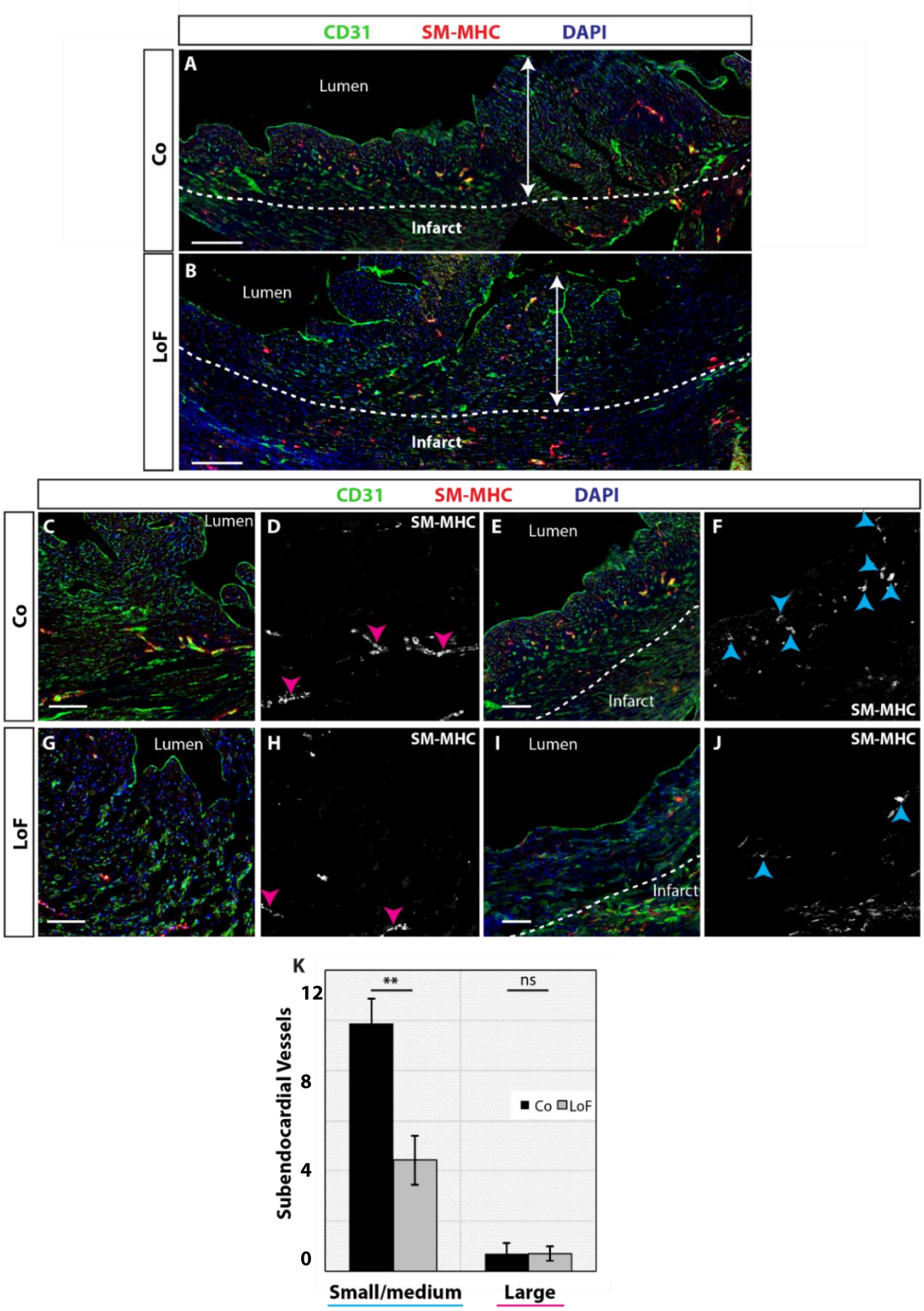

Figure 5.7. SM-MHC labelling shows a reduction in sub-endocardial vessels in Notch1 LoF at 7 days post-MI

Subendocardial vessels were examined in control and Notch1 LoF hearts at 7 days post-MI. The subendocardial region (A,B, arrows) was defined as between the endocardium and the infarct border zone (A,B, dotted line), taking care to exclude neovascularisation of the infarct. CD31 labelled endothelial cells (green), and SM-MHC positive vessels in this region were counted and grouped into small/medium (<50µm) and large (>50µm) categories for comparison. Example images are shown for control (C-F) and Notch1 LoF (G-J) hearts, with the infarct (dotted line), large vessels (pink arrows) and small/medium vessels (blue arrows) indicated. A significant reduction in the number of small/medium subendocardial vessels was observed, and no difference in large vessels with the Notch1 LoF (K). *N = 4 hearts per group, P = 0.01 (small/med), scale bars: A, B = 200µm, C-J = 100µm.*

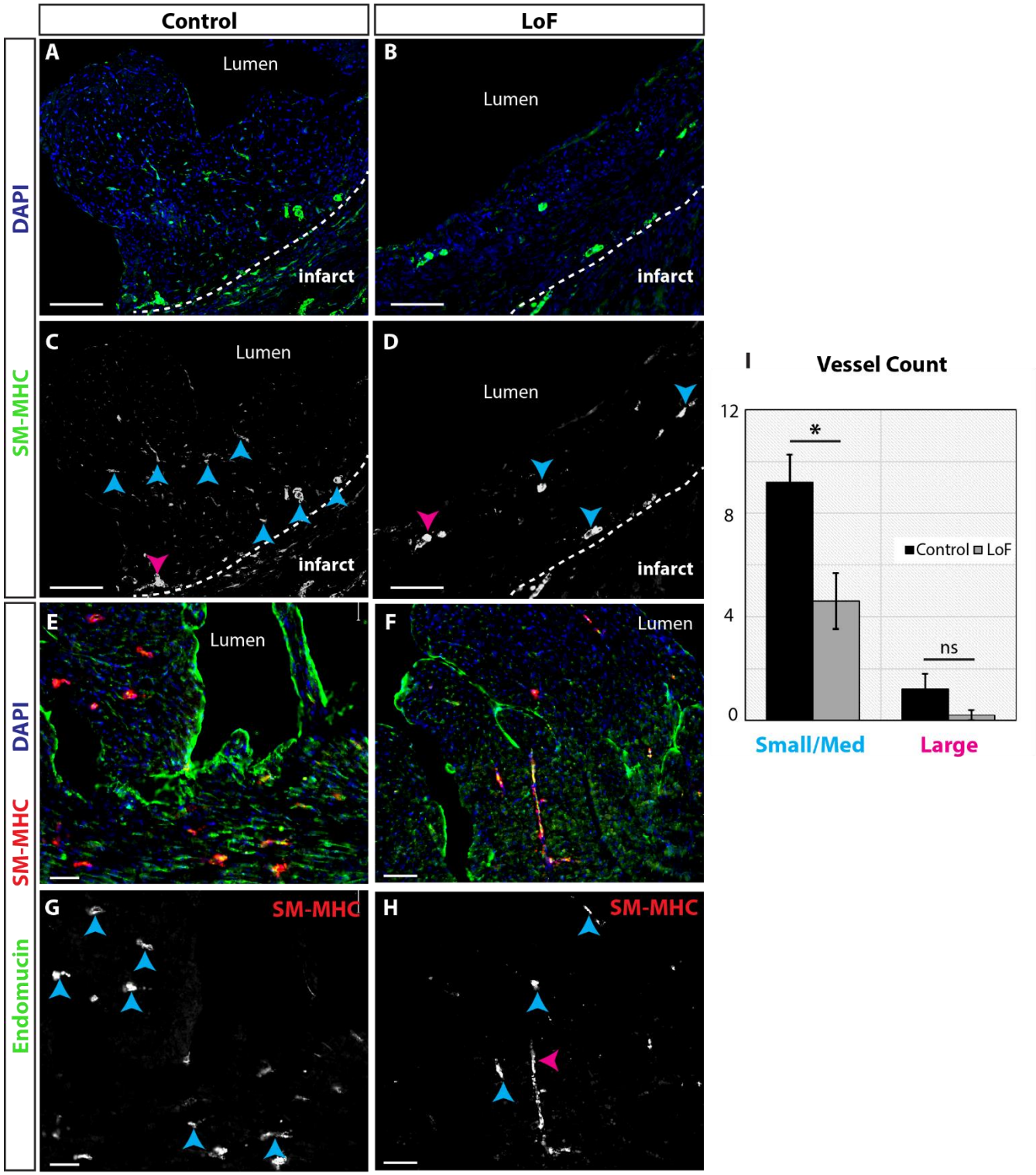

Figure 5.8. Sub-endocardial vessels are reduced in Notch1 LoF 14 days post-MI

Sub-endocardial vessels were examined in control and Notch1 LoF hearts at 14 days post-MI with sub-endocardial region and vessel sizes defined as in Figure 5.7. The subendocardial region is shown by the dotted line (A-B) and small/medium (blue arrows) and large (pink arrows) vessels are indicated (C, D, G, H). Vessels were labelled by SM-MHC (red) and endothelium was labelled by endomucin (green). At this time point, a significant reduction was observed in small/medium subendocardial vessels and a trend towards a reduction in large subendocardial vessels with the Notch1 LoF (I). *N = 3 hearts per group, P =0.03*

5.3.1 Lineage tracing of endothelial cells post-MI confirms subendocardial EndMT

Whilst the aim was to generate endothelial-specific Notch1 LoF and GoF models with TdTomato labelling targeted cells, due to breeding inefficiency, surgical losses and time constraints of the project, many of the samples used for the LoF and GoF analysis in did not contain the TdTomato reporter. Whilst this did not affect the assessment of a LoF and GoF phenotype, it provided challenges for tracing targeted cells, and it was not possible to investigate an endothelial cell contribution to other cell types in these samples. A small number of samples were positive for TdTomato, which allowed a preliminary endothelial cell lineage trace, however this requires additional n numbers before compelling conclusions can be made. Power calculations were used to determine the number of mice required per experimental group: considering a predicted 30% effect size (this is a conservative estimate, based on our pilot study), standard deviation in the order of 25%, criterion of statistical significance set at 5%, and statistical power of 85%, the approximate number required per experimental group is 8 animals. The preliminary analysis of TdTomato hearts is described below.

TdTomato was used to label endothelial cells expressing the *VE Cadherin-Cre*, with recombination induced at least 12 days prior to LAD ligation. Tamoxifen has a half-life of 12 hours, so this protocol ensured full clearance from the body prior to the surgical procedure, such that any cells labelled by TdTomato post-operatively were derived from pre-existing endothelial cells. Co-staining with α-SMA revealed TdTomato$^+$ cells closely associated with α-SMA$^+$ cells in the subendocardium of remodelling regions, at 7 days post-MI (**Figure 5.9A-C**, arrows). At this stage it was difficult to determine whether TdTomato and α-SMA were expressed in the same cells, or the α-SMA$^+$ cells were closely localised to the endothelial cells.

At 14 days post-MI, clear overlap was observed between TdTomato and SM-MHC which resulted in co-expressing cells appearing yellow (**Figure 5.9D**). In a representative image, yellow arrows indicate endocardial cells labelled with TdTomato which also

expressed SM-MHC, a mature smooth muscle marker, which were seen frequently in the subendocardium of this sample. This is the first evidence of endocardial cells showing expression of SM-MHC, and supports the hypothesis that smooth muscle cells in subendocardial vessels are derived from the endocardium (**Figure 5.9D**, box shows inset in **G,H**). Subendocardial vessels also appeared yellow at this stage, indicating TdTomato^{+} SM-MHC^{+} cells in this region (**Figure 5.9E-F**, yellow arrows). It is not possible to define whether these cells are derived from the endocardium or endothelium with the Cre model used here, however evidence is provided for an EndMT contribution to neovascularisation in the subendocardium post-MI. These data were confirmed with endomucin staining, which identified subendocardial vessels expressing TdTomato that were negative for endomucin, suggesting a non-endothelial cell type which may either be arterial endothelial cells, or smooth muscle cells (**Figure 5.9I-K**, red arrows). Preexisting endothelial cells are indicated by yellow arrows which show co-expression of endomucin and TdTomato (**Figure 5.9J**).

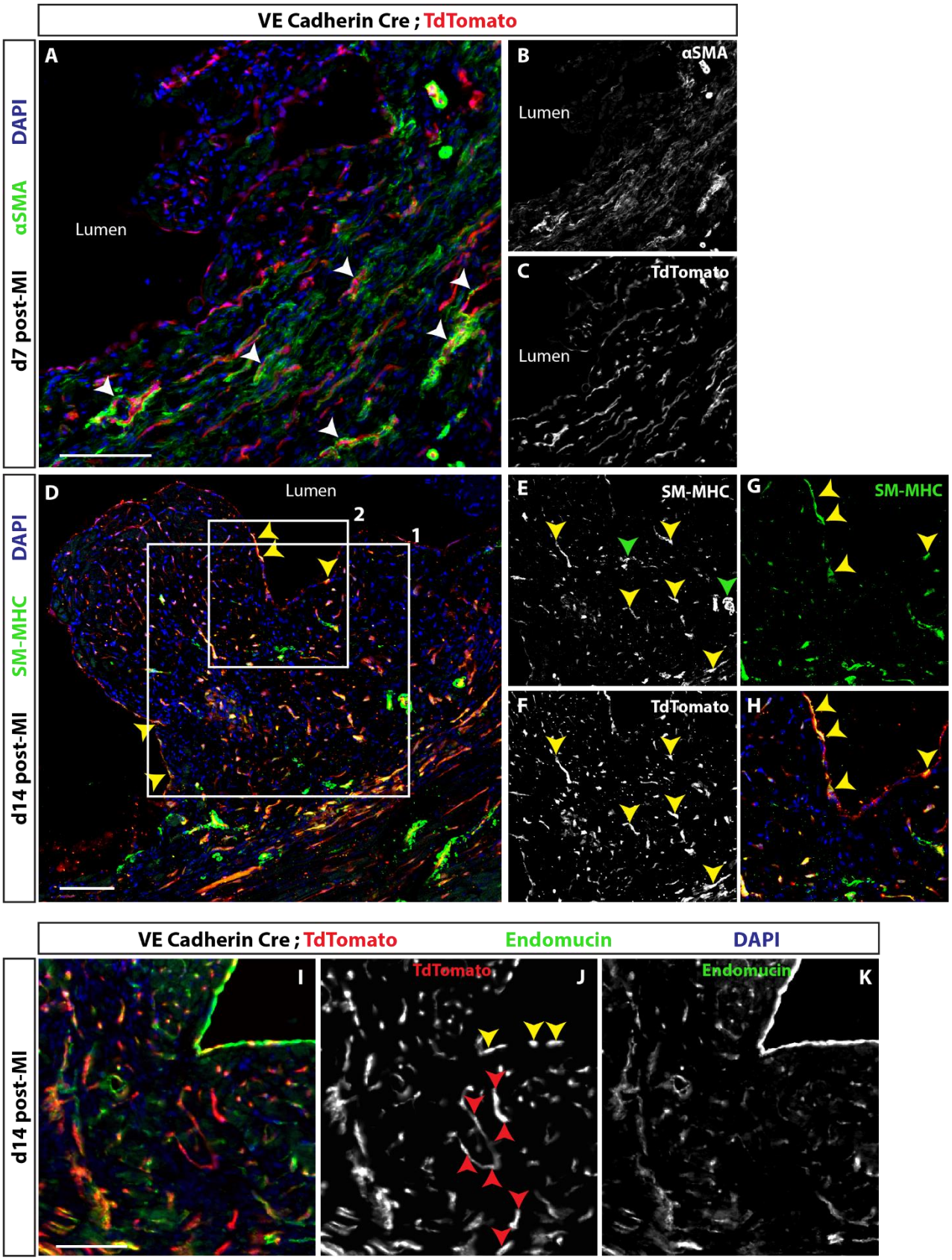

Figure 5.9. Lineage tracing shows an endothelial contribution to SM-MHC positive smooth muscle cells post-MI

Figure 5.9. Lineage tracing shows an endothelial contribution to SM-MHC positive cells post-MI

TdTomato labelling of endothelial cells using the *VE Cadherin-Cre* enabled lineage tracing of cells from the endocardium to subendocardial vessels. At 7 days post-MI α-SMA positive cells (green) were observed near the endocardial surface and in subendocardial vessels (A). Many α-SMA positive cells were localised with TdTomato cells (red), with some appearing co-labelled (A, arrows), however it is difficult to conclude whether TdTomato and α-SMA were expressed in the same cells, or in closely associated cells (B,C). At day 14 post-MI there was clearer overlap between SM-MHC and TdTomato expression, with many cells appearing orange/yellow (D). Box 1 in (D) indicates inset shown in E-F, box 2 in (D) indicates inset shown in G-H. Yellow arrows in (D) indicate endocardial cells expressing SM-MHC, and yellow arrows in (D-E) indicate the same cells which are labelled with SM-MHC and TdTomato, suggesting these are smooth muscle cells with an endothelial origin. Green arrows in (E) indicate SM-MHC positive cells that are TdTomato negative, suggesting that some sub-endocardial vessels are derived from a source that was unlabelled by TdTomato when the *VE Cadherin-Cre* was induced. (G-H) show a close up image of SM-MHC positive endocardial cells (also labelled by TdTomato). TdTomato expression is shown in combination with endomucin (green) in (I-K), and whilst many cells were overlapping to indicate these are endothelial cells, subendocardial vessels were observed which did not express endomucin (green) (I-K, red arrows). These data together suggest that a subset of subendocardial vessels are derived from endothelial cells which previously expressed *VE Cadherin* and now have a SM-MHC^{+}endomucin^{-} expression profile, supporting the theory of endocardial cells undergoing EndMT to contribute to neovascularisation post-MI. *n = 1 per timepoint. Scale bars: A, D = 100μm, I = 50μm.*

5.3.2 EndMT is impaired or delayed in Notch1 LoF post-MI

SM-MHC$^+$ cells were observed beneath the endocardium in remodelling regions at 7 days post-MI (**Figure 5.10A-D**). Arrows indicate SM-MHC$^+$ cells which appeared to align with the endocardium in remodelling regions which include newly formed lumina (**Figure 5.10A-B**). Clusters of SM-MHC$^+$ cells were also observed directly beneath the endocardial surface, suggesting a possible endocardial derivation (**Figure 5.10C-D**, arrows). Conversely, in the Notch1 LoF, SM-MHC$^+$ cells were not observed underlying the endocardium of remodelling regions in any samples at this stage. A representative image shows a few SM-MHC$^+$ vessels in the subendocardium (**Figure 5.10E-F**) with no other SM-MHC$^+$ cells, however it was unclear whether these vessels were endocardial or endothelial derived, or pre-existing coronary vessels.

In control hearts at 14 days post-MI, mature subendocardial vessels were observed, with support of SM-MHC+ cells, as described in chapter 3 and shown in figures 5.8, 5.9 and **Figure 5.11G-H**. At the same stage in the Notch1 LoF, some unusual observations were made, which suggest a delay in EndMT, and a possible migratory defect. CD31 was used to label the endocardium and endothelial cells, and SM-MHC$^+$ cells were investigated. Large clusters of SM-MHC$^+$ cells were observed beneath the endocardial surface at this stage, (**Figure 5.11A**) and when analysed at higher magnification (**Figure 5.11B**, inset from A) these cells appeared to co-express CD31 and SM-MHC. This expression profile matches that of intermediary migratory mesenchymal cells in the infarcted adult heart described by Aisagbonhi et. al., 2011, during the process of EndMT (**Figure 5.11C**). This study did not describe an endocardial origin for injury-induced EndMT, although they used an endothelial Cre and only analysed endothelial cells within the infarcted myocardium (Aisagbonhi et. al., 2011). Cell type (1), defined as endothelium, were CD31^{high}SM-MHC^{low}, and are indicated in **Figure 5.11A** as endocardium, and cell type (2) defined as migratory mesenchymal cells, were CD31^{low}SM-MHC^{low} and are indicated as the sub-endocardial cell clusters (**Figure**

5.11B). The overlap between CD31 and SM-MHC in the region outlined was calculated using the “analyse particles” tool in ImageJ, and showed 93% overlap.

Figure 5.11E shows another section of the same region, where the subendocardial SM-MHC$^+$ cells appeared to have a more mature morphology. Whilst some endocardial cells still expressed SM-MHC (yellow arrows), the majority of SM-MHC$^+$ cells were negative for the endothelial marker, endomucin (white arrows).

In another remodelling region of the same heart, mature SM-MHC$^+$ cells were observed in close association with the endocardium (**Figure 5.11F**, white arrows), with some cells co-expressing endomucin and SM-MHC (yellow arrows). Additionally, in this region which includes a large subendocardial lumen, the endocardial cells displayed an unusual cobblestone morphology which was never observed in control hearts.

In addition to the clusters of SM-MHC$^+$ cells close to the endocardium at 14 days post-MI, more subendocardial lumina were observed in the Notch1 LoF which were unsupported by SM-MHC. Lumina appeared to form beneath the endocardial surface, which were lined by endomucin, but not SM-MHC (**Figure 5.12A-F**). Vessels are indicated with green arrows, and the subendocardial lumina outlined in **Figure 5.12C, F**, were completely negative for SM-MHC.

When compared with the control sample at 14 days post-MI shown in **Figure 5.9** and **Figure 5.11G-H**, the morphology of the Notch1 LoF was very different. Fewer mature subendocardial vessels were present, and large subendocardial lumina were retained, rather than compacting in combination with subendocardial vessel maturation.

These data together suggest that the loss of endothelial Notch1 signalling did not completely repress subendocardial EndMT, but instead has led to a delay or impairment which results in fewer subendocardial vessels at 7 and 14 days post-MI, and excessive clusters of SM-MHC$^+$ cells beneath the endocardium. Since some of the SM-MHC$^+$ subendocardial cell clusters appear mature, this raises the possibility of a Notch1-

induced migration defect which has prevented the cells from moving into the myocardium to surround the newly derived lumina. Further investigations are needed to distinguish EndMT from migratory defects and to characterise the molecular mechanisms driving the formation of these SM-MHC^{+} subendocardial clusters.

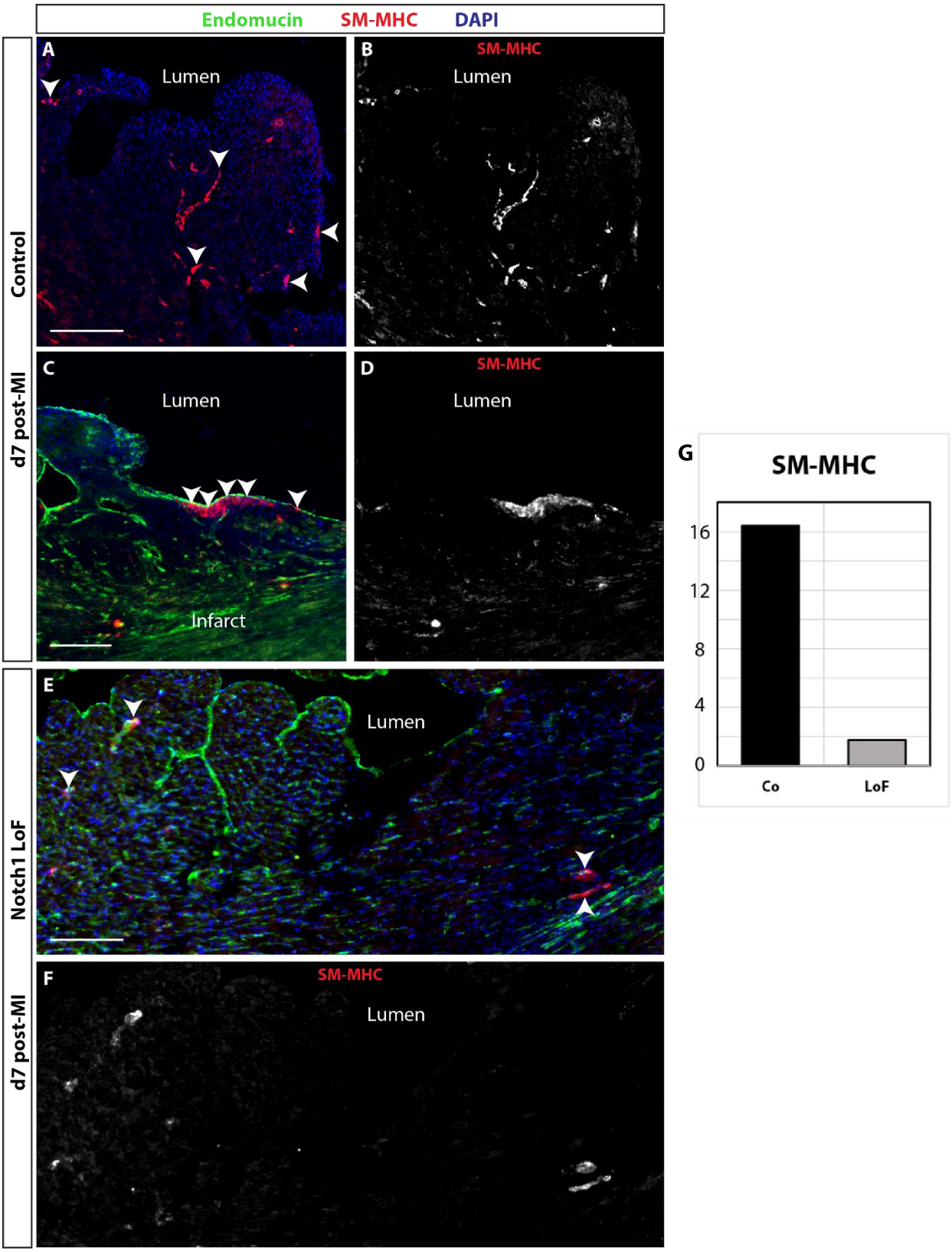

Figure 5.10. EndMT is impaired or delayed in Notch1 LoF

Expression of SM-MHC (red) is shown in control hearts at 7 days post-MI; positive cells were observed underlying the endocardium (endomucin, green) in remodelling regions (A-D, arrows), suggesting that these cells may be endocardial-derived. In the Notch1 LoF samples, very few SM-MHC positive cells were observed in the subendocardium (E-F, arrows), with none captured underlying the endocardial surface. Data have been quantified in (G). These data are suggestive of impaired EndMT or a delay in this process with the Notch1 LoF. *Scale bars = 200μm, n = 4 per condition.*

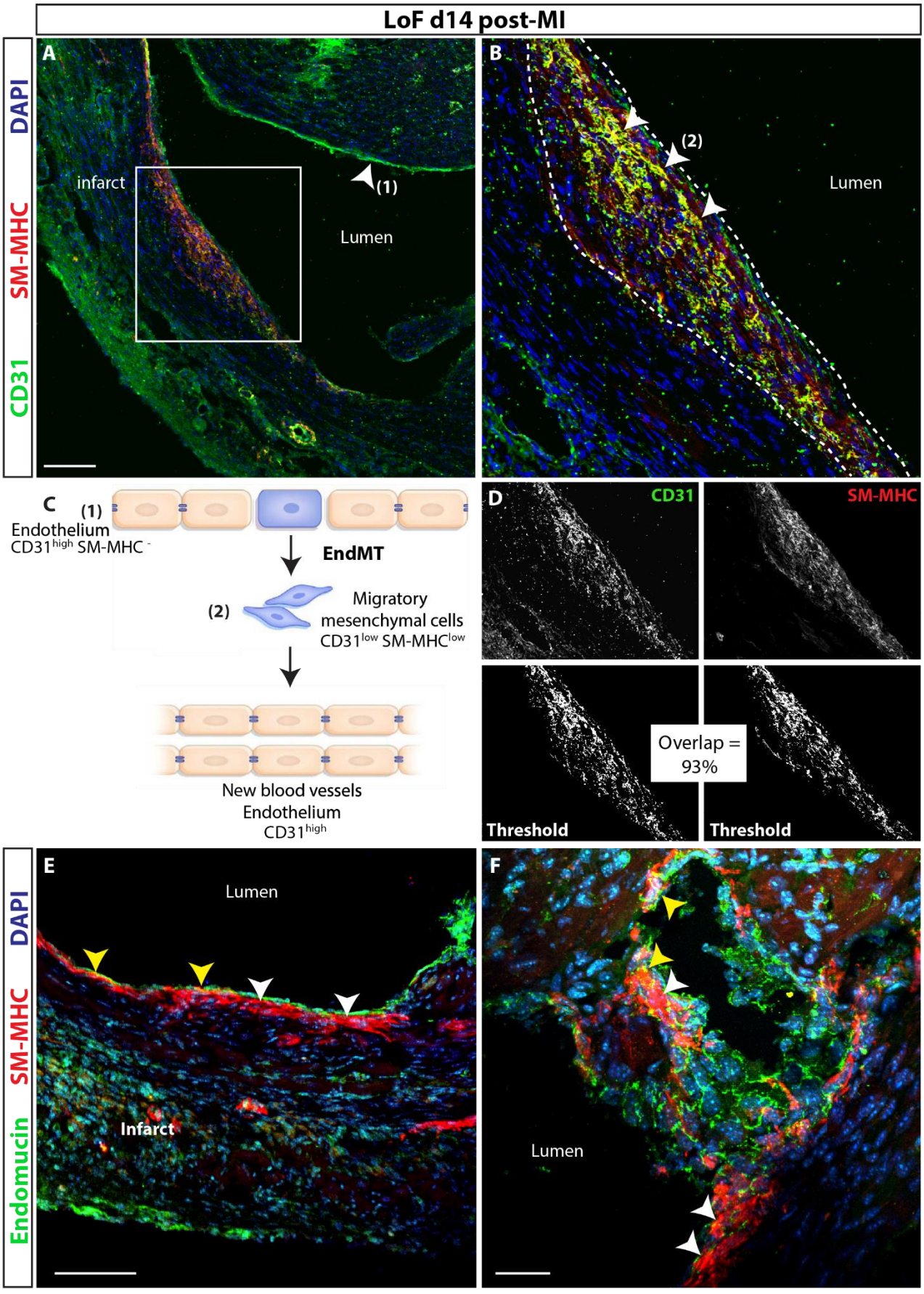

Fig. 5.11. Impaired neovascularisation in Notch1 LoF at day 14 post-MI

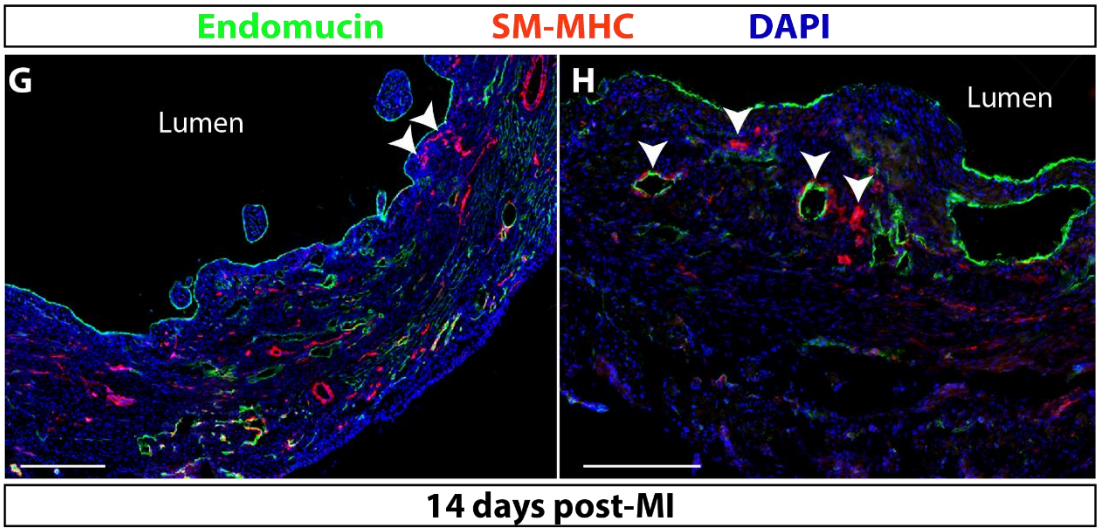

Figure 5.11. Impaired neovascularisation in Notch1 LoF at day 14 post-MI

Impaired neovascularisation was observed at 14 days post-MI in the Notch1 LoF. In control hearts at this stage (**Figure 5.9 and** panels G, H), the endocardium is mostly compacted with mature subendocardial vessels formed. However, clusters of SM-MHC (red) positive cells were observed underlying the endocardial surface in Notch1 LoF (A). This region is shown at higher magnification (B,D) and the cluster of cells co-expressed CD31 (green), an endothelial cell marker, along with SM-MHC. Migratory mesenchymal cells produced as an intermediate cell type during EndMT have been identified with low $CD31^{+}SM\text{-}MHC^{+}$ expression (C, Aisagbonhi et. al., 2011), and the overlap of CD31 and SM-MHC was calculated as 93% in this subendocardial cell cluster. These data suggest that EndMT occurs in the Notch1 LoF model, however the later observation of cells undergoing EndMT suggests that the process has been disrupted. A consecutive section of the same region shows more mature like $SM\text{-}MHC^{+}$ cells beneath the endocardium (E, white arrows), which was labelled with endomucin (green) and in some areas co-expressed SM-MHC (E, yellow arrows). SM-MHC+ cells were also observed in a region of endocardial remodelling to form a subendocardial lumen (F, white arrows), however the cells appear to be trapped at the endocardial surface, with some co-expressing endomucin (F, yellow arrows) and the endocardial cells showing an unusual cobblestone morphology (F). d14 controls are shown in G-H, indicating SM-MHC supported subendocardial vessels at this stage (arrows). *Scale bars: A, G = 500µm, E, H = 200µm, F = 50µm. N = 2.*

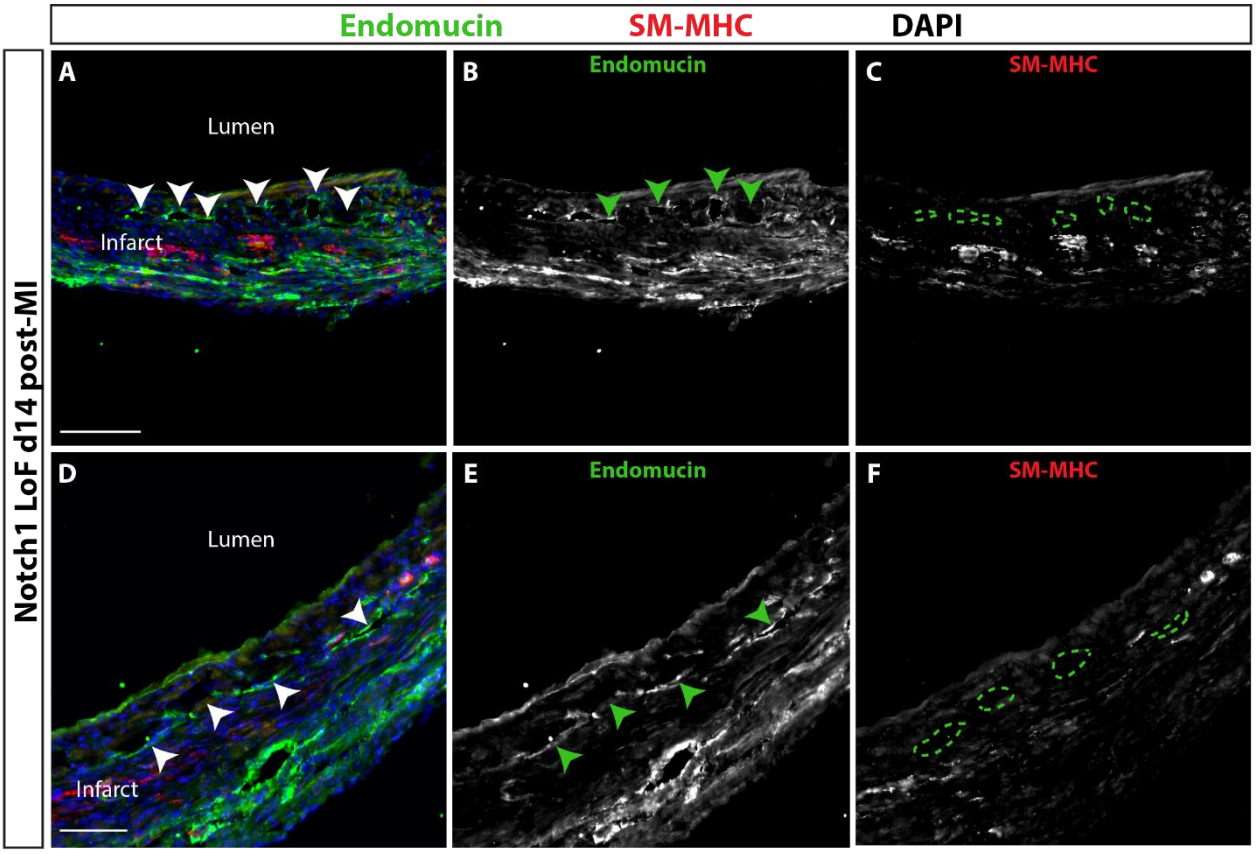

Figure 5.12. Sub-endocardial lumina lack SM-MHC positive cells in Notch1 LoF 14 days post-MI

Subendocardial vessels (lumina) were observed in Notch1 LoF hearts at day 14 that lacked SM-MHC (red) support (A-F). Lumina beneath the endocardial surface are indicated with arrows (A, B, D, E) and express endomucin (green) (B, E), but no SM-MHC (C,F). This supports Figure 5.11 and provides further evidence for an impairment in neovascularisation in the Notch1 LoF. *Scale bars = 100μm. N = 2.*

5.4.1 Constitutive activation of endothelial Notch1 induces subendocardial remodelling in the uninjured adult heart

The endothelial Notch1 GoF was induced by 5 doses of tamoxifen as described in Chapter 4, and hearts were harvested 10 days later (**Figure 5.13A**). Hearts showed an unusual endocardial morphology and dilatation of the left ventricle (representative images in **Figure 5.13B-C**) in the Notch GoF group, compared with control. DAPI staining was used to create endocardial traces (D-E), and these were analysed using FracLac software. An increase in endocardial projections was observed (**Figure 5.13D,E**, arrows), however when analysed statistically, this trend was not significant (**Figure 5.13F**).

Subendocardial vessels were also investigated in the Notch1 GoF model without MI, and an obvious increase was observed. Vessels were labelled with SM-MHC and endomucin, and, as expected, minimal subendocardial vessels were observed in control hearts without MI (**Figure 5.14A,C,E**). In contrast, the Notch1 GoF hearts appeared to have an increased number of SM-MHC^{+} vessels in the subendocardium (**Figure 5.14B,D,F**). Interestingly, these vessels were co-labelled with endomucin and SM-MHC, which is usually only observed in post-MI hearts, since endomucin primarily labels veins and capillaries, but not arteries, whereas SM-MHC labels the smooth muscle surrounding arteries. Given the effects observed in the Notch1 LoF on EndMT and subendocardial vessels post-MI, it is plausible to speculate that this increase in SM-MHC^{+} vessels in non-MI Notch1 GoF hearts may be induced by EndMT, which has been triggered by endothelial Notch1 signalling. However, due to the small sample size, statistical analysis was not undertaken and additional samples are required to cofirm these results.

To identify the source of the SM-MHC+ vessels in the Notch1 GoF hearts, the *VE Cadherin-Cre;TdTomato* line was crossed with the Notch1 GoF model, to label the endothelial cells targeted with the Notch1 GoF. Endocardial remodelling was observed in these samples with large lumina formed beneath the endocardial surface (**Figure**

5.15A, yellow box), and SM-MHC^{+} vessels were present in the subendocardium (**Figure 5.15A**, arrows). Some of the cells in these subendocardial vessels appeared to co-express TdTomato and SM-MHC (**Figure 5.15B-C**, arrows), which supports the possibility of induced EndMT in this model. A large subendocardial vessel in another sample also showed clear overlap between TdTomato and α-SMA (**Figure 5.15C-E**), which may be similar to the migratory mesenchymal cells observed post-MI. Another representative image provides supporting evidence, with large subendocardial lumina clearly evident (yellow boxes), and a mature subendocardial vessel which co-expressed TdTomato and SM-MHC. These data are supportive of a role for endothelial Notch1 in neovascularisation, and provide evidence of this pathway being induced, even in non-MI hearts.

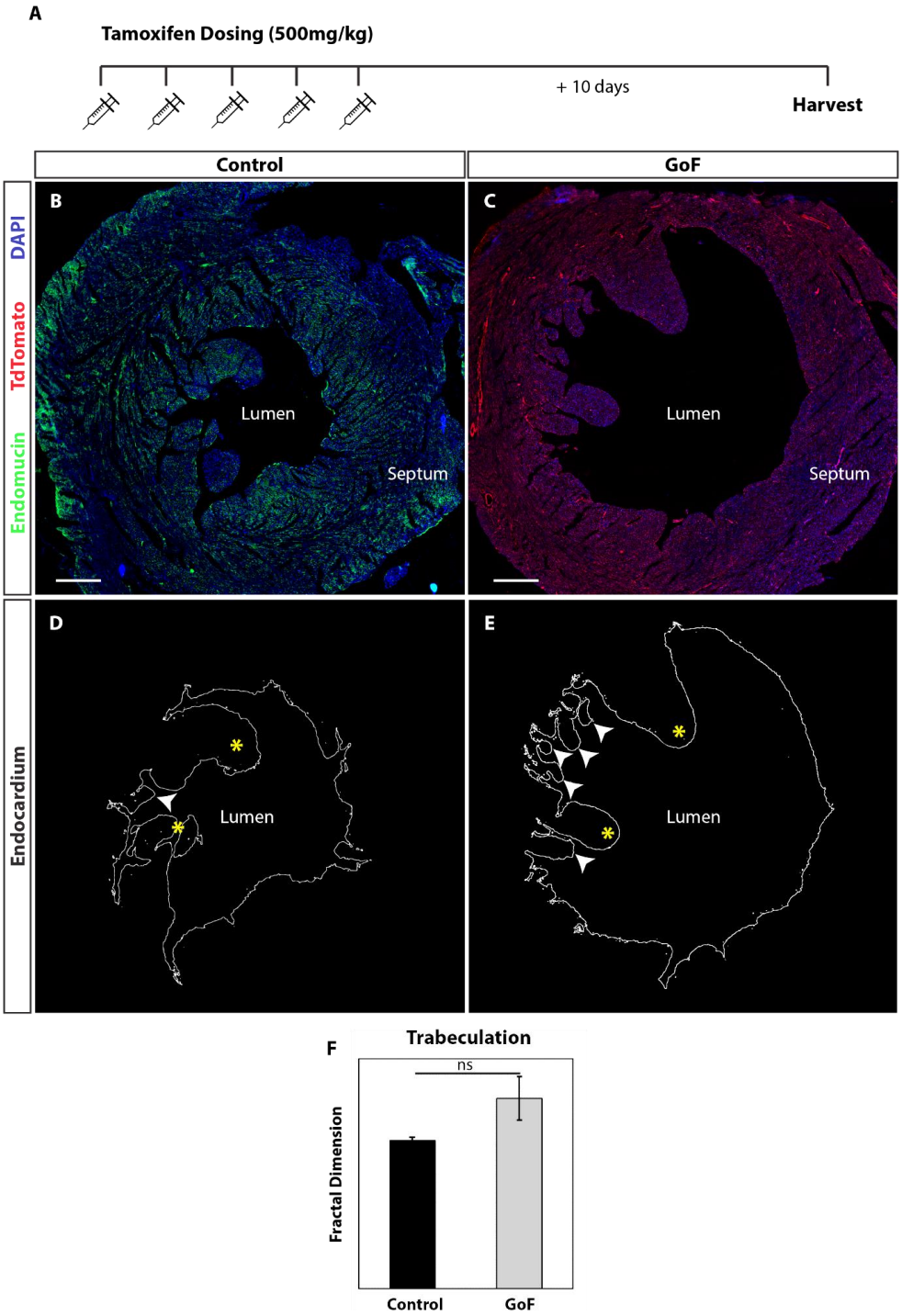

Figure 5.13. Notch1 GoF hearts show a trend towards increased endocardial remodelling without injury

Notch1 GoF hearts were examined without injury and compared with control hearts. Mice were harvested 10 days after being dosed with tamoxifen (A, endomucin green, TdTomato red), and analysed using immunofluorescent imaging and fractal analysis. Representative images are shown in (B, C), where the GoF heart appears to be more dilated. The endocardial traces highlight differences in endocardial trabeculation (D, E, arrows), with the GoF trace appearing to have more endocardial projections than the control. Papillary muscles are indicated by yellow asterisks (D, E). The traces were run through FracLac software in ImageJ and a comparison was made between the groups. A trend towards increased trabeculation in the Notch1 GoF was observed, however this was not significant with the N number tested (F). *n = 3 per group, P = 0.23, scale bars = 1mM*.

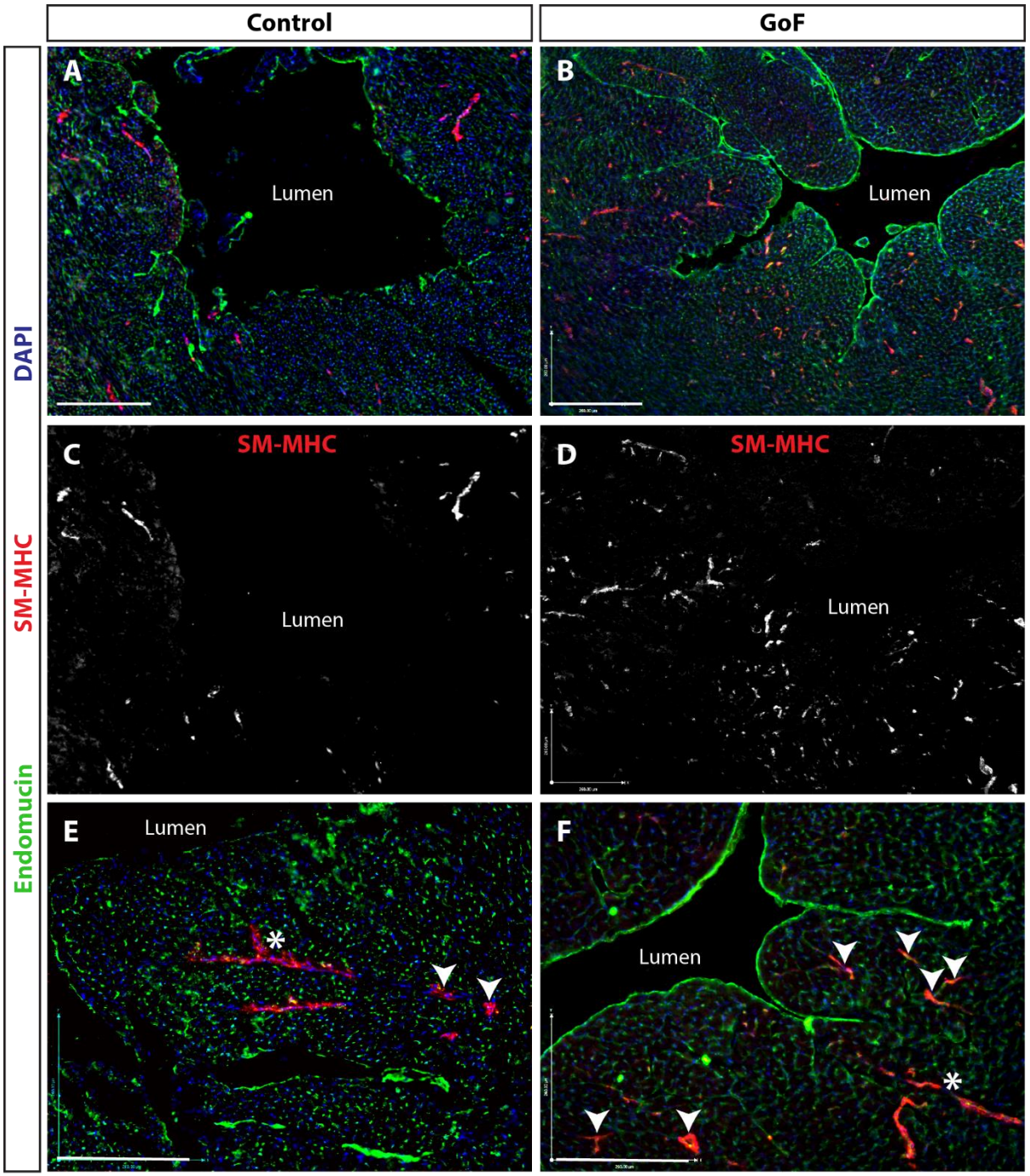

Figure 5.14. Increased neovascularisation in Notch1 GoF without injury

SM-MHC (red) expression was investigated in Notch1 GoF hearts without injury to examine any changes in neovascularisation. An increase in the number of vessels was observed in the Notch1 GoF (A, B, red), with more vessels appearing close to the endocardium (B). SM-MHC expression is shown in (C, D) where more vessels are visible close to the lumen in (D), endomucin (green) labelled endothelium. Additional examples are shown at higher magnification in (E, F) and vessels are indicated by arrows. Asterisks highlight large vessels which are often seen in the uninjured adult heart, however the small vessels labelled in (F) are unusual in their close proximity to the endocardium. In the control hearts, endomucin did not label SM-MHC$^+$ vessels since it is generally a marker of veins, however in the GoF hearts, most of the SM-MHC$^+$ vessels appeared to be co-labelled by endomucin, which is more reminiscent of the infarcted heart, suggesting that these vessels may be derived as a consequence of Notch1 GoF. *n = 2, scale bars: A, B = 200μm, E, F = 100μm.*

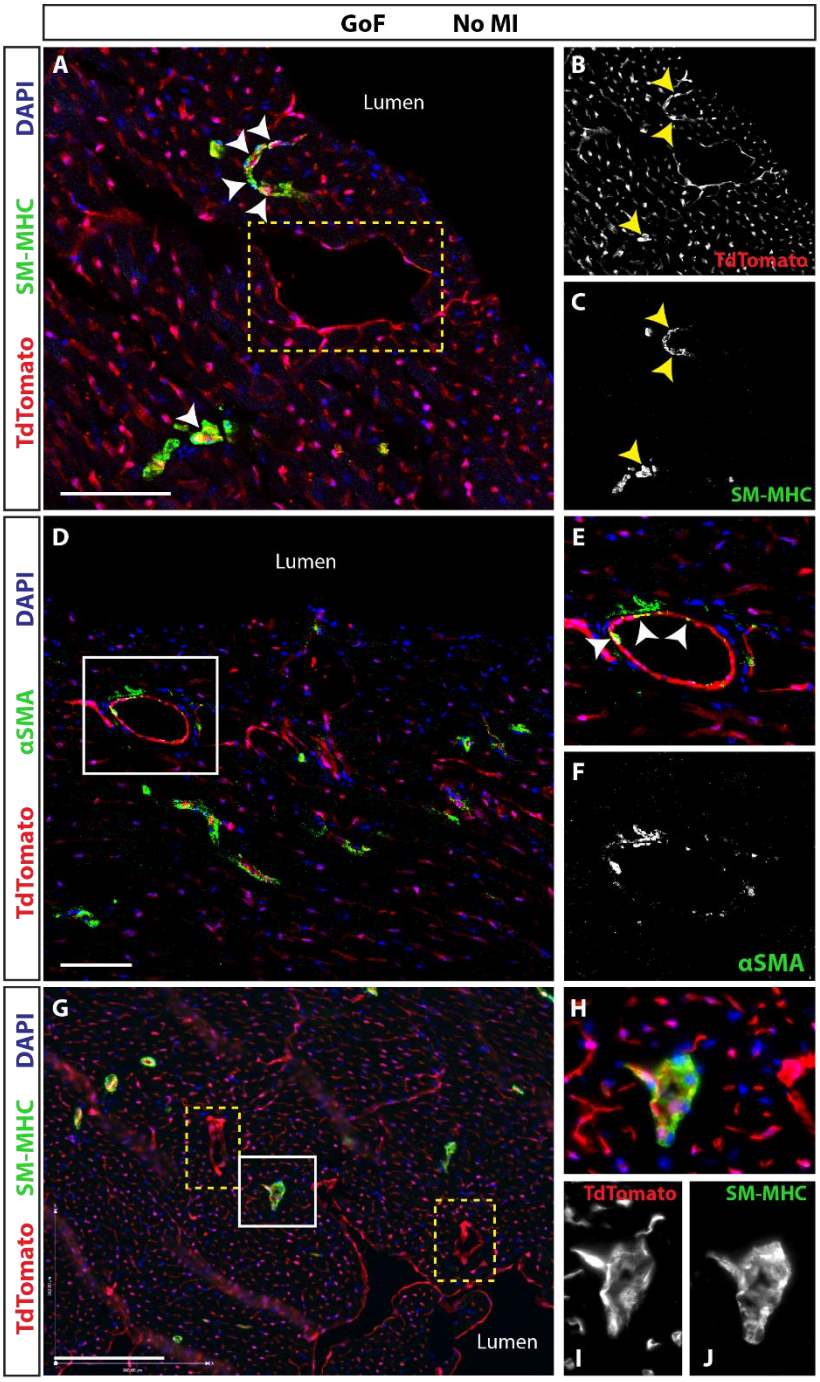

Figure 5.15. TdTomato lineage tracing shows evidence of an endothelial contribution to SM-MHC positive cells in Notch1 GoF hearts without injury

TdTomato (red) labelling of endothelial cells in the Notch1 GoF enabled lineage tracing in uninjured adult hearts. SM-MHC$^+$ vessels (green) were observed close to the endocardial surface, with apparent co-expression of TdTomato in the same cell (A-C, arrows), suggesting and endothelial source. Large lumina were also observed beneath the endocardial surface (A, C, yellow boxes) which is uncharacteristic of an uninjured heart, and some of these TdTomato lined vessels contained cells co-expressing αSMA$^+$ (B-F, arrows). These lumina may be in the process of developing into mature vessels, with the TdTomato$^+$ αSMA$^+$ cells being migratory mesenchymal cells that are undergoing EndMT to give rise to smooth muscle cells. In support of this, a mature vessel was observed co-expressing TdTomato and SM-MHC in another sample (G-J), suggesting an endothelial contribution to smooth muscle of subendocardial vessels in the Notch1 GoF uninfarcted heart. *n = 2. Scale bars: A, F = 100μm, B = 200μm.*

5.4.2 Increased trabeculation and subendocardial vessels with constitutive activation of endothelial Notch1 post-MI

The Notch1 GoF was activated prior to LAD ligation and samples compared with control hearts over a time course post-MI. The sample size for the Notch1 GoF was low (n=2 for day 2, n=1 for day 7) so quantification and statistical analysis was not possible, however interesting observations were made from the samples harvested, which supports the value of further investigation. At 2 days post-MI, endocardial remodelling appeared to be increased, with many more endocardial projections overlaying the infarcted myocardium than in control hearts (**Figure 5.16A-D**, arrows). Whilst endocardial remodelling was also observed in control hearts at this stage, the Notch1 GoF hearts appeared to have already formed large, enclosed subendocardial lumina (**Figure 5.16D**, yellow arrows) which have not been observed until 4 days post-MI in control hearts. Additionally, subendocardial α-SMA$^+$ vessels were observed in remodelling regions (**Figure 5.16E**, arrows), as well as α-SMA$^+$ cells associated with endothelial cells close to the endocardial surface. These cells, which were proposed to be the intermediary migratory mesenchymal cells observed at day 7 in control hearts, appear to have arisen earlier in the Notch1 GoF model (**Figure 5.16F-G**).

An increase in TdTomato labelled subendocardial vessels was observed at 7 days post-MI in the Notch1 GoF (**Figure 5.17A-C**, arrows). These vessels were co-labelled with SM-MHC, suggesting that they are mature vessels, and potentially derived from pre-existing endothelial cells which have undergone EndMT. Individual channels showed expression of SM-MHC and TdTomato in the same vessels (**Figure 5.17D-F**, arrows), but it is unclear whether these are the same cells or closely associated endothelial and smooth muscle cells. A representative control heart at day 7 showed fewer SM-MHC labelled subendocardial vessels, and certainly fewer co-expressing the endothelial marker (**Figure 5.17G-H**).

Whilst these data are descriptive, and from a small sample size, they complement the findings shown with the Notch1 LoF, and suggest a role for endothelial Notch1 in endocardial remodelling and subendocardial neovascularisation post-MI.

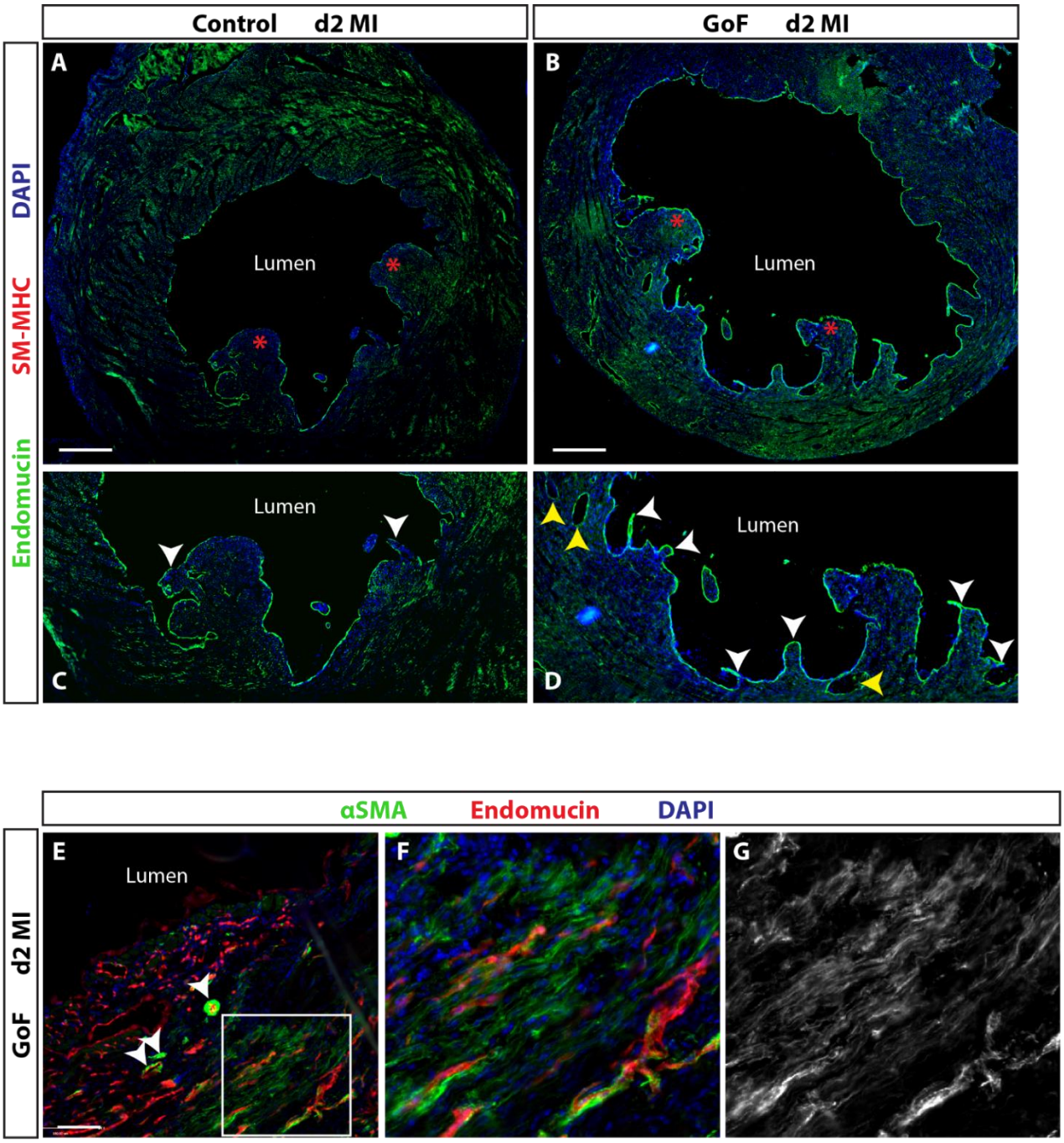

Figure 5.16. Increased trabeculation and precocious EndMT observed in Notch GoF at 2 days post-MI

Whilst the N number for Notch1 GoF samples post-MI was too low for quantification, the samples collected revealed interesting preliminary observations. A clear increase in endocardial remodelling was observed at 2 days post-MI with Notch1 GoF (A-B). More endocardial projections were observed in the Notch1 GoF than the control (C, D, white arrows) and multiple lumina formed beneath the endocardial surface (D, yellow arrows), which were not observed in control hearts at this stage. αSMA$^+$ vessels were observed close to the endocardial surface (E, arrows) and αSMA$^+$ cells appeared in the subendocardial region of the Notch1 GoF at 2 days post-MI (F-G). These cells showed a similar pattern to the αSMA$^+$ cells seen in control hearts at 7 days post-MI (Figure 5.9) which were localised with TdTomato$^+$ cells, supporting a role for endothelial Notch1 in EndMT. *Scale bars: A, B = 1mM, E = 100μm. N =2.*

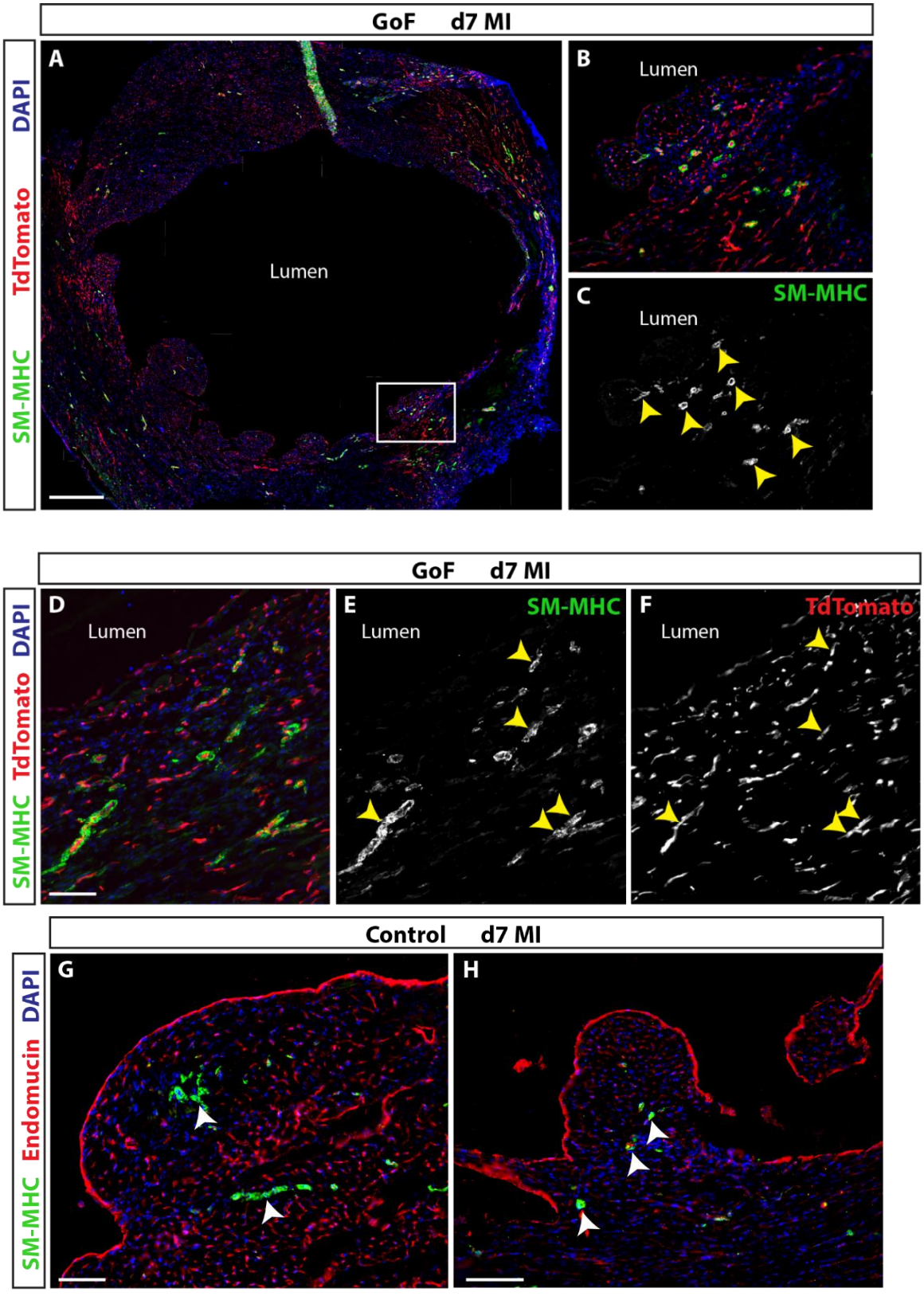

Figure 5.17. Increased density of mature sub-endocardial vessels observed in Notch1 GoF 7 days post-MI

TdTomato^{+} vessels were observed in the subendocardium of a remodelling region in the Notch1 GoF heart at 7 days post-MI (A-C, arrows). Whilst vessels appeared to co-express SM-MHC and TdTomato, it is difficult to conclude whether the SM-MHC^{+} cells are also TdTomato^{+}, or cells closely aligned (A-F, arrows). The density of mature subendocardial vessels appeared to be higher in this Notch1 GoF sample, when compared with a control at the same time point (G-H). *Scale bars: A, D, G = 100μm, H = 200μm, n = 1.*

5.5.1 Discussion

This chapter has expanded upon the findings from Chapters 3 and 4, and provided supportive evidence of a role for endothelial Notch1 in endocardial remodelling and subendocardial neovascularisation post-MI.

CBF:H2B-Venus was used to investigate Notch activity in the post-MI setting, in support of the immunofluorescence data shown in Chapter 3. Whilst this tool was useful in identifying clusters of Notch signalling cells in regions of endocardial and subendocardial remodelling, expression of Venus was also observed widely throughout the myocardium in sham and MI hearts. This reporter of Notch signalling is not specific to the Notch1 receptor, since signalling through any of the Notch receptors, 1-4, results in cleavage of the intracellular domain, binding with CBF1 and translocation to the nucleus to activate transcription factors. Therefore, whilst the data shown using this reporter confirmed the observations with the N1ICD antibody, it was not possible to decipher whether the antibody was an unreliable readout of Notch1 activity, or the additional activity seen with the *CBF:H2B-Venus* was through the other three Notch receptors.

Notch signalling has been studied extensively in cardiac repair post-MI, although these studies have focused primarily on cardiomyocyte proliferation, and cardiac progenitor cell proliferation and differentiation (Gude et. al., 2012). Since this project aimed to focus on endothelial Notch1 signalling, the lack of specificity of the *CBF:H2B-Venus* reporter proved to be a limiting factor, and whilst the strong Venus fluorescence was useful for visualising Notch in remodelling regions, it was not possible to clearly identify all cell types undergoing Notch signalling, nor to assess which receptor was activated. The data acquired from this reporter, in combination with the antibody staining observations, provided sufficient rationale to target Notch1 in the endothelium, but additional experiments were not undertaken to further characterise *CBF:H2B-Venus* reporter activity.

Changes in endocardial remodelling were analysed using FracLac software plugin for ImageJ, which defined trabeculation by FD. Whilst the morphology of the endocardium appeared to be different in the Notch1 LoF at 2 days post-MI, a significant difference in FD was only found at 7 and 14 days post-MI, when a reduction in FD was identified. Although all endothelial cells were targeted with the *VE Cadherin-Cre*, this analysis focused specifically on the morphology of the endocardium, and it is therefore reasonable to assume that the phenotype observed is due to disrupted Notch1 signalling in endocardial cells. This finding supports the hypothesis of developmental mechanisms driving trabeculation and compaction being recapitulated in the pathological setting. Endocardial Notch1 has been established as the key regulator of proliferation, differentiation and maturation for left ventricular patterning in the embryo (D'amato et. al., 2015), however this study provides the first evidence of the pathway being reactivated in the adult heart. Future work should focus on the forces driving the redeployment of this developmental pathway, with consideration given to hypoxia and mechanical changes due to their impact on developmental remodelling and cardiac patterning (Campernolle et. al., 2003, Shyu, 2009, Khokhlova et al., 2016). The number of subendocardial vessels was analysed in control and Notch1 LoF, and a significant reduction in small/medium SM-MHC^{+} vessels between the endocardium and the infarct was observed at 7 and 14 days post-MI. The discovery of subendocardial vessels in the adult injured heart is a novel finding that we published in 2017 (Dubé et. al., 2017), and the data provided here gives an insight into the mechanisms underlying the formation of these vessels. The methods used allow us to conclude that endothelial Notch1 has a role in subendocardial neovascularisation post-MI, however they do not provide a detailed interrogation into the exact signalling cascade taking place. Further investigation is required to elicit the full mechanism, and to determine whether the neovascularisation and trabeculation phenotypes are interlinked or independent of each other.

To examine the role of Notch1 as a cell fate regulator, TdTomato was used to label cells targeted by the endothelial *VE Cadherin-Cre* prior to LAD ligation surgery. This allowed us to analyse whether TdTomato was expressed in any non-endothelial cells post-MI, which would suggest that pre-existng endothelial cells had changed fate and transitioned to another cell type. TdTomato was observed in SM-MHC+ cells both in the endocardium and in subendocardial vessels, which suggests that endocardial cells have undergone some form of EndMT, and may possibly be the source of mesenchymal cells for the contribution of smooth muscle cells to *de novo* subendocardial vessels. Whilst the TdTomato/SM-MHC expression observed in the endocardium and subendocardial vessels provides strong supporting evidence of an endocardial contribution, without a specific endocardial Cre, this cannot be categorically concluded. Bin Zhou's group recently published an Npr3-Cre model which was reported to be specific to the endocardium (Tang et. al., 2018), however, when they used this to lineage trace endocardial cells after LAD ligation, cryoinjury and ischemia-reperfusion they found that the endocardium minimally contributed new coronary vessels. However, in a model which involved trapping endocardial cells, they showed an endocardial contribution to vascular endothelial cells of newly derived vessels. It is unclear why their findings from the LAD ligation model do not align with the results shown here, although some of their infarcted samples appeared to show a scar much larger than 30%, which as described in Chapter 4, would have impaired trabeculation and the subendocardial neovascular response. Future work should aim to assess the utility of this line and determine the effect of Npr3 haploinsufficiency, since the heterozygous deletion of the gene may have impacted neovascularisation. By rigorously lineage tracing the endocardium using the methodology described in chapter 4, it should be possible to clarify any endocardial contribution to subendocardial vessels, and ideally confirm the suitability of Npr3-Cre for targeting the adult endocardium.

Notch1 is known to induce EndMT during development (Luna-Zurita et. al., 2010), however this process takes place in the atrioventricular canal, whereas trabeculation occurs in the ventricles (D'amato et. al., 2015). It is unclear from the data shown in this thesis, which downstream signalling mechanisms are activated by Notch1 to induce neovascularisation. However, the role of Notch1 in EndMT was investigated in a small number of samples at 14 days post-MI to determine whether this process has a role in the formation of subendocardial vessels post-MI.

Whilst EndMT was apparent relatively early in control hearts, with SM-MHC^{+} cells observed beneath the endocardium at 7 days post-MI and mature subendocardial vessels expressing TdTomato at 14 days post-MI, the Notch1 LoF samples did not replicate these results. Instead, at 14 days post-MI unusual morphological changes were observed, with SM-MHC^{+} cells clustered beneath the endocardial surface and gathered around remodelling subendocardial lumina. These data suggest that Notch1 plays a role in orchestrating EndMT post-MI, and that the process is either impaired or delayed with the loss of function. The presence of migratory mesenchymal cells suggests that the endocardium retains its capacity to undergo EndMT, albeit delayed, therefore further investigation should be focus on a migratory defect, since the clusters of mature SM-MHC^{+} cells appear to have failed to migrate into the myocardium to surround the newly formed subendocardial lumina. This finding requires considerable future work to fully uncover the effect of Notch1 LoF on EndMT, and experiments to investigate this mechanism are discussed further in Chapter 7.

Alongside the Notch1 LoF studies, evidence has been provided for EndMT in the uninjured adult heart and after LAD ligation with constitutive activation of endothelial Notch1. The formation of large subendocardial lumina and mature subendocardial vessels in non-MI hearts is a novel observation, and supports a role for Notch1 in orchestrating subendocardial EndMT. This is perhaps the most convincing data to prove the importance of Notch1 signalling in this setting, providing confirmation that Notch1

activation is sufficient to drive the formation of subendocardial vessels, even without injury. Whilst these data are limited due to sample size, the findings could uncover a novel mechanism for neovascularistion in the adult heart, and reveal a therapeutically relevant target. The additional remodelling observed in the infarcted Notch1 GoF hearts provide further support for the activation of this pathway, and with increased N numbers and a thorough analysis, this model has the potential to uncover the full mechanism driving this process. Further experiments to build on this finding are described in Chapter 6.

5.5.2 Conclusions

- Endothelial Notch1 is a key regulator of endocardial trabeculation after MI
- Formation of subendocardial vessels is driven by endothelial Notch1 in the infarcted adult heart
- Subendocardial EndMT contributes to neovascularisation post-MI
- Subendocardial EndMT is impaired with the loss of endothelial Notch1
- Neovascularisation is induced by constitutive activation of endothelial Notch1 in both uninjured and injured adult hearts
- EndMT is induced by constitutive activation of endothelial Notch1 in the uninjured adult heart
- Notch1 appears to be a key regulator of EndMT, contributing to subendocardial neovascularisation in the infarcted adult heart

CHAPTER 6

DISCUSSION, CONCLUSIONS AND FUTURE WORK

Chapter 6

General Discussion, Conclusions and Future Work

6.1 Discussion

The findings of this project are discussed with reference to the objectives described in Chapter 1:

- ***Characterisation of endocardial remodelling post-MI and screen for recapitulation of developmental pathways***

- ***Development of surgical, analytical and genetic tools to analyse trabeculation and the role of endocardial Notch1 post-MI***

- ***Investigate the role of Notch1 in endocardial remodelling and neovascularisation post-MI***

This chapter aims to consider the extent to which these objectives were achieved, and to discuss limitations associated with the methodology and results described. Conclusions are made, where relevant, and future work to expand upon the findings of this thesis is outlined.

6.1.1 An endocardial contribution to neovascularisation post-MI?

This thesis evaluated evidence for an endocardial contribution to neovasucularisation in the adult ischemic heart. A combination of descriptive and quantitative methods were utilised and the conclusions overall support a role for the endocardium in the processes of trabeculation and compaction, and subendocardiual EndMT, in what appears to be a recapitulation of developmental mechanisms in the post-MI setting. Extensive endocardial remodelling was characterised and the mechanism underlying the formation of *de novo* sub-endocardial vessels was rigorously examined, with Notch1 identified as a key regulator in orchestrating distinct morphological changes in response to injury. This is the first description of an endocardial mechanism being reactivated in the adult heart, and proposes a new direction for neovascularisation studies, and the potential for novel pharmacological interventions in the treatment of heart failure.

The challenges associated with targeting the adult endocardium have been described in detail throughout this thesis. The lack of a specific gene to label the adult endocardium is an ongoing limitation of the field, which will continue to limit studies of this tissue until a novel marker is identified. A pulse-chase lineage tracing study that investigated three well-established endothelial markers, *Cdh5-CreER*, *ApInCreER* and *Fabp4CreER* concluded that almost 100% endothelial cells were labelled prior to MI, and almost 100% vascular endothelial cells were labelled post-MI with all three transgenic models (He et. al., 2017). This study provided conclusive evidence that there is no non-endothelial contribution to neovascularisation in the ischemic adult heart, after a previous study claimed a fibroblast contribution to vascular endothelial cells via a mesenchymal-endothelial-transition (Ubil et. al., 2014). The confirmation of an exclusive endothelial contribution to vascular endothelial cells post-MI supports the findings presented here, since the endocardium is also labelled by all three endothelial models used by He et. al., 2017. At the time of developing the experiments described in this thesis, the only model available to distinguish endocardial cells from endothelial cells was *Pdgfb-iCreER*, which labels all endothelial cells except the endocardium. Whilst a specific endocardial lineage

trace is the only way to unequivocally prove an endocardial source of vascular endothelial cells post-MI, evidence of subendocardial vessels that were unlabelled by *Pdgfb-Cre;YFP* (Dubé et. al., 2017), being the only difference from the endothelial lineage traces used by He et al, collectively provide a convincing proposal for an endocardial contribution in this setting.

In combination with investigating the formation of subendocardial vessels, consideration was given to the process of EndMT in the adult MI setting. The *Pdgfb-Cre* reporter showed some overlap between TdTomato and α-SMA in regions of capillary expansion, but large clusters of α-SMA$^+$ cells beneath the endocardial surface which were unlabelled by tdTomato suggested a non-endothelial source. This line of investigation was followed up via a *VE Cadherin-Cre*-driven reporter, where the only difference in the profile of cells labelled by this marker was the endocardium. Sub-endocardial α-SMA$^+$ cells were associated with tdTomato labelled cells at 7 days post-MI in this model, and at 14 days post-MI co-expression of tdTomato and SM-MHC was observed in sub-endocardial vessels, as well as in the endocardium. These data suggest that endocardial EndMT may contribute to mature sub-endocardial vessels in the infarcted heart. The sample size of the post-MI *VE Cadherin-Cre;tdTomato* cohort was low, and additional samples are required to perform a quantitative analysis of SM-MHC$^+$ tdTomato$^+$ subendocardial vessels, in support of this interesting finding. SM-MHC$^+$ endocardial cells should also be quantified in this model in an attempt to distinguish between an endothelial and endocardial origin of EndMT.

The key limitation of this method lies with the transgenic model used to lineage trace the endocardium, as the *VE Cadherin-Cre* provides no definitive method of tracing SM-MHC$^+$ cells specifically to the endocardium, however, with the use of morphological features and the potential identification of a specific marker to label the endocardium immunohistochemically in the samples described here, and the subsequent development of a novel Cre to generate new samples, we hope to provide a convincing case in future, for a portion of the cells contributing to EndMT being endocardial-derived.

An additional limitation of the methods used to investigate EndMT in this setting is the long window between harvest time points at days 2, 7 and 14 post-MI, which may have concealed important components of this molecular process that would provide an insight into how the mechanism unfolds. At the earliest time-point, EndMT does not appear to be activated, at 7 days post-MI some tdTomato^{+} cells were associated with α-SMA^{+} cells, and by 14 days post-MI, co-expressing vessels were observed in the sub-endocardium. Whilst these snapshots are useful for investigating the presence of EndMT in the post-MI heart, a more in-depth study which includes samples at days 4 and 10 in addition to those investigated here, may reveal important aspects of the endocardial contribution that were missed by this strategy.

6.1.2 Endocardial remodelling in the infarcted heart

A detailed time-course was provided as a novel demonstration of recapitulated trabeculation and compaction in the post-MI heart. This was evaluated morphologically and molecularly with the analysis of trabecular projections and investigation of recapitulated developmental pathways. Whilst it is unclear whether the process of endocardial remodelling contributes to neovascularisation, the lack of trabecular projections in sham samples suggests that this is an injury response to myocardial ischemia which is conceivable in this setting as a method of accessing the blood-filled lumen. Attempts to determine whether sub-endocardial “lumina” became perfused using IV injection of lectin were unsuccessful, and the technique requires further optimisation to determine a suitable dose and administration regime for post-MI mice. However, Kobayashi et. al., 2018 showed evidence of perfused vessels close to the endocardial surface, and it would be interesting to analyse whether these vessels are the Pdgfb^{-} vessels suggested to be endocardial-derived here.

Adaptive induction of trabeculae in the adult heart is not a novel discovery and clinical evidence of hypertrabeculation in pregnant women, athletes and patients with anaemia is supportive of this post-MI phenomenon (Gati et. al., 2013, Gati et. al., 2014). The study of pregnant women proposed increased preload as a trigger for hypertrabeculation, as

an adaptive response to wall tension, leading to increased left ventricular volume and mass, and the development of trabeculations. They suggested that individuals subjected to a longer preload stress such as intense athletic training or heart failure, would incur more obvious changes in remodelling (Gati et. al., 2014). Further investigations are required to determine whether the endocardial projections observed here are also induced by increased cardiac pressure, or through another mechanism, such as myocardial hypoxia. The identification of a trigger for endocardial remodelling may provide insight into whether this response is independent of neovascularisation, and employed to increase the surface area of the endocardium whilst vascular expansion occurs, or whether the processes of trabeculation and compaction are interlinked with neovascularisation, in order to provide the additional endocardial cells for subsequent compaction and an EndMT contribution to sub-endocardial vessels.

A limitation of studying morphological changes in fixed sections is the ability to visualise trabeculae in only one plane. 11µm transverse heart sections were used to analyse trabeculation, and a comparison with sagittal sections may provide further insight into the role of endocardial projections, and how they connect with the left ventricle. Our group is currently exploring the use of high resolution episcopic microscopy (HREM), which offers the ability to visualise endocardial remodelling three dimensionally, providing an invaluable approach for expanding our understanding of the morphological changes induced by MI, and their role in revascularising the heart. Additionally, a longitudinal within-subject analysis would be insightful to determine changes in the same heart at various timepoints post-MI; MRI imaging could be useful in this manner for providing a basic readout of trabeculation and heart function, although this would not provide the required resolution to study molecular changes associated with remodelling.

Since the identification of the endocardium as a primary source of coronary endothelial cells in development, consideration has been extended to its role in pathological neovascularisation, and during the course of this DPhil project, three studies were published examining endocardial remodelling in the post-MI setting. Whilst recapitulation

of developmental mechanisms was not the focus of these investigations, the findings must be considered alongside the results shown here in an attempt to uncover the complex interplay resulting in sub-endocardial vessels post-MI.

Miquerol et. al., 2015 described “Endocardial flowers” on the endocardial surface connected with the underlying coronary vasculature via “stalks”; flowers expressed VEGFR2, a signalling molecule involved in angiogenesis, although the endocardium itself did not show evidence of angiogenesis. Sub-endocardial vessels also showed presence of α-SMA^{+} cells suggestive of possible EndMT leading to an arterial phenotype (Miquerol et. al., 2015). Whilst this was the first evidence of an endocardial role in post-MI neovascularistaion, it is unclear whether the “endocardial flowers” described were derived from the endocardium or from pre-existing coronary vessels, since the molecular expression profile of the “flowers” did not match that of the endocardium.

Kobayashi et. al., 2018, described endocardial sprouting, which was driven by VEGF signalling, and resulted in expansion of perfused subendocardial vessels. They observed a reduction in subendocardial vessels with an endothelial-specific VEGFR2 knockout, confirming that a subset of subendocardial vessels were formed via angiogenesis from endothelial cells, although clear evidence was not provided for these being endocardial-derived. The lack of endocardial VEGFR2 observed in Chapter 3, and the disappointing results of VEGF-targeted proangiogenic therapies, suggest that angiogenesis is not the primary mechanism for endocardial neovascularisation post-MI and alternative mechanisms should therefore be considered. In support of this, recent unpublished data from our group, in collaboration with Sarah De Val (Oxford) demonstrates an active repression of VEGF-mediated signalling in the infarcted heart, compared with detectable, albeit low level, baseline VEGF signalling in the uninjured adult heart.

The Zhou group, responsible for two of the endocardial development studies, created an endocardial-specific Npr3-Cre model after identifying enrichment of Npr3 in endocardium vs. endothelium through single cell RNA-Sequencing analysis of the embryonic heart (Zhang et. al., 2016). This model was used to investigate an endocardial contribution to

vascular endothelial cells in the post-MI setting, as a recapitulation of the developmental mechanism they previously described (Tang et. al., 2018). Four models of injury were used, and all showed extensive sub-endocardial remodelling with “endocardial tubes” formed beneath the endocardial surface connecting to the left ventricle. However, the study concluded that these tubes did not become vessels due to the lack of associated α-SMA^{+} cells, and an endocardial contribution to coronary endothelial cells was only observed in a model involving entrapment of endocardial cells, either a PSSL injury or transplantation of FACS-sorted endocardial cells into the infarcted myocardium. In this setting, endocardial cells contributed vascular endothelial cells to vessels which went on to acquire α-SMA. Whilst this study concluded that the adult endocardium minimally contributes to vascular endothelial cells post-MI, due to the lack of smooth muscle support surrounding endocardial tubes and the failure of endocardial tubes to connect with the coronary vasculature, it provides evidence for the endocardium retaining its capacity to contribute vascular endothelial cells in the adult heart, under suitable conditions. Still, their conclusion contradicts the endocardial angiogenesis study which claims that “endocardial flowers” do connect with coronary vessels and show a mature vascular phenotype (Miquerol et. al., 2015), and our observations of mature sub-endocardial vessels (Chapter 3, Dubé et. al., 2017).

Thus, controversy remains surrounding an endocardial contribution to vascular endothelial cells post-MI, and the processes underlying endocardial remodelling are evidently complex. The mechanism described here, involving recapitulation of Notch1 signalling may only drive part of the process, alongside VEGFR2 signalling and other undiscovered mechanisms. However, the key to uncovering a definitive endocardial contribution and the underlying mechanisms driving the process, lies in finding a reliable, accurate method to target the endocardium specifically.

Tang et. al., 2018, attempted this with the Npr3-Cre, however, the suitability of Npr3 for targeting the endocardium should be fully examined before analysis of its effects on neovascularisation. A recent study which provided a single cell RNA-Sequencing

analysis of murine tissues culminating in an online searchable platform, confirmed the localisation of Npr3 to endocardial cells, although a small percentage of fibroblasts also expressed the gene (**Figure 6.1A**). This platform also provided support for the Pdgfb-driven reporter described in Chapter 3, with no endocardial expression seen, and pdgfb restricted to endothelial cells and leukocytes (**Figure 6.1B**) (The Tabula Muris Consortium, 2018). Whilst this supports the use of Npr3-Cre to target the endocardium, the contradictory findings in relation to neovascularisation post-MI remain, which poses the question of whether the heterozygous deletion of Npr3 in this model has an impact on neovascularisation. Npr3 has an established role in endothelial cell growth and proliferation, and epithelial-mesenchymal transition (EMT) (Khambata et. al., 2011, El Andalousi et.al., 2013, Moyes et. al., 2014, Suffee et. al., 2017), and whilst Tang et. al., 2018, investigated the effect of inducing the heterozygous deletion in adult mice by ECG, ejection fraction and cellular analysis via immunostaining, this was not performed in the ischemic heart after LAD ligation. In response to these inconsistent findings, our group aims to fully characterise the Npr3-Cre line to examine its suitability for targeting the endocardium, in order to determine whether this approach should be adopted by the group or further consideration should be extended to identifying a specific endocardial-expressed gene.

In summarising these studies, alongside the findings described in this thesis, sufficient evidence has been provided for consideration of endocardial activation in the injured adult heart, with rationale for investigating alternative mechanisms to angiogenesis. However, it is clear that the underlying processes are likely to be complex, and considerable future work is required to establish the predominant mechanism driving this process endogenously and to identify targets for therapeutic enhancement.

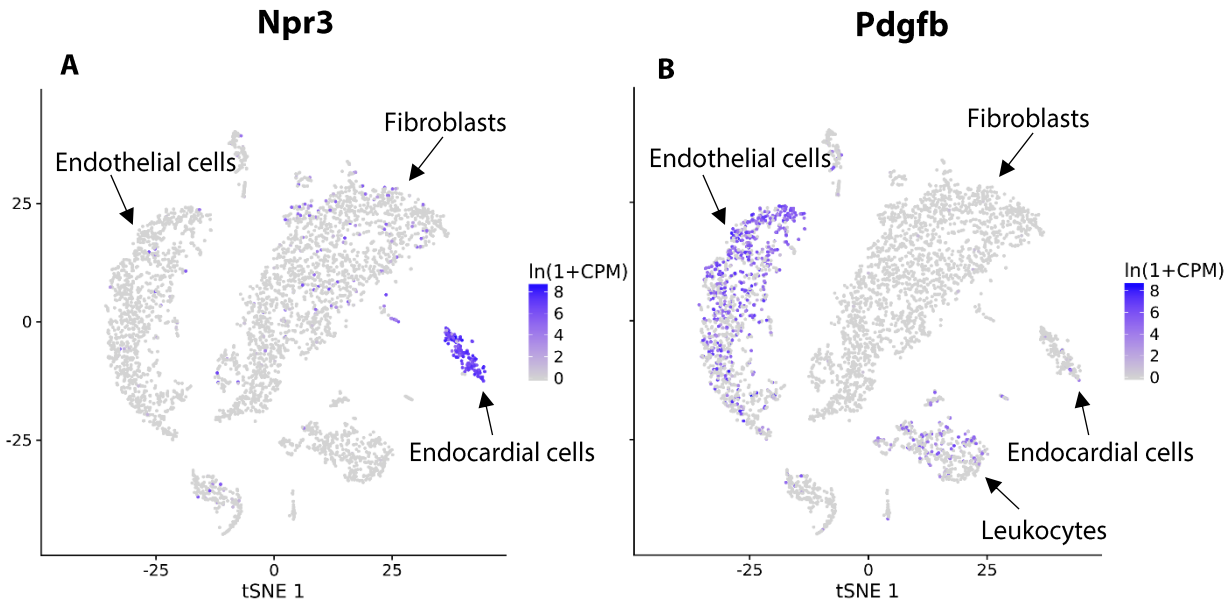

Figure 6.1. The Tabula Muris Consortium: Single cell sequencing of the adult mouse heart shows Npr3 and Pdgfb expression

The Tabula Muris Consortium performed single cell RNA-sequencing on tissues from an adult mouse and expression of Npr3 and Pdgfb in FACS isolated heart cells is shown. Dark purple indicates high expression and grey indicates low expression. (A) provides confirmation of Npr3 expression in endocardial cells of the adult heart, with some expression observed in fibroblasts. (B) is supportive evidence for the expression pattern shown in Chapter 3 with pdgfb, as this endothelial marker is not expressed in the adult endocardium. *(The Tabula Muris Consortium, 2018)*

6.1.3 Developmental pathways recapitulated in the infarcted adult heart

In an attempt to uncover the signalling processes that drive endocardial remodelling post-MI, consideration was extended to the molecular mechanisms underlying trabeculation and compaction in development. Through this work, novel evidence was provided for reactivation of various elements of these pathways, which were previously thought to be inactive postnatally. The reactivation of Brg1, Nrg1 and Notch pathway elements suggests that embryonic ventricular modelling is redeployed in response to ischemia in the infarcted heart. Whilst this study focused on investigating Notch signalling in this setting, due to its endocardial role as a key regulator in developmental

trabeculation and EndMT, further examination of Brg1 and Nrg1 controlled mechanisms may reveal additional insights into the intricate pathways driving endocardial remodelling post-MI.

Since these mechanisms have not previously been examined in adult coronary endothelial or endocardial cells, the use of cultured endothelial cell models such as primary explants, endothelial cells isolated by FACS or induced pluripotent stem cell (iPSC) -derived coronary endothelial cells, would be beneficial for screening the mechanisms, and investigating the effect of attenuating or enhancing them, alongside *in vivo* applications. This approach would enable the use of pharmacological agents to manipulate signalling, providing preliminary data for follow-up by *in vivo* analysis, and the potential, in the case of human iPSC, to investigate translational relevance using human cell-based assays.

Much of the data provided for identifying molecular pathways involved in endocardial remodelling is descriptive, and whilst this provides an informative morphological report of endocardial signalling, a quantitative comparison of relevant signalling molecules would also be advantageous. Attempts were made to examine changes in expression of Notch pathway genes from whole heart MI samples, however no significant differences were observed between sham and post-MI hearts. The use of the *pdgfb-Cre* reporter line for this analysis would be beneficial to permit RNA isolation separately from endothelial and endocardial cells after FACS, allowing the comparison of relevant gene expression between the two cell types before and after MI. This technique could also extend to analysing genes involved with EndMT and other pathways such as Brg1/BMP signalling and proliferation, enabling a comparison of these pathways, in endocardial and endothelial post-MI samples.

6.2.1 Development of surgical and analytical tools to determine extent of trabeculation post-MI

Investigation of MI-induced endocardial projections in multiple strains revealed consistent, and reproducible hypertrabeculation overlying the infarct region. Optimisations were made to reduce known variability associated with the LAD ligation surgery, and a rigorous analysis process was employed to ensure that samples with infarct sizes outside the defined range (10-30% left ventricle) were excluded. However, whilst the LAD ligation model is an important tool to allow the investigation of post-MI pathologies, the procedure maintains some limitations. The use of a larger sample size would improve consistency and ensure reliable results, however the challenges associated with breeding transgenic mice, the time required to perform the procedure and post-operative care, and higher than average mortality rates in the lines used, prevented this possibility. Improved efficiency may be employed by testing infarct size shortly after the procedure to exclude samples with a very small or no injury, prior to harvesting and processing the samples. Blood plasma levels of cardiac troponin T are used as a biomarker of MI clinically, and has been reported as an effective measure of infarct size in rodents (Kolk et. al., 2009). This test can be performed 6-8 hours after LAD ligation surgery without euthanizing the animal, and would permit those which are non-infarcted or present with small infarcts, to be sacrificed at an earlier point of the experiment.

Another caveat of the murine model of MI is the use of young healthy animals (10-16 weeks) which translates to a human age of approx. 25 years. Coronary artery disease develops clinically through the build-up of atherosclerotic plaques over many years, with progression to MI in primarily middle- to old-aged adults. Studies of infarction in diabetic, db/db mice, and atherosclerotic, ApoE$^{-/-}$ mice, showed impaired infarct healing when compared with controls, suggesting that the results observed in young, healthy mice may not be representative of the clinical response (Greer et. al., 2006, Majmudar et. al.,

2013). Despite these limitations, the surgical model of MI is the most suitable tool currently available, and home office guidelines restrict the use of aged animals in this process.

The semi-automated, digital analysis of trabeculation in post-MI samples was developed based on clinical MRI studies that analysed trabeculation in patients with LVNC. This method proved to be a reliable, unbiased measure of endocardial remodelling in this setting, however there is scope for improvement, as the presence of papillary muscles could not be controlled for, and variation due to the degree of ventricular contraction may have influenced fractal analysis measurements. A recent publication outlined a semi-automatic detection method for analysing trabeculation from cardiac MRI images in a murine model of LVNC. Semi-automatic software was used to calculate compacted mass (M_c), trabeculated mass (M_t) and percentage of trabeculation (M_t/M_c) (Frandon et. al., Oct 2018). This method allowed the papillary muscles to be excluded and the results were validated by histology. For incorporation of another analysis method to investigate post-MI trabeculation in future studies, similar adaptations and optimisations need to be completed as shown here for fractal analysis, to ensure its compatibility with immunofluorescent microscopy images. This may be worth considering in order to identify the most accurate and reproducible method of analysing trabeculation in post-MI hearts.

6.2.2 The use of transgenic models for investigating endothelial Notch1 post-MI

Two endothelial specific mouse lines were developed to investigate the role of Notch1 in neovascularisation of the heart after MI. *VE Cadherin-Cre* was used to target endocardial cells through endothelial expression, and while this model efficiently labelled the endocardium with and without MI, it required a high dose of tamoxifen that was not easily compatible with the LAD ligation surgery. The dose of tamoxifen required to induce Cre recombination should be a consideration when identifying suitable Cre models for future studies employing complex surgical procedures, which require a considerable period of

anaesthesia, due to the respiratory challenges experienced here with the combination of high tamoxifen dose, anaesthesia and opioid analgesic. Additional consideration should also be made for alternative administration routes of tamoxifen, as IP injection can be unreliable and may have contributed to the low efficiency of recombination. Oral gavage may be considered as an alternative method for future studies, however this was not employed here due to optimisation being performed using the IP route of administration, and experimental consistency being maintained.

The Notch1 LoF model was validated using immunofluorescence and RNAScope, which showed a reduction of Hes1 when compared with control. The GoF was analysed using FACS for GFP-labelled cells, as although the GFP was too weak for detection by microscopy, it was detectable by flow cytometry. RNA extraction was attempted from the FACS sorted cells, however this technique requires further optimisation for use with low cell yields. Once refined, this technique will allow analysis of candidate signalling pathways that may be upregulated in the GoF model, such as those involved with EndMT.

6.3.1 A role for Notch1 in endocardial remodelling post-MI

Evidence has been provided here for significantly reduced trabeculation in Notch1 LoF mice at 7 and 14 days post-MI. This was analysed via fractal analysis software which was validated in Chapter 4. Whilst *VE Cadherin-Cre* did not target the endocardium specifically, the endocardial phenotype observed is consistent with a role for endocardial Notch1. To confirm this finding is endocardial-driven, an endocardial specific Cre should be crossed with the Notch1 LoF, and the same analysis performed. Alternatively, if this tool remains unavailable, the Notch1 LoF may be crossed with the *Pdgfb-Cre*, and if the phenotype is not observed in this setting, we can conclude that the trabeculation phenotype observed is controlled by endocardial Notch1 signalling.

It was hypothesised here that the endocardial Notch1 mechanism described by D'amato et. al., 2015, was recapitulated in the ischemic heart to drive trabeculation and compaction in support of neovascularisation. Whilst a role for Notch1 in trabeculation has been confirmed, and early investigations showed expression of Dll4 and Jag1, the ligands mediating Notch1 signalling in development, it is not possible to unequivocally confirm the full pathway without further establishment of ligand-receptor interactions. Since the development of additional animal models targeting the ligands would be time and labour intensive, in vitro methods would be more suitable to analyse the presence of Dll4 and Jag1. Isolation of post-MI endocardial cells using the *Pdgfb-Cre* would allow the analysis of the Notch1 ligands expressed by the endocardium post-MI, and an endocardial-like cell-based assay could be used to activate Notch1 signalling by the addition of Dll4 through coating culture plates with the ligand fused to IgG (Parker et. al., 2012), or addition of active Jag1 for a specified period (Yamamura et. al., 2014), and morphological and molecular changes analysed to determine activation of proliferation and cell migration.

Once a suitable transgenic model is developed to specifically target the endocardium in mice, further investigations should also aim to establish what triggers hypertrabeculation, and whether the process is part of the neovascular response, playing a role in contributing subendocardial vessels, or is a mechanism employed to combat increased preload by remodelling the mass and volume of the myocardium.

6.3.2 Notch1 signalling in subendocardial neovascularisation post-MI

Sub-endocardial vessels were counted at days 7 and 14 post-MI, and a significant reduction was observed in small/medium sub-endocardial vessels in the Notch1 LoF. This confirms a role for Notch1 in neovascularisation post-MI, however it is unclear from the techniques employed here, whether this is a result of the increased trabeculation which was also observed, or an independent Notch1 driven neovascular pathway. Tracing of endothelial cells was performed using TdTomato as a reporter of *VE*

Cadherin-Cre, and tdTomato^{+} cells were detected in SM-MHC^{+} subendocardial vessels, suggestive of EndMT. In the Notch1 mutants, evidence of EndMT was not observed at 7 days post-MI, and at 14 days post-MI, the process appeared to be impaired, with large clusters of SM-MHC^{+} cells restricted beneath the endocardial surface. Notch1 has been shown to regulate EndMT in the AVC where the endocardium contributes mesenchymal cells to the cardiac cushions for valve development, and whilst in wild type embryos, endocardial cells transitioned to invading mesenchymal cells in the cardiac cushions, RBPJ knockout embryos showed a lack of mesenchymal cells invading the cushion, and instead appeared to maintain the closely associated endocardial structure. The mutant endocardium did appear to activate EndMT, however the study concluded that junctional complexes must be locally disassembled for cells to migrate in wild-type embryos, and RBPJ mutants appeared to maintain an activated, premigratory cell type with junctional complexes intact (Timmerman et. al., 2004). This data suggests that endocardial Notch mediates a later step in the progression of EndMT, and the phenotype observed in the day 14 post-MI mutants here, appears to replicate this developmental finding. Further support is therefore provided for recapitulation of developmental mechanisms in the adult ischemic heart, and Notch1-regulated endocardial EndMT may be activated in the left ventricle to contribute mesenchymal cells in a similar manner to the endocardial-pericyte contribution observed in development (Chen et. al., 2016).

Whilst the aim of this project was to investigate a role for Notch1 in a hypothesised recapitulation of trabeculation and compaction post-MI, these findings appear to confirm reactivation of two independent endocardial Notch1 pathways from distinct regions of the developing heart. Further investigation is required to interrogate the EndMT phenotype in the Notch1 LoF, with increased sample size and analysis of transcription factors Snai1 and Zeb1 required to clarify the role of EndMT in this model.

Endocardial Notch signalling has also been implicated in zebrafish heart regeneration, where a highly dynamic endocardium was shown to regulate endocardial maturation,

cardiomyocyte proliferation and dedifferentiation through Notch and Serpine1, a developmental endocardial gene involved with cell proliferation and migration (Münch et. al., 2017). Whilst the zebrafish model is less representative of the human heart due to its capacity to fully regenerate within 60 days, useful mechanistic insights can be gained from the study of regenerative processes, and the relevance of endocardial Notch may be conserved across species.

The Notch1 phenotypes observed here, which appear to be a recapitulation of developmental processes contributing to the formation of valves and coronary vessels, suggest an important role for Notch1 signalling in the adult infarcted heart. Whilst endocardial Notch has been implicated in cardiac regeneration of the zebrafish, this study provides the first evidence of a role for endocardial Notch1 in a mammalian model of MI, and identifies a novel mechanism of neovascularisation for potential therapeutic approaches in the treatment of HF.

When considering therapeutic agents to target Notch signalling in disease, consideration must be made for the challenges associated with specifically targeting a receptor on endocardial or endothelial cells, which may also be present in other cell types throughout the body. Notch inhibitors and activators are in development for targeting tumour angiogenesis, however these studies are in the early stages, with investigations into ligand-mimicking proteins and activating antibodies still being considered pre-clinically (Hernandez et. al., 2014). An alternative strategy targeting downstream transcription factors induced by Notch may be preferable, with the aim of promoting trabeculation, compaction and EndMT in the ischaemic heart. However, this therapeutic approach would require tight regulation to prevent over-activation of the pathway which could lead to excessive trabeculation, cell proliferation and activation of angiogenic pathways, which could be detrimental for cardiac repair.

The findings detailed here propose an endogenous mechanism that provides potential avenues for therapeutic targeting of neovascularisation post-MI, and with further

investigations to uncover the subsequent signalling cascade leading to the formation of mature subendocardial vessels, may reveal a novel approach for vascular repair in the ischaemic heart.

6.4 Conclusions

The work presented in this thesis provides novel insights into the pathways controlling neovascularisation in the ischemic heart and, to our knowledge, the first evidence of recapitulating developmental endocardial mechanisms in the adult pathological setting.

The presence of subendocardial vessels at 7 and 14 days post-MI was confirmed in wild type hearts and a negative *Pdgfb-Cre* lineage trace showed unlabelled subendocardial vessels that are suggestive of an endocardial contribution. The *Pdgfb-Cre;tdTomato* was also validated with FACS as a method of isolating endocardial cells, and provides a useful tool for analysing specific genes and pathways in the endocardium vs endothelium with and without MI. EndMT was investigated as a process contributing to vascular endothelial cells in the post-MI setting, and lineage tracing with *VE Cadherin;tdTomato* showed an endothelial contribution to subendocardial vessels by 14 days post-MI.

The developmental processes of trabeculation and compaction were investigated in the ischemic adult heart and evidence of recapitulation was provided, with mechanisms underlying cell proliferation and migration in the embryonic heart appearing to drive the remodelling process post-MI

Models and analysis tools were developed and optimised to allow investigation of the effect of attenuating and activating endothelial Notch1 on the post-MI response; WGA was validated as a method to analyse infarct size, and fractal dimension was confirmed as a reliable measurement of trabeculation in the murine adult heart. As expected, extent of trabeculation was shown to increase with infarct size, in injuries up to 30% of the left ventricle, after which remodelling was impaired.

Analysis of the effects of endothelial Notch1 on trabeculation in the infarcted heart revealed endothelial Notch1 as a key regulator of this process, as in the developmental setting. Reduced trabeculation was identified in Notch1 LoF and a hypertrabeculation phenotype was observed in the Notch1 GoF. Notch1 LoF mutants also showed reduced

neovascularisation with significantly fewer subendocardial vessels than controls, and the Notch1 GoF appeared to have more mature subendocardial vessels present at 7 days post-MI.

An insight into the mechanism driving subendocardial neovascularisation was provided with the mutant EndMT phenotype. EndMT appeared impaired in the Notch1 LoF at 14 days post-MI with activation of the endocardium observed, but clusters of SM-MHC^{+} cells remained localised to the endocardial surface instead of invading the myocardium beneath. This is replicative of the developmental process driving endocardial EndMT in the AVC, and an RBPJ KO model which revealed a similar phenotype in the embryo.

Sub-endocardial neovascularisation was also initiated in the uninjured adult heart by induction of constitutive activation of endothelial Notch1. Whilst a significant difference was not observed in trabeculation of these samples, the number of sub-endocardial vessels was clearly increased and evidence of an endocardial contribution to these vessels via EndMT was observed with the tdTomato reporter. The capacity for the uninjured adult heart to initiate sub-endocardial neovascularisation through activation of endothelial Notch1, is a novel finding that poses considerable translational potential for targeting neovascularisation in the clinical setting.

Whilst further investigation is required to fully uncover the mechanisms described here, this study provides a strong basis for consideration of the endocardium in neovascularisation post-MI and manipulation of developmental mechanisms via therapeutic approaches to improve cardiac repair.

6.5 Future Work

This study establishes a rational basis for considerable future work to uncover the full mechanism driving subendocardial neovascularisation in the ischemic heart. Key experiments which may be employed for future investigations are described below:

- Transcriptomic analysis of endocardial cells isolated from *Pdgfb-Cre;tdTomato* mice with and without MI
- Characterisation of the Npr3-Cre model to determine its suitability for analysing neovascularisation post-MI
- 3d visualisation of trabeculation in the adult infarcted heart: Control vs. GoF
- Characterisation of post-MI endocardial EndMT
- Further examination of tdTomato-labelled Notch1 LoF and GoF models to confirm EndMT phenotype observed
- Ex vivo analysis of mechanisms involved in neovascularisation post-MI

6.5.1 Transcriptomic analysis of endocardial cells isolated from *Pdgfb-Cre;tdTomato* mice with and without MI

A novel isolation method was developed and optimised to obtain adult endocardial cells from the *Pdgfb-Cre;tdTomato* mouse using an enzymatic digestion followed by FACS. This method proved to derive approximately 10,000 endocardial cells and 100,000 endothelial cells per 1 million isolated cells from adult heart tissue, and analysis of extracted RNA confirmed intact RNA isolation is possible from endothelial cells. Endocardial cell RNA extraction was prevented by the relatively harsh method of Trizol reagent RNA extraction and the low endocardial cell count. Further experimentation is required to adapt RNA extraction methods, and develop an optimal protocol for extraction from small amounts of starting material. Recent work within the Smart and Mommersteeg groups (Oxford) has focused on extracting RNA from small populations of mouse embryonic cells, and FACS isolated cavefish cells, and expertise from these investigations will be shared to improve the outcome of extracting endocardial cell RNA.

The extraction of RNA from adult endocardial cells will be invaluable for novel characterisation of this tissue. A full transcriptomic analysis will reveal differentially expressed genes, and possibly a specific endocardial marker which could be used to develop transgenic tools to target the endocardium. Isolation of this cell population from post-MI samples will provide an insight into the pathways regulating sub-endocardial neovascularisation, and, moreover, a single cell RNA-sequencing approach would permit the characterisation of sub-populations of endocardial cells which may reveal additional mechanistic information relating to endocardial trabeculation and EndMT in the post-MI setting. Novel findings could then be followed up ex vivo to confirm anatomical and functional differences in relevant endocardial sub-populations and how their interaction orchestrates neovascularisation in the ischemic heart.

6.5.2 Characterisation of the Npr3-Cre model to determine its suitability for analysing neovascularisation post-MI

As stated, the key limitation of this study is the lack of a specific transgenic tool for targeting the adult endocardium. Bin Zhou (Shanghai) has developed an Npr3-Cre mouse which is reported to be endocardial specific during development and in the adult heart. Images shown by Tang et. al., 2018, revealed strong endocardial expression, however low expression also appeared in the epicardium, and a recent single cell RNA-Sequencing analysis also showed expression in fibroblasts (The Tabula Muris Consortium, 2018). Considering the well-established role of Npr3 in vascular homeostasis and endothelial cell proliferation, and the possibility of a fibroblast-mesenchymal-transition to neovascularisation post-MI (Ubit et. al., 2014), full characterisation of the effect of this Npr3 heterozygous deletion on neovascularisation post-MI would be informative.

Our group has recently imported the Npr3-CreER model, which will be crossed to the tdTomato reporter to allow tracing of endocardial cells. Analysis of subendocardial vessels after LAD ligation will provide a clear indication of whether the Npr3-CreER deletion affects neovascularisation via the endocardium. If the model proves to be reliable, the Notch1 LoF and GoF mice will be crossed to it, to enable endocardial specific Notch1 loss- and gain-of-function analysis. The tools developed here to investigate trabeculation, neovascularisation and EndMT will be employed for the same rigorous examination of endocardial Notch1 post-MI.

6.5.3 Three-dimensional visualisation of trabeculation in the adult infarcted heart: Control vs. GoF

Whilst immunofluorescent imaging of cryosections provides an insight into endocardial remodelling in the adult heart, a three-dimensional visualisation of the morphological changes would be invaluable for expanding our knowledge of how endocardial

remodelling supports cardiac recovery of the ischemic heart. Recent HREM expertise has been developed within the department, and use of this advanced microscopy technique is being developed for use in the uninjured adult heart. The use of this 3d-imaging method is proposed to gain a digital, interactive, 3-dimensional representation of endocardial remodelling in control and Notch1 GoF post-MI hearts.

Alongside this, it would be beneficial to investigate perfusion of subendocardial vessels post-MI using a fluorescein lectin. Kobayashi et. al., 2018 observed perfusion of subendocardial vessels from 3 days post-MI, and with the use of *Pdgfb-Cre;tdTomato* to label endothelial-derived vessels, IV injection of leptin prior to harvesting at 2 and 7 days post-MI would allow analysis of perfused tdTomato labelled and unlabelled sub-endocardial vessels.

6.5.4 Characterisation of post-MI endocardial EndMT

Evidence of EndMT has been provided at 7 and 14 days post-MI using the *VE Cadherin-Cre;tdTomato* model to label endocardial- and endothelial-derived cells in sub-endocardial vessels. The presence of SM-MHC^{+} cells in the endocardium provides the first indication of endocardial EndMT in the adult heart and Notch1 mutants exhibited an impaired EndMT phenotype supportive of a role for Notch1.

The analysis here has provided a snapshot of sub-endocardial EndMT in the ischemic heart, and to fully characterise this mechanism, an extensive time-course should be performed with the *VE cadherin-Cre;tdTomato* model to gauge morphologically whether the SM-MHC+ cells observed at 14 days post-MI were contributed from the endocardium or the endothelium. Samples should be harvested at 2, 4, 7, 10 and 14 days post-MI and immunofluorescence analysis of overlap between tdTomato and α-SMA^{+} cells performed to identify intermediary migratory mesenchymal cells, and tdTomato and SM-MHC^{+} cells to identify vascular smooth muscle with an endothelial or endocardial origin.

6.5.5 Increased sample size of tdTomato-labelled Notch1 LoF and GoF models to confirm EndMT phenotype observed

In addition to the EndMT investigations of *VE Cadherin;tdTomato* mice, additional samples at 7 and 14 days post-MI should be obtained from the Notch1 LoF and Notch1 GoF with tdTomato labelling the cells targeted. Whilst informative Notch1 LoF examples were shown here at 14 days post-MI, suggesting an effect of Notch1 on EndMT, the finding can only be unequivocally concluded by tracing the subendocardial clusters of mature SM-MHC^{+} cells to an endothelial/endocardial source.

Further characterisation of the Notch1 GoF without MI should be performed. Samples should be harvested at a range of time-points after inducing constitutive activation of endothelial Notch1, to analyse morphological changes and trace tdTomato labelled cells on their route to changing fate. A quantitative analysis may also be informative alongside the morphological investigations; isolation of tdTomato labelled cells at equivalent times after induction would allow investigation of candidate signalling pathways involved with EndMT. An expression timecourse of transcription factors, such as Zeb1 and Snai1, would provide further insight into Notch1-regulated EndMT in the adult heart and potentially uncover suitable targets for therapeutic manipulation of this pathway.

6.5.6 Ex vivo analysis of mechanisms involved in neovascularisation post-MI

The final addition to the in vivo analysis performed here would be a thorough investigation of the mechanisms identified in a cell-based assay. Ex vivo approaches are beneficial, alongside the in vivo models, as cell culture assays provide a tool for manipulating signalling pathways and examining the effect on the morphology and molecular identity of the cells. Notch1 ligands such as Dll4 and Jag1 could be added to the assay, via coating the culture plate with the IgG tagged to the ligand, transient addition of the activated ligand, viral transfection or a small interfering RNA (siRNA), to activate Notch signalling, and any downstream effects (methods reported by Jaleco et.

al., 2001, Choi et. al., 2009, Parker et. al., 2012, Yamamara et. al., 2014). Expression of EndMT transcription factors could be validated in this setting providing a readout of Notch1-regulated EndMT and supporting in vivo mechanistic analysis.

Whilst there are currently no adult endocardial cell models available, our collaborator Dr Amer Rana, University of Cambridge, has developed a human induced pluripotent cell (iPSC) based differentiation assay to produce endocardial-like cells in culture. This protocol is currently being validated against an iPSC-derived endothelial model for confirmation of its suitability as an endocardial assay, and if proven reliable, Notch1 regulated EndMT would be interrogated with pharmacological manipulation. This translational approach would confirm whether the mechanism observed in mice is conserved in a human cell model, and provide rationale for therapeutic targeting to improve clinical cardiac outcomes.

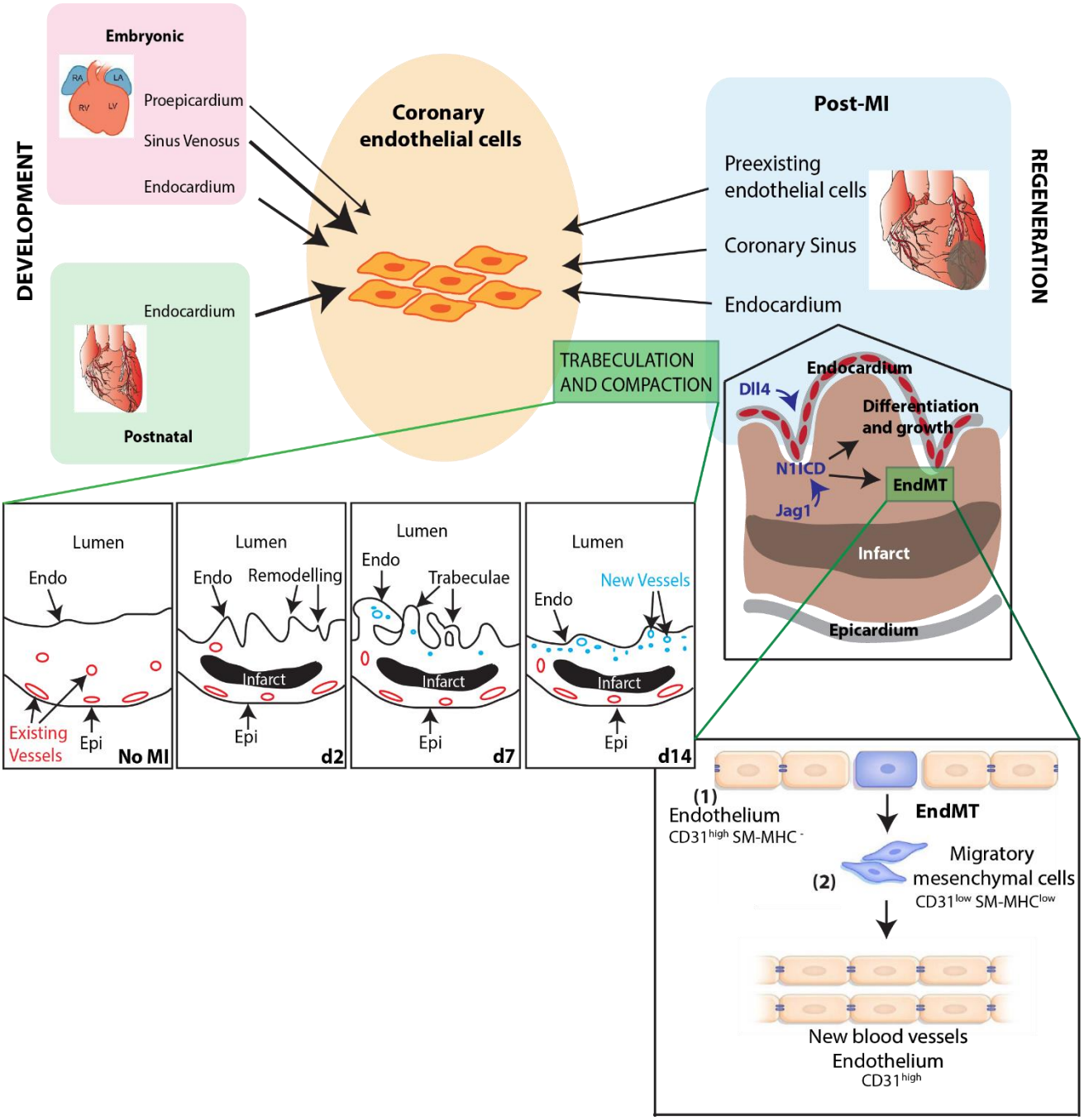

Final Remarks

This thesis has defined a possible endocardial contribution to neovascularisation post-MI, via recapitulation of the developmental mechanisms driving trabeculation and compaction. A role for endothelial Notch1 has been identified in endocardial remodelling, and regulation of EndMT in the ischaemic heart, providing a novel therapeutic pathway for further investigation.

APPENDIX

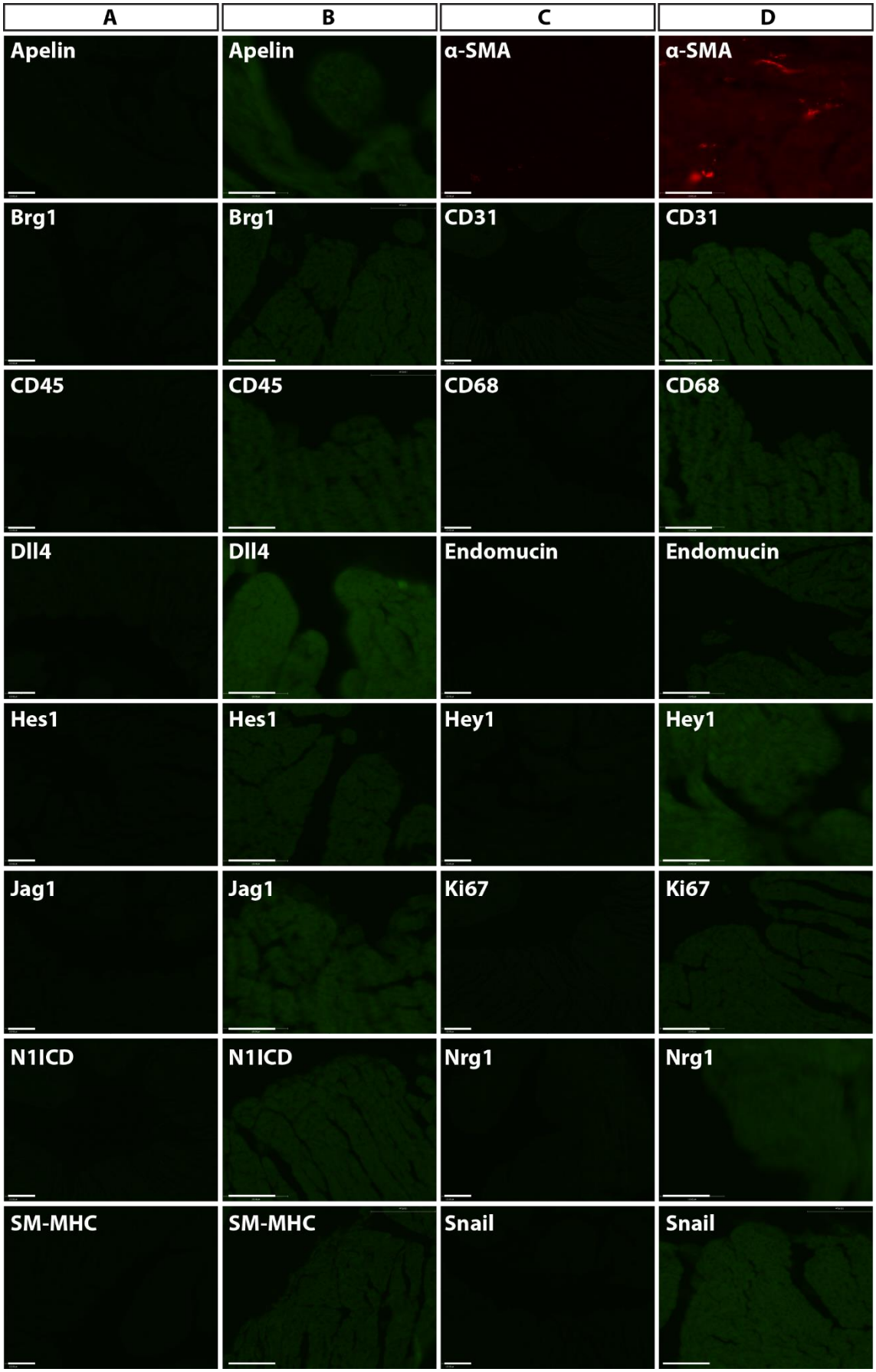

Appendix 1: Primary antibody controls

All key antibodies used throughout the thesis shown with primary only. Columns A and C, scale bars = 200 μm, columns B and D, scale bars = 100 μm.

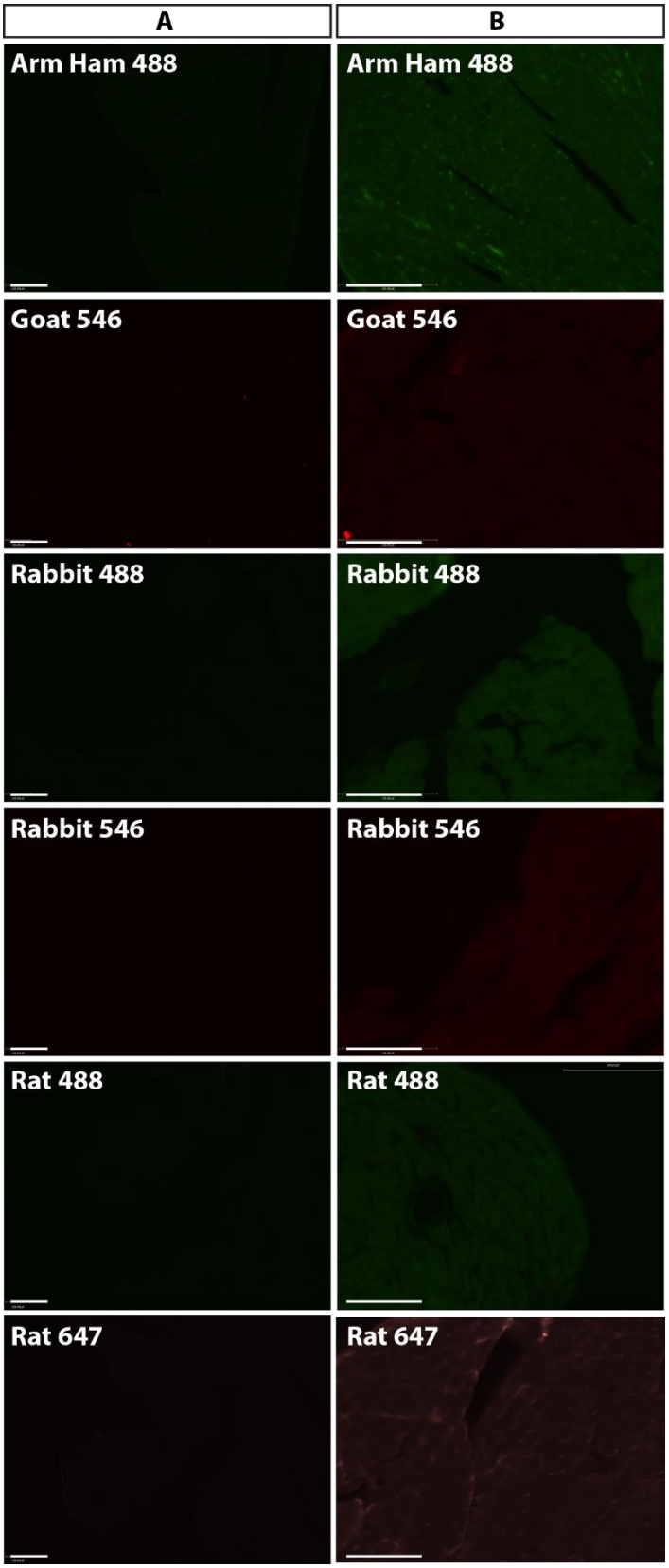

Appendix 2: Secondary antibody controls

All secondary antibodies used throughout the thesis shown without primary antibody. Column A, scale bars = 200 µm, column B, scale bars = 100 µm.

Bibliography

Aisagbonhi, O., Rai, M., Ryzhov, S., Atria, N., Feoktistov, I., & Hatzopoulos, A. K. (2011). Experimental myocardial infarction triggers canonical Wnt signaling and endothelial-to-mesenchymal transition. *Disease Models & Mechanisms*, *4*(4), 469–483. https://doi.org/10.1242/dmm.006510

Arai, A., Yamamoto, K., & Toyama, J. (1997). Murine cardiac progenitor cells require visceral embryonic endoderm and primitive streak for terminal differentiation. *Developmental Dynamics*, *210*(3), 344–353. https://doi.org/10.1002/(SICI)1097-0177(199711)210:3<344::AID-AJA13>3.0.CO;2-A

Artavanis-Tsakonas, S., Rand, M. D., & Lake, R. J. (1999). Notch signaling: Cell fate control and signal integration in development. *Science*. https://doi.org/10.1126/science.284.5415.770

Bhatia, N. L., Tajik, A. J., Wilansky, S., Steidley, D. E., & Mookadam, F. (2011). Isolated Noncompaction of the Left Ventricular Myocardium in Adults: A Systematic Overview. *Journal of Cardiac Failure*, *17*(9), 771–778. https://doi.org/10.1016/j.cardfail.2011.05.002

Braunwald, E. (2013). Heart failure. *JACC: Heart Failure*. https://doi.org/10.1016/j.jchf.2012.10.002

Bray, S. J. (2006). Notch signalling: A simple pathway becomes complex. *Nature Reviews Molecular Cell Biology*, *7*(9), 678–689. https://doi.org/10.1038/nrm2009

Cao, J., Navis, A., Cox, B. D., Dickson, A. L., Gemberling, M., Karra, R., … Poss, K. D. (2016). Single epicardial cell transcriptome sequencing identifies Caveolin 1 as an essential factor in zebrafish heart regeneration. *Development (Cambridge, England)*, *143*(2), 232–243. https://doi.org/10.1242/dev.130534

Captur, G., Zemrak, F., Muthurangu, V., Petersen, S. E., Li, C., Bassett, P., … Moon, J. C. (2015). Fractal Analysis of Myocardial Trabeculations in 2547 Study Participants: Multi-Ethnic Study of Atherosclerosis. *Radiology*, *277*(3), 707–715. https://doi.org/10.1148/radiol.2015142948

Chen, H. I., Sharma, B., Akerberg, B. N., Numi, H. J., Kivelä, R., Saharinen, P., … Red-Horse, K. (2014). The sinus venosus contributes to coronary vasculature through VEGFC-stimulated angiogenesis. *Development (Cambridge, England)*, *141*(23), 4500–4512. https://doi.org/10.1242/dev.113639

Chen, H., Shi, S., Acosta, L., Li, W., Lu, J., Bao, S., … Shou, W. (2004). BMP10 is essential for maintaining cardiac growth during murine cardiogenesis. *Development*, *131*(9), 2219–2231. https://doi.org/10.1242/dev.01094

Chen, J., Ceholski, D. K., Liang, L., Fish, K., & Hajjar, R. J. (2017). Variability in coronary artery anatomy affects consistency of cardiac damage after myocardial infarction in mice. *American Journal of Physiology-Heart and Circulatory Physiology*, *313*(2), H275–H282. https://doi.org/10.1152/ajpheart.00127.2017

Chen, Q., Zhang, H., Liu, Y., Adams, S., Eilken, H., Stehling, M., … Adams, R. H. (2016). Endothelial cells are progenitors of cardiac pericytes and vascular smooth muscle cells. *Nature Communications*. https://doi.org/10.1038/ncomms12422

Choi, K., Ahn, Y.-H., Gibbons, D. L., Tran, H. T., Creighton, C. J., Girard, L., … Kurie, J. M. (2009). Distinct biological roles for the notch ligands Jagged-1 and Jagged-2. *The Journal of Biological Chemistry*, *284*(26), 17766–17774. https://doi.org/10.1074/jbc.M109.003111

Claxton, S., Kostourou, V., Jadeja, S., Chambon, P., Hodivala-Dilke, K., & Fruttiger, M. (2008). Efficient, inducible Cre-recombinase activation in vascular endothelium. *Genesis*, *46*(2), 74–80. https://doi.org/10.1002/dvg.20367

Cohen-Gould, L., & Mikawa, T. (1996). The Fate Diversity of Mesodermal Cells within the Heart Field during Chicken Early Embryogenesis. *Developmental Biology*, *177*(1), 265–273. https://doi.org/10.1006/dbio.1996.0161

Cohen, J., & Cohen, J. (2003). *Applied multiple regression/correlation analysis for the behavioral sciences*. L. Erlbaum Associates.

Compernolle, V. (2003). Cardia bifida, defective heart development and abnormal neural crest migration in embryos lacking hypoxia-inducible factor-1α. *Cardiovascular Research*, *60*(3), 569–579. https://doi.org/10.1016/j.cardiores.2003.07.003

Cooley, M. A., Fresco, V. M., Dorlon, M. E., Twal, W. O., Lee, N. V., Barth, J. L., … Argraves, W. S. (2012). Fibulin-1 is required during cardiac ventricular morphogenesis for versican cleavage, suppression of ErbB2 and Erk1/2 activation, and to attenuate trabecular cardiomyocyte proliferation. *Developmental Dynamics*, *241*(2), 303–314. https://doi.org/10.1002/dvdy.23716

Corada, M., Liao, F., Lindgren, M., Lampugnani, M. G., Breviario, F., Frank, R., … Dejana, E. (2001). Monoclonal antibodies directed to different regions of vascular endothelial cadherin extracellular domain affect adhesion and clustering of the protein and modulate endothelial permeability. *Blood*, *97*(6), 1679–1684. https://doi.org/10.1182/BLOOD.V97.6.1679

D'Amato, G., Luxán, G., del Monte-Nieto, G., Martínez-Poveda, B., Torroja, C., Walter, W., … de la Pompa, J. L. (2016). Sequential Notch activation regulates ventricular chamber development. *Nature Cell Biology*, *18*(1), 7–20. https://doi.org/10.1038/ncb3280

De Haas, S., Ghossein-Doha, C., Geerts, L., van Kuijk, S. M. J., van Drongelen, J., & Spaanderman, M. E. A. (2017). Cardiac remodeling in normotensive pregnancy and in pregnancy complicated by hypertension: systematic review and meta-analysis. *Ultrasound in Obstetrics & Gynecology*, *50*(6), 683–696. https://doi.org/10.1002/uog.17410

De la Pompa, J. L., & Epstein, J. A. (2012). Coordinating Tissue Interactions: Notch Signaling in Cardiac Development and Disease. *Developmental Cell*. https://doi.org/10.1016/j.devcel.2012.01.014

De La Pompa, J. L., Timmerman, L. A., Takimoto, H., Yoshida, H., Elia, A. J., Samper, E., … Mak, T. W. (1998). Role of the NF-ATc transcription factor in morphogenesis of cardiac valves and septum. *Nature*. https://doi.org/10.1038/32419

Del Monte, G., & Harvey, R. P. (2012). An endothelial contribution to coronary vessels. *Cell*, *151*(5), 932–934. https://doi.org/10.1016/j.cell.2012.11.004

Deng, Y., Larrivee, B., Zhuang, Z. W., Atri, D., Moraes, F., Prahst, C., … Simons, M. (2013). Endothelial RAF1/ERK activation regulates arterial morphogenesis. *Blood*, *121*(19), 3988–3996. https://doi.org/10.1182/blood-2012-12-474601

Deveza, L., Choi, J., & Yang, F. (2012). Therapeutic angiogenesis for treating cardiovascular diseases. *Theranostics*, *2*(8), 801–814. https://doi.org/10.7150/thno.4419

Dolber, P. C., & Spach, M. S. (1987). Picrosirius Red Staining of Cardiac Muscle Following Phosphomolybdic Acid Treatment. *Stain Technology*, *62*(1), 23–26. https://doi.org/10.3109/10520298709107961

Dubé, K. N., Thomas, T. M., Munshaw, S., Rohling, M., Riley, P. R., & Smart, N. (2017). Recapitulation of developmental mechanisms to revascularize the ischemic heart. *JCI Insight*, *2*(22). https://doi.org/10.1172/jci.insight.96800

Eisenberg, L. M., & Markwald, R. R. (1995). Molecular regulation of atrioventricular valvuloseptal morphogenesis. *Circulation Research*. https://doi.org/10.1161/01.RES.77.1.1

El Andalousi, J., Li, Y., & Anand-Srivastava, M. B. (2013). Natriuretic Peptide Receptor-C Agonist Attenuates the Expression of Cell Cycle Proteins and Proliferation of Vascular Smooth Muscle Cells from Spontaneously Hypertensive Rats: Role of Gi Proteins and MAPkinase/PI3kinase Signaling. *PLoS ONE*, *8*(10). https://doi.org/10.1371/journal.pone.0076183

Emde, B., Heinen, A., Gödecke, A., & Bottermann, K. (2014). Wheat germ agglutinin staining as a suitable method for detection and quantification of fibrosis in cardiac tissue after myocardial infarction. *European Journal of Histochemistry*, *58*(4), 315–319. https://doi.org/10.4081/ejh.2014.2448

Fang, L., Moore, X.-L., Dart, A. M., & Wang, L.-M. (2015). Systemic inflammatory response following acute myocardial infarction. *Journal of Geriatric Cardiology : JGC*, *12*(3), 305–312. https://doi.org/10.11909/j.issn.1671-5411.2015.03.020

Ferdous, A., Caprioli, A., Iacovino, M., Martin, C. M., Morris, J., Richardson, J. A., … Garry, D. J. (2009). Nkx2–5 transactivates the *Ets-related protein 71* gene and specifies an endothelial/endocardial fate in the developing embryo. *Proceedings of the National Academy of Sciences*, *106*(3), 814–819. https://doi.org/10.1073/pnas.0807583106

Fernández, B., Durán, A. C., Fernández, M. C., Fernández-Gallego, T., Icardo, J. M., & Sans-Coma, V. (2008). The coronary arteries of the C57BL/6 mouse strains: implications for comparison with mutant models. *Journal of Anatomy*, *212*(1), 12–18. https://doi.org/10.1111/j.1469-7580.2007.00838.x

Flamme, I., Frölich, T., & Risau, W. (1997). Molecular mechanisms of vasculogenesis and embryonic angiogenesis. *Journal of Cellular Physiology*, *173*(2), 206–210. https://doi.org/10.1002/(SICI)1097-4652(199711)173:2<206::AID-JCP22>3.0.CO;2-C

Frandon, J., Bricq, S., Bentatou, Z., Marcadet, L., Barral, P. A., Finas, M., … Jacquier, A. (2018). Semi-automatic detection of myocardial trabeculation using cardiovascular magnetic resonance: correlation with histology and reproducibility in a mouse model of non-compaction. *Journal of Cardiovascular Magnetic Resonance : Official Journal of the Society for Cardiovascular Magnetic Resonance*, *20*(1), 70. https://doi.org/10.1186/s12968-018-0489-0

Frangogiannis, N. G. (2014). The Immune System and the Remodeling Infarcted Heart. *Journal of Cardiovascular Pharmacology*, *63*(3), 185–195. https://doi.org/10.1097/FJC.0000000000000003

Garg, V., Muth, A. N., Ransom, J. F., Schluterman, M. K., Barnes, R., King, I. N., … Srivastava, D. (2005). Mutations in NOTCH1 cause aortic valve disease. *Nature*, *437*(7056), 270–274. https://doi.org/10.1038/nature03940

Garside, V. C., Chang, A. C., Karsan, A., & Hoodless, P. A. (2013). Co-ordinating Notch, BMP, and TGF-β signaling during heart valve development. *Cellular and Molecular Life Sciences*, *70*(16), 2899–2917. https://doi.org/10.1007/s00018-012-1197-9

Gassmann, M., Casagranda, F., Orioli, D., Simon, H., Lai, C., Klein, R., & Lemke, G. (1995). Aberrant neural and cardiac development in mice lacking the ErbB4 neuregulin receptor. *Nature*, *378*(6555), 390–394. https://doi.org/10.1038/378390a0

Gati, S., Chandra, N., Bennett, R. L., Reed, M., Kervio, G., Panoulas, V. F., … Sharma, S. (2013). Increased left ventricular trabeculation in highly trained athletes: do we need more stringent criteria for the diagnosis of left ventricular non-compaction in athletes? *Heart (British Cardiac Society)*, *99*(6), 401–408. https://doi.org/10.1136/heartjnl-2012-303418

Gati, S., Papadakis, M., Papamichael, N. D., Zaidi, A., Sheikh, N., Reed, M., … Sharma, S. (2014). Reversible De Novo Left Ventricular Trabeculations in Pregnant Women. *Circulation*, *130*(6), 475–483. https://doi.org/10.1161/CIRCULATIONAHA.114.008554

Gati, S., Van Niekerk, N., Reed, M., Cox, A., Zaidi, A., Ghani, S., … Sharma, S. (2013). 156 THE PREVALENCE OF INCREASED LEFT VENTRICULAR TRABECULATION IN INDIVIDUALS WITH SICKLE CELL ANAEMIA? *Heart*, *99*(suppl 2), A91.2-A92. https://doi.org/10.1136/heartjnl-2013-304019.156

Greer, J. J. M., Ware, D. P., & Lefer, D. J. (2006). Myocardial infarction and heart failure in the *db/db* diabetic mouse. *American Journal of Physiology-Heart and Circulatory Physiology*, *290*(1), H146–H153. https://doi.org/10.1152/ajpheart.00583.2005

Grego-Bessa, J., Luna-Zurita, L., del Monte, G., Bolós, V., Melgar, P., Arandilla, A., … de la Pompa, J. L. (2007). Notch Signaling Is Essential for Ventricular Chamber Development. *Developmental Cell*. https://doi.org/10.1016/j.devcel.2006.12.011

Gude, N., & Sussman, M. (2012). Notch signaling and cardiac repair. *Journal of Molecular and Cellular Cardiology*, *52*(6), 1226–1232. https://doi.org/10.1016/j.yjmcc.2012.03.007

Hang, C. T., Yang, J., Han, P., Cheng, H.-L., Shang, C., Ashley, E., … Chang, C.-P. (2010). Chromatin regulation by Brg1 underlies heart muscle development and disease. *Nature*, *466*(7302), 62–67. https://doi.org/10.1038/nature09130

He, L., Huang, X., Kanisicak, O., Li, Y., Wang, Y., Li, Y., … Zhou, B. (2017). Preexisting endothelial cells mediate cardiac neovascularization after injury. *Journal of Clinical Investigation*. https://doi.org/10.1172/JCI93868

Heffner, C. S., Herbert Pratt, C., Babiuk, R. P., Sharma, Y., Rockwood, S. F., Donahue, L. R., … Murray, S. A. (2012). Supporting conditional mouse mutagenesis with a comprehensive cre characterization resource. *Nature Communications*, *3*(1), 1218. https://doi.org/10.1038/ncomms2186

Henry, T. D., Annex, B. H., McKendall, G. R., Azrin, M. A., Lopez, J. J., Giordano, F. J., … McCluskey, E. R. (2003). The VIVA trial: Vascular endothelial growth factor in ischemia for vascular angiogenesis. *Circulation*. https://doi.org/10.1161/01.CIR.0000061911.47710.8A

Hernandez Tejada, F. N., Galvez Silva, J. R., & Zweidler-McKay, P. A. (2014). The challenge of targeting notch in hematologic malignancies. *Frontiers in Pediatrics*, *2*, 54. https://doi.org/10.3389/fped.2014.00054

High, F. A., & Epstein, J. A. (2008). The multifaceted role of Notch in cardiac development and disease. *Nature Reviews Genetics*, *9*(1), 49–61. https://doi.org/10.1038/nrg2279

Huh, W. J., Khurana, S. S., Geahlen, J. H., Kohli, K., Waller, R. A., & Mills, J. C. (2012). Tamoxifen induces rapid, reversible atrophy, and metaplasia in mouse stomach. *Gastroenterology*. https://doi.org/10.1053/j.gastro.2011.09.050

Jaleco, A. C., Neves, H., Hooijberg, E., Gameiro, P., Clode, N., Haury, M., … Parreira, L. (2001). Differential effects of Notch ligands Delta-1 and Jagged-1 in human lymphoid differentiation. *The Journal of Experimental Medicine*, *194*(7), 991–1002. https://doi.org/10.1084/JEM.194.7.991

Jelinek, H. F., Jones, C. L., Warfel, M. D., Lucas, C., Depardieu, C., & Aurel, G. (2006). Understanding fractal analysis? The case of fractal linguistics. In *Complexus*. https://doi.org/10.1159/000094189

Jenni, R., Oechslin, E. N., & van der Loo, B. (2007). Isolated ventricular non-compaction of the myocardium in adults. *Heart*, *93*(1), 11–15. https://doi.org/10.1136/hrt.2005.082271

Kaipainen, A., Korhonen, J., Mustonen, T., van Hinsbergh, V. W., Fang, G. H., Dumont, D., … Alitalo, K. (1995). Expression of the fms-like tyrosine kinase 4 gene becomes restricted to lymphatic endothelium during development. *Proceedings of the National Academy of Sciences of the United States of America*, *92*(8), 3566–3570. https://doi.org/10.1073/pnas.92.8.3566

Kasaai, B., Caolo, V., Peacock, H. M., Lehoux, S., Gomez-Perdiguero, E., Luttun, A., & Jones, E. A. V. (2017). Erythro-myeloid progenitors can differentiate from endothelial cells and modulate embryonic vascular remodeling. *Scientific Reports*, *7*(1), 43817. https://doi.org/10.1038/srep43817

Kelly, R. G., Brown, N. A., & Buckingham, M. E. (2001). The arterial pole of the mouse heart forms from Fgf10-expressing cells in pharyngeal mesoderm. *Developmental Cell*, *1*(3), 435–440. Retrieved from http://www.ncbi.nlm.nih.gov/pubmed/11702954

KERN, M. J. (1999). Angiogenesis, Arteriogenesis, and Physiological Perfusion: Review of Natural History and Concepts. *Journal of Interventional Cardiology*, *12*(4), 313–318. https://doi.org/10.1111/j.1540-8183.1999.tb00251.x

Khambata, R. S., Panayiotou, C. M., & Hobbs, A. J. (2011). Natriuretic peptide receptor-3 underpins the disparate regulation of endothelial and vascular smooth muscle cell proliferation by C-type natriuretic peptide. *British Journal of Pharmacology*, *164*(2 B), 584–597. https://doi.org/10.1111/j.1476-5381.2011.01400.x

Khokhlova, A. D., & Iribe, G. (2016). Transmural Differences in Mechanical Properties of Isolated Subendocardial and Subepicardial Cardiomyocytes. *Bulletin of Experimental Biology and Medicine*, *162*(1), 48–50. https://doi.org/10.1007/s10517-016-3542-8

Kisanuki, Y. Y., Hammer, R. E., Miyazaki, J., Williams, S. C., Richardson, J. A., & Yanagisawa, M. (2001). Tie2-Cre Transgenic Mice: A New Model for Endothelial Cell-Lineage Analysis in Vivo. *Developmental Biology*, *230*(2), 230–242. https://doi.org/10.1006/dbio.2000.0106

Kitajima, S., Takagi, A., Inoue, T., & Saga, Y. (2000). MesP1 and MesP2 are essential for the development of cardiac mesoderm. *Development (Cambridge, England)*, *127*(15), 3215–3226. Retrieved from http://www.ncbi.nlm.nih.gov/pubmed/10887078

Kloner, R. A. (2006). Foreword - No-reflow: Basic science to a clinical phenomenon. *Basic Research in Cardiology*. https://doi.org/10.1007/s00395-006-0614-3

Kobayashi, K., Maeda, K., Takefuji, M., Kikuchi, R., Morishita, Y., Hirashima, M., & Murohara, T. (2017). Dynamics of angiogenesis in ischemic areas of the infarcted heart. *Scientific Reports*, *7*(1), 1–13. https://doi.org/10.1038/s41598-017-07524-x

Kolk, M. V. V, Meyberg, D., Deuse, T., Tang-Quan, K. R., Robbins, R. C., Reichenspurner, H., & Schrepfer, S. (2009). LAD-ligation: a murine model of myocardial infarction. *Journal of Visualized Experiments : JoVE*, (32). https://doi.org/10.3791/1438

Krijnen, P. A. J., Nijmeijer, R., Meijer, C. J. L. M., Visser, C. A., Hack, C. E., & Niessen, H. W. M. (2002). Apoptosis in myocardial ischaemia and infarction. *Journal of Clinical Pathology*, *55*(11), 801–811. Retrieved from http://www.ncbi.nlm.nih.gov/pubmed/12401816

Lambert, J. M., Lopez, E. F., & Lindsey, M. L. (2008). Macrophage Roles Following Myocardial Infarction. *International Journal of Cardiology*, *130*(2), 147. https://doi.org/10.1016/J.IJCARD.2008.04.059

Lee, K.-F., Simon, H., Chen, H., Bates, B., Hung, M.-C., & Hauser, C. (1995). Requirement for neuregulin receptor erbB2 in neural and cardiac development. *Nature*, *378*(6555), 394–398. https://doi.org/10.1038/378394a0

Lescroart, F., Wang, X., Lin, X., Swedlund, B., Gargouri, S., Sànchez-Dànes, A., … Blanpain, C. (2018). Defining the earliest step of cardiovascular lineage segregation by single-cell RNA-seq. *Science (New York, N.Y.)*, *359*(6380), 1177–1181. https://doi.org/10.1126/science.aao4174

Li, Y., Hiroi, Y., & Liao, J. K. (2010). Notch signaling negatively regulates cardiac differentiation (Nemir, 2006). *Trends Cardiovasc Med.*, *20*(7), 228–231. https://doi.org/10.1021/nl061786n.Core-Shell

Libby, P., Maroko, P. R., Bloor, C. M., Sobel, B. E., & Braunwald, E. (1973). Reduction of experimental myocardial infarct size by corticosteroid administration. *The Journal of Clinical Investigation*, *52*(3), 599–607. https://doi.org/10.1172/JCI107221

Lin, L. Y., Su, M. Y. M., Pham, V. T., Tran, T. T., Wang, Y. H., Tseng, W. Y. I., … Lin, J. L. (2016). Endocardial Remodeling in Heart Failure Patients with Impaired and Preserved Left Ventricular Systolic Function-A Magnetic Resonance Image Study. *Scientific Reports*, *6*(February), 1–8. https://doi.org/10.1038/srep20868

Liu, J., Bressan, M., Hassel, D., Huisken, J., Staudt, D., Kikuchi, K., … Stainier, D. Y. R. (2010). A dual role for ErbB2 signaling in cardiac trabeculation. *Development*, *137*(22), 3867–3875. https://doi.org/10.1242/dev.053736

Livak, K. J., & Schmittgen, T. D. (2001). Analysis of Relative Gene Expression Data Using Real-Time Quantitative PCR and the 2−ΔΔCT Method. *Methods*, *25*(4), 402–408. https://doi.org/10.1006/meth.2001.1262

Lowery, J. W., & de Caestecker, M. P. (2010). BMP signaling in vascular development and disease. *Cytokine & Growth Factor Reviews*, *21*(4), 287–298. https://doi.org/10.1016/j.cytogfr.2010.06.001

Luna-Zurita, L., Prados, B., Grego-Bessa, J., Luxán, G., Del Monte, G., Benguría, A., … De La Pompa, J. L. (2010). Integration of a Notch-dependent mesenchymal gene program and Bmp2-driven cell invasiveness regulates murine cardiac valve formation. *Journal of Clinical Investigation*. https://doi.org/10.1172/JCI42666

Luna-Zurita, L., Prados, B., Grego-Bessa, J., Luxán, G., del Monte, G., Benguría, A., … de la Pompa, J. L. (2010). Integration of a Notch-dependent mesenchymal gene program and Bmp2-driven cell invasiveness regulates murine cardiac valve formation. *Journal of Clinical Investigation*, *120*(10), 3493–3507. https://doi.org/10.1172/JCI42666

Luxán, G., Casanova, J. C., Martínez-Poveda, B., Prados, B., D'Amato, G., MacGrogan, D., … de la Pompa, J. L. (2013). Mutations in the NOTCH pathway

regulator MIB1 cause left ventricular noncompaction cardiomyopathy. *Nature Medicine*, *19*(2), 193–201. https://doi.org/10.1038/nm.3046

MacGrogan, D., Münch, J., & de la Pompa, J. L. (2018). Notch and interacting signalling pathways in cardiac development, disease, and regeneration. *Nature Reviews Cardiology*, *15*(11), 685–704. https://doi.org/10.1038/s41569-018-0100-2

Madeddu, P., Emanueli, C., Spillmann, F., Meloni, M., Bouby, N., Richer, C., … Levy, B. I. (2006). Murine models of myocardial and limb ischemia: Diagnostic end-points and relevance to clinical problems. *Vascular Pharmacology*. https://doi.org/10.1016/j.vph.2006.08.008

Mahmoud, M., Allinson, K. R., Zhai, Z., Oakenfull, R., Ghandi, P., Adams, R. H., … Arthur, H. M. (2010). Pathogenesis of arteriovenous malformations in the absence of endoglin. *Circulation Research*. https://doi.org/10.1161/CIRCRESAHA.109.211037

Majmudar, M. D., Keliher, E. J., Heidt, T., Leuschner, F., Truelove, J., Sena, B. F., … Nahrendorf, M. (2013). Monocyte-directed RNAi targeting CCR2 improves infarct healing in atherosclerosis-prone mice. *Circulation*, *127*(20), 2038–2046. https://doi.org/10.1161/CIRCULATIONAHA.112.000116

Malliaras, K., Zhang, Y., Seinfeld, J., Galang, G., Tseliou, E., Cheng, K., … Marbán, E. (2013). Cardiomyocyte proliferation and progenitor cell recruitment underlie therapeutic regeneration after myocardial infarction in the adult mouse heart. *EMBO Molecular Medicine*, *5*(2), 191–209. https://doi.org/10.1002/emmm.201201737

Meier, C. K., & Oyama, M. a. (2004). Myocardial Infarction. *Small Animal Critical Care Medicine*. https://doi.org/10.1016/B978-1-4160-2591-7.10041-4

Meilhac, S. M., Kelly, R. G., Rocancourt, D., Eloy-Trinquet, S., Nicolas, J.-F., Buckingham, M. E., … Stainier, D. Y. R. (2003). A retrospective clonal analysis of the myocardium reveals two phases of clonal growth in the developing mouse heart. *Development*, *130*(16), 3877–3889. https://doi.org/10.1242/dev.00580

Meyer, D., & Birchmeier, C. (1995). Multiple essential functions of neuregulin in development. *Nature*, *378*(6555), 386–390. https://doi.org/10.1038/378386a0

Milgrom-Hoffman, M., Harrelson, Z., Ferrara, N., Zelzer, E., Evans, S. M., & Tzahor, E. (2011). The heart endocardium is derived from vascular endothelial progenitors. *Development*, *138*(21), 4777–4787. https://doi.org/10.1242/dev.061192

Miquerol, L., Thireau, J., Bideaux, P., Sturny, R., Richard, S., & Kelly, R. G. (2015). Endothelial Plasticity Drives Arterial Remodeling Within the Endocardium After Myocardial Infarction. *Circulation Research*, *116*(11), 1765–1771. https://doi.org/10.1161/CIRCRESAHA.116.306476

Moore-Morris, T., Guimarães-Camboa, N., Banerjee, I., Zambon, A. C., Kisseleva, T., Velayoudon, A., … Evans, S. M. (2014). Resident fibroblast lineages mediate pressure overload-induced cardiac fibrosis. *The Journal of Clinical Investigation*, *124*(7), 2921–2934. https://doi.org/10.1172/JCI74783

MOORMAN, A. F. M., & CHRISTOFFELS, V. M. (2003). Cardiac Chamber Formation: Development, Genes, and Evolution. *Physiological Reviews*, *83*(4), 1223–1267. https://doi.org/10.1152/physrev.00006.2003

Moorman, A., Webb, S., Brown, N. A., Lamers, W., & Anderson, R. H. (2003). Development of the heart: (1) formation of the cardiac chambers and arterial trunks. *Heart (British Cardiac Society)*, *89*(7), 806–814. Retrieved from http://www.ncbi.nlm.nih.gov/pubmed/12807866

Moyes, A. J., Khambata, R. S., Villar, I., Bubb, K. J., Baliga, R. S., Lumsden, N. G., … Hobbs, A. J. (2014). Endothelial C-type natriuretic peptide maintains vascular homeostasis. *Journal of Clinical Investigation*, *124*(9), 4039–4051. https://doi.org/10.1172/JCI74281

Münch, J., Grivas, D., González-Rajal, Á., Torregrosa-Carrión, R., & de la Pompa, J. L. (2017). Notch signalling restricts inflammation and serpine1 expression in the dynamic endocardium of the regenerating zebrafish heart. *Development (Cambridge, England)*, *144*(8), 1425–1440. https://doi.org/10.1242/dev.143362

Murtaugh, L. C., Stanger, B. Z., Kwan, K. M., & Melton, D. A. (2003). Notch signaling controls multiple steps of pancreatic differentiation. *Proceedings of the National Academy of Sciences*, *100*(25), 14920–14925. https://doi.org/10.1073/pnas.2436557100

Muthuramu, I., Lox, M., Jacobs, F., & De Geest, B. (2014). Permanent ligation of the left anterior descending coronary artery in mice: a model of post-myocardial infarction remodelling and heart failure. *Journal of Visualized Experiments : JoVE*, (94). https://doi.org/10.3791/52206

Mysliwiec, M. R., Bresnick, E. H., & Lee, Y. (2011). Endothelial Jarid2/Jumonji is required for normal cardiac development and proper Notch1 expression. *The Journal of Biological Chemistry*, *286*(19), 17193–17204. https://doi.org/10.1074/jbc.M110.205146

Nadeau, M., Georges, R. O., Laforest, B., Yamak, A., Lefebvre, C., Beauregard, J., … Nemer, M. (2010). An endocardial pathway involving Tbx5, Gata4, and Nos3 required for atrial septum formation. *Proceedings of the National Academy of Sciences*. https://doi.org/10.1073/pnas.0914888107

Neuhaus, H., Rosen, V., & Thies, R. S. (1999). Heart specific expression of mouse BMP-10 a novel member of the TGF-beta superfamily. *Mechanisms of Development*, *80*(2), 181–184. Retrieved from http://www.ncbi.nlm.nih.gov/pubmed/10072785

Niessen, K., & Karsan, A. (2008). Notch signaling in cardiac development. *Circulation Research*. https://doi.org/10.1161/CIRCRESAHA.108.174318

Nossuli, T. O., Lakshminarayanan, V., Baumgarten, G., Taffet, G. E., Ballantyne, C. M., Michael, L. H., & Entman, M. L. (2000). A chronic mouse model of myocardial ischemia-reperfusion: essential in cytokine studies. *American Journal of Physiology: Heart and Circulatory Physiology*. https://doi.org/10.1152/ajpheart.2000.278.4.H1049

Nowotschin, S., Xenopoulos, P., Schrode, N., & Hadjantonakis, A.-K. (2013). A bright single-cell resolution live imaging reporter of Notch signaling in the mouse. *BMC Developmental Biology*, *13*(1), 15. https://doi.org/10.1186/1471-213X-13-15

Orban, P. C., Chui, D., & Marth, J. D. (1992). Tissue- and site-specific DNA recombination in transgenic mice. *Proceedings of the National Academy of Sciences of the United States of America*, *89*(15), 6861–6865. https://doi.org/10.1073/PNAS.89.15.6861

Paige, S. L., Plonowska, K., Xu, A., & Wu, S. M. (2015). Molecular Regulation of Cardiomyocyte Differentiation. *Circulation Research*, *116*(2), 341–353. https://doi.org/10.1161/CIRCRESAHA.116.302752

Parker, M. H., Loretz, C., Tyler, A. E., Duddy, W. J., Hall, J. K., Olwin, B. B., … Tapscott, S. J. (2012). Activation of Notch Signaling During *Ex Vivo* Expansion Maintains Donor Muscle Cell Engraftment. *STEM CELLS*, *30*(10), 2212–2220. https://doi.org/10.1002/stem.1181

Payne, S., De Val, S., & Neal, A. (2018). Endothelial-Specific Cre Mouse Models. *Arteriosclerosis, Thrombosis, and Vascular Biology*, *38*(11), 2550–2561. https://doi.org/10.1161/ATVBAHA.118.309669

Pedram, A., Razandi, M., Hu, R., & Levin, E. R. (1997). Vasoactive Peptides Modulate Vascular Endothelial Cell Growth Factor Production and Endothelial Cell Proliferation and Invasion *, *272*(27), 17097–17103.

Pérez-Pomares, J. M., & de la Pompa, J. L. (2011). Signaling During Epicardium and Coronary Vessel Development. *Circulation Research*, *109*(12), 1429–1442. https://doi.org/10.1161/CIRCRESAHA.111.245589

Porrello, E. R., Mahmoud, A. I., Simpson, E., Hill, J. A., Richardson, J. A., Olson, E. N., … Zhou, B. (2011). Transient regenerative potential of the neonatal mouse heart. *Science (New York, N.Y.)*, *331*(6020), 1078–1080. https://doi.org/10.1126/science.1200708

Pratumvinit, B., Reesukumal, K., Janebodin, K., Ieronimakis, N., & Reyes, M. (2013). Isolation, characterization, and transplantation of cardiac endothelial cells. *BioMed Research International*, *2013*, 359412. https://doi.org/10.1155/2013/359412

Radtke, F., Wilson, A., Stark, G., Bauer, M., van Meerwijk, J., MacDonald, H. R., & Aguet, M. (1999). Deficient T cell fate specification in mice with an induced inactivation of Notch1. *Immunity*, *10*(5), 547–558. https://doi.org/10.1016/S1074-7613(00)80054-0

Ramjane, K., Han, L., & Jin, C. (2008). The diagnosis and treatment of the no-reflow phenomenon in patients with myocardial infarction undergoing percutaneous coronary intervention. *Experimental and Clinical Cardiology*, *13*(3), 121–128. Retrieved from http://www.ncbi.nlm.nih.gov/pubmed/19343126

Red-Horse, K., Ueno, H., Weissman, I. L., & Krasnow, M. A. (2010). Coronary arteries form by developmental reprogramming of venous cells. *Nature*, *464*(7288), 549–553. https://doi.org/10.1038/nature08873

Reffelmann, T., Hale, S. L., Dow, J. S., & Kloner, R. A. (2003). No-Reflow Phenomenon Persists Long-Term After Ischemia/Reperfusion in the Rat and Predicts Infarct Expansion. *Circulation*, *108*(23), 2911–2917. https://doi.org/10.1161/01.CIR.0000101917.80668.E1

Rentschler, S., Harris, B. S., Kuznekoff, L., Jain, R., Manderfield, L., Lu, M. M., … Epstein, J. A. (2011). Notch signaling regulates murine atrioventricular conduction and the formation of accessory pathways. *Journal of Clinical Investigation*, *121*(2), 525–533. https://doi.org/10.1172/JCI44470

Riley, P. R., & Smart, N. (2011). Vascularizing the heart. *Cardiovascular Research*. https://doi.org/10.1093/cvr/cvr035

Rivard, A., & Isner, J. M. (1998). Angiogenesis and vasculogenesis in treatment of cardiovascular disease. *Molecular Medicine (Cambridge, Mass.)*, *4*(7), 429–440. Retrieved from http://www.ncbi.nlm.nih.gov/pubmed/9713822

Roberts, R., DeMello, V., & Sobel, B. E. (1976). Deleterious effects of methylprednisolone in patients with myocardial infarction. *Circulation*, *53*(3 Suppl), I204-6. Retrieved from http://www.ncbi.nlm.nih.gov/pubmed/1253361

Roger, V. L. (2013). Epidemiology of heart failure. *Circulation Research*. https://doi.org/10.1161/CIRCRESAHA.113.300268

Saffitz, J. E., & Kléber, A. G. (2004). Effects of Mechanical Forces and Mediators of Hypertrophy on Remodeling of Gap Junctions in the Heart. *Circulation Research*, *94*(5), 585–591. https://doi.org/10.1161/01.RES.0000121575.34653.50

Samsa, L. A., Yang, B., & Liu, J. (2013). Embryonic cardiac chamber maturation: Trabeculation, conduction, and cardiomyocyte proliferation. *American Journal of Medical Genetics. Part C, Seminars in Medical Genetics*, *163C*(3), 157–168. https://doi.org/10.1002/ajmg.c.31366

Savio-Galimberti, E., Frank, J., Inoue, M., Goldhaber, J. I., Cannell, M. B., Bridge, J. H. B., & Sachse, F. B. (2008). Novel features of the rabbit transverse tubular system revealed by quantitative analysis of three-dimensional reconstructions from confocal images. *Biophysical Journal*. https://doi.org/10.1529/biophysj.108.130617

Sedmera, D., Pexieder, T., Vuillemin, M., Thompson, R. P., & Anderson, R. H. (2000). Developmental patterning of the myocardium. *The Anatomical Record*, *258*(4), 319–337. https://doi.org/10.1002/(SICI)1097-0185(20000401)258:4<319::AID-AR1>3.0.CO;2-O

Selye, H., Bajusz, E., Grasso, S., & Mendell, P. (1960). Simple Techniques for the Surgical Occlusion of Coronary Vessels in the Rat. *Angiology*. https://doi.org/10.1177/000331976001100505

Shyu, K.-G. (2009). Cellular and molecular effects of mechanical stretch on vascular cells and cardiac myocytes. *Clinical Science*. https://doi.org/10.1042/CS20080163

Silvestre, J.-S., Mallat, Z., Tedgui, A., & Levy, B. I. (2008). Post-ischaemic neovascularization and inflammation. *Cardiovascular Research*, *78*(2), 242–249. https://doi.org/10.1093/cvr/cvn027

Simons, M., Annex, B. H., Laham, R. J., Kleiman, N., Henry, T., Dauerman, H., … Chronos, N. A. (2002). Pharmacological treatment of coronary artery disease with recombinant fibroblast growth factor-2: Double-blind, randomized, controlled clinical trial. *Circulation*. https://doi.org/10.1161/hc0802.104407

Smart, N., & Riley, P. R. (2012). The epicardium as a candidate for heart regeneration. *Future Cardiology*, *8*(1), 53–69. https://doi.org/10.2217/fca.11.87

Song, A. J., & Palmiter, R. D. (2018). Detecting and Avoiding Problems When Using the Cre–lox System. *Trends in Genetics*. https://doi.org/10.1016/j.tig.2017.12.008

Sorensen, I., Adams, R. H., & Gossler, A. (2009). DLL1-mediated Notch activation regulates endothelial identity in mouse fetal arteries. *Blood*, *113*(22), 5680–5688. https://doi.org/10.1182/blood-2008-08-174508

Srinivas, S., Watanabe, T., Lin, C. S., William, C. M., Tanabe, Y., Jessell, T. M., & Costantini, F. (2001). Cre reporter strains produced by targeted insertion of EYFP and ECFP into the ROSA26 locus. *BMC Developmental Biology*, *1*, 4. https://doi.org/10.1186/1471-213X-1-4

Stankunas, K., Hang, C. T., Tsun, Z.-Y., Chen, H., Lee, N. V, Wu, J. I., … Chang, C.-P. (2008). Endocardial Brg1 represses ADAMTS1 to maintain the microenvironment for myocardial morphogenesis. *Developmental Cell*, *14*(2), 298–311. https://doi.org/10.1016/j.devcel.2007.11.018

Sternberg, N., Hamilton, D., & Hoess, R. (1981). Bacteriophage P1 site-specific recombination. II. Recombination between loxP and the bacterial chromosome. *Journal of Molecular Biology*. https://doi.org/10.1016/0022-2836(81)90376-4

Stewart, D. J., Hilton, J. D., Arnold, J. M. O., Gregoire, J., Rivard, A., Archer, S. L., … Rasmussen, H. S. (2006). Angiogenic gene therapy in patients with nonrevascularizable ischemic heart disease: A phase 2 randomized, controlled trial of AdVEGF121(AdVEGF121) versus maximum medical treatment. *Gene Therapy*. https://doi.org/10.1038/sj.gt.3302802

Su, T., Stanley, G., Sinha, R., D'Amato, G., Das, S., Rhee, S., … Red-Horse, K. (2018). Single-cell analysis of early progenitor cells that build coronary arteries. *Nature*, *559*(7714), 356–362. https://doi.org/10.1038/s41586-018-0288-7

Suffee, N., Moore-Morris, T., Farahmand, P., Rücker-Martin, C., Dilanian, G., Fradet, M., … Hatem, S. N. (2017). Atrial natriuretic peptide regulates adipose tissue accumulation in adult atria. *Proceedings of the National Academy of Sciences of the United States of America*, *114*(5), E771–E780. https://doi.org/10.1073/pnas.1610968114

Sugi, Y., & Markwald, R. R. (1996). Formation and early morphogenesis of endocardial endothelial precursor cells and the role of endoderm. *Developmental Biology*. https://doi.org/10.1006/dbio.1996.0096

Tang, J., Zhang, H., He, L., Huang, X., Li, Y., Pu, W., … Zhou, B. (2018). Genetic Fate Mapping Defines the Vascular Potential of Endocardial Cells in the Adult Heart. *Circulation Research*, *122*(7), 984–993. https://doi.org/10.1161/CIRCRESAHA.117.312354

Tayebjee, M. H., Lip, G. Y. H., & MacFadyen, R. J. (2004). Collateralization and the response to obstruction of epicardial coronary arteries. *QJM : Monthly Journal of the Association of Physicians*, *97*(5), 259–272. Retrieved from http://www.ncbi.nlm.nih.gov/pubmed/15100419

Teekakirikul, P., Kelly, M. A., Rehm, H. L., Lakdawala, N. K., & Funke, B. H. (2013). Inherited cardiomyopathies: Molecular genetics and clinical genetic testing in the postgenomic era. *Journal of Molecular Diagnostics*. https://doi.org/10.1016/j.jmoldx.2012.09.002

Thygesen, K., Alpert, J. S., White, H. D., Joint ESC/ACCF/AHA/WHF Task Force for the Redefinition of Myocardial Infarction, Jaffe, A. S., Apple, F. S., … Al-Attar, N. (2007). Universal definition of myocardial infarction. *Circulation*. https://doi.org/10.1161/CIRCULATIONAHA.107.187397

Tian, X., Hu, T., Zhang, H., He, L., Huang, X., Liu, Q., … Zhou, B. (2014). De novo formation of a distinct coronary vascular population in neonatal heart. *Science*. https://doi.org/10.1126/science.1251487

Timmerman, L. A., Grego-Bessa, J., Raya, A., Bertrán, E., Pérez-Pomares, J. M., Díez, J., … de la Pompa, J. L. (2004). Notch promotes epithelial-mesenchymal transition during cardiac development and oncogenic transformation. *Genes & Development*, *18*(1), 99–115. https://doi.org/10.1101/gad.276304

Tomlinson, J. E., Žygelytė, E., Grenier, J. K., Edwards, M. G., & Cheetham, J. (2018). Temporal changes in macrophage phenotype after peripheral nerve injury. *Journal of Neuroinflammation*, *15*(1), 185. https://doi.org/10.1186/s12974-018-1219-0

Ulvmar, M. H., Martinez-Corral, I., Stanczuk, L., & Mäkinen, T. (2016). *Pdgfrb-Cre* targets lymphatic endothelial cells of both venous and non-venous origins. *Genesis*, *54*(6), 350–358. https://doi.org/10.1002/dvg.22939

Van Den Akker, N. M. S., Caolo, V., Wisse, L. J., Peters, P. P. W. M., Poelmann, R. E., Carmeliet, P., … Gittenberger-De Groot, A. C. (2008). Developmental coronary maturation is disturbed by aberrant cardiac vascular endothelial growth factor expression and Notch signalling. *Cardiovascular Research*. https://doi.org/10.1093/cvr/cvm108

Van Vliet, P., Wu, S. M., Zaffran, S., & Puceat, M. (2012). Early cardiac development: a view from stem cells to embryos. *Cardiovascular Research*, *96*(3), 352–362. https://doi.org/10.1093/cvr/cvs270

VanDusen, N. J., Casanovas, J., Vincentz, J. W., Firulli, B. A., Osterwalder, M., Lopez-Rios, J., … Firulli, A. B. (2014). Hand2 is an essential regulator for two Notch-dependent functions within the embryonic endocardium. *Cell Reports*, *9*(6), 2071–2083. https://doi.org/10.1016/j.celrep.2014.11.021

Virag, J. A. I., & Lust, R. M. (2011). Coronary artery ligation and intramyocardial injection in a murine model of infarction. *Journal of Visualized Experiments : JoVE*, (52). https://doi.org/10.3791/2581

Vogel, B., Siebert, H., Hofmann, U., & Frantz, S. (2015). Determination of collagen content within picrosirius red stained paraffin-embedded tissue sections using fluorescence microscopy. *MethodsX*. https://doi.org/10.1016/j.mex.2015.02.007

Wang, Y., Nakayama, M., Pitulescu, M. E., Schmidt, T. S., Bochenek, M. L., Sakakibara, A., … Adams, R. H. (2010). Ephrin-B2 controls VEGF-induced angiogenesis and lymphangiogenesis. *Nature*, *465*(7297), 483–486. https://doi.org/10.1038/nature09002

Weber, H., Symes, C. E., Walmsley, M. E., Rodaway, A. R., & Patient, R. K. (2000). A role for GATA5 in Xenopus endoderm specification. *Development (Cambridge, England)*, *127*(20), 4345–4360. Retrieved from http://www.ncbi.nlm.nih.gov/pubmed/11003835

Whittaker, P., Kloner, R. A., Boughner, D. R., & Pickering, J. G. (n.d.). Quantitative assessment of myocardial collagen with picrosirius red staining and circularly polarized light. *Basic Research in Cardiology*, *89*(5), 397–410. Retrieved from http://www.ncbi.nlm.nih.gov/pubmed/7535519

Williams, R., Lendahl, U., & Lardelli, M. (1995). Complementary and combinatorial patterns of Notch gene family expression during early mouse development. *Mechanisms of Development*. https://doi.org/10.1016/0925-4773(95)00451-3

Withey, S. L., Hill, R., Lyndon, A., Dewey, W. L., Kelly, E., & Henderson, G. (2017). Effect of Tamoxifen and Brain-Penetrant Protein Kinase C and c-Jun N-Terminal Kinase Inhibitors on Tolerance to Opioid-Induced Respiratory Depression in Mice. *Journal of Pharmacology and Experimental Therapeutics*. https://doi.org/10.1124/jpet.116.238329

Wu, B., Wang, Y., Lui, W., Langworthy, M., Tompkins, K. L., Hatzopoulos, A. K., … Zhou, B. (2011). Nfatc1 Coordinates Valve Endocardial Cell Lineage Development Required for Heart Valve Formation. *Circulation Research*, *109*(2), 183–192. https://doi.org/10.1161/CIRCRESAHA.111.245035

Wu, B., Zhang, Z., Lui, W., Chen, X., Wang, Y., Chamberlain, A. A., … Zhou, B. (2012). Endocardial cells form the coronary arteries by angiogenesis through myocardial-endocardial VEGF signaling. *Cell*, *151*(5), 1083–1096. https://doi.org/10.1016/j.cell.2012.10.023

Xu, X., Friehs, I., Zhong Hu, T., Melnychenko, I., Tampe, B., Alnour, F., … Zeisberg, E. M. (2015). Endocardial fibroelastosis is caused by aberrant endothelial to mesenchymal transition. *Circulation Research*, *116*(5), 857–866. https://doi.org/10.1161/CIRCRESAHA.116.305629

Xu, Z., Alloush, J., Beck, E., & Weisleder, N. (2014). A murine model of myocardial ischemia-reperfusion injury through ligation of the left anterior descending artery. *Journal of Visualized Experiments : JoVE*, (86). https://doi.org/10.3791/51329

Yamamura, H., Yamamura, A., Ko, E. A., Pohl, N. M., Smith, K. A., Zeifman, A., … Yuan, J. X.-J. (2014). Activation of Notch signaling by short-term treatment with Jagged-1 enhances store-operated Ca(2+) entry in human pulmonary arterial smooth muscle cells. *American Journal of Physiology. Cell Physiology*, *306*(9), C871-8. https://doi.org/10.1152/ajpcell.00221.2013

Yanagida, K., Liu, C. H., Faraco, G., Galvani, S., Smith, H. K., Burg, N., … Hla, T. (2017). Size-selective opening of the blood-brain barrier by targeting endothelial sphingosine 1-phosphate receptor 1. *Proceedings of the National Academy of Sciences of the United States of America*, *114*(17), 4531–4536. https://doi.org/10.1073/pnas.1618659114

Yang, L., Cai, C.-L., Lin, L., Qyang, Y., Chung, C., Monteiro, R. M., … Evans, S. (2006). Isl1Cre reveals a common Bmp pathway in heart and limb development. *Development*, *133*(8), 1575–1585. https://doi.org/10.1242/dev.02322

Yarden, Y., & Sliwkowski, M. X. (2001). Untangling the ErbB signalling network. *Nature Reviews Molecular Cell Biology*, *2*(2), 127–137. https://doi.org/10.1038/35052073

Zachary, I., & Morgan, R. D. (2011). Therapeutic angiogenesis for cardiovascular disease: biological context, challenges, prospects. *Heart (British Cardiac Society)*, *97*(3), 181–189. https://doi.org/10.1136/hrt.2009.180414

Zhang, H., Pu, W., Li, G., Huang, X., He, L., Tian, X., … Zhou, B. (2016). Endocardium Minimally Contributes to Coronary Endothelium in the Embryonic Ventricular Free Walls. *Circulation Research*, *118*(12), 1880–1893. https://doi.org/10.1161/CIRCRESAHA.116.308749

Zhang, J., Chu, L.-F., Hou, Z., Schwartz, M. P., Hacker, T., Vickerman, V., … Thomson, J. A. (2017). Functional characterization of human pluripotent stem cell-derived arterial endothelial cells. *Proceedings of the National Academy of Sciences*, 201702295. https://doi.org/10.1073/pnas.1702295114

Zhang, W., Chen, H., Qu, X., Chang, C.-P., & Shou, W. (2013). Molecular mechanism of ventricular trabeculation/compaction and the pathogenesis of the left ventricular noncompaction cardiomyopathy (LVNC). *American Journal of Medical Genetics Part C: Seminars in Medical Genetics*, *163*(3), 144–156. https://doi.org/10.1002/ajmg.c.31369

Zhao, L., Borikova, A. L., Ben-Yair, R., Guner-Ataman, B., MacRae, C. A., Lee, R. T., … Burns, C. E. (2014). Notch signaling regulates cardiomyocyte proliferation during zebrafish heart regeneration. *Proceedings of the National Academy of Sciences of the United States of America*, *111*(4), 1403–1408. https://doi.org/10.1073/pnas.1311705111

Zhou, B., & Pu, W. T. (2011). Epicardial epithelial-to-mesenchymal transition in injured heart. *Journal of Cellular and Molecular Medicine*, *15*(12), 2781–2783. https://doi.org/10.1111/j.1582-4934.2011.01450.x